VILNIUS UNIVERSITY
CENTER FOR PHYSICAL SCIENCES AND TECHNOLOGY

Augustina Jozeliūnaitė

Dynamic hydrogen-bonded tubular supramolecular assemblies

DOCTORAL DISSERTATION

Natural sciences,
Chemistry (N 003)

VILNIUS 2022

This dissertation was prepared between 2017 and 2021 (Vilnius University). The research was supported by Research Council of Lithuania.

This doctoral dissertation will be defended in a public meeting of the Dissertation Defence Panel:

Chairman – Prof. Habil. Dr. Albertas Malinauskas (Center for Physical Sciences and Technology, Natural Sciences, Chemistry – N 003).
Members:
Prof. Dr. Riina Aav (Tallinn University of Technology, Natural Sciences, Chemistry – N 003).
Doc. Dr. Jelena Dodonova – Vaitkūnienė (Vilnius University, Natural Sciences, Chemistry – N 003).
Prof. Dr. Vytautas Getautis (Kaunas University of Technology, Natural Sciences, Chemistry – N 003).
Prof. Habil. Dr. Gediminas Niaura (Center for Physical Sciences and Technology, Natural Sciences, Chemistry – N 003).
The dissertation shall be defended at a public meeting of the Dissertation Defence Panel at 1.00 pm on 30th September 2022 in Room A101 of the Center for Physical Sciences and Technology.
Address: Saulėtekio av. 3, LT-10257 Vilnius, Lithuania
Tel. +370 5 264 9211; e-mail office@ftmc.lt

The text of this dissertation can be accessed at the libraries of Center for Physical Sciences and Technology of Vilnius University as well as on the website of Vilnius University: www.vu.lt/lt/naujienos/ivykiu-kalendorius

VILNIAUS UNIVERSITETAS
FIZINIŲ IR TECHNOLOGIJOS MOKSLŲ CENTRAS

Augustina Jozeliūnaitė

Dinaminės vandeniliniais ryšiais sudarytos supramolekulinės vamzdelinės struktūros

DAKTARO DISERTACIJA

Gamtos mokslai,
Chemija (N 003)

VILNIUS 2022

TABLE OF CONTENTS

LIST OF ABBREVIATIONS

AFM	Atomic force microscopy
AIBN	Azobisisobutyronitrile
CD	Circular dichroism
COSY	Correlation spectroscopy
DABCO	1,4-diazabicyclo[2.2.2]octane
DAN	2,7-Diamino-1,8-naphthyridine
DCM	Dichloromethane
DFT	Density-functional theory
DIPEA	N,N-Diisopropylethylamine
DLS	Dynamic light scattering
DMF	Dimethylformamide
DMSO	Dimethylsulfoxide
DNA	Deoxyribonucleic acid
DOSY	Diffusion ordered spectroscopy
EA	Ethyl acetate
ECHBM	Electrostatic-covalent hydrogen bond model
EtOH	Ethanol
FS	Fullerene soot
GPC	Gel permeation chromatography
HATU	Hexafluorophosphate Azabenzotriazole Tetramethyl Uronium
HOMO	Highest occupied molecular orbital
HSQC	Heteronuclear single quantum coherence spectroscopy
ICyt	Isocytosine
ISC	Intersystem crossing
LUMO	Lowest unoccupied molecular orbital
MOFs	Metal organic frameworks
NDI	Naphthalene diimide
NMR	Nuclear Magnetic Resonance
NOE	Nuclear Overhouser effect
OFETs	Field-effect transistors
OLEDs	Light-emmiting diodes
PDI	Perylene diimide
RAHB	Resonance-assisted hydrogen bonding
RNA	Ribonucleic acid
ROESY	Rotating frame nuclear Overhauser effect spectroscopy
SEI	Secondary electrostatic interactions
SEM	Scanning electron microscopy

SET	Single electron transfer
TEA	Triethylamine
TEMPO	(2,2,6,6-tetramethylpiperidin-1-yl)oxyl
TFA	Trifluoroacetic acid
THF	Tetrahydrofuran
TMSCN	Trimethylsilyl cyanide
TMV	Tobacco mosaic virus
TPP	Tetraphenyl porphyrin
TTF	Tetrathiafulvalene
Upy	Ureidopyrimidinone

ACKNOWLEDGEMENTS

OBJECTIVES AND OUTLINE OF THE THESIS

Supramolecular chemistry serves as an excellent tool for the construction of complex functional architectures at the molecular level. The interest in these systems arises from the ability of small building blocks to spontaneously arrange into highly organized systems driven by reversible noncovalent interactions. Even though widely abundant in nature, self-assembly is still underdeveloped and many challenges still need to be addressed in order to achieve fully operational molecular devices. For instance, the smallest building components have to be encoded with essential information required to impose great level of control over spontaneous self-assembly. Hence, the synthesis of monomers often can be quite challenging and time consuming. A vast array of supramolecular architectures still partially relies on conventional covalent bonds to ensure highly ordered systems with limited dynamic properties. Therefore, it is essential to design structures fully based on noncovalent interactions in order to achieve reversible biomimetic systems which could operate in a controlled manner.

The main aim of this thesis is to develop discrete and tubular supramolecular architectures exhibiting dynamic properties based on C_2-symmetric bicyclo[3.3.1]nonane backbone with well-defined inner cavity which could potentially serve as functional supramolecular materials in future applications.

In order to achieve the set goals, self-complementary building blocks comprising flexible linker were synthesized for hydrogen-bonded tubular architectures in chapter 2. The precise tailoring of the linker is essential for the reduction of the steric repulsion arising from overcrowded bulky substituents in the periphery of a tubular polymer, which could prevent further orthogonal propagation. The incorporation of nucleophilic anchor into the scaffold opens up possibility for further introduction of various functional chromophores. Furthermore, tubular polymer can be converted into discrete cyclic tetramer by converting isocytosine moieties into ureidopyrimidinones. The host-guest properties of the resulting aggregates were probed by encapsulation of fullerene C_{60} within its well-defined cavity. Unprecedently, the obtained inclusion complex enhanced the propensity of the fullerene to abstract electron from sulfide side chains even in the dark. Owing to the fact that the application of fullerenes as catalysts for oxidation of organic substrates has been previously investigated very scarcely, its

potential as a green heterogenous photocatalyst was addressed in this work. Blue light-mediated chemoselective oxidation of sulfides in the presence of fullerene soot or fullerene nanodispersion yielded corresponding sulfoxides in good yields.

In chapter 3 the main focus is on dynamic nature of concave capsule comprising tetraphenyl porphyrin (TPP) moieties. During the complexation, the cavity underwent conformational changes in order to provide suitable shape for C_{60} guest molecule. Conformational changes of the system were achieved by guest induced cooperative effect of the tautomerization from the keto to enolic form of ureidopyrimidinone alongside CH-π interactions which offsets TPP units from the center of opening and provides the entrance for the guest molecule.

In chapter 4 the hydrogen-bonded tubular polymer comprising segregated n- and p-type channels was synthesized based on azabicyclo[3.3.1]nonane backbone. Simultaneous orthogonal propagation was provided by the combination of bifurcated hydrogen atoms situated on the rims of tetramer and π-π interactions occurring from newly incorporated planar tetrathiafulvalene units. Tetrathiafulvalene scaffold could potentially exhibit excellent hole mobility, whereas fullerene entrapped within cavity of supramolecule would serve as a n-type channel.

Finally, reversibility of ureidopyrimidinone hydrogen-bonding site was tackled in chapter 5. Tetrameric cyclic construct was transformed into reversible supramolecular tweezer by employing heterocomplexation with rival 2,7-diamino-1,8-naphthyridine agent. Full reversibility between the tetrameric structure, the open-ended tweezer or the monomeric unit was demonstrated by using chemical or light external stimuli.

1. HYDROGEN-BONDED SUPRAMOLECULAR ARCHITECTURES POSSESING WELL-DEFINED CAVITY

A new level of elegance and complexity has to be achieved in pursue of immense technological advances. The emergence of supramolecular chemistry as a concept of organized entities held together by weak intermolecular forces has opened up the opportunities for scientists to take the so-called "engineering up" approach to build new functional materials at the molecular scale. The idea of self-assembly originally came by exploring complex biological systems exhibiting high-level cooperativity and fidelity, such as viruses, lipid membranes, nucleic acid duplexes and triplexes, folded proteins, and their ability to associate into functional aggregates.[1,2] Such pre-organized entities might be essential for the emergence of life. Thus, by learning fundamentals of self-assembly and self-organization we are one step closer to understanding origin of life.[3]

The term self-assembly has been defined by George M. Whitesides as the autonomous organization of components into patterns or structures without human intervention.[4] In 1959 Richard Feynman in his famous lecture titled "There is plenty of room at the bottom" envisioned the possibility to manipulate matter at the atomic level to create small scale devices.[5] D. J. Cram, J.-M. Lehn and C. J. Pedersen have fulfilled that vision by providing foundation for supramolecular chemistry based on host-guest interactions and self-assembly to produce functional superstructures.[6] However, supramolecular architectures have to meet certain requirements to be able to aggregate in well-defined, controlled manner and to overcome the entropic penalty arising from the loss of disorder. The system has to organize itself to attain the thermodynamic minimum with the highest complementary interface. Therefore, the molecular component has to be encoded with all the necessary information for anticipated aggregation mode to occur. These instructions rely on noncovalent interactions such as metal-ligand coordination, π-π stacking, hydrophobic interactions and hydrogen bonds.[1] The reversible nature of noncovalent bonding allows for error-checking and elimination of defective features in the assembly (Figure **1**).[3,7] Thus, the building blocks can re-adjust once in contact ultimately resulting in the most stable arrangement.

Irreversible aggregation:
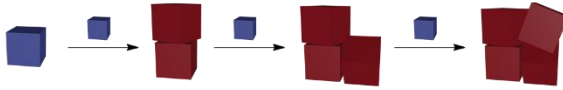
Reversible self-correcting aggregation:
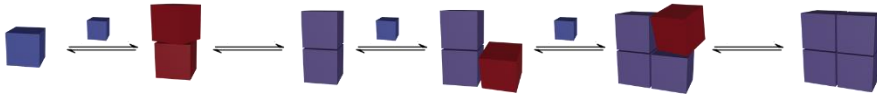
Figure 1. Schematic representation of irreversible and reversible aggregation modes.

Perhaps the most prominent example of hydrogen-bonded structures in living systems is the double-strand assembly of oligonucleotides in deoxyribonucleic acid (DNA).[8] The intermolecular hydrogen bonding in Watson-Crick base pairs reinforced by other noncovalent forces such as π-π interaction and hydrophobicity contribute to the association into the most stable double helix structure at thermodynamic equilibrium.[1] Even though some errors during nucleation of propagation might occur leading to the formation of loops and hairpins, the reversible nature of assembly followed by an error-checking allows the elimination of faulty patterns.[3] Due to high selectivity and fidelity, the different sequences of base pairs reliably encode genetic information within DNA.

Another example studied in great detail is rod-shaped tobacco mosaic virus (TMV) with dimensions 300 nm by 18 nm comprising 2130 identical subunits of 158 amino residues each (Figure **2**). Protein units assemble around a single strand of RNA by forming helical coat with size corresponding to 16 1/3 subunits per turn. Utilization of single protein in the outer layer is enough to ensure sufficient interactions between the subunits in order to hold the whole structure together. Reversible noncovalent interactions permit the virus to be dismantled by releasing its viral RNA strand during the replication and to spontaneously re-assemble again into functioning viral particle once the multiplication is complete.[1–3,9]
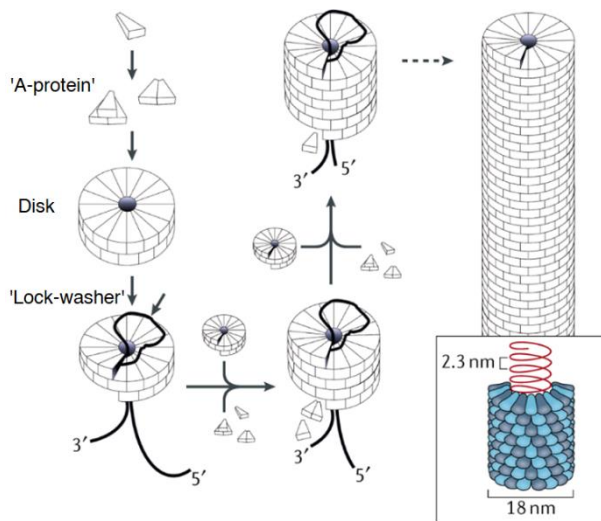
Figure 2. Stepwise self-assembly of tobacco mosaic virus. Reproduced from ref. 9 with permission from Beilstein Institut, 2016.

Over the past decades combination of nature inspired self-assembly alongside conventional synthetic methods have resulted in remarkable progress towards functional nanoarchitectures, for example, helical dendrimers[10], gels[11], nanoribbons[12], nanowires[13], capsules[14], nanotubes[15], etc. Such sophisticated multicomponent systems have led to broad application ranging from medicinal chemistry to microelectronics or photonics. In the latter fields, the major driving force for further improvements is to fulfill the demands of decreasing devices' dimensions with higher performance. Self-assembly facilitates manufacturing of devices by offering economical and flexible synthetic route from cheap-raw materials at the molecular level.[1,16] Furthermore, new supramolecular materials may pave the way as state-of-the-art stimuli-responsive nanocarriers in drug delivery. Recently, stable supramolecular micelles with high drug loading capacity were reported. *In vitro*, they displayed an excellent control of drug release and were successfully endocytosed by cancer cells showcasing its effectiveness.[17] A plethora of various nanostructures have been developed utilizing noncovalent interactions. Herein, however, the major focus will be on hydrogen bonded supramolecular architectures.

1.1 Hydrogen Bonding in Supramolecular Assemblies

Noncovalent interactions play an essential role in the development of functional supramolecular structures. The main noncovalent interactions employed in self-assembly include hydrogen bonding, dipole-dipole and

ionic interactions, π-π stacking and metal coordination.[15,18] Among them, hydrogen bonds are the most commonly utilized due its strength[19], reversibility, directionality[18] and sensitivity to external stimuli like solvent[20,21], pH[22,23] and temperature[24,25].

According to the commonly accepted classification, the hydrogen bonds are formed between a donor with a positively polarized hydrogen (D—H) and a proton acceptor (A), where donors are typically an electronegative atoms, such as O, N, S, C or halogens, and acceptors carrying nonbonding electron lone pairs or a π-bond of an unsaturated systems.[20] Thus, hydrogen bond can be simply described as a proton shared by two lone electron pairs.[26]

The nature of hydrogen bonding is still discussed up to today, whether it is predominantly electrostatic or partially covalent. Partially covalent character of hydrogen bond was proven by Compton scattering[27] and NMR[28] experiments. Based on the so-called electrostatic-covalent hydrogen bond model (ECHBM) described by Gilli *et al*., strong hydrogen bond is partially covalent, but if bond strength decreases, covalent contribution is reduced and the nature of bond becomes purely electrostatic interaction.[28–30] Typically, the strength of hydrogen bond is characterized by bond energy and can be classified as strong (14 – 40 kcal/mol), moderate (5 – 15 kcal/mol) and weak (0 – 5 kcal/mol).[20] However, the majority of supramolecular structures are obtained in solutions, therefore the strength of an intermolecular hydrogen bond in solution is defined by the association constant K_a of the aggregate or the change in Gibbs free energy. Thus, hydrogen bond strength depends not only on its length and angle[31], but is affected by the nature of the solvent, i.e. polar solvents compete with the solute molecules and suppress the supramolecular interactions.[20,21]

Typically, a single hydrogen bond is not strong enough to ensure well-defined supramolecular assemblies. Therefore, multiple hydrogen bond motifs come into play when stronger interactions are required. For example, complementary base pairs of guanine **1** – cytosine **2** complex are two to three orders of magnitude more stable in comparison to adenine **3** – thymine **4** pair (Figure **3**).[32,33] Many more useful structures usually employ three to four intermolecular hydrogen bonds since they assemble into robust yet reversible supramolecular architectures.
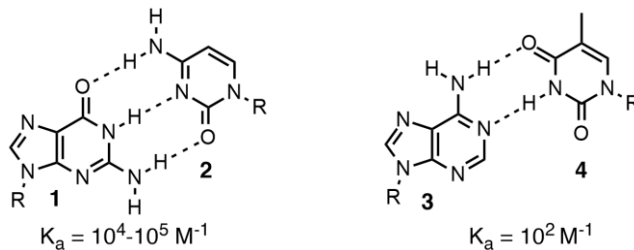
Figure 3. Schematic representation of DNA base pairs

1.1.1 Strength of hydrogen bonds

Even though higher number of hydrogen bonds establishes stronger association in supramolecular arrays, this should not be used as a sole guiding principle. Jorgensen and Pranata with co-workers have introduced term of so-called secondary electrostatic interactions (SEI).[34,35] According to SEI model, stabilization arises from the proper arrangement of donors (D) and acceptors (A), where attractive forces (SI$_a$) between positively and negatively polarized atoms in adjacent hydrogen bonds predominate, and repulsive forces (SI$_r$) between two positively or negatively polarized atoms are being minimized or diminished completely.[36] Hence DDA-AAD array will exhibit stronger association compared to DAD-ADA due to maximized number of attractive interactions in the former array.[20,37] The most stable structure is obtained when multipoint hydrogen-bonded arrays with hydrogen donors are in one moiety while acceptors are in the another because of all favorable secondary attraction forces (Figure **4**). As shown by Schneider, the strength of multiple hydrogen-bonded arrays can be anticipated from empirical free energy increments based on total free energies ΔG of 58 complexes in chloroform. Each primary and secondary electrostatic interaction contribute 7.9 kJ/mol and ±2.9 kJ/mol to ΔG, respectively. Sign of the latter value depends on the nature of secondary interactions.[32,38]
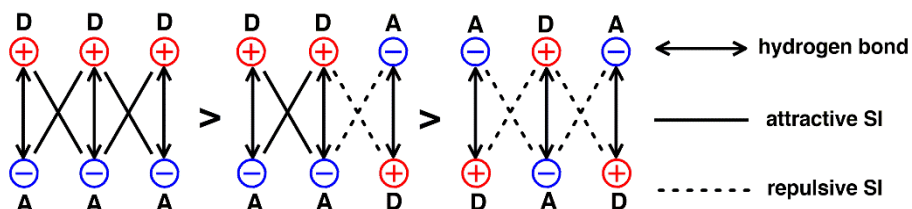
Figure 4. Schematic representation illustrating secondary electrostatic interactions on linear arrays of hydrogen bonds.

Jorgensen *et al.* have developed a series of triple hydrogen-bonded arrays with corresponding association constants in full support of this concept. Namely, ADA-DAD heterodimer **5:6** has a weakest affinity ($K_a = 140$ M^{-1}), because it contains four repulsive SEI while AAD-DDA array's **7:8** association constant is $K_a = 10^4$ M^{-1} due to secondary interactions canceling each other out (Figure **5**).[34,35] Zimmerman *et al.* reaffirmed previous reports by obtaining consistent results which included at that time unknown DDD-AAA dimer **13:14** that led to the strongest affinity because of all four attractive secondary interactions.[39] In addition, extension of anthyridine aromatic scaffold led to complex **15:16** with improved stability up to $K_a = 10^7$ M^{-1} in CH$_2$Cl$_2$ due to increased planarity of the framework.[40]
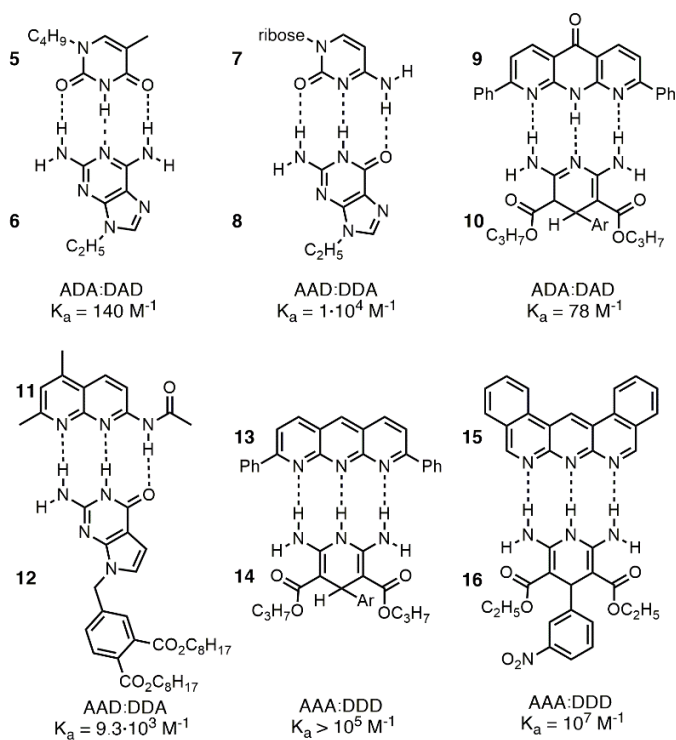
Figure 5. Linear arrays **5**-**16** comprising triple hydrogen bonds.

To improve the binding affinity further, the linear arrays comprising four hydrogen bonds have been established. In general, four different dimers DDDD-AAAA, DDDA-AAAD, DDAD-AADA and DAAD-ADDA may be conceived. However, the self-complementary DDAA and DADA arrays are significantly more important with respect to the application in supramolecular chemistry.[20] DADA-ADAD hydrogen-bonded dimers **17:17** and **18:18** which undergo self-assembly were initially reported by Meijer *et*

al. (Figure **6a**).[38,41,42] The significant difference in their association constant is due to pre-organization within molecule **18** by forming an additional intramolecular hydrogen bond between the hydrogen of ureido moiety and nitrogen atom of heterocycle ring which constrains the urea moiety in space and makes the self-assembly more facile.
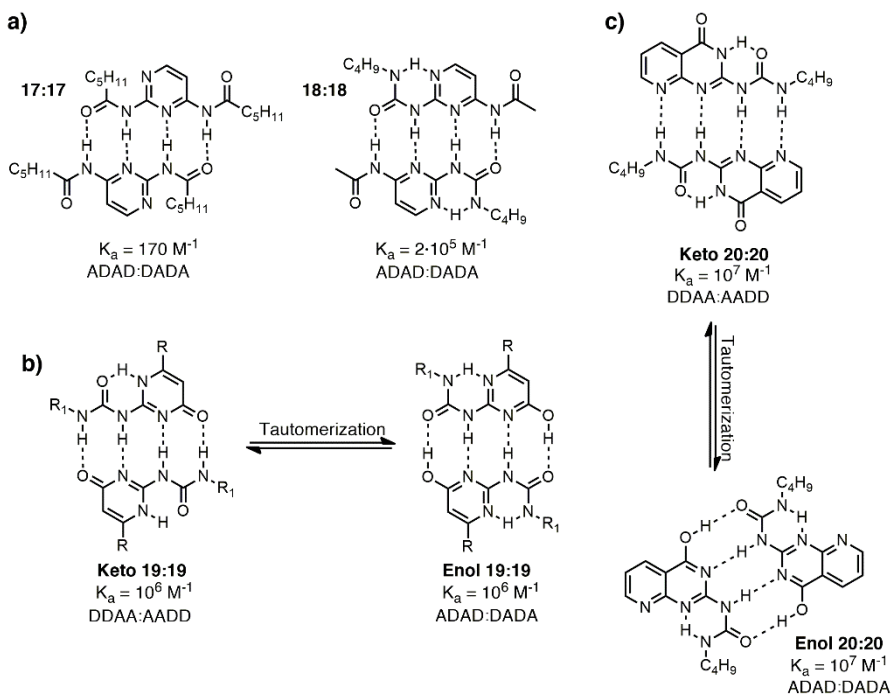
Figure 6. Examples of quadruple hydrogen-bonded arrangements.

Furthermore, Meijer *et al.* introduced self-complementary molecules, based on ureidopyrimidinone (Upy) backbone, which can dimerize using either DDAA or DADA hydrogen-bonded arrays depending on the predominant tautomeric form of Upy (Figure **6b**).[42] Typically, the more predominant DDAA motif encompasses fewer repulsive secondary electrostatic interactions compared to DADA complementary motif. Nevertheless, Upy moiety can exist in either self-complementary keto or enolic forms which undergoes association via pre-organized DDAA or DADA arrays, respectively. The shift in tautomeric equilibrium can be controlled just by changing the nature of substituents from electron-donating to electron-withdrawing and *vice versa*.[43] In order to address the issue of tautomerism, Zimmerman *et al.* proposed a monomer **20**, where the majority of tautomer self-dimerize through DDAA hydrogen bond pattern despite negligible amount of DADA array appearing as well (Figure **6c**).[44]

Nevertheless, incorporation of all binding subunits into one linear backbone is synthetically challenging. Therefore, changing the spacings between hydrogen binding subunits represents an alternative approach. It leads to elimination of secondary interactions; hence stability of the structure is solely proportional to the number of hydrogen bonds. Gong *et al*. presented highly cooperative self-complementary DDAA **21** and DADA **22** components with association constants in the range of 10^4 M^{-1} (Figure **7a**).[45] Changing the linker from glycine in **21:21** and **22:22** to rigid aromatic linkers in **23:23** and **24:24** has no significant effect on the binding strength (Figure **7b**). Spacers can also be used to prevent homodimerization when needed by alternating the gap between bonding units (Figure **7c**).[46,47] Longer heterodimers comprising six or eight hydrogen bonds have also been prepared with increased stability accordingly.[48,49]
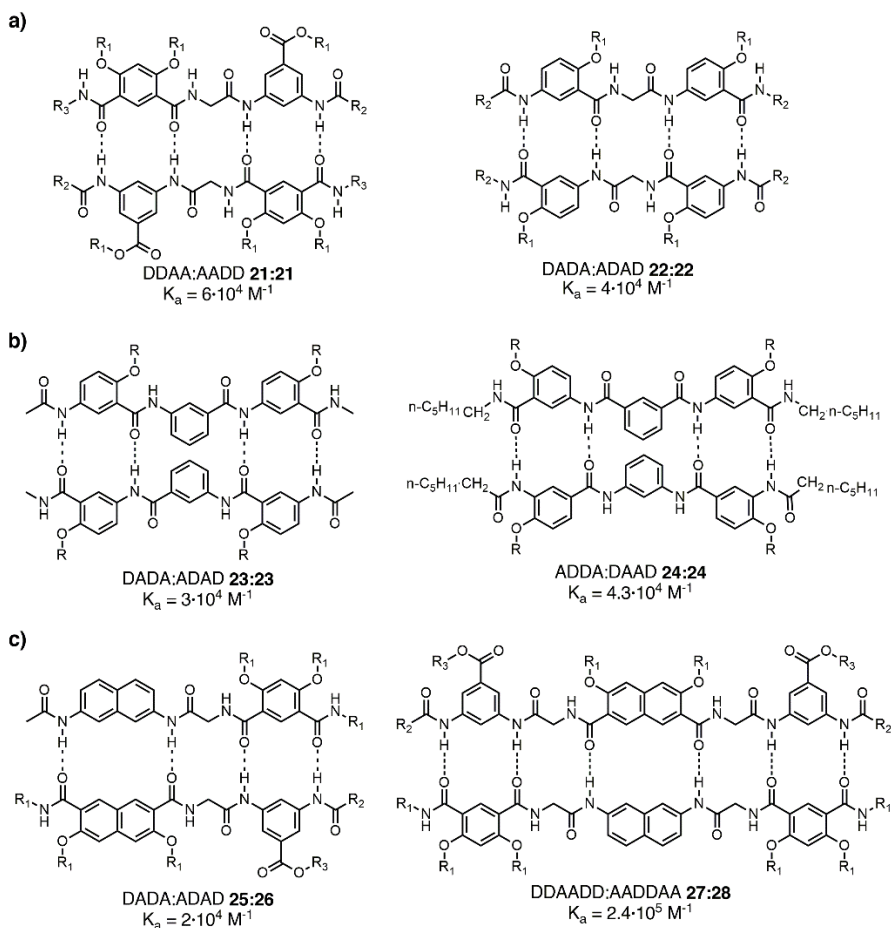
Figure 7. Molecular dimers with hydrogen-bonding arrays separated by spacers.

Several possible tautomeric forms can have a negative impact on the binding properties of a monomer which directly affects association constant of the dimer.[50] Despite this caveat, Bell *et al.* have further improved association in cationic DDD⁺-AAA systems by combining cooperative secondary interactions with positively charged species which enhances proton acidity of the donating unit while providing electrostatic stability arising from favorable attractive interactions (Figure **8a**).[51] However, for this particular cationic complex **13:29** they could not accurately measure association constant by employing different techniques, and therefore it was suggested that due to lack of curvature in the binding isotherm, the association constant must be greater than $5 \cdot 10^5$ M^{-1} in CH$_2$Cl$_2$. Leigh *et al.* measured the remarkable association constant $K_a = 3 \cdot 10^{10}$ M^{-1} of cationic complex **15:30** by fluorescence titration experiments performed in CH$_2$Cl$_2$.[50]
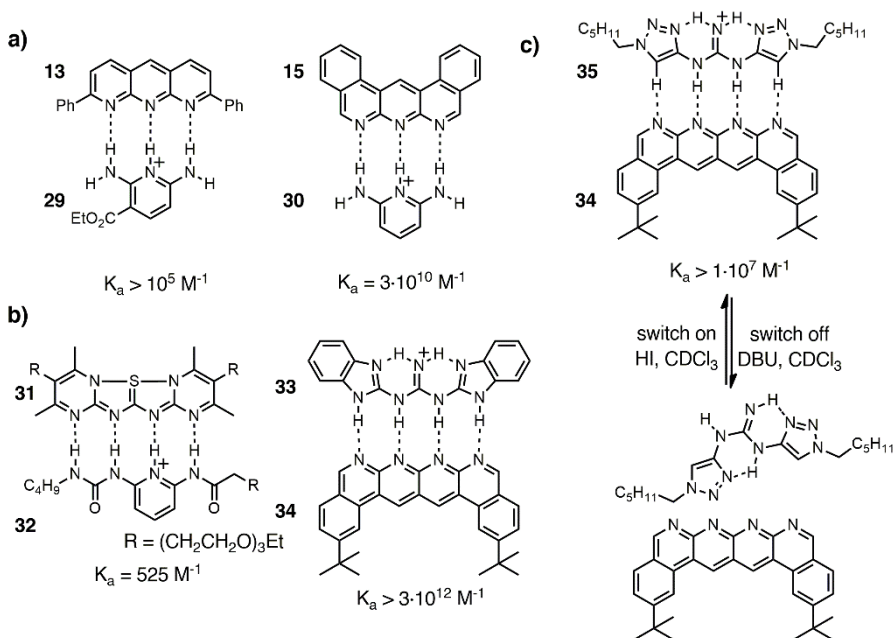
Figure 8. Cationic complexes comprising remarkably strong hydrogen-bonding motifs.

To further enhance the association process, quadruple cationic hydrogen bonded motifs have been proposed by Lüning *et al.* where sulfurane **31** together with cationic counterpart **32** gives the desired hetero dimer DDDD⁺-AAAA (Figure **8b**). Unfortunately, **31:32** exhibits impeded dimerization with a mediocre association constant due to lack of pre-organization in cationic pyridine urea **32** which can undergo folding via single bond rotation

resulting in the formation of an intramolecular hydrogen bond between the protonated pyridine nitrogen and carbonyl groups.[52] To overcome a detrimental folding, readily accessible AAAA-DDDD$^+$ hydrogen bonded array comprising planar rigid heteroaromatic system was reported.[53] Incorporation of two intramolecular hydrogen bonds into the backbone restricts undesired tautomerization and together with enhanced donor strength arising from positive charge promotes the formation of the well-defined **33:34** arrays with remarkably high affinity ($K_a > 3 \cdot 10^{12}$ M^{-1} in CH$_2$Cl$_2$). Replacing two benzimidazole groups of the **33** to triazole moieties **35** results in reduced association due to changing NH···N hydrogen bonds to two newly formed weaker CH···N interactions in a quadruple hydrogen-bonded array **35:34**. Additionally, such system could be disassembled and re-assembled in fully reversible manner simply by deprotonation of guanidinium moiety via successive addition of base and acid (Figure **8c**).[54] Utilizing such supramolecular architectures controlled by simple stimulus may broaden the scope of their application in self-healing polymers or other functional materials.

Despite the SEI model's effective estimates of the strength of hydrogen bonds, many state-of-the-art quantum calculations and experimental evidence have indicated that other key factors including charge-transfer interactions, Pauli repulsive interactions, dispersion interactions, cooperativity and resonance-assisted hydrogen bonding (RAHB) reciprocate in the formation of hydrogen bond.[19,55,56] In accordance with Guerra *et al.,* oversimplified secondary electrostatic interaction model is coinciding so well with empirical methods due to its correlation with charge accumulation in monomers. They pointed out that a larger charge accumulation at the frontier atoms is obtained when proton donors and acceptors are grouped. This leads to an improved orbital interaction and a decreased HOMO-LUMO gap because a more positive donor atoms better stabilizes LUMO while negatively charged acceptor atoms destabilizes HOMO. Thus, tautomeric hydrogen-bonded DDAA arrays result in a higher binding affinity due to a greater charge accumulation compared to DADA motifs.[19,55,57] Their findings are further supported by RAHB theory initially introduced by Gilli *et al*., suggesting that in β-diketones partial charges are generated by π-electron delocalization which enhances the strength of hydrogen bond (Figure **9a**). It follows from these insights that the basicity of hydrogen bond donor can be increased by π-resonance assistance. Hernández-Rodríguez, and Rocha-Rinza *et al.* proposed that hydrogen bond stability could be refined by considering Brønsted-Lowry acid-base properties of proton donor

and acceptor moieties, respectively. Thus, the binding strength might be modulated in a rational way by incorporating various electron-withdrawing and electron-donating groups.[58,59] In line with these ideas, Wu *et al*. found that arrays comprising same SEI patterns can have different binding affinity depending on the aromatic nature of the interacting dimers.[60] The hydrogen bond is reinforced if delocalized π-conjugation pattern coincides with Hückel's rule and the number of π-electrons is equal to 4n+2. Such effect can be observed in guanine **1** – cytosine **2** and adenine **3** – thymine **4** nucleobase pairs or Upy DDAA dimer **19**:**19** (Figure **9b**).[36,60,61] In sharp contrast to the SEI model, extended π-conjugation in the quadruple multipoint hydrogen bonded dimers can explain such tremendous difference of association constants between complexes **36**:**37** and **36**:**38** despite having the same DAAD-ADDA hydrogen bonding pattern (Figure **9c**).[61,62]
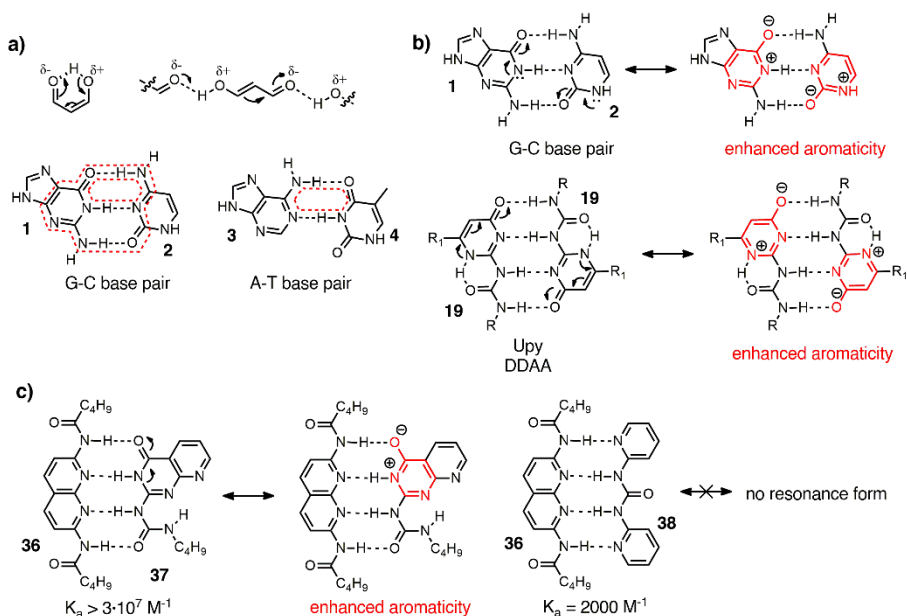
Figure 9. a) Resonance-assisted hydrogen bonding in β-diketones and GC and AT base pairs; b) aromaticity modulated hydrogen bonding in GC base pair and Upy dimer; c) changes in the aromatic character of heterocycles can affect association between DAAD-ADDA arrays.

Clear exceptions to the SEI model were also explained by Lukin and Leszynski, who noted that DAA-ADD hydrogen-bonded dimers form weak complexes in comparison to DDD-AAA arrays due to solvation of DAA and ADD units in wet polar solvents such as DMSO or even occasionally chloroform might contain a significant amount of water which could

interfere with the stability of hydrogen-bonded complexes.[63] For instance, binding energy can be increased by more than 3.5 kcal/mol upon changing the nature of the solvent from dichloromethane to tetrachloroethane. These examples highlight the more intricate solvent effects over hydrogen-bonded structures. Hydrogen bond strength can be reduced in polar solvents since they usually demonstrate the strongest release in enthalpy and entropy upon associative interactions with the monomer, thus stabilizing the unbound state.[64–66] Therefore, nonpolar solvents have greatly facilitated the development of hydrogen-bonded arrays.

Multipoint hydrogen-bonded arrays are of great interest in self-assembly due to its capability to form well-defined larger entities from low molecular weight components. However, structural information such as molecular shape, placement of various functionalities and directionality has to be encoded into the building blocks in order to obtain a supramolecular structure with envisaged properties. In addition, for the effective applicability in supramolecular chemistry, monomer should also possess characteristics like readily accessible synthesis, high fidelity and complex stability with tunable affinity. In search of desired synthons only few have been shown to possess required key properties for the construction of self-assembly systems. The widely exploited minority that fits the criteria are ureidopyrimidinones, ureas, guanines, barbiturates, cyclic peptides and deazapterins.

1.2 Development of ureidopyrimidinone as a hydrogen bonded synthon

Among the multiple hydrogen-bonded arrays, the 2-ureido-4[1H]-pyrimidinone (Upy) has taken a prominent position as a versatile building block owing to its self-complementary nature, strong dimerization and availability from cheap starting materials. Upy was initially developed in 1998 by Meijer *et al*. as a preorganized quadruple hydrogen-bonded DDAA array. The Upy can be conveniently synthesized in a gram scale in two step synthesis by reaction of β-keto esters with guanidine, followed by acylation with isocyanate.[38,67–71] As discussed above, its extremely high association constant ($K_a > 10^7 \cdot M^{-1}$ in chloroform) could be justified by attractive secondary electrostatic interactions which are supplemented by increased aromaticity due to π-electron delocalization in six membered rings.[61,72]

Despite its versatility, one important shortcoming of this hydrogen-bonding motif cannot be ignored. Namely, the presence of different tautomeric forms in Upy scaffold can cumber the formation of well-defined structures. Keto-enol tautomerism is the most studied because it plays an essential role in the interaction of active molecules with proteins, enzymes or other receptors. In addition, tautomerism of base pairs in cells can cause improper recognition, replication or transfer of genetic information. Hence, tautomerism potentially can facilitate spontaneous point mutations in DNA.[73,74]

The ureidopyrimidinones can exist in three different tautomeric forms depending on the polarity of solvent and the nature of substituents, among which two tautomers 4-[1H]-pyrimidinone (**4-keto**) and pyrimidin-4-ol (**enol**) are self-complementary and can form DDAA and DADA homodimers, respectively (Figure **10**).[68,73,75] For instance, in polar aprotic DMSO solvent intermolecular hydrogen bonding is inhibited, thus Upy is present in 6-[1H]-pyrimidinone (**6-keto**) monomeric form while a mixture of **4-keto** and **enol** prevail in less polar solvents like toluene or CHCl$_3$ as a result of acquired stabilization by self-association.[38,71,73,76]
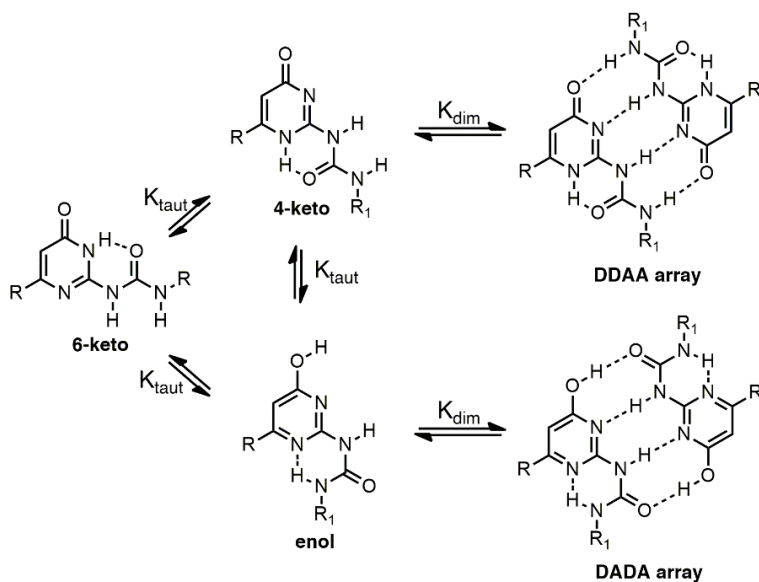

Figure 10. Tautomeric forms of ureidopyrimidinone (Upy) derivatives.

Study on various Upy monomers and their corresponding dimers by DFT methods has given a more comprehensive insight how the change in polarization of the surrounding environment affects tautomeric distribution. It was shown that the order of tautomer stability changes from **enol** > **6-keto**

24

> **4-keto** in vacuum to **4-keto > enol > 6-keto** in chloform.[70] In addition, Meijer *et al.* have deduced from ^{1}H NMR dilution experiments in d$_8$-THF that distribution of **4-keto** and **enol** forms is concentration-dependent since N-H resonances corresponding to **4-keto** form do not shift while N-H and O-H resonances belonging to **enol** form shift upon dilution. These findings indicate higher robustness of the **4-keto** tautomer.[42] Moreover, the alteration of substituents' electronic properties can remarkably shift equilibrium towards particular tautomeric form. For instance, Upy bearing electron-withdrawing substituents like p-nitrophenyl- and trifluoromethyl- on the 6-position of the isocytosine ring favors **enol** tautomer in chloroform while the presence of electron-donating substituent favors **4-keto** form.[38,42,70,71,73,76] Further control over tautomeric distribution can be obtained by incorporating electron-withdrawing groups at the terminal urea nitrogen atom which leads to even greater preference for **4-keto** form.[42] It was demonstrated that larger substituents on 6-position promote the dimerization via DDAA – AADD mode shifting the equilibrium towards **4-keto** form. Computational investigations on structural features of Upy showed that dimers bearing adamantyl groups have shorter hydrogen bonds in comparison to methyl-substituted congeners as evidenced by an apparent red shift in IR spectrum indicating reduced stretching frequencies of hydrogen bonds.[70]

Tautomerization might lower association fidelity of the targeted DDAA arrays by promoting undesired complex dimerization leading to complicated supramolecular architectures. Therefore, Sanjayan *et al.* sought to eliminate prototropy related issues by exploiting intramolecular bifurcated hydrogen bonding to restrain proton transfer in self-assembling systems (Figure **11**).
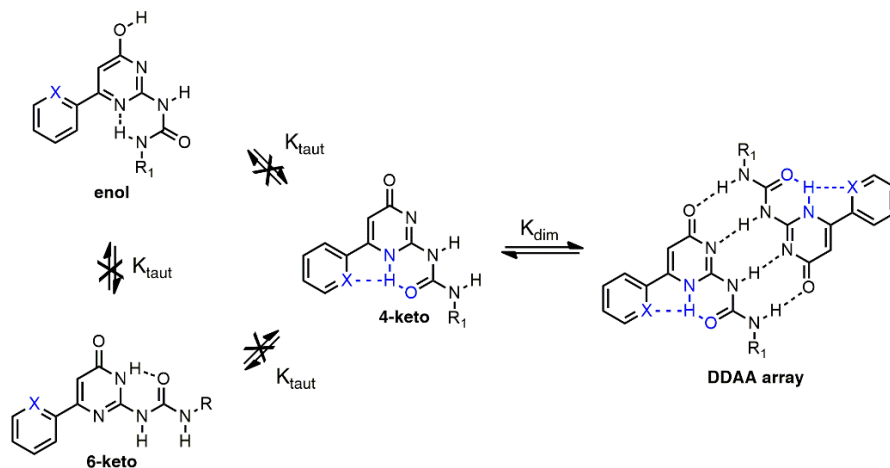
Figure 11. Representative diagram of prototropy-free DDAA dimers.

To this end, additional hydrogen bonding acceptors such as methoxy-, quinoline and hydroquinone were introduced into 6-position of heterocycle in order to form an additional hydrogen bonding with N-H of pyrimidine and to prevent the proton shifting (Figure **12a**). A single set of N-H peaks in ^{1}H NMR spectra of **39:39**, **40:40** and **41:41** dimers in CDCl$_3$ indicated a formation of a self-complementary keto tautomers. The substantial downfield shift of N-Hs is in accord with intramolecular hydrogen bonding to two acceptors. The high stability of the complexes without competition from parasitic tautomers was demonstrated by increasing DMSO-d$_6$ amount up to 20 % in NMR dilution titration experiments with insignificant chemical shifts of N-H involved in dimerization being observed.[77] Dong *et al.* developed Upy derivative **42** comprising pyridine moiety at 6-position which embedded intramolecular hydrogen bonding amongst N-H of pyrimidine with nitrogen atom of pyridine to promote desired **4-keto** tautomer shown to exist both in solution and solid phase.[73]
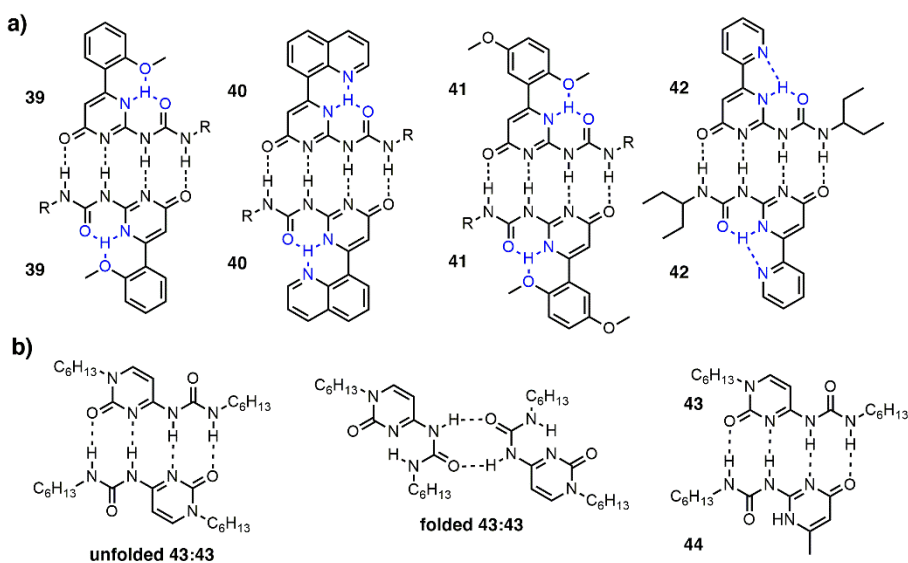
Figure 12. a) quadruple hydrogen bonded dimers with inhibited prototropy; b) unfolded and folded conformers of cytosine and dimerization of former conformer to heterocomplex **43:44**.

Another approach to prevent tautomerization is N alkylation in ureidocytosine system introduced by Hailes *et al.* (Figure **12b**). The lack of intramolecular interactions resulted in flexible ureido scaffold and appearance of two conformers, folded and unfolded. It was shown that dimer of preferred unfolded form mainly exists in nonpolar solvents with

association constant $K_a = 9 \cdot 10^6$ M^{-1} in C_6D_6 as DDAA – AADD quadruple hydrogen-bonded dimer. Furthermore, its potential to disrupt robust Upy complex by heterocomplex formation was confirmed by ^1H NMR studies of a 1:1 mixture unfolded **43** with UPy **44** in CDCl$_3$ in ratio 5:6:5 of **43**:**43**, **43**:**44**, **44**:**44** accordingly.[78]

For further development of supramolecular structures, the dimeric architectures comprising two bisureidopyrimidinone moieties **45** linked by m-xylylene spacer were reported (Figure **13a**). Even though more than three isomers of this dimeric structure can exist, only two different conformers were characterized by single-crystal X-ray analysis in solid state. The interconversion between syn-conformer **I**, with both Upy moieties on the same plane, and anti-conformer **II**, with Upy units on opposite sides of plane, is fast, whereas equilibration into keto-enol configuration **III** is relatively sluggish process (Figure **13b**).[79] However, tautomerization between keto-enol forms can be efficiently controlled by incorporation of different substituents. **46** bearing alkyl chain mainly exists in **III** configuration, whereas DDAA-AADD dimeric module is predominant in **47** due to additional intramolecular hydrogen bonding interlocking the system in keto tautomer (Figure **13c**).[73] Hence, it is necessary to find novel strategies to gain superior control over tautomerization to establish well-ordered architectures exhibiting higher degree of complexity.
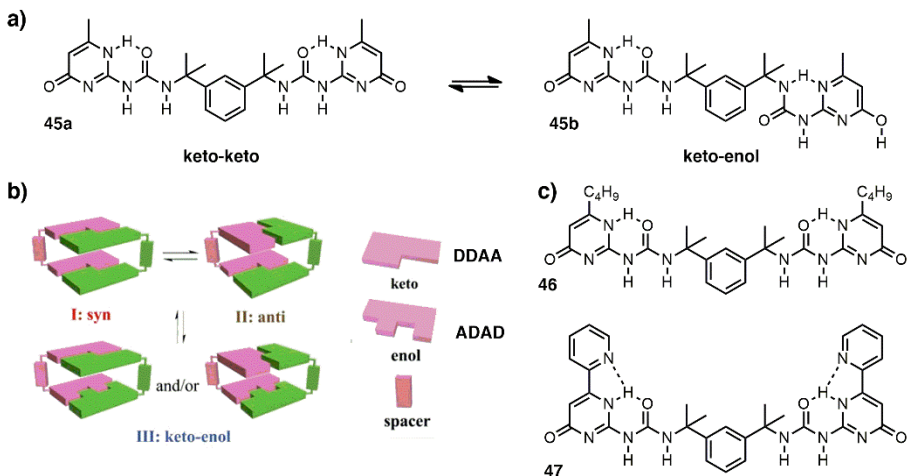

Figure 13. Supramolecular architecture comprising two bisureidopyrimidinone moieties **45** linked via m-xylynene spacer.

1.3 Supramolecular frameworks possessing cavity based on discrete hydrogen-bonded building blocks

The creation of well-defined nanostructures with the same precision as exhibited by nature is still a challenge. Although self-assembly of individual components mostly rely on noncovalent interactions, further formation of hierarchical 2D and 3D networks is reinforced by the so-called cooperative effect, where a combination of two or more forces come into play. The newly obtained structure may behave in a unique manner and exhibit different properties with respect to its constituents. Cooperative effects can be distinguished into 4 groups: cooperative aggregation, allosteric cooperativity, interannular cooperativity and chelate cooperativity. The latter applies for cyclic assemblies such as macrocycles, rosettes, capsules, cages, nanotubes, etc., which benefit from increased thermodynamic stability compared to linear open form species.[80]

1.3.1 Hydrogen bond driven cyclic aggregates

The primary rosette structures were elegantly introduced by the groups of Lehn,[81,82] Mascal,[83,84] Whiteside[85,86] and Fenniri[87–89]. The Janus-type fused heterocycles form rigid cyclic hexamer utilizing hydrogen bonding pattern DDA-AAD, in similar fashion to GC nucleobases.[83] According to Lehn *et al.*, co-crystallization of triaminopyrimidines **48** with complementary barbituric acid derivatives **49** gives rise to a mixture of ribbon-like polymeric strands and hexameric macrocycles in solid state (Figure **14**).[81] Thus, fused heterocycles **50** comprising two hydrogen bonding arrays on both ends with 120° angle geometry between complementary entities direct rosette-type cyclization with enhanced chelate cooperativity and hindered formation of linear strands.[82,84]
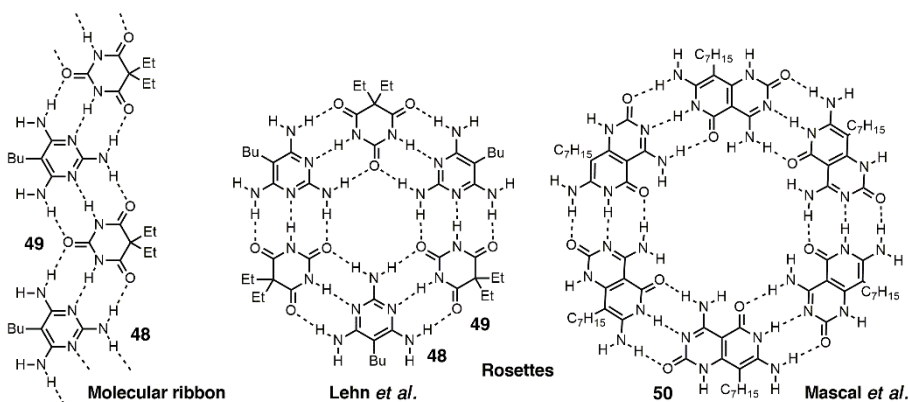
Figure 14. Examples of hexameric rosettes and ribbon-like polymer.

The prominent representatives of discrete rosette family comprising cyanuric acid **CA** and melamine **M** derivative in solid state were designed by Whiteside *et al.* Replacement of methyl groups on melamine with sterically encumbering *tert*-butyl substituents impedes formation of other possible supramolecular isomers.[85] Further, hierarchical supramolecular aggregates necessitate at least some degree of pre-organization. BisM **51** and bisCA **52** units comprising various rigid linkers form nanotubes from preorganized **CA-M** rosettes. Subsequently, it further assembles into mesoscopic aggregates of rod structures due to attractive intermolecular van der Waals interactions between adjacent lauryloxypropyl groups (Figure **15a**).[86]
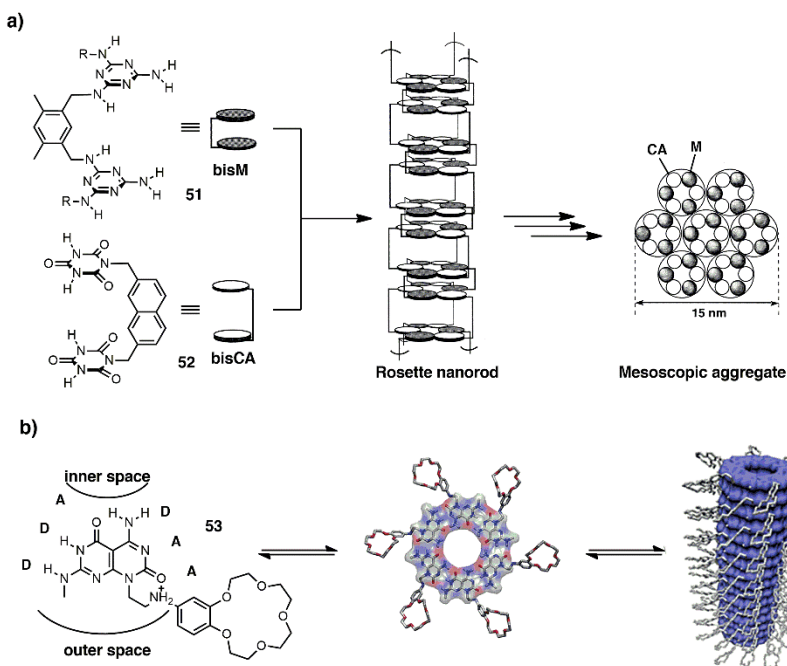
Figure 15. Self-assembly of a) **bisM** with **bisCA** to give polymeric nanorods which tend to aggregate into bundles of rods and b) **GC** fused heterocycles into chiral tubular nanorods. Adapted from ref. 86, 89 with permission from American Chemical Society, 1999 and 2002, respectively.

Janus-type hexameric macrocycles **53** comprising **GC** fused heterocycles were later on exploited by Fenniri *et al.* to construct hierarchical tubular architectures through π-π stacking and hydrophobic effect in organic and aqueous media (Figure **15b**). Electron-donor properties can be controlled by modulation of inner cavity via extension of the bicyclic scaffold. Incorporation of one or two pyridine rings increases cavity size to ca. 1.4 nm

and 1.7 nm, respectively, without disrupting the topology of the rosette macrocycle. Thus, enlarged cavity opens up the possibilities for larger guest encapsulation and inner channel functionalization.[87,88] Chiroptical properties and outer surface properties can be tuned by attaching various pendant groups. For instance, incorporation of benzocrown ethers to its exterior ensues prochiral binding sites to chiral auxiliary – L- or D-Ala amino acids which induces a prominent Cotton effect in circular dichroism (CD) spectra, whereas control experiments with only amino acid or crown ether derivative do not exhibit any CD activity.[89]

Some of the recent works on this subject are focused on the ability to control topology of the secondary structure in order to develop 1D nanoassemblies with high degree of internal order similar to proteins. Rosettes of barbiturate derivatives **54** bearing naphthalene units can either stack with a small inclination angle between adjacent macrocycles into windmill **55** or watermill **56** shape in methylcyclohexane depending on its geometry (Figure **16**). Stacking with rotational and translational offset or just only rotational displacement corresponding to J- and H-type aggregation can lead to toroidal or linear supramolecular polymers, respectively.[90]
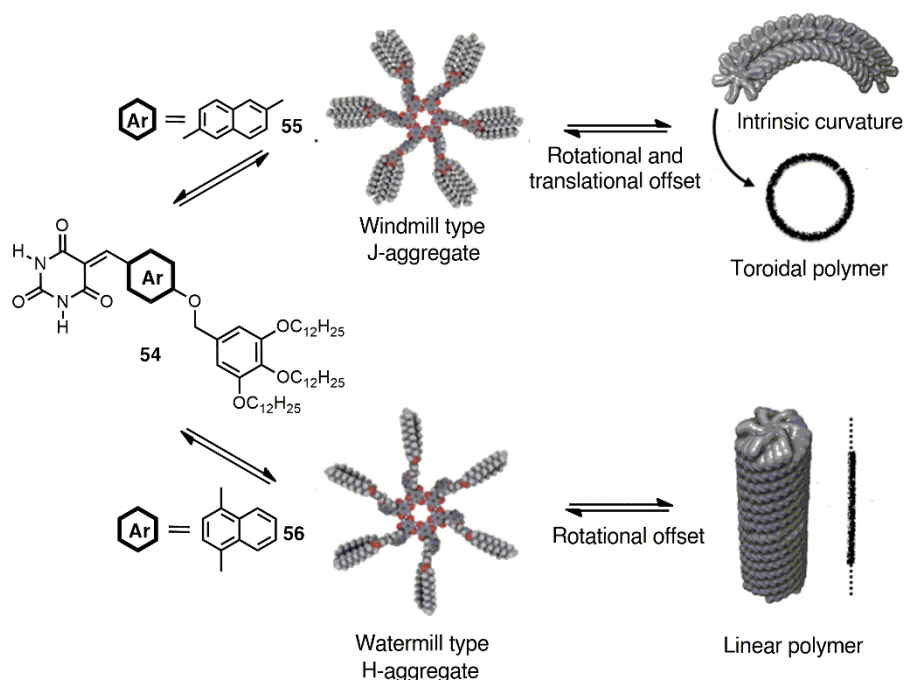
Figure 16. Impact of π-conjugated core on the secondary structure. Adapted from ref. 90 with permission from American Chemical Society, 2019.

Extension of aromatic scaffold to anthracene results in linear structure with suppressed intrinsic curvature because of stronger π-π interactions leading to smaller displacement of stacked rosettes. Surprisingly, a mixture of two monomers comprising naphthalene and anthracene core exhibit narcissistic self-sorting which generates segregated helical and linear topologies in a single fiber.[91]
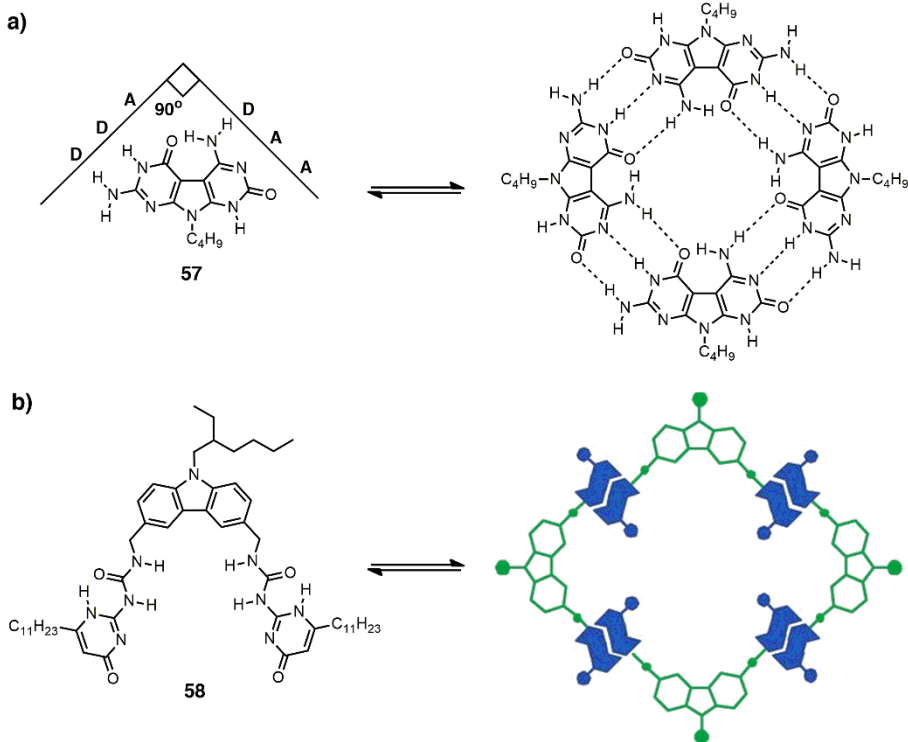
Figure 17. Examples of well-defined tetrameric aggregates.

An analogous Janus-type building block **57** comprising GC pair interlinked with the pyrrole moiety was introduced by Perrin *et al.* Embedded pyrrole governs both hydrogen bonding AAD and DDA arrays to associate through 90° angle into corresponding tetrameric macrocycle held by 12 hydrogen bonds (Figure **17a**). A novel tetrameric topology was elucidated by variable temperature ^{1}H NMR, whereas NH_2 unit of guanine resolves into two distinct signals at 5.75 and 7.3 ppm at –65°C due to reduced rotation along C-N bond, and at –10°C broad coalesced signal belonging to NH_2 of cytosine split into two resonances at 6.8 and 7.5 ppm. The diffusion ordered ^{1}H NMR spectroscopy (DOSY) revealed the presence of a single species with corresponding diffusion coefficient D = 0.7·10^{-10} m^{2}s^{-1}, much smaller

compared to monomeric carbazole reference (D = 1.43·10⁻¹⁰ m²s⁻¹). This value is consistent with ESI-MS analysis which further corroborated the formation of solely tetrameric assemblies.[92] In this context, Mendoza *et al.* designed Upy moieties embedded in carbazole scaffold **58** with methylene linkers, which preferentially lead to well-defined tetrameric architectures (Figure **17b**). The binding sites are symmetrically arranged on the same plane, facing the same direction with 90° angle and it favors belt-like formation without torsional strain. Alkyl groups pointing outside towards the bulk solvent decrease the steric hindrance while enhancing the solubility in organic solvents. DOSY experiment revealed only one type of discrete species assigned as tetramer with an approximate hydrodynamic radius of 9.29 Å.[93]
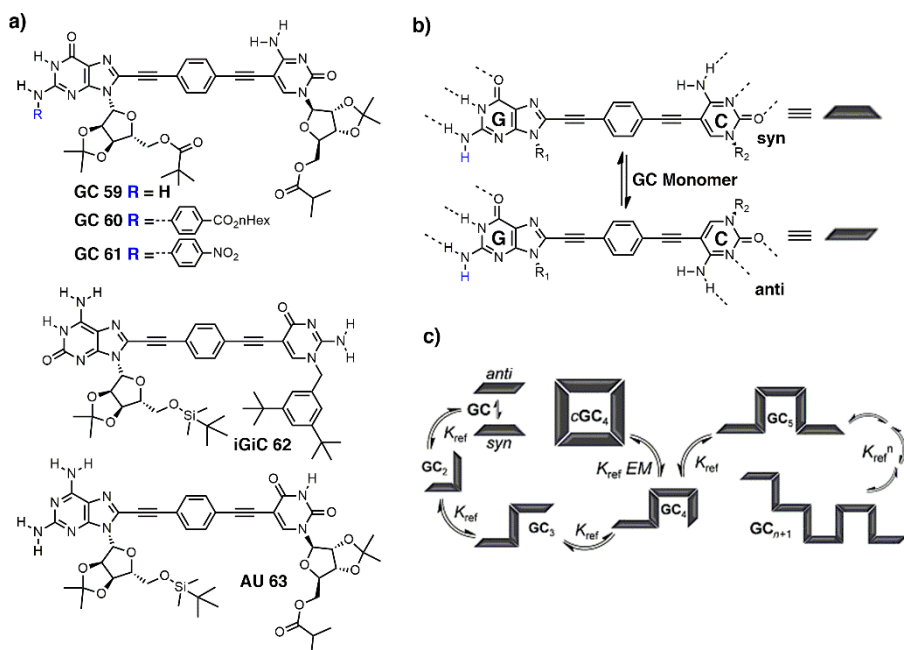
Figure 18. a) Structure of rigid dinucleoside monomers GC, iGiC, AU; b) equilibrium established between syn and anti-conformations; c) self-assembly of GC monomer to form cyclic tetramer or linear oligomer. Adapted from ref. 94 with permission from John Wiley and sons, 2015.

Another synthetic strategy encompasses high-fidelity cyclic tetramers through rationally designed GC **59**, iGiC **62**, AU **63** monomers, where chelate cooperativity is enhanced by incorporating linear p-diethynylbenzene linker between nucleobases (Figure **18a**). σ-bonds in the spacer still allow the rotation between nucleobases, thus monomer can adopt syn or anti

conformations depending on mutual orientation of bases (Figure **18b**). Its rigid nature with reduced rotational motion to a certain extent is a key factor to favor square-shape over polymerization in "all or nothing" fashion with minimal conformation entropy loss and strain generated upon cyclization (Figure **18c**). The remarkable thermodynamic stability of the tetrameric assembly was confirmed by competition studies. Addition of rival cytosine in excess should interfere with tetramerization and compete with GC **59** monomer for binding to complementary hydrogen bonded array. Author monitored competition by ^{1}H NMR titrations and estimated that 60 equivalents of cytosine in CHCl$_3$, 40 in THF or 35 in DMF were needed in order to disrupt the macrocycle. AU **63** forms significantly less stable tetramer due to weaker binding (K = 2.5·10^2 M^{-1}) which is two folds of magnitude lower in comparison to GC **61** and iGiC **62**.[94,95] Guanosine arylation with electron-deficient substituents increased acidity of guanosine amine **GC 60** and **GC 61** resulting in further enhanced stability.[96]

1.3.2 Hollow discrete host assemblies

Self-assembly of concave pre-organized molecules into discrete capsules or cages comprising well-defined internal space has emerged as a fascinating class of supramolecules due to their applicability in host-guest chemistry, catalysis, drug delivery and molecular devices. The walls of host isolate accommodated molecules by providing mechanical barrier to guest molecules from the outer environment. Covalent macrocycles, including cyclodextrins, cucurbiturils, calixarenes, pilaranes, resorcinarenes have been utilized as a nanocontainers with high affinity for various small guest entities. Although, covalently bonded architectures ensure well retained shape of the inner space, the rigid scaffold limits the conformational freedom needed in order to fit required guest molecule. Thus, more dynamic hosts could be established utilizing supramolecular approach.

Rebek *et al.* have pioneered the construction of reversible molecular capsules by presenting the so-called tennis ball, where the self-complementary glycoluril scaffold **64** dimerizes into pseudospherical shape held together by eight hydrogen bonds in chloroform (Figure **19a**). The curvature of monomers is ensured by methylene linkages between glycoluril moieties.[97] However, such closed shell cavity could not accommodate molecules larger than ethane. The capsule with larger cavity was obtained by fusing 13 rings together and extending the backbone of monomer **65** (Figure **19b**). The substituents appended on the same plane to ethylene bridge ensure that the backbone takes a lowest energy C shape conformation with R groups

pointing outwards. Encapsulations of 1-ferrocenecarboxylic acid and adamantane derivatives in *para*-xylene-d_{10} were confirmed by the upfield shifted signals observed in NMR spectrum due to anisotropic environment induced by four benzene rings of the host. During encapsulation, favorable host-guest interactions compete with entropy loss due to reduced freedom of distinct components. Hence, guest molecules must possess the shape and size complementarity to the cavity in order to maximize favorable van der Waals interactions between host and guest for successful confinement of an individual molecules within inner space.[98] For instance, cylindrical capsule with flattened interior cavity can trap two different disc-shaped molecules like benzene, cyclohexane, etc (Figure **19c**). Moreover, a preferential confinement of benzene together with p-xylene is observed in a mixture of benzene, toluene and p-xylene, because two benzene molecules are too small for optimal filling of the cavity, whereas two p-xylene molecules are too large.[99]
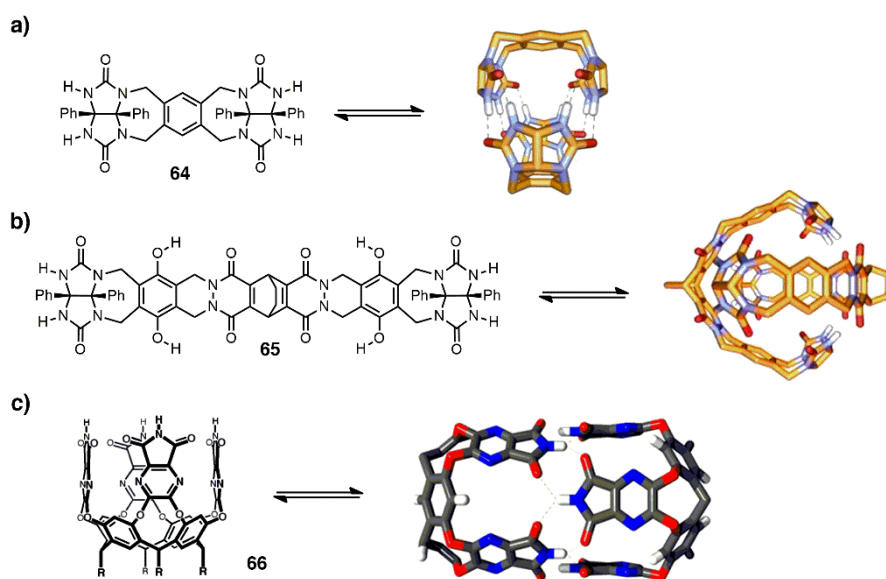
Figure 19. Reversible capsules based on glycoluril backbone.

Symmetrical molecular capsules displaying a significantly larger cavity (ca. 1400 Å^3) were assembled by spontaneous association of resorcinarenes **67** and pyrogallolarenes **68** when proper guests are present (Figure **20a**). The latter is also a precursor for bowl-shaped cavitands, obtained by covalently connecting hydroxyl groups on adjacent aromatic rings. Main difference between the two is that pyrogallolarenes associate in both anhydrous and wet

solvents, where eight water molecules, at each corner of the cage, are essential to facilitate the construction of resorcinarene capsule.[100,101] In another example, octameric hydrogen bonded capsule comprising cavity of 2300 Å^3 volume were obtained by employing chiral-assisted aggregation (Figure **20b**). Using enantiopure (+)-(P)-isatin-**69** building block instead of racemate was envisioned to prevent the formation of ill-defined aggregates and polymeric species. Additionally, the large tetrahexadecylammonium cation was encapsulated successfully due to favorable cationic-π interactions inside the cavity.[102]

67a: R_1 = H, R = CH_3;
67b: R_1 = H, R = C_4H_9; **68b**: R_1 = H, R = C_4H_9;
67c: R_1 = H, R = $C_{11}H_{23}$; **68c**: R_1 = H, R = $C_{11}H_{23}$;

(+)-(P)-isatin-**69**

Figure 20. a) Structure of resorcin[4]arenes **67**, pyrogallol[4]arenes **68** and their hexameric form; b) octameric capsule comprising isatin **69** building block.

Recently, the largest hexameric molecular cage was reported with corresponding cavity volume of 2800 Å^3 based on resorcinar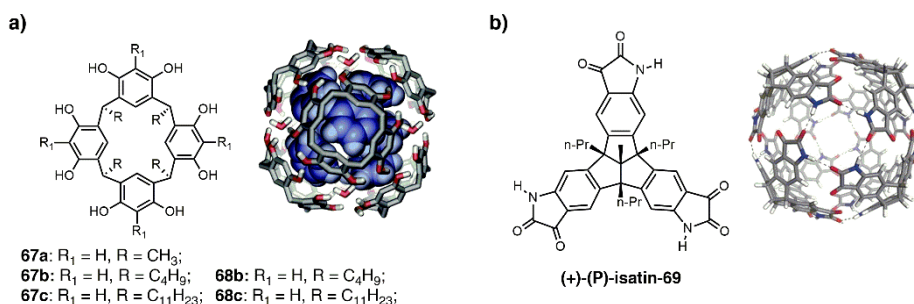ene building block. Furthermore, encapsulation of C_{60} in $CDCl_3$ and C_{70} in toluene-d_8 were confirmed by a downfield shift of the resonances corresponding to encapsulated fullerene in ^{13}C NMR. However, the size of cage strongly depends on the concentration. At higher concentration (5 mM in $CDCl_3$) all major signals belong to a single diffusion coefficient D = $2.39 \cdot 10^{-10}$ m^2s^{-1}, whereas by lowering concentration a new set of peaks appears corresponding to higher diffusion coefficient (D = $3.53 \cdot 10^{-10}$ m^2s^{-1}), suggesting the presence of a smaller monomeric species.[103]

1.3.3 Hierarchical self-assembly of encoded synthons into organic nanotubes

Self-assembly has enabled the bottom-up approach for engineering the 1D and 2D versatile architectures, such as spontaneously produced organic nanotubes. Compared to capsules and cages, nanotubes comprising open ends enable their potential application in size- and shape-discriminating encapsulation, transport, separation or flowthrough catalysis, where guests can move freely in and out of the cavity. In principle, several feasible approaches to design open-ended tubular structures have been reported,

including helical coiling of linear precursors[104,105], assembly of rod-like monomers into barrels[106], orthogonal stacking of macrocycles[107-113] and hierarchical formation of supramolecular aggregates[114-119]. For instance, previously described mesoscopic nanorods consisting of rosette macrocycles falls into the latter category, although it hardly offers any control of cavity size and functionality, thereby only exceedingly small guest molecules can be accommodated (Figure **14**-**16**).
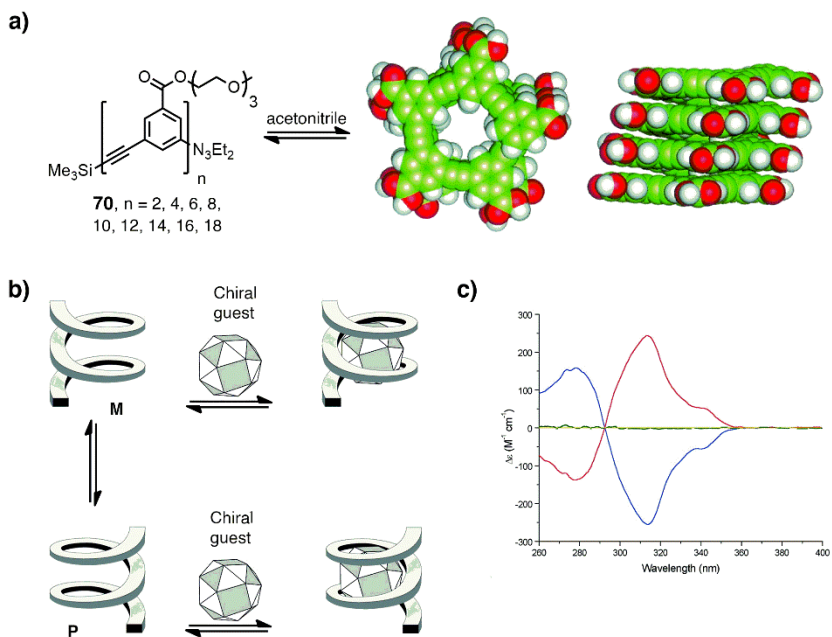
Figure **21**. a) Phenylacetylene oligomers folding into helical polymers; b) encapsulation of chiral guest by enantiomeric M and P helical conformations; c) CD spectrum of encapsulated (+)-α-pinene (red) and (-)-α-pinene (blue), free (-)-α-pinene (yellow), oligomer (green). Adapted from ref. 104, 105 with permission from AAAS, 1997 and American Chemical Society, 2000, respectively.

Analogous to α-helix, where amino acids are encoded to arrange in helical secondary structure of protein, synthetic polypeptide derivatives with tendencies to fold into helical conformations have been reported. Linear oligophenylacetylenes are guided into helical arrangement by local constraints enforced upon rigid backbone in concert with further stabilization of the secondary structure by intramolecular hydrogen bonds, hydrophobic and van der Waals interactions (Figure **21a**). The helix formation for foldamers **70** (n > 8) in acetonitrile was inferred on the basis of ¹H NMR

spectrum. Upfield shifts in the aromatic region are in accord with solvophobically driven intramolecular stacking of phenyl rings which maximizes collateral polar groups interaction with solvent while hindering hydrocarbon backbone.[104] Encapsulation of various chiral monoterpenes within well-defined inner hollow of dodecamer **70** (n=12) was assessed by circular dichroism studies. Uncomplexed dynamic racemate of enantiomeric M and P helical conformations results in a pair of diastereomers upon trapping a chiral guest molecule (Figure **21b**). (+)-α-pinene and (-)-α-pinene induce CD signals with same intensity but in opposite direction (Figure **21c**).[105]

Altering the backbone of β-peptides can exert rational control over secondary structure resulting in helical nanotubes. For instance, manipulating torsional preference of the backbone composed of cyclohexyl or cyclopentyl amino acids facilitate stable helical assembly by adopting 14- and 12-membered ring conformations, respectively (Figure **22**). Trans-2-aminocyclohexanecarboxylic acid derivatives **71a** and **71b** have high propensity to coil into 14-helix form and trans-2-aminocyclopentanecarboxylic acid derivatives **72a** and **72b** into 12-helical shape in solid state, which is the most stable among helices bearing three-, four-, five- and six-membered cycloalkyl rings according to molecular mechanics studies. Stability of the conformers was further supported by amide proton exchange experiments in methanol. Suppressed NH/ND exchange rate indicated the presence of a stable helical conformation of hexamer **71a** held together by strong intramolecular hydrogen bonds.[108–110]
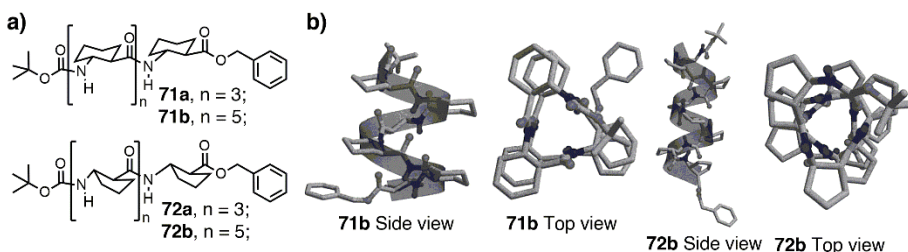
Figure **22**. Folding of linear monomers into helical nanotubes. Adapted from ref. 109 with permission from American Chemical Society, 1998.

Even number of alternating D- and L-amino acids form flat cyclic peptides which can further stack in an antiparallel β-sheet manner to obtain hollow tubular assemblies with inner cavity of 7-8 Å. When glutamic acid is protonated in an eight-residue cycle **73** -(D-Ala-Glu-D-Ala-Gln)$_2$-, it reduces

charge repulsion between macrocycles and carbonyl units form intermolecular hydrogen bonds with amide moieties from the opposite macrocycles, while all the carboxylate groups protrude outwards in the same plane as peptide rings to prevent steric interactions between lateral chains (Figure **23a,b**). Functional side chains of amino acids can be modified to equip structure with necessary solubility or site-specific functionality. Electron diffraction patterns exhibit 4.73 Å axial periodicity which completely coincide with packing of β-sheets.[107]
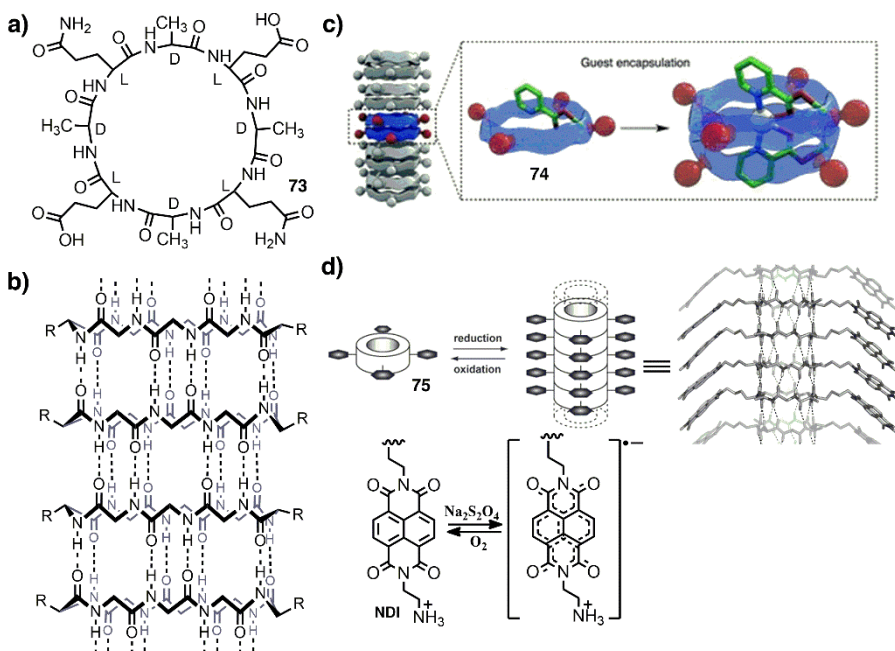
Figure **23**. a) Structure of D,L-alternating polypeptide **73**; b) self-assembled tubular structure stacked in an antiparallel β-sheet pattern; c) guest encapsulation of polypeptide comprising pyridine group inside its cavity. Reproduced from ref. 111 with permission from the Royal Society of Chemistry, 2016; d) redox-controlled nanotube aggregation and the model of self-assembled tubular structure with stacking of NDI side groups. Reproduced from ref. 113 with permission from Wiley-VCH Verlag GmbH & Co, 2005.

Later on, dimeric structures of alternating α,γ-cyclopeptides **74** comprising 3-aminocycloalkanecarboxylic acid moieties were designed, which could facilitate functionalization of internal cavity by attaching various entities through simple ester linkage and allow encapsulation of various guests like metal ions, alcohols and dicarboxylic acids (Figure **23c**). Incorporation of one pyridine unit per one peptide macrocycle via ester linker led to

successful complexation of silver ion and oxalic acid inside the cavity of dimeric structure.[111] The nanotube structure was probed via fluorescence measurements of intermolecular charge transfer occurring between naphthalene diimide (NDI) incorporated onto parallel cyclopeptides.[112] In fact, intermolecular π-π interactions between NDI entities promote tubular stacking of the macrocycles (Figure **23d**). The reversible nature of such aggregates can be manipulated in aqueous environment by oxidation/reduction utilizing chemical and electrochemical methods. Formation of radical anion increases NDI π-stacking behavior and reduces the overall charge on cyclic peptide, whilst increasing length of aggregate.[113]

This concept was further developed by preparation of D,L-alternating eight-residue building block comprising hydrophobic -Leu-Trp-Leu- motif linked to hydrophilic (-Glu-His-)$_2$Gln amino acid residues. Well-thought-out design of cyclopeptide with necessary information encoded into the amino acids scaffold led to hierarchical self-assembly of the dynamic 2D nanosheets in solution (Figure **24**). Macrocycles are held together in an anti-parallel β-sheet manner via eight hydrogen bonds between the adjacent rings. The hydrophobic nature of Leu-Trp-Leu motifs forces the hollow nanotubes to aggregate further into nanotube bilayers by alleviating unfavorable interactions in aqueous media. The cooperativity effect of leucine zippers alongside π-π stacking of tryptophan indoles provides additional stability for this 2D architecture.[114]
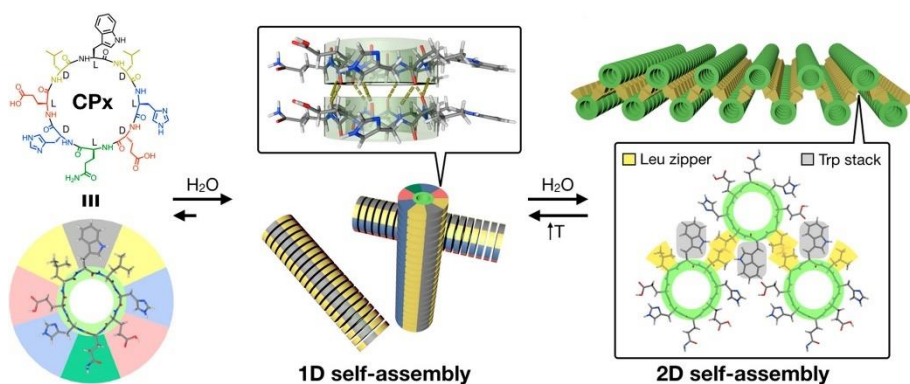

Figure **24.** Multi-step self-assembly of cyclic peptides with increasing hierarchy. Reproduced from ref. 114 with permission from American Chemical Society, 2022.

Recently, a promising approach to self-assembly of supramolecular nanotubes from discrete components utilizing noncovalent interactions has

been reported. Modification of initial building block at early stages facilitates access to modulation of inner cavity's size and functionality as well as control over precise structure and dimensions of the tubular aggregate. For instance, amino acids interlinked with NDI moiety tends to adopt syn geometry in respect to NDI scaffold. The obtained monomer **76** can serve as a smallest building block and undergo isodesmic polymerization into helical nanotubes (Figure **25**). Supramolecular structure is held together solely by intermolecular hydrogen bonds between carboxylic acids in chloroform while the walls of nanotube encompassing NDI are reinforced by two weak CH···O hydrogen bond interactions. In aprotic environment π-π stacking is negligible due to electron deficient properties of NDI backbone and steric hindrance associated with side chains of amino acids. The chirality of nanotube is determined by stereochemistry of amino acids and ensues uniform assembly into M-helical aggregates in solid state and aprotic solvents like chloroform.[115,116] Helical nanotube comprises inner cavity with a 12.4 Å diameter which is well-fitting for C_{60} fullerene. An apparent color change from pale yellow to dark orange of solution containing monomer and C_{60} clearly indicates a successful encapsulation in chloroform.[117]
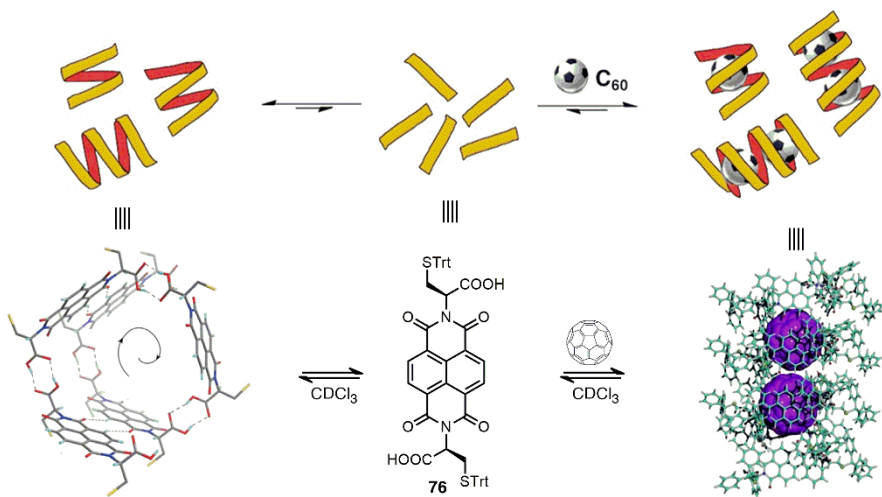
Figure **25**. NDI monomer **76** helical self-assembly into hollow nanotubes and subsequential C_{60} encapsulation. Reproduced from ref. 116 and 117 with permission from American Chemical Society, 2022 and John Wiley and Sons, 2007.

Subsequently, high chelate cooperativity displaying tetrameric macrocycle was obtained from GC Watson-Crick hydrogen bonding through 90° angle. Tetramer participated in collateral nanotube growth in orthogonal direction

guided by the hydrogen bonding between the peripheral amide units on the adjacent macrocycles and π-π interactions (Figure **26**). The well-preorganized monomer consists of complementary guanine and cytosine nucleobases connected through a rigid π-conjugated linker and equipped with alkyl chains protruding outwards to increase its solubility in nonpolar solvents. Temperature-dependent studies provided detailed information upon process of polymerization. CD changes within 329 – 268K temperature range could be fitted to a successive nucleation-elongation polymerization model as was anticipated by the authors.[118]
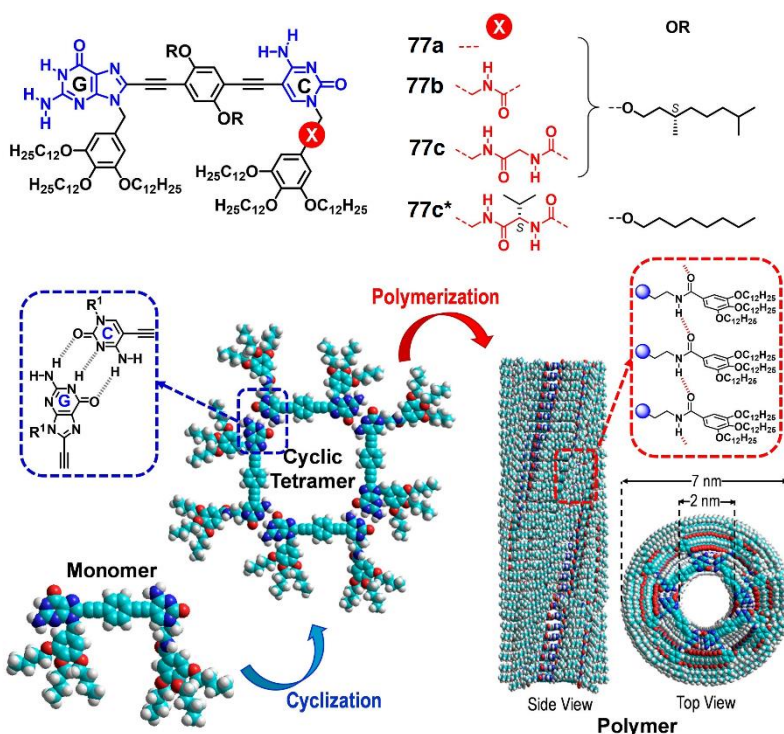
Figure **26.** Structure of building blocks and their two-step hierarchical self-assembly into tubular aggregates. Reproduced from ref. 119 with permission from John Wiley and Sons, 2021.

Preparation of three monomers **77a, 77b, 77c** featuring 0, 1 and 2 peripheral amides demonstrated their vital role in the polymerization mechanism and for the stability of the tubular structure. Expectedly, **77a** did not participate in macrocycle aggregation due to lack of an intermolecular hydrogen bonding site, whereas **77b** exhibited cooperative polymerization and **77c** showed isodesmic polymerization. Differences between polymerization mechanism of **77b** and **77c** were not expected to be observed, but the authors

postulated it might be due to competition among intra- and intermolecular hydrogen bonding arising from different pendent groups.[119]

Another example of stimuli-responsive tubular aggregation with dynamic control over the stages of hierarchical assembly was reported by Yagai *et al.* The monomer **78** comprising two alkoxyazobenzene entities linked with 3,4,5-(tridodecyloxy)-xylylene spacer tends to self-dimerize into cone-shaped building block via π-π stacking in nonpolar methylcyclohexane solution at 20 °C (Figure **27**). Azobenzene functionalization with amide groups prevents antiparallel stacking and promotes assembly into toroidal shape by creating hydrogen bonding sites along the inner circle of newly obtained structure. Upon cooling down solution to 0°C, large π-conjugated surface acquired on the top and bottom planes of the toroid ensued further orthogonal stacking of the rings into tubular rod-shaped architecture.
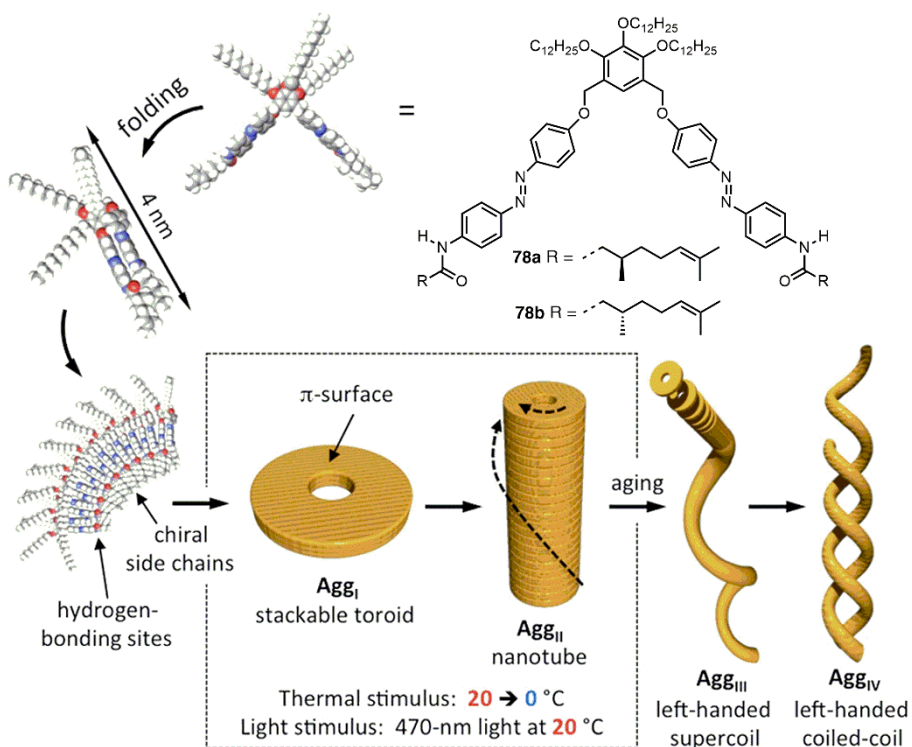
Figure **27**. Hierarchical self-assembly of monomer **78** into nanotoroids followed by further aggregation to hollow nanotubes. Reproduced from ref. 120 with permission from American Chemical Society, 2022.

Solution aging resulted in elongated left-handed supercoils which were intertwined and produced left-handed double helices. Reversible trans-cis isomerization of azobenzene can be manipulated by an external light stimulus; hence irradiation with 365nm UV light promotes trans to cis isomerization and disrupts assembly into smaller components. Visible light induced cis-trans isomerization results in the recovery of initial supramolecular aggregate.[120]

2. Discrete supramolecular aggregates based on C_2-symmetric bicyclo[3.3.1]nonane scaffold

An attractive concept for cyclic self-assembly utilizing enantiomerically pure C_2-symmetric bicyclo[3.3.1]nonane framework encompassing non-natural nucleobase isocytosine (ICyt) **79** was introduced by Orentas *et al.* (Figure **28a**). This approach is based on ability of ICyt to alternate between N^1-H and N^3-H tautomeric forms, thus offering DDA and AAD hydrogen bonding patterns on the edges of same monomer and resulting in self-complementary monomer of C_1-symmetry. Such homo-tautoleptic aggregation facilitate the covalent synthesis of chiral building blocks since only one type of monomer is needed. Furthermore, extensive preorganization of rigid scaffold with ca. 90° angle between the hydrogen bonding arrays results in exclusive tetrameric cyclization **79₄** in nonpolar organic solvents.
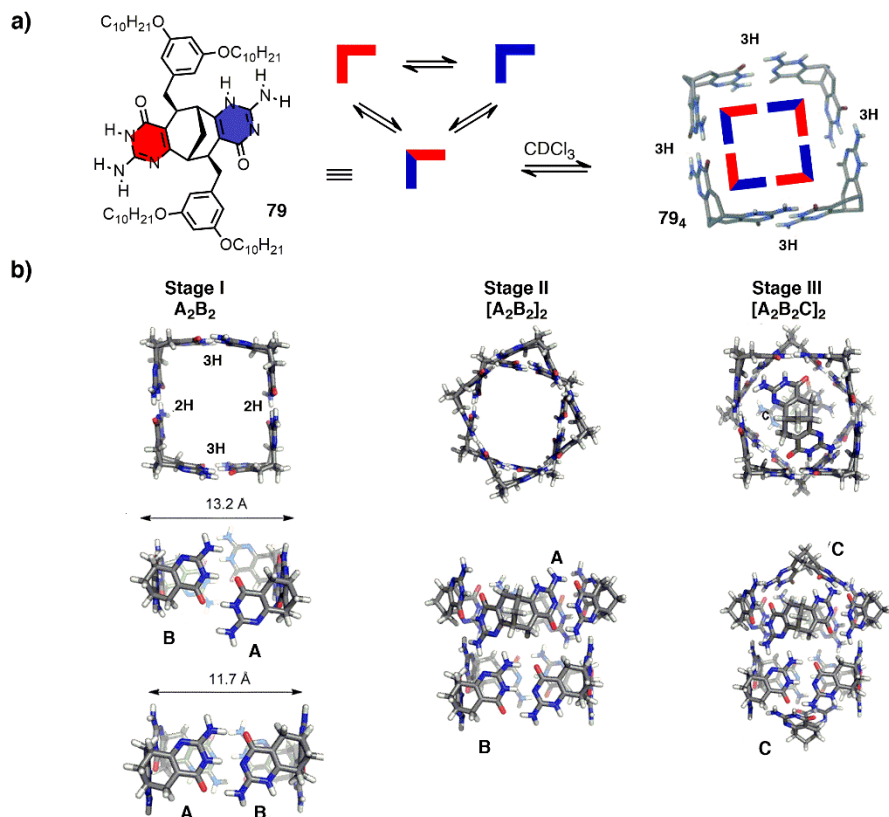

Figure 28. a) Homo-tautoleptic aggregation of bicyclo[3.3.1]nonane monomer **79** possesing two isocytosine units; b) assembly of decameric capsule in three distinct stages. Adapted from ref. 121, 122 with permission from John Wiley and Sons, 2011 and American Chemical Society, 2015.

Branched 3,5-didecyloxybenzyl groups were incorporated in the scaffold to improve solubility in organic solvents. Topology and homoleptic aggregation of belt-shaped tetramer 79_4 with high-fidelity were unambiguously confirmed by 2D NMR, GPC, DOSY experiments in CDCl$_3$, whereas hydrodynamic radius R$_H$ = 13.2 Å obtained from diffusion coefficient (D = 2.71·10^{-10} m^{2}s^{-1}) using Stokes-Einstein equation was consistent with theoretical value obtained from molecular dynamics (MD) simulations.[121] Subsequently, the obtained cyclic tetramer **A$_2$B$_2$** was able to aggregate even further to produce unique decameric capsule **[A$_2$B$_2$C]$_2$** in nonpolar carbon disulfide by utilizing additional bifurcated hydrogen bonding sites along the rim (Figure **28b**). It was evident that supramolecular structure consists of three different types of monomer with two distinct aggregation modes, 2H-bonding between two N^3-H keto forms and 3H-bonding between N^1-H and N^3-H keto forms. Thus, the final structure consists of two tetrameric aggregates stacked on top of each other comprising alternating 3H- and 2H-bonding of two ICyt tautomers and the obtained octamer **[A$_2$B$_2$]$_2$** is subsequently capped with two monomer molecules with embedded N^3-H keto tautomers on both sides of the backbone. In addition, the resulting capsule can participate in host-guest complexation by entrapping C$_{60}$ fullerene molecule inside its cylindrical cavity.[122]

Later on, the hydrogen bonding array was extended by incorporating ureidopyrimidinone (Upy) module into chiral bicyclic structure, which would enable structure and function modulation (Figure **29a**). Unlike the previous supramolecular structures, the enantiomerically pure supramolecular tetrameric cycle **80$_4$** possessing large cavity, was assembled using self-complementary quadruple hydrogen-bonding DDAA Upy motifs in chloroform. However, in other less polar solvents like, toluene and benzene, another type of pentameric aggregate **80$_5$** emerged, possibly because less polar solvents can maintain larger deviations from 90° hydrogen-bonding angle allowing larger undesirable structures (Figure **29b**). Nonetheless, fullerenes C$_{60}$ and C$_{70}$ were efficiently encapsulated by tetramers **80a$_4$** and **80b$_4$**, thus shifting equilibrium towards exclusive formation of tetrameric inclusion complex **C$_{60}$@80$_4$** and removing parasitic pentamers in toluene. The 1:1 host-guest stoichiometry between **80a$_4$** and both fullerenes was reaffirmed by molar ratio method utilizing ^{1}H NMR titration. The higher stability of complex **C$_{70}$@80a$_4$** was corroborated by ^{1}H NMR measurements of a 1:1 mixture of both fullerenes, showing the formation of **C$_{60}$@80a$_4$** and **C$_{70}$@80a$_4$** in 1:2 ratio. Higher stability of

complex with C_{70} was observed arguably due to larger π-surface of C_{70} available for the interaction with isocytosine walls.[123]
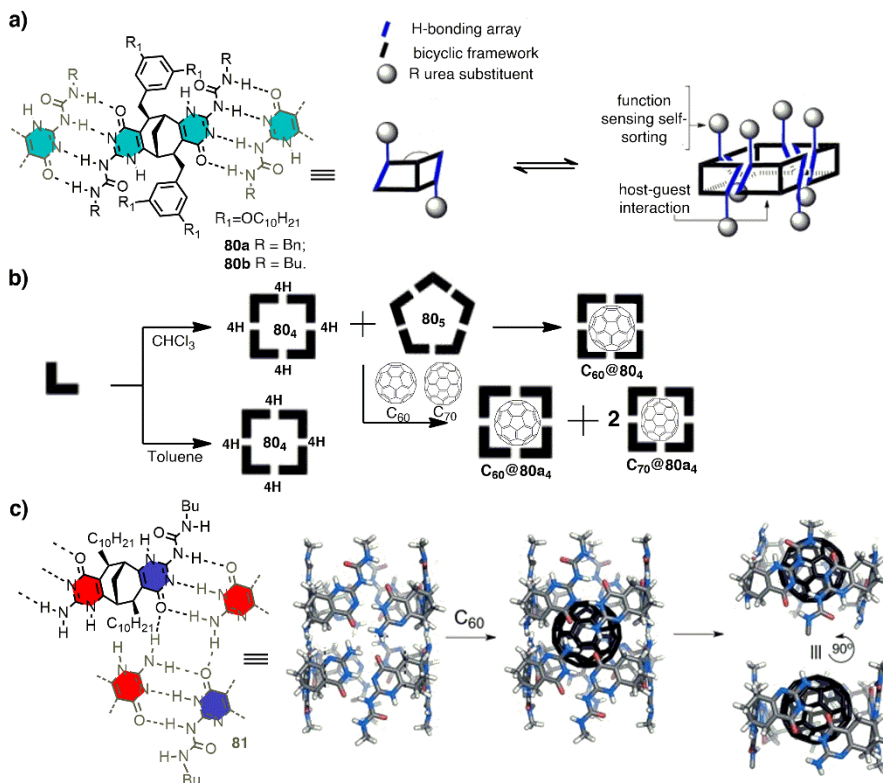
Figure 29. a) Quadruple hydrogen-bonded belt-shaped tetrameric aggregate 80_4 with an inner cavity; b) solvent and guest controlled self-sorting between tetrameric and pentameric forms; c) Rearrangement of octameric capsule into tetrameric cycles due to C_{60} encapsulation. Adapted from ref. 123, 124 with permission from American Chemical Society, 2013 and John Wiley and Sons, 2015.

In the following studies, synthesis of unsymmetrical building block **81** containing Upy and ICyt on both sides was developed (Figure **29c**). This approach allowed the formation of octameric aggregate 81_8 with large cavity from eight identical low molecular weight components. The assembly between two tetrameric belts occurs because one proton of ICyt participates in cyclic aggregation, while the bifurcated hydrogen maintains edge-to-edge connection of two tetrameric cycles. Hypothetically, the length and open-end topology of the cavity could allow for encapsulation of either two C_{60} molecules or one C_{120} molecule. However, the substantial simplification of

^{1}H NMR spectrum in accordance with significant shift from 5.6 ppm to 11.0 ppm of NH proton corresponding to butyl urea group clearly indicates the dismantling of the octameric structure into cyclic tetramer 81_4 with entrapped C_{60} within the cavity. Additionally, bulky solubilizing substituents like 3,5-bis-(decyloxy)benzyl hinders formation of octameric aggregate due to steric repulsion occurring between the collateral chains of parallel monomers.[124] Hence, manipulation of the size of substituents or its spatial arrangement can provide the means to control successive stacking of the cyclic tetramers into hierarchical tubular polymers (Figure **30a,b**).
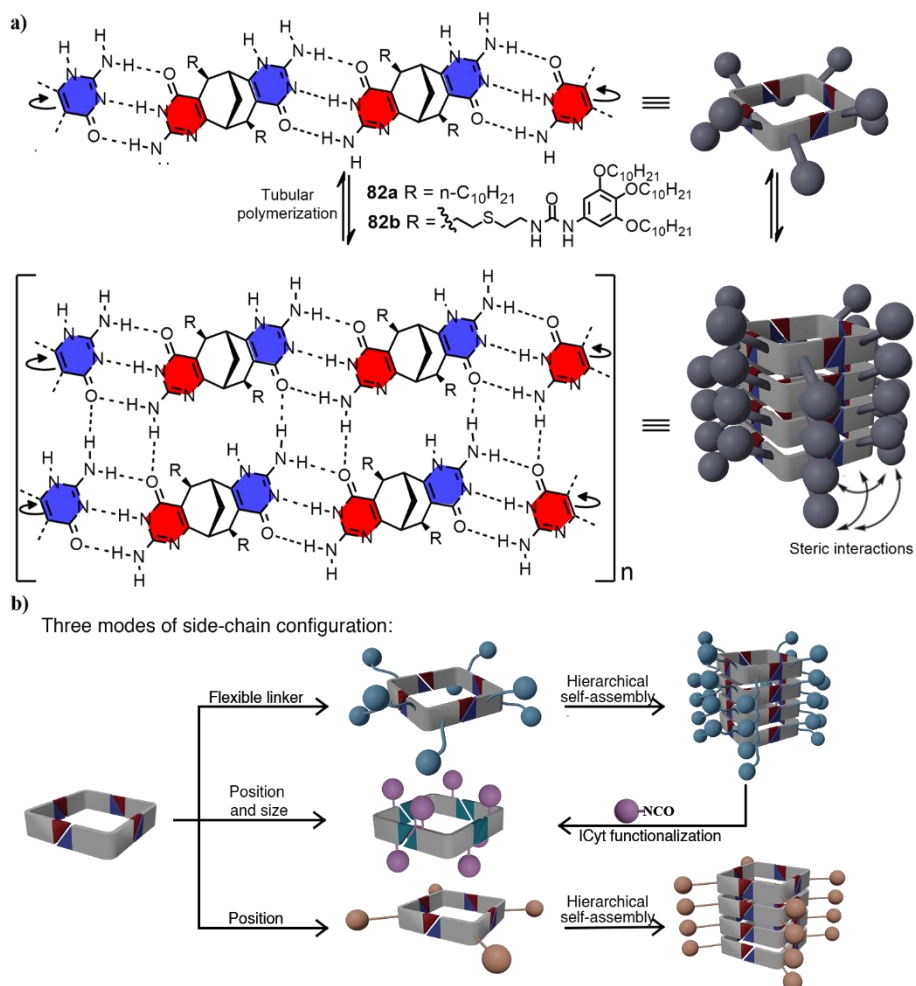

Figure 30. a) Orthogonal aggregation of building block **82** comprising isocytosine. Adapted from ref. 125 with permission from John Wiley and sons, 2018 ; b) three possible strategies for side-chain incorporation.

An orthogonal tautoleptic aggregation was achieved using complementary DDA-AAD hydrogen-bonding motifs between tautomeric forms of isocytosine entity and reducing the size of the solubilizing groups to linear decyl chains or, alternatively, by placing substituents into radial position of the bicyclic monomer. Another approach was to incorporate flexible linker between the bicyclo[3.3.1.]nonane scaffold and bulky substituent, which provides additional space for more favorable spatial positioning. Orthogonal propagation was corroborated from the extremely broad signals in ^{1}H NMR spectrum in chloroform and toluene which was consistent with high viscosity of the solution. The evaluation of particle size by dynamic light scattering (DLS) indicated distribution of aggregates **82a** and **82b** with hydrodynamic radius of 250 nm and 50 nm, respectively.[125]

The latter strategy will be further elaborated in this chapter by providing the means for efficient incorporation of substituents of various size with different functional properties via flexible linker to facilitate construction of novel smart materials.

2.1 Design and synthesis of self-complementary synthons comprising flexible linkers

In this work the corresponding bicyclo[3.3.1]nonane derivatives have been prepared on large scale based on previously developed and optimized synthetic route by Orentas group.[126] This particular scaffold has attracted attention due its ability to adopt V-shape when two heteroaromatic rings are fused on opposing termini of backbone. Even though bicyclo[3.3.1]nonane can exist in chair-chair, boat-chair, boat-boat conformations, cyclohexane rings fused with aromatic rings are planarized and conformationally restricted placing aromatic rings at 90° angle. Furthermore, utilization of the enantiomerically pure synthons over the racemates is a necessity to prevent unwanted linear assemblies over cyclic aggregates.

The synthesis was carried out first by obtaining Meerwein ester **83** in two steps by a condensation of formaldehyde with dimethylmalonate in 67 % yield. Subsequent decarboxylation while performing acidic hydrolysis resulted in 54 % yield of bicyclo[3.3.1]nonane-2,6-dione **85**. Enantiomerically pure **(+)-85** was isolated in 48 % yield from racemic mixture by kinetic resolution using Baker's yeast for sweet dough (Figure **31**).[127]
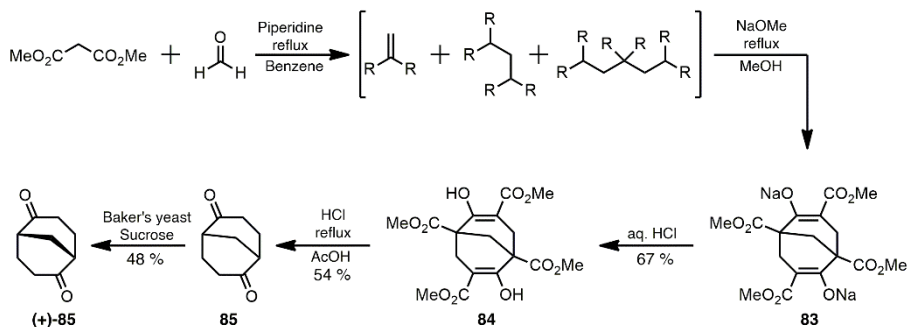
Figure **31**. Synthesis of enantiomerically pure diketone (+)-**85**.

The acylation of diketone **(+)-85** was carried out in 50 % yield by treating with dimethyl carbonate and NaH base in anhydrous DMF (Figure **32**). The isolated bis-β-ketoester **(+)-86** was used in selenation reaction with phenylselenyl chloride followed by oxidative elimination with hydrogen peroxide. This step had to be repeated two times in order to obtain unsaturated bis-β-ketoester **(+)-87** in 52 %, otherwise even when using an excess of PhSeCl only mono-selenated product was obtained.
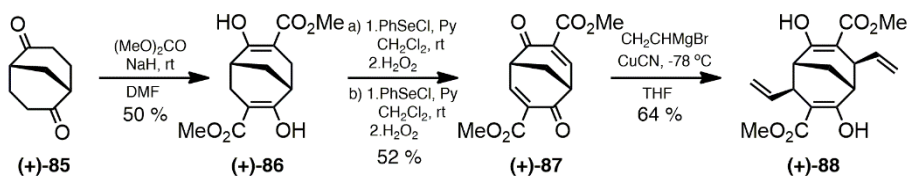
Figure **32**. Synthesis of enantiomerically pure synthon required for tiol-ene click reaction.

At this point, various solubilizing groups were incorporated into bicyclo[3.3.1]nonane backbone to ensure the solubility of the building blocks needed for further supramolecular assembly in nonpolar media. It was accomplished by performing Michael 1,4-addition of organocopper reagents to unsaturated **(+)-87**. This approach, however, necessitate the preparation of organometallic reagent for each separate solubilizing chain, which significantly complicates chemical diversification of the monomers. For this reason, a universal "anchor" was envisioned to which freely modifiable side chains could be connected. Moreover, the variety of substituents was limited due to unfavorable steric repulsion occurring between sidechains. Placing bulky groups too close to bicyclo[3.3.1] backbone prevents the cyclic tetramer from further aggregation to supramolecular nanotubes.[121,124,125] Thus, we envisioned that steric overcrowding could be prevented by introducing a flexible linker between backbone and bulky substituent. The

introduction of nucleophilic anchor would provide the means to incorporate various chromophores into the system without the tedious organometallic chemistry. Hence, the development of novel and efficient synthetic pathway was based on thiol-ene click chemistry between nonactivated double bond and thiol. The divinyl diketone (+)-88 was obtained in 64 % yield by performing Michael 1,4-addition reaction of vinyl cuprate at –78 °C. It is known from our previous work in the group, that this type of addition occurs only from the bridge side of the backbone providing exclusively an exo,exo-disubstituted diastereomer.

The versatility of a thiol-ene reaction as a synthetic tool has been previously demonstrated in material chemistry. Its application ranges from usage by polymer chemists for synthesis of dendrimers and crosslinked networks to implementation in lithography[128], and even found its way as a chemical ligation tool for peptides[129] and oligosaccharides[130]. The great potential of radical thiol-ene coupling was spotted because it can be initiated either thermally or photochemically with a catalytical amount of photocatalyst under mild conditions. Reaction exerts high tolerance for a wide range of functional groups and does not require expensive toxic metal-based catalysts. Thus, thioacetic acid[131] was selected for the photoinitiated radical-based addition to divinyl diketone (+)-88 in order to obtain HS-precursor bearing a nucleophilic site. At first, reaction was carried out by irradiating reaction mixture with a UV lamp (254 nm) and using quartz cuvette as a reaction vessel. Divinyl diketone was treated with 3 equivalents of thioacetic acid in the presence of 20 mol% of benzophenone as a photoinitiator. However, thioacetate 89 was obtained in low 36 % yield. Prolonging reaction time or increasing excess of thioacetic acid still resulted in low yields. Surprisingly, irradiation of (+)-88 with household UVA lamp (365 nm, 4 x 9W) in standard borosilicate glassware under inert atmosphere with 3 equivalents of thioacetic acid in toluene at room temperature produced targeted product 89 in a presence of 10 mol% of azobisisobutyronitrile (AIBN) as a photoinitiator (Figure 33). The reaction displayed high reproducibility and excellent 90 – 99 % yields.
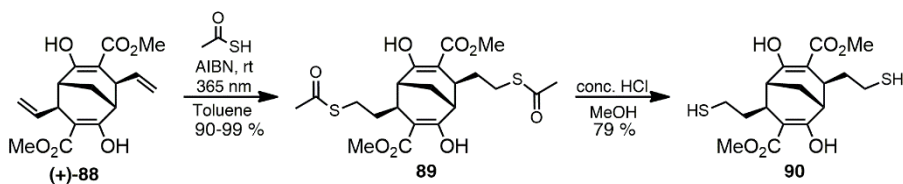

Figure 33. Synthesis of nucleophilic thiolated precursor 90.

Thiol-ene coupling proceeds via radical mechanism, where AIBN undergoes homolytic cleavage generating two 2-cyanoprop-2-yl radicals which initiate the reaction by abstracting hydrogen atom from thioacetic acid (Figure **34**). Activated thioacetic acid S-radical adds to alkene **(+)-88** in anti-Markovnikov regioselective fashion and proceeds to initiate reaction further by removing hydrogen atom from another molecule of thioacetic acid. Subsequently, the hydrolysis of the intermediate thioacetate **89** produced targeted thiol. The hydrolysis can be accomplished either under basic conditions with K_2CO_3 or acidic conditions with concentrated HCl in MeOH. Performing the hydrolysis under acidic conditions, however, led to a much greater yield (79 %) compared to basic conditions (57 %).
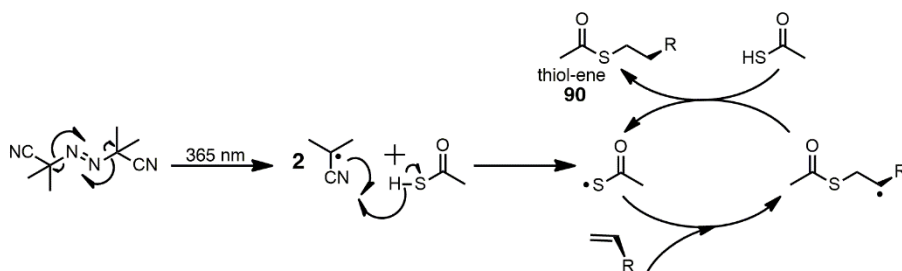

Figure **34.** Mechanism of radical thiol-ene coupling.

Newly synthesized thiolated **90** facilitated the incorporation of various chromophores by simple nucleophilic substitution reaction utilizing the corresponding bromides to obtain **91a-e** (Figure **35**). The substituents were attached using mild conditions, i.e., treating **90** with 2.2 equiv. bromide derivative and 2.2 equiv. K_2CO_3 in DMF at 80 °C for 1-3 hours. The groups of different size and shapes ranging from linear tetraethylene glycol- to branched 3,5-bis(decyloxy)benzyl- were successfully engaged in the alkylation reaction. The above groups of varying size were chosen for further evaluation of their impact on hierarchical assembly of tetrameric cycles into greater aggregates.

The synthesis of 3,5-bis(decyloxy)benzyl bromide[132], bis(MeO-PEG4)benzyl bromide[133] and 13-bromo-2,5,8,11-tetraoxatridecane[134] have been previously reported in literature. Pyrene derivatives **92** and **93** were synthesized starting from 1-pyrenecarboxaldehyde. First, it was reduced to the corresponding alcohol in 82 % yield with NaBH₄ followed by addition of respective linker via nucleophilic substitution to afford **92** and **93** in 77 % and 38 % yields, respectively (Figure **36**).
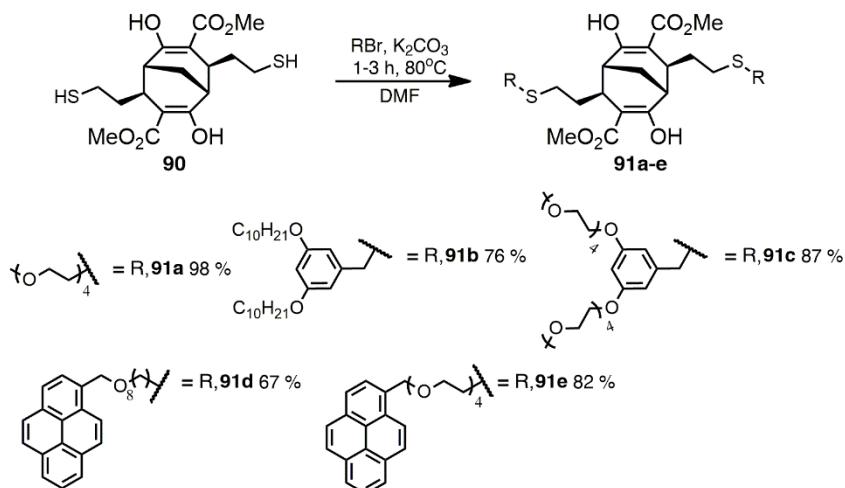
Figure **35.** Nucleophilic substitution reactions of **90a-e** bearing thiol groups.
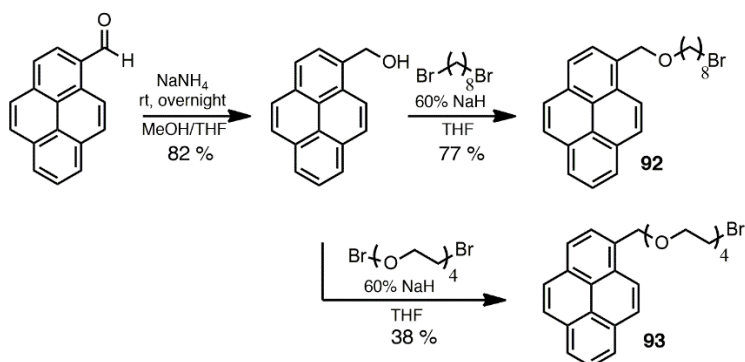
Figure **36**. Synthesis of pyrene derivatives **92** and **93** comprising linear alkyl and tetraethylene glycol linkers.

Subsequently, self-complementary hydrogen bonding DDA-AAD sites were embedded into enantiomerically pure bicyclo[3.3.1]nonane backbone at each end through condensation of bis-β-ketoester **91a-e** with excess of guanidinium carbonate or guanidinium chloride and KOtBu in MeOH at 100 °C (Figure **37**). The isocytosine moieties in **94a-e** act as self-complementary hydrogen bonding arrays due to their ability to alternate between N^1-H and N^3-H tautomeric forms. The resulting tetrameric cyclic aggregate can undergo further orthogonal stacking through bifurcated hydrogens along both rims (Figure **38**). The formation of tubular polymers was apparent from extremely broad signals in ^{1}H NMR spectra in nonpolar CDCl$_3$ and high viscosity of solution. Further structural characterization using NMR was thus not possible due to the absence of well-resolved resonances.
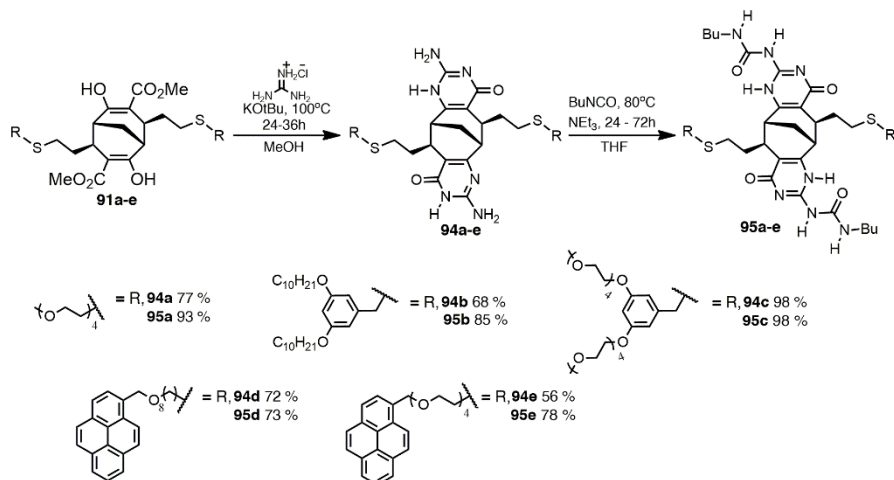
Figure **37**. Synthesis of enantiomerically pure C_2-symmetric synthon with embedded self-complementary hydrogen bonded sites.

The orthogonal stacking of ICyt derivatives **94a-e** were mitigated by converting isocytosines into Upy derivatives **95a-e** as a result of conversion of -NH$_2$ group into the corresponding urea moiety. Resulting C_2-symmetric Upy building blocks were obtained in 73 – 97 % yields by treating corresponding ICyt with an excess of n-butyl isocyanate in presence of TEA in THF at 80 °C for 24 – 72 hours. The self-complementary Upy moieties possess quadruple DDAA hydrogen bonding sites which ensues association into tetrameric cycles via self-dimerization. Therefore, these monomers were used in the following aggregation studies in solution.
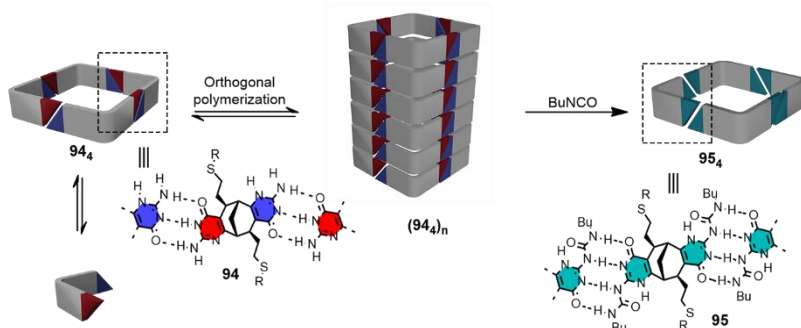
Figure **38**. Conversion between supramolecular tubular and tetrameric architectures.

53

2.2 Self-assembly and host-guest studies of tetrameric cavitands

To fully characterize obtained supramolecular tetrameric aggregate, NMR was used as a primary tool. The high symmetry of ^{1}H NMR spectrum indicated the formation of a well-defined cyclic aggregate via self-complementary quadruple hydrogen bonding motifs (Figure **39a**). Dimeric or polymeric association was dismissed straightaway due to geometric preorganization of the bicyclo[3.3.1]nonane scaffold. Tetrameric cavitand of monomer **95a** was investigated as a representative example to provide insight into aggregation mode of all monomers **95a-e**. Single set of downfield shifted NHs resonances at 12.93, 11.89, 9.64 ppm confirmed intermolecular hydrogen bonding interactions between urea moieties in chloroform (Figure **39b**).
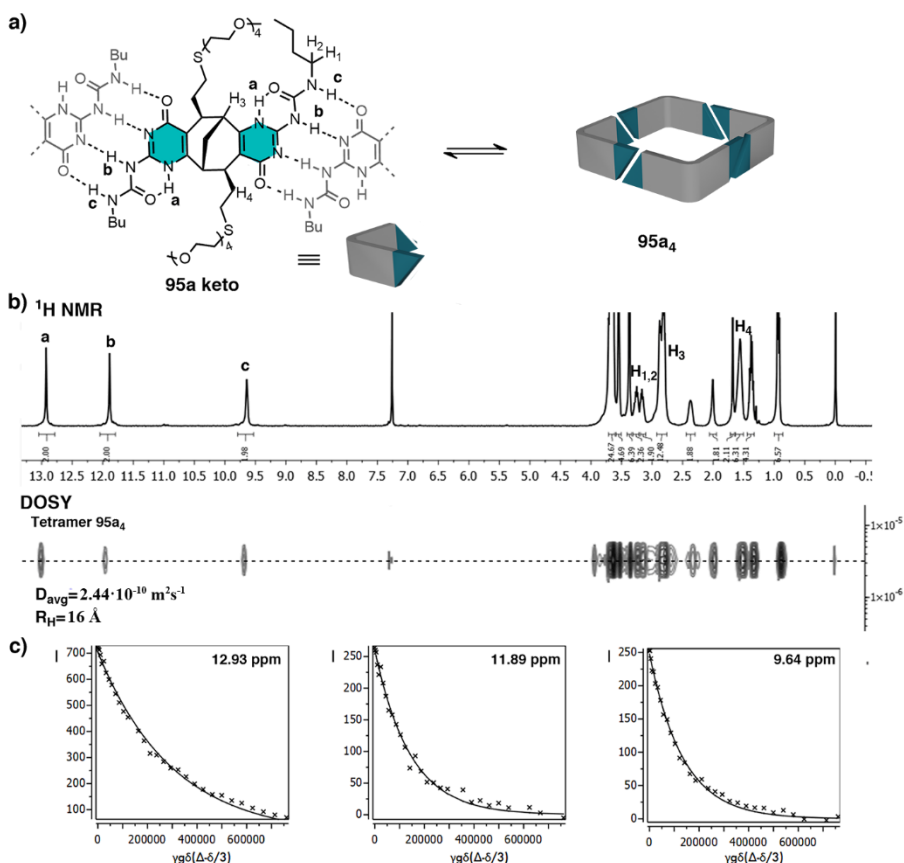
Figure **39**. a) Self-assembly of tetrameric aggregate; b) ^{1}H NMR spectrum of 10mM tetramer **95a₄** in CDCl$_3$ with DOSY trace stacked at the bottom; c) fitting of signal decay to Stejskal−Tanner equation for each corresponding NH.

In addition, to confirm the existence of a tetrameric aggregate as a single species in solution, DOSY experiments were performed on a 10 mM solution in CDCl$_3$ at 296 K. All proton resonances correspond to a single diffusion coefficient D = 2.44·10^{-10} m^{2}s^{-1}, which converts into the hydrodynamic radius R$_H$ = 16 Å using Stokes – Einstein relation (D = k$_b$T/6πηR$_H$). The results obtained are in accordance to previously reported values for structurally related tetrameric aggregates.[121,123] All three NH resonances at 12.93, 11.89 and 9.64 ppm were analyzed to estimate the average diffusion coefficient (Figure **39c**). Based on literature, Upy motifs can potentially self-aggregate by keto or enol tautomers via DDAA-AADD or DADA-ADAD hydrogen-bonding modes, respectively (Figure **40a**).
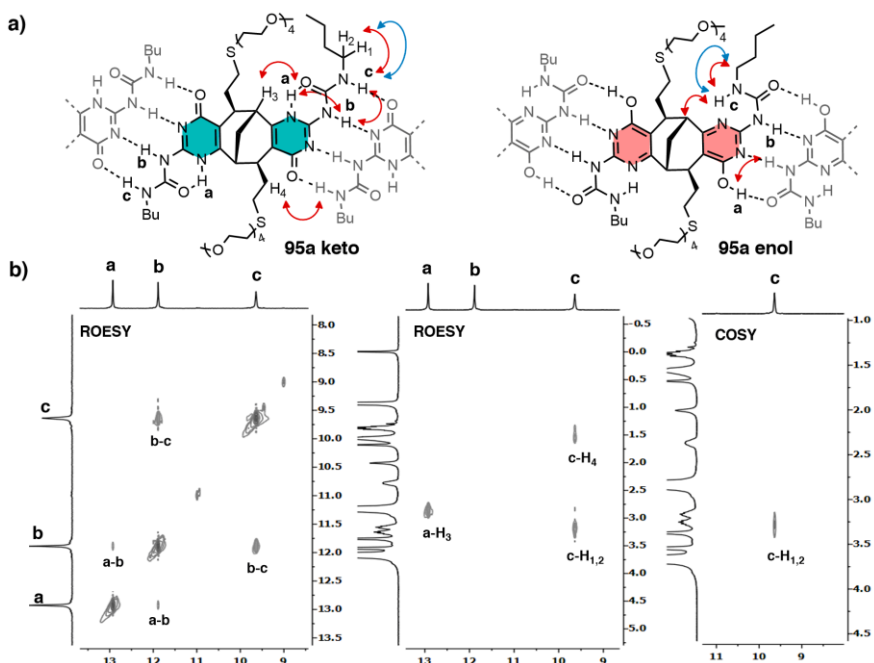
Figure **40**. a) Schematic representation of through-bond and through-space interactions for keto and enol tautomers of **95a** in CDCl$_3$ (ROESY red arrows, COSY blue arrows); b) main COSY and ROESY cross-peaks used for structural assignment.

In our case, keto form was predominant based on through-bond and through-space interactions in ROESY and COSY NMR spectra in CDCl$_3$ (Figure **40b**). NOE cross-peaks between the protons **a-b** and **b-c**, **c-H$_4$** and **a-H$_3$** fully corroborated involvement of the keto form in quadruple hydrogen bonding while dismissing participation of the enolic form. Additionally, interactions observed in ROESY and COSY spectra between urea NH proton

c and N-CH$_2$ group of the butyl chain (C-H$_1$,H$_2$) confirmed correct assignment of the N-H resonances within the Upy fragment.

Other aggregates **95b-e$_4$** in CDCl$_3$ displayed identical pattern in ^{1}H NMR spectra with corresponding diffusion coefficients ranging between 2.12 – 2.17·10^{-10} m^{2}s^{-1} (Figure **41a**). Remarkably, the same pattern of quadruple hydrogen-bonding mode occurs even in such polar solvents like acetonitrile indicating high stability of the tetrameric aggregate (Figure **41b**). On the other hand, new set of signals was observed in a nonpolar benzene-d$_6$. It is known from previous studies by Orentas *et al.* that a mixture of tetrameric and pentameric species can co-exist in toluene or benzene solutions (Figure **42a**).[123]
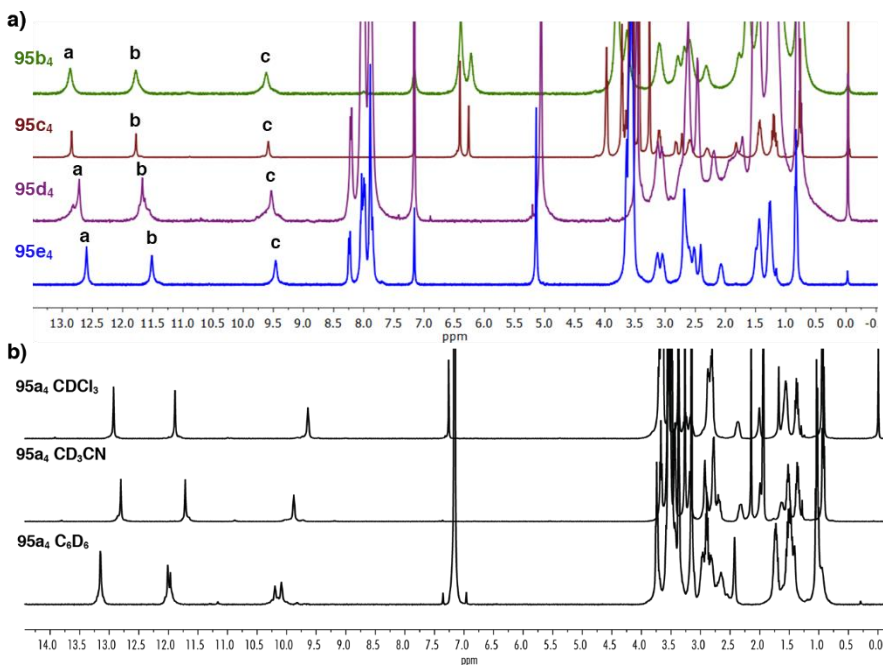
Figure **41**. a) ^{1}H NMR spectra of tetramers **95b-e$_4$** in CDCl$_3$ b) ^{1}H NMR spectra of tetramer **95a$_4$** in CDCl$_3$, acetonitrile-d$_3$ and benzene-d$_6$.

The possibility of the formation of enolic tautomer was initially ruled out by DOSY based on the presence of two distinguishable species of different sizes (Figure **42b**). Apparently, stronger hydrogen bonding in less polar C$_6$D$_6$ allows higher deviation from planarity within Upy:Upy dimer permitting association of larger supramolecular homologues. Diffusion coefficients 2.09·10^{-10} and 1.89·10^{-10} m^{2}s^{-1} at 15 mM concentration were

attributed to tetrameric and pentameric aggregates, respectively. Resulting values were translated into hydrodynamic radii 15.8 Å and 17.5 Å for tetramer and pentamer, respectively. The ratio of diffusion coefficients was calculated to be 1.11, which is expected to be roughly equal to the reciprocal ratio between molecular masses of the tetramer (M_T = 3939.6) and the pentamer (M_P = 4924.5).[135] The obtained values fitted within the range of theoretical ratios estimated for spherical molecules by utilizing eq.(1) and were in agreement with previously reported experimental data and molecular modeling. [123]

$$\sqrt[3]{\frac{M_P}{M_T}} \leq \frac{D_P}{D_P} \leq \sqrt{\frac{M_P}{M_T}} = 1.08 \leq 1.11 \leq 1.12 \qquad (1)$$

Figure **42**. a) Schematic representation of cyclic tetramer and pentamer aggregates in nonpolar solvents; b) DOSY spectrum of 15 mM **95a** in C_6D_6 indicating two different species in solution; c) NH region of stacked ^{1}H NMR spectra of aggregates **95a-e** in C_6D_6.

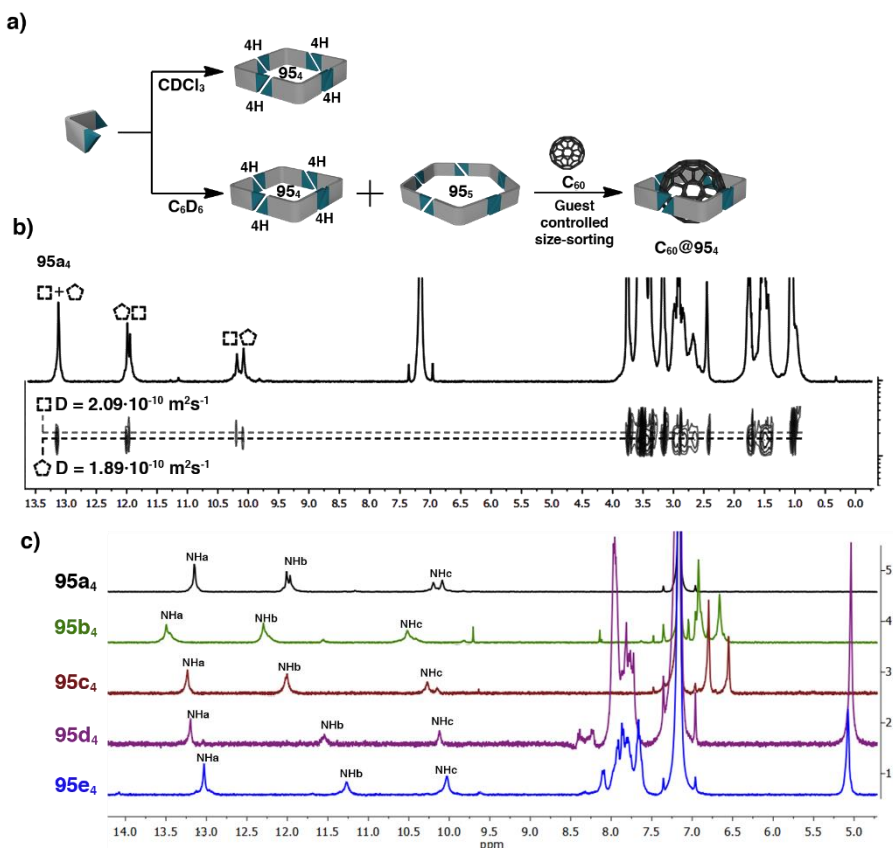However, single set of NHs resonances of other aggregates **95b-e₄** comprising bulkier substituents were observed in ^{1}H NMR implying presence solely of one kind species in C_6D_6 (Figure **42c**). In this case, association of pentamers might be impaired due to increased unfavorable steric repulsion emerging from overcrowding of large solubilizing groups in periphery of the aggregate's walls. Diffusion coefficients for **95c₄** and **95d₄** ($D = 2.06 \cdot 10^{-10}$ and $2.13 \cdot 10^{-10}$ m^{2}s^{-1}) suggested predominant presence of tetrameric supramolecules, however, $D = 1.715 \cdot 10^{-10}$ and $1.874 \cdot 10^{-10}$ m^{2}s^{-1} for **95b₄** and **95e₄** were obtained, which could be attributed to either pentameric species or increased radius of tetramer due to greater rate of solvation or spatial arrangement of larger substituents.

Additionally, the geometry of tetrameric cycle was calculated using semi-empirical PM3 method as implemented in Spartan'14. The resulting molecular model (MM) of tetramer **95₄** indicated the size of empty cavity to be 13.4 Å from face to face (Figure **43a**). In all models, the solubilizing side groups were omitted for clarity. The cavity can provide the means to encapsulate C_{60} since its dimensions almost perfectly coincide with the size of guest molecule.

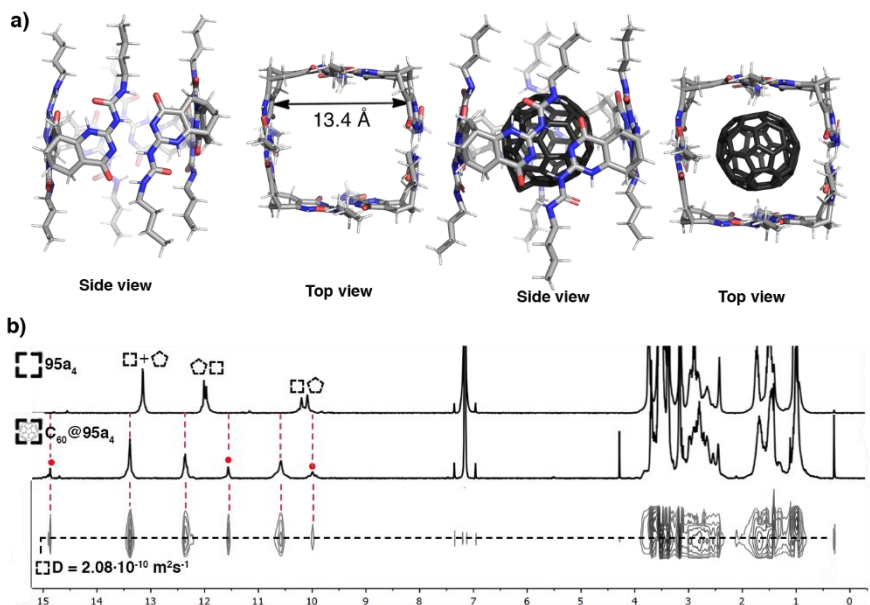
Figure **43**. a) Molecular model (semi-empirical, PM3) of tetramer **95₄** and its complex with C_{60}; b) ^{1}H NMR spectra of **95a** in C_6D_6 in the presence of 0.25equiv. C_{60} with DOSY stacked bellow. Red dot indicates resonances corresponding to enol tautomer.

The host-guest chemistry of **95a-e** was carried out in benzene-d_6 and acetonitrile-d_3. Although, C_{60} solubility in the latter solvent is poor, encapsulation took place over time. Successful encapsulation of 0.25 equiv. C_{60} in 9 days was supported by apparent downfield shift of NHs proton peaks in ^1H NMR spectra upon complexation of guest with electron acceptor character in benzene-d_6 (Figure **43b**). Diffusion coefficient of complex **C_{60}@95a$_4$** was obtained identical to free tetramer (D = $2.08 \cdot 10^{-10}$ $m^2 s^{-1}$), thus indicating that host does not undergo any considerable structural changes. In fact, the encapsulation imposed guest-controlled self-sorting of cavity size and removed pentamer rendering tetramer as a prevailing species in the solution (Figure **42a**). A minor set of new resonances emerged in ^1H NMR spectrum which could most likely be assigned to the enolic tautomer.

The encapsulation of C_{60} in benzene-d_6 was completed with all aggregates **95a-e$_4$** in 4 – 9 days. Unexpectedly, substantial degradation of the host-guest complex was observed over time in all cases (Figure **44a)**.
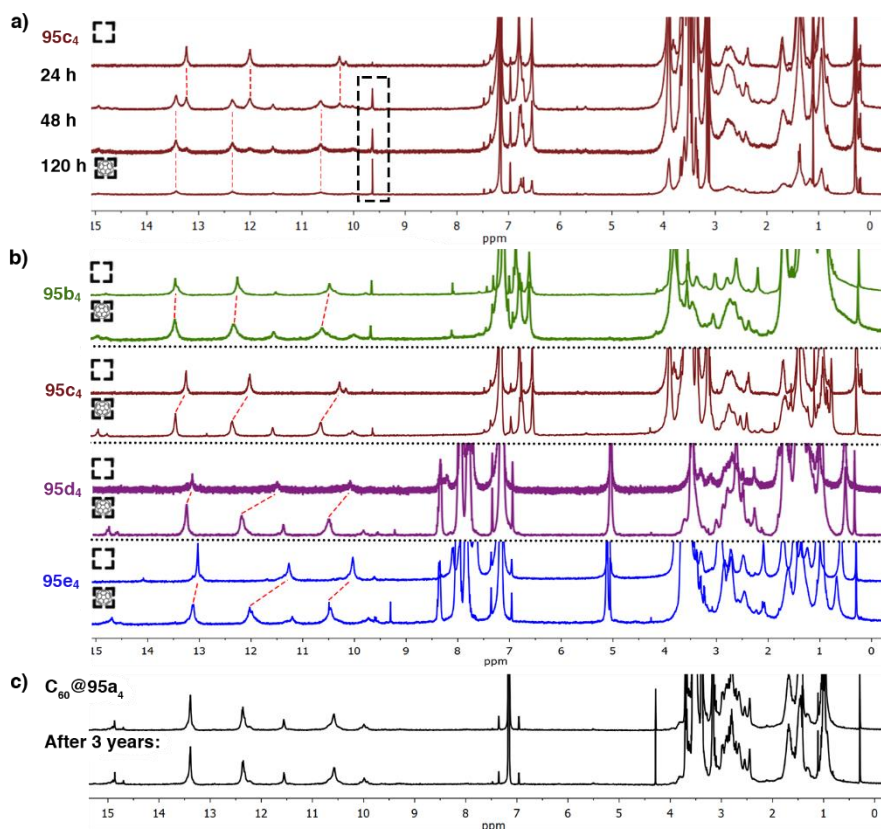

Figure **44**. a) degradation of complex **C_{60}@95c$_4$**; b) stacked ^1H NMR spectra of **95b-e$_4$** in presence of C_{60}; c) stability of complex **C_{60}@95a$_4$** over three years.

The appearance of a new resonance at 9.64 ppm in the spectra and the formation of an insoluble brown solid from the solution was observed overtime. Thus, all host-guest experiments were repeated under argon atmosphere in the dark to increase the stability of newly formed complex (Figure **44b**). Remarkably, complex C_{60}@**95a₄** under argon was still intact after three years based on obtained ^{1}H NMR spectrum in C_6D_6 (**Figure 44c**).

In addition, cyclic tetramer **95a₄** successfully entrapped C_{60} within cavity in polar acetonitrile (Figure **45**). The degradation of the tetramer was observed instantly along with sluggish complexation; therefore, the experiment was carried out under inert atmosphere in the dark while heating at 50 °C for 16 days. However, **95c₄** did not fully encapsulate C_{60} due to low stability of formed complex even under argon.
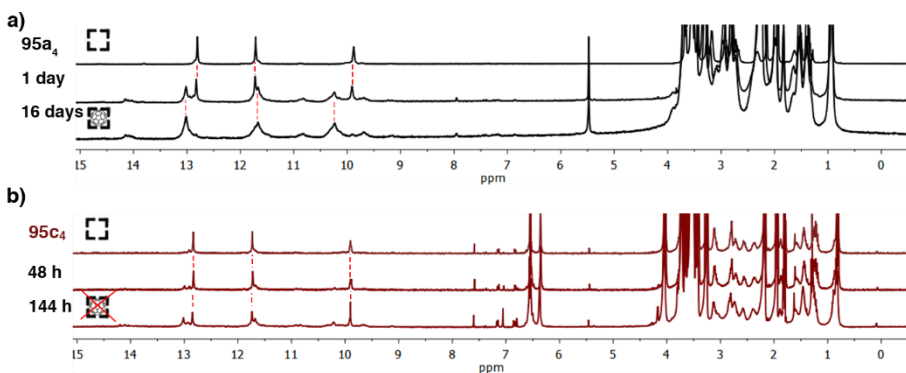
Figure **45**. ^{1}H NMR spectra of C_{60} guest encapsulation by a) **95a₄** and b) **95c₄** CD₃CN.

We speculated that introduction of fullerene guest molecule into the cavity of our supramolecular aggregate locks side chains in proximity to guest and enhances fullerene's known ability to generate singlet oxygen[136] or to abstract an electron[137,138] from the sulfide without external stimuli which generates sulfide cation radicals **A** in the collateral chains of the cyclic tetramer (Figure **46a**). Thus, cation radical can undergo oxidation with molecular oxygen resulting in persulfoxide **B**, whereas labile acidic α-proton are prone to abstraction which results to formation of hydroperoxylsulfonium ylide **C**. The latter intermediate can rearrange into hydroperoxysulfide **D** leading to hydrolysis and subsequent C-S bond cleavage.[130,139] Hence, ensuing degradation of the tetrameric capsule and appearance of benzaldehyde corresponding to resonance observed at around 10 ppm in ^{1}H NMR spectrum. The control experiments were performed at

daylight by treating keto ester **91c** with C_{60} in CD_3CN and **95c** with C_{60} in MeOD. In either case no apparent formation of benzaldehyde was observed because ketoester cannot form cavitand or the association of tetrameric aggregates was hindered by polar solvent, thus encapsulation could not take place. Thereby, stability of complex **C_{60}@95a$_4$** can be justified by the lack of reactive benzylic site for oxidative cleavage.

Figure **46**. a) Proposed degradation of tetrameric complex mechanism; b) Oxidation of PPh$_3$ in presence of molecular oxygen and complex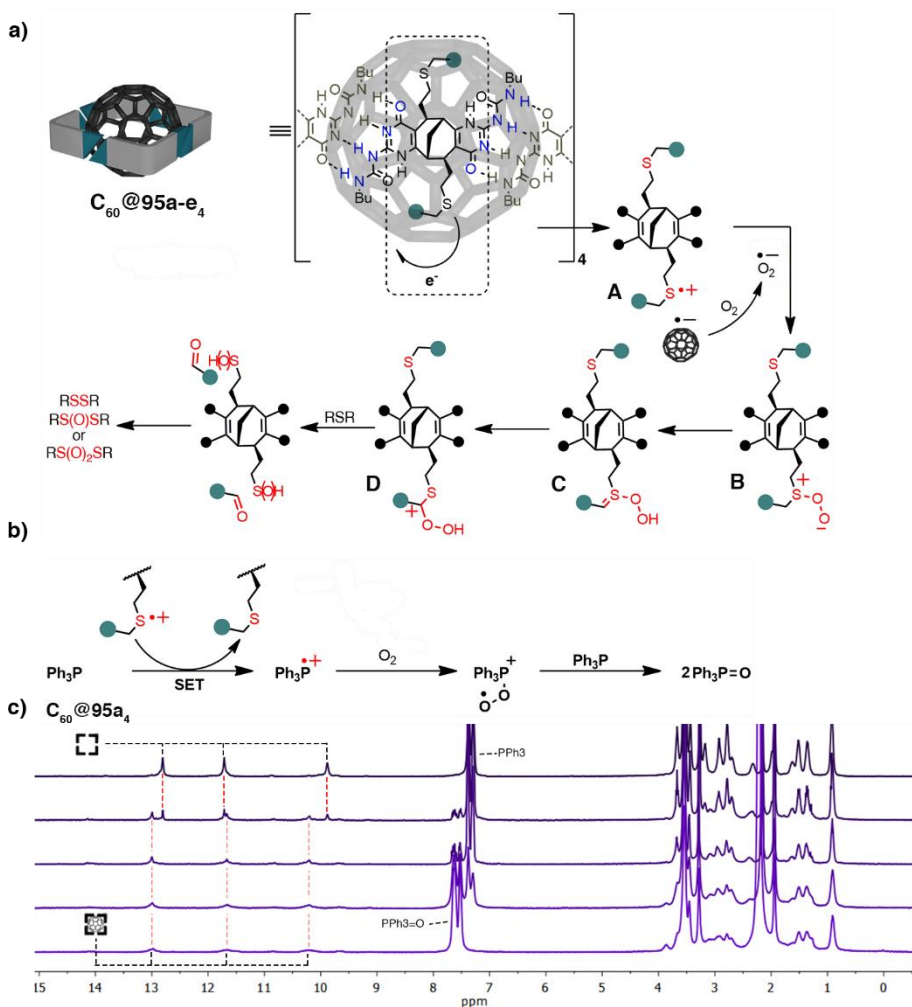 **C_{60}@95a$_4$** as a catalyst in CD_3CN; c) Stacked ^{1}H NMR spectra of PPh$_3$ oxidation over time in CD_3CN.

Furthermore, triphenylphosphine was selected as an inhibitor due its efficient electron donating properties in order to prevent detrimental C-S

bond cleavage reactions. Reduction of sulfide cation radical with PPh_3 proceeds via single electron transfer (SET) to generate phosphine radical cation (Figure **46b**). The latter intermediate binds with molecular oxygen to produce the dioxygen cation radical adduct which reacts with another molecule of PPh_3 to yield two molecules of final oxidized product. Similarly, a final oxygenated product can be obtained by a radical coupling between phosphine cation radical and superoxide radical anion $O_2^-\cdot$ which is produced by transferring electron from $C_{60}^-\cdot$ anion radical to molecular oxygen.[140–142] A mixture of monomer **95a**, C_{60} and PPh_3 in ratio 1:0.25:1 in CD_3CN was sparged with oxygen and heated at 50 ºC in the dark until all PPh_3 was successfully converted into triphenylphosphine oxide. As seen in spectra of ^1H NMR in Fig. **46c**, oxidation did not occur without the presence of complex $\mathbf{C_{60}@95a_4}$. Once the complex started to form, the oxidation of triphenylphosphine utilizing molecular oxygen took place without any other external stimuli, such as light. The aforementioned electron transfer is unique and was never reported before as it occurs between fullerene C_{60} forcibly positioned in close proximity to R-S-R and without any source of light.

While there are a few attempts reported in oxidation of organic substrates utilizing fullerene derivatives, overall, this topic is addressed very scarcely. Thus, we decided to probe C_{60} utility in detail as a heterogenous catalyst in singlet oxygen mediated reactions.

2.3 Photooxidation of sulfides to sulfoxides using heterogenous carbon-based catalyst

Catalysis research firmly stands at a forefront of chemistry which is reflected by a plethora of publications being produced every year on various metal-based catalysts like metal oxides[143], porous zeolites or metal organic frameworks (MOFs)[144]. Additionally, metal-based materials operating under visible light in photoredox reactions have opened the door for more sustainable chemical transformations with higher selectivity under mild conditions.[145,146] Though, environmentally benign metal-free catalysts still remain largely underdeveloped, so the emphasis of this chapter is placed on fullerene as a prospective carbon-based candidate in photoredox catalysis. Prominent electron acceptor properties of C_{60} were exploited in chemoselective oxidation of sulfides to corresponding sulfoxides using oxygen as a terminal oxidant in order to expand the scope of green photocatalytic synthesis.

Oxidation of sulfides plays a significant role in numerous fields such as wastewater treatment, chemical warfare agent disposal and fossil fuels desulfurization. Various sulfoxides have biological activity and are extensively used in pharmaceuticals.[147–149] Thus, unquestionable importance of these compounds is reflected in high demand from industry and academia. It demonstrates necessity to develop the facile synthesis of sulfoxides without toxic waste or overoxidation to unwanted sulfones, using renewable catalyst with high stability; challenges that have not been fully solved so far. Most common synthetic approaches rely either on hazardous oxidizing agents like peroxides and hypervalent iodine reagents, require expensive and toxic transition metals as catalysts[150–152] or photosensitizers such as Rose Bengal[153], Eosin Y[154], Bodipy[155], etc. Nevertheless, poor chemoselectivity and low catalytic activity still limit their prospective application.

To the best of our knowledge, there are a few attempts reported on fullerene mediated oxidation which requires initial preparation of catalyst like functionalization[156], incorporation into miceles[157] or covalent immobilization on solid supports[158]. Herein, we utilize fullerene C_{60} and fullerene soot (FS) as an off-the-shelf photocatalyst without any prior modification. FS is a cheap raw material obtained by vaporizing the pure carbon under inert atmosphere and condensing the vapor to produce a wide range of structures that include fullerenes C_{60} and C_{70}. Further implementation of pristine C_{60} in the industry might be limited due its high price, thus we proposed FS as an inexpensive alternative with hope it meets expectations concerning catalytical activity, chemoselectivity and tolerance to various functional groups.

To probe the substrate scope of blue light mediated oxidation, a collection of sulfide derivatives was prepared having linear alkyl or branched *tert*-butyl units and various functionalities like esters, amides, nitriles or oxidation sensitive alkenes. The precursors **96a, b, e, f, j–m, p, q** for oxidation were prepared simply by nucleophilic substitution reactions using bromide derivatives and the corresponding thiols in the presence of K_2CO_3 in DMF at room temperature. The rest of sulfides **96c, d, n, o** were readily synthesized by treating thiols with acrylates or acrylonitriles, respectively, using methoxide or triethylamine as a base. Additionally, in order to compare effectiveness between fullerene C_{60} and FS as heterogenous catalyst, FS was used as a powder or suspension in toluene, whereas C_{60} was used as a stable colloidal nanodispersion[159]. The latter was prepared by first dissolving fullerene in toluene and then mixing with polar reaction medium. Oxidation

reactions of each sulfide were carried out with all three mentioned forms of catalyst in ethanol or acetonitrile sparged with oxygen and using blue LED (100 W 450 nm) as an external light source with an air cooling. All the obtained results are summarized in Figure **47**.
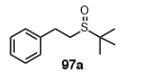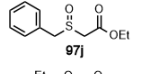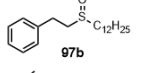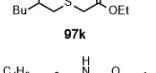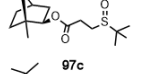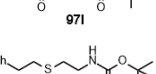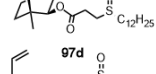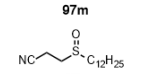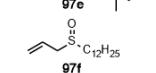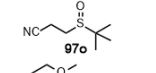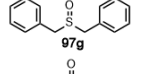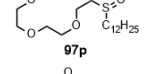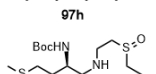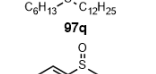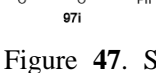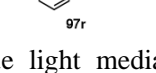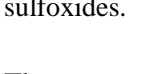
Figure **47**. Summarized results of blue light mediated sulfide oxidation to sulfoxides.

Compound	[FS] EtOH	[FS] CH$_3$CN	[FS in Tol] EtOH	[FS in Tol] CH$_3$CN	[C$_{60}$ in Tol] EtOH	[C$_{60}$ in Tol] CH$_3$CN
97a	93%	0%	97%	81%	78%	48%
97b	99%	0%	93%	82%	99%	60%
97c	74%	0%	74%	55%	84%	35%
97d	88%	0%	92%	78%	69%	86%
97e	77%	0%	85%	94%	92%	59%
97f	81%	0%	90%	70%	68%	71%
97g	81%	0%	94%	0%	98%	69%
97h	82%	0%	57%	90%	79%	93%
97i	35%	0%	92%	36%	73%	51%
97j	58%	0%	44%	18%	56%	21%
97k	47%	0%	53%	16%	56%	36%
97l	72%	0%	98%	65%	95%	97%
97m	98%	0%	42%	78%	82%	60%
97n	67%	0%	96%	80%	92%	61%
97o	70%	0%	53%	59%	72%	89%
97p	88%	79%	97%	82%	99%	80%
97q	98%	85%	92%	82%	95%	80%
97r	<5%	0%	<5%	<5%	<5%	<5%

The corresponding sulfoxides were obtained without any further overoxidation to sulfones in moderate to high yields with all three types of catalysts, whereas ethanol displayed slightly better performance due to its ability to stabilize key intermediates involved in oxidation. In several cases nanodispersion [FS in tol] outperformed C$_{60}$, which could be reasoned by joint effect of C$_{60}$ and C$_{70}$ existing in soot. In order to confirm this point, sulfide **96f** oxidation using nanodispersion of C$_{60}$/C$_{70}$ (1:1 molar ratio) as a catalyst produced sulfoxide in 5 % higher yield than using nanodispersion of C$_{60}$ alone. However, FS as a powder exhibited lower activity in comparison to colloidal solution. This could be accounted to a greater effective surface area resulting from the finer powder obtained by stirring FS in toluene in

relation to untreated FS. The difference in particle size from 1.43 µm to 0.80 µm was observed in scanning electron microscopy (SEM) measurements (Figure **48**).[160] High tolerance towards steric hindrance was confirmed by successful oxidation of sulfides comprising *tert*-butyl group. Sulfide **96g** is known to undergo visible light induced oxidative C-S cleavage to afford benzaldehydes, but in this case corresponding sulfoxide **97g** was obtained without any noticeable degradation. Oxidation sensitive alkene moieties of **96e-f** were not susceptible for oxidative cleavage under these mild conditions. Unfortunately, lower yields were observed with **97j** and **97k** due to increased acidity of the CH_2 protons between the sulfur atom and ester group which contributes to enolization followed by substrate fragmentation. Oxidation of sulfides was not observed in the absence of catalyst, light or oxygen as indicated by control experiments. Furthermore, oxidation of sulfide **96b** with fullerene depleted FS afforded sulfoxide in a tremendously decreased yield (20 %). Fullerene C_{60} was removed by continuous extraction with 1,2-dichlorobenzene following previously reported procedure.[161] However, carbon nanotube residue in fullerene depleted soot might be accountable for minor sulfide oxidation, since using single walled carbon nanotubes as a heterogenous catalyst produced sulfoxide **97b** in 13 % yield, whereas activated charcoal did not display any catalytic activity.
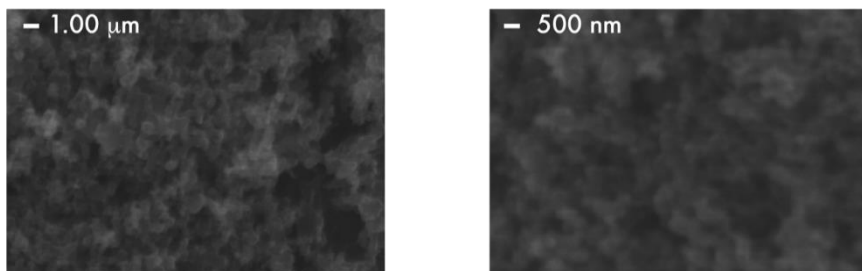
Figure **48**. SEM image of fullerene soot: commercial material (left) and from toluene suspension (right). Significant particle size reduction is observed after stirring fullerene soot in toluene.

In addition, the ability to recover and reuse a heterogeneous catalyst is of great importance from the economical point of view. In this regard, FS recyclability and stability were tested by performing oxidation of sulfide **96b** under general conditions. After each cycle, FS was recovered by centrifugation and washed prior next reaction. At least 10 successive oxidation cycles were completed without losing its intrinsic catalytic activity (Figure **49**). Raman measurements of fresh and recycled FS were carried

out.[160] Indistinguishable images of both samples imply robustness of FS as a heterogeneous catalyst.
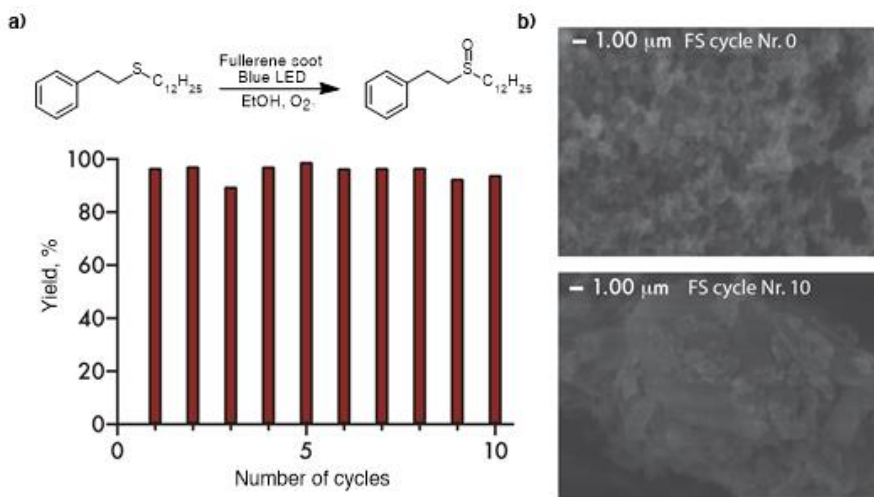
Figure **49**. a) recycling experiments of the FS heterogeneous catalyst; b) SEM images of the FS powder before and after 10 cycles.

The sulfide photooxidation can take place by two different mechanisms: either by energy transfer mechanism generating singlet oxygen or by an electron transfer mechanism employing triplet oxygen. Oxidation can occur via both mechanisms simultaneously or one of them might predominate over the other depending on precursor's structure or solvent. However, there is still an ongoing debate over the exact mechanistic pathways and the intermediates involved. Insights into possible intermediate species and detailed mechanisms have been reported by Foote[162], Clennan[163] and Albini[164–166] *et al.* As far as we are concerned, fullerene acts as a photocatalyst, where it absorbs light to give singlet excited state C_{60}^* followed by intersystem crossing (ISC) to the triplet excited state $^3C_{60}^*$ (Figure **50a**). The generated triplet excited state reacts with molecular oxygen $^3O_2$ by an energy transfer process producing singlet oxygen $^1O_2$.[136,137,167] The resulting $^1O_2$ subsequently reacts with sulfide **96** to produce two molecules of sulfoxide **97** via persulfoxide **A** intermediate. Foote *et al.* had reasoned that formation of zwitterionic **A** is more plausible over diradical or cyclic dioxirane species based on his intermediate entrapment studies with trimethyl phosphite[168] as well as observing increased rate of oxidation in protic solvents. Protic polar solvent, for example ethanol, tends to form hydrogen bonding with persulfoxide and reduces negative charge

density on intermediate **B**, thereby, facilitates subsequent nucleophilic attack by second sulfide.[169]
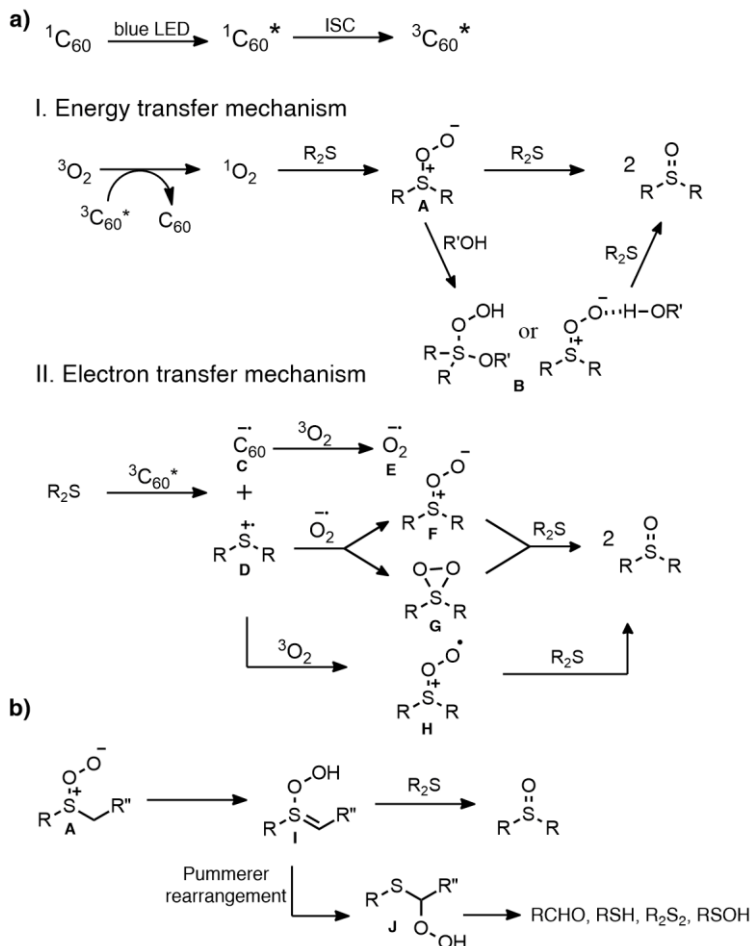
Figure **50**. Potential mechanism for C$_{60}$-catalyzed sulfide oxidation.

In the electron transfer mechanism, excited ^{1}C$_{60}$* acts as a strong oxidant and reacts with sulfide to form reduced fullerene radical anion **C** and sulfide radical cation **D**. Then fullerene species transfer electrons to molecular O$_2$ to generate superoxide radical anion O$_2^-$$^\bullet$ **E** which combines with radical cation **D** and produces identical persulfoxide **A** intermediate like in energy transfer mechanism. On the other hand, Baciocchi *et al.* have argued that another intermediate – thiadioxirane **G** is involved instead. For instance, photooxidation of the same substrate PhSMe via electron transfer and ^{1}O$_2$ pathway resulted in different product distribution, whereas sulfone was only detected in a singlet oxygen promoted reaction. Additionally, electrophilic

diphenyl sulfoxide can capture persulfoxide **A** by converting itself to diphenyl sulfone. In this case, trapping experiments of electron transfer mediated oxidation did not result in diphenylsulfone formation, which coincide with no occurrence of intermediate with nucleophilic nature.[170] Accordingly, cyclic adduct thiadioxirane **G**, possessing electrophilic characteristics, can react with sulfide but not with diphenyl sulfoxide. On the other hand, sulfide radical cation **D** can potentially react directly with molecular oxygen yielding persulfoxide radical **H** which interacts with another sulfide and releases sulfoxide.

Sulfides **96g, j-k** bearing acidic α-proton are susceptible to abstraction of labile proton which leads to hydroperoxylsulfonium ylide **I** formation (Figure **50b**). The latter intermediate can undergo oxidation to yield sulfoxide or proceed through Pummerer rearrangement to form hydroperoxide **J** which decomposes into aldehydes and other cleavage byproducts.[171]

In our case, to gain better insight into the contribution of energy and electron transfer mechanisms in the photooxidation reaction, quenching experiments using dialkylsulfide **96a** with different additives were executed (Table **1**).

Table 1. Control experiments of **96a** oxidation using C_{60} in toluene nanodispersion.

Entry	Catalyst	Solvent	O_2	Quencher	Yield (%)
1	+	EtOH	+	none	99
2	+	EtOH	+	2 equiv. TEMPO	29
3	+	EtOH	+	2 equiv. DABCO	41
4	+	EtOH	+	2 equiv. 1,4-benzoquinone	31
5	+	EtOH	+	2 equiv hydroquinone	50
6	+	EtOH	+	6mol% Co(acac)$_3$	41
7	+	EtOH	+	1,3-dinitrobenzene	90
8	+	EtOH	+	1,4-dimethoxybenzene	85

For instance, a well-known radical scavenger (2,2,6,6-tetramethylpiperidin-1-yl)oxyl (TEMPO) inhibits oxidation tremendously indicating the presence of radical species. The singlet oxygen pathway was confirmed since oxidation yield was noticeably suppressed with both $^1O_2$ quenchers – 1,4-

diazabicyclo[2.2.2]octane (DABCO) and Co(acac)$_3$, whereas sulfide radical cation scavengers 1,4-dinitrobenzene and 1,4-dimethoxybenzene had almost no influence on reaction yield whatsoever. Though, 1,4-benzoquinone, responsible for superoxide radical anion entrapment, had suppressed oxidation yield significantly. Thereby, in our case sulfide oxidation takes place by combination of both mechanisms.

Thioanisole resistance to oxidations limits the scope of our method to dialkyl sulfides. To our delight, however, the addition of TEA as a mediator significantly improved reaction outcome. Synergy between photocatalysts and TEA as a redox mediator in sulfide oxidation reactions has been reported previously[172,173] C$_{60}$ comprises low reduction potentials, thus is susceptible to electron transfer interactions with good electron donors, such as tertiary aliphatic amines.[174,175] Presumably, fullerene can effectively abstract electron from TEA resulting in amine radical cation which subsequently transforms thioanisole to reactive sulfide radical cation while restoring amine to initial form. Only catalytic amount (0.2 equiv) of TEA as a mediator is needed to ensure high yields (>85%) of methylphenyl sulfoxide derivates **97r-u** (Figure **51**).
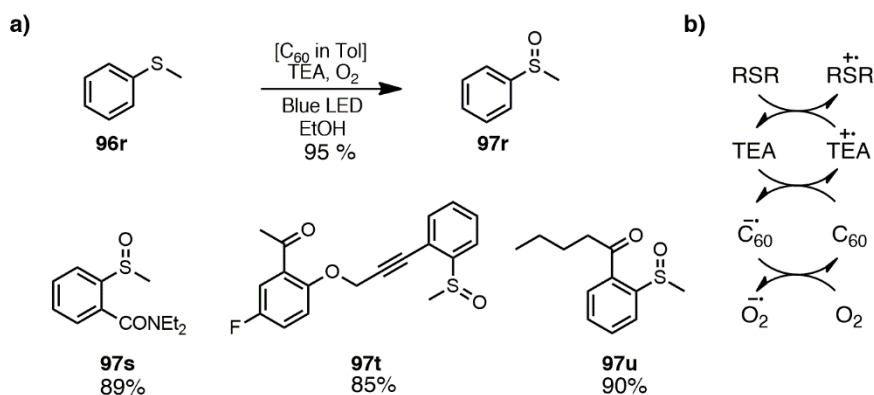
Figure **51**. a) TEA mediated oxidation of thioanisole derivatives **96r-u** under blue LED irradiation; b) proposed mechanism of oxidation by cooperative C$_{60}$ and TEA catalysis.

The synthetic potential of the blue light-mediated photocatalysis was screened further by performing chemoselective oxidation of bisulfide **96v** containing both dialkyl and arylalkyl sulfide moities (Figure **52**). To our surprise, disulfoxides were successfully obtained with 68 – 81 % yield in ethanol. Such chemoselective oxidation occurred indirectly due to

intramolecular oxygen transfer from dialkylpersulfoxide intermediate to arylalkyl sulfide. The effectiveness of this type of oxidation was evaluated using a triphenylphosphite as an external nucleophilic quencher. No substantial changes in the distribution of oxidated products were noted, although $P(OPh)_3$ is considered to be a much better electrophilic oxygen acceptor in comparison to sulfide. Furthermore, diphenylsulfoxide did not participate in co-oxidation as anticipated, sustaining the supposition of electrophilic intermediate being involved. Yields of oxidation in acetonitrile were somewhat lower owing to the lack of persulfoxide stabilization via hydrogen bonds unlike with ethanol.

EtOH:
[FS] **97v** 72%, 97v/97w = 2.6
[FS in tol] **97v** 68%, 97v/97w = 4.7
[C$_{60}$ in tol] **97v** 81%, 97v/97w = 5.9

CH$_3$CN:
[FS] **97v** 31%, 97v/97w = 1.4
[FS in tol] **97v** 61%, 97v/97w = 1.5
[C$_{60}$ in tol] **97v** 45%, 97v/97w = 1.6
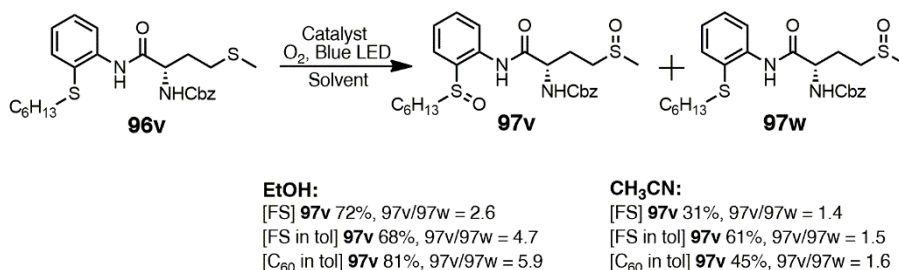
Figure **52**. Chemoselective oxidation of bisulfide **96v** via intramolecular oxygen transfer.

2.3.1 Other environmentally friendly synthetic applications of heterogeneous fullerene catalyst

In this context, other potential applications of the blue LED mediated photooxidation using fullerene as a heterogeneous catalyst were explored. In reference to previously distinguished ability of photo-excited fullerene to abstract electron from TEA, the oxidative cyclization-addition between N,N-dimethylanilines and maleimides were probed under environmentally benign conditions. The necessary steps involved in the formation of tetrahydroquinolines **99** were extensively studied by several groups using different photocatalysts.[176,177] In suggested mechanism, photoexcited C$_{60}$ produces α-aminoalkyl radical **98a** through single electron transfer followed by deprotonation (Figure **53**). Resulting species **98a** are capable to attack double bond of electron deficient maleimides and further undergo cyclization followed by successive electron and hydrogen atom transfer steps to afford tetrahydroquinoline **99** as a final product.
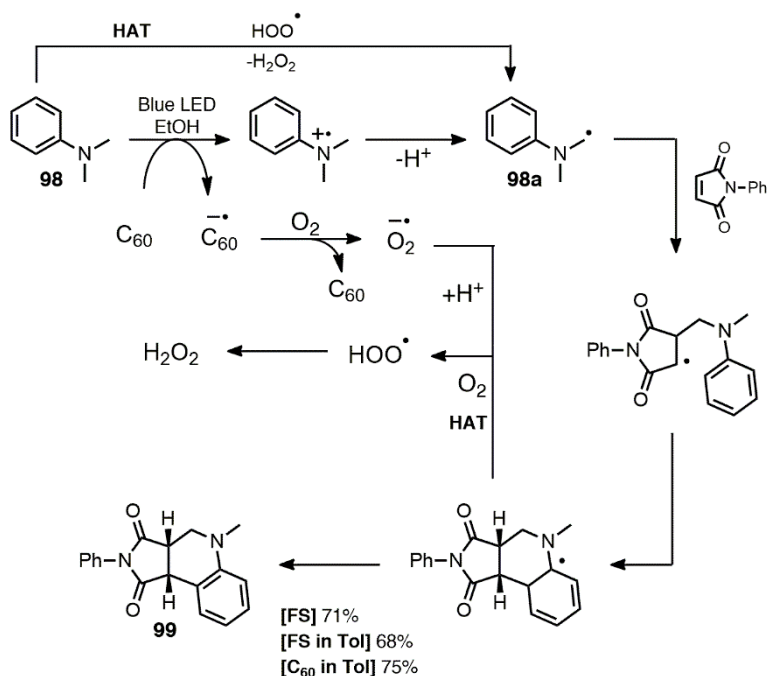
Figure **53**. Reaction mechanism of radical cyclization

Furthermore, N-benzyl anilines can be easily converted into imines in a similar manner, whereas amino cation radical undergoes α-deprotonation followed by oxidation to yield the corresponding product.[178–180] To facilitate imine **100b** formation, the reaction efficiency was compared in EtOH, CH_3CN and $CHCl_3$ (Figure **54a**). Surprisingly, the latter solvent was the most effective with yields ranging between 78 – 100 % with all three forms of fullerene catalyst. The outcome might be associated with the longest lifetime of $^1O_2$ in $CHCl_3$ while comparing to the rest of the solvents.

Subsequently, oxidative α-cyanation of tertiary amine 2-phenyl-1,2,3,4-tetrahydroisoquinoline **101a** was carried out with trimethylsilyl cyanide (TMSCN) in presence of heterogenous fullerene catalyst to afford α-amino nitrile **101b** in moderate yields without further formation of dicyanated products (Figure **54b**). Such adaptation of our catalyst to already established one-pot cyanation method provides the means for efficient synthesis of α-aminonitriles which is used as a versatile intermediate for plethora of bioactive compounds.[180–182]

a)

EtOH:
[FS] **100b** 0%;
[FS in tol] **100b** 0%;
[C$_{60}$ in tol] **100b** 88%;

CH$_3$CN:
[FS] **100b** 0%;
[FS in tol] **100b** 85%;
[C$_{60}$ in tol] **100b** 86%;

CHCl$_3$:
[FS] **100b** 78%;
[FS in tol] **100b** 91%;
[C$_{60}$ in tol] **100b** 100%;

b)

EtOH:
[FS] **101b** 86%;
[FS in tol] **101b** 74%;
[C$_{60}$ in tol] **101b** 70%;

CH$_3$CN:
[FS] **101b** 0%;
[FS in tol] **101b** 52%;
[C$_{60}$ in tol] **101b** 63%;

CHCl$_3$:
[FS] **101b** 84%;
[FS in tol] **101b** 65%;
[C$_{60}$ in tol] **101b** 0%;
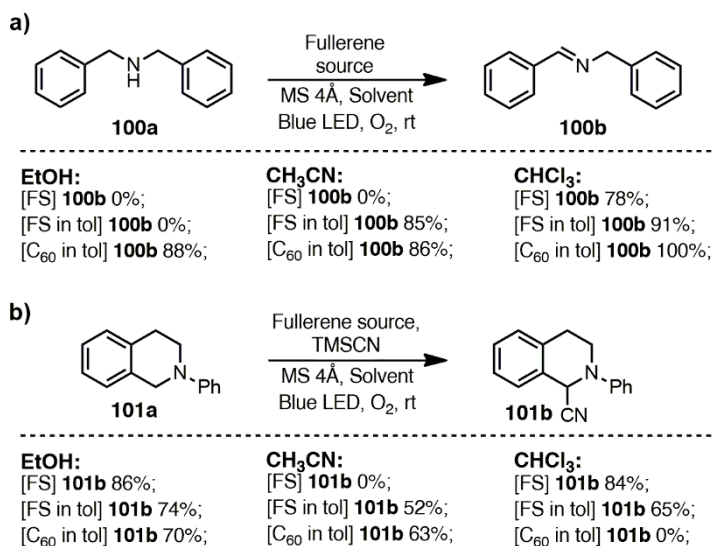
Figure **54**. a) Blue-light mediated oxidation of N-benzyl anilines; b) oxidative α-cyanation of 2-phenyl-1,2,3,4-tetrahydroisoquinoline.

In similar manner, heterogenous fullerene catalyst together with sterically hindered DIPEA as an electron donor was effectively employed in *ipso*-hydroxylation of aryl boronic acids **102a** and **103a** to corresponding phenols (Figure **55**).[183,184] Photooxidative hydroxylation of arylboronic acid **102a** were performed in EtOH and CHCl$_3$ in excellent yields, whereas pyridin-4-ol **103b** was obtained only in EtOH because it did not dissolve in neither acetonitrile nor chloroform.

EtOH:
[FS] **102b** 99%;
[FS in tol] **102b** 89%;
[C$_{60}$ in tol] **102b** 96%;

CHCl$_3$:
[FS] **102b** 93%;
[FS in tol] **102b** 59%;
[C$_{60}$ in tol] **102b** 48%;

EtOH:
[FS] **103b** 63%;
[FS in tol] **103b** 67%;
[C$_{60}$ in tol] **103b** 100%;
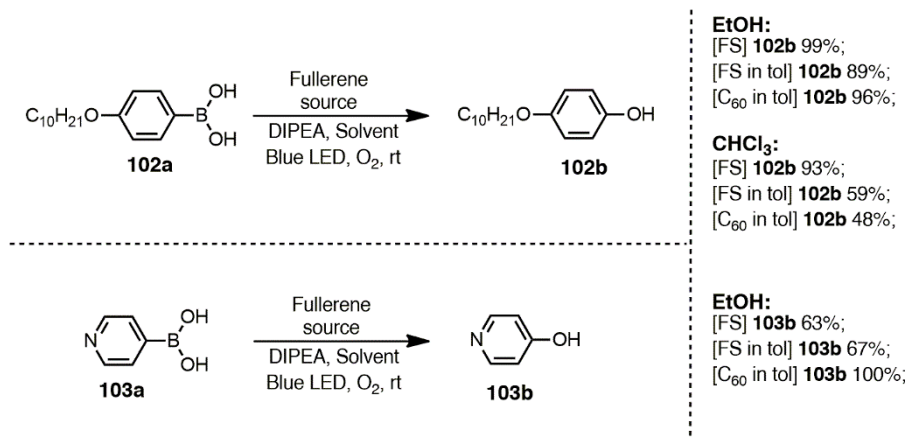
Figure **55**. Photoinduced hydroxylation of arylboronic acids to corresponding phenols **102b** and **103b**.

2.3.2 Development of continuous-flow strategy for sulfide photooxidation

Having established suitable sulfide oxidation conditions, the next step was to achieve sulfide oxidation in gram scale. However, it is difficult to apply photochemistry in batch reactions due to short penetration distance of light into the reaction vessel. Thus, continuous-flow reactor was exploited as a means to obtain high surface area to volume ratio which ensures uniform and effective irradiation of reaction mixture.

In order to examine the feasibility of continuous-flow strategy application for our environmentally benign method, flow reactor with a non-immobilized heterogenous fullerene soot was assembled (Figure **56**). In comparison to previously reported flow reactors, it does not require any additional modification or catalyst immobilization into stationary phase.[185,186]
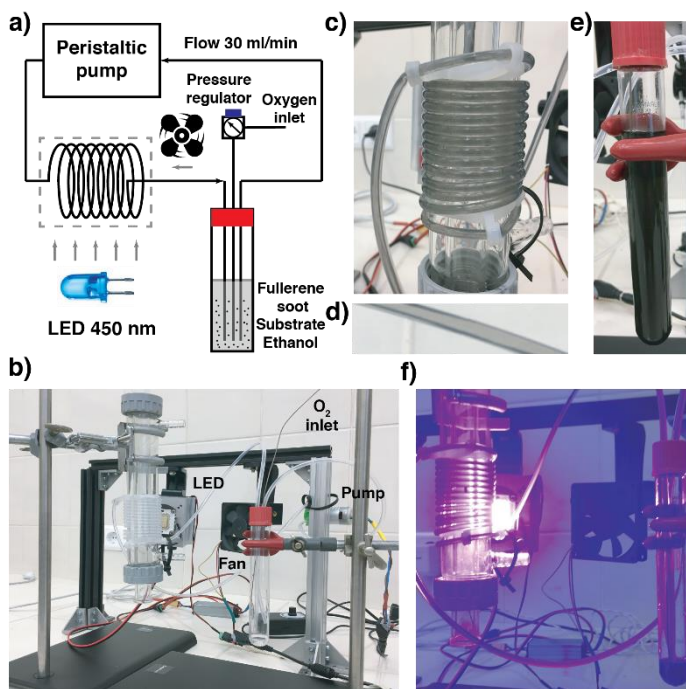
Figure **56**. a) Schematic representation of the continuous-flow system; b) setup of flow reactor; close-up of fullerene soot flowing through the c) coil and d) tubing; e) reservoir filled of reaction mixture comprising well-dispersed FS in ethanol; f) flow reaction under irradiation.

The initial photoreactor consisted of 3 mm Teflon tubing attached to a mini-peristaltic pump and passing through a reservoir of FS suspension in ethanol

and a coil with high surface area for efficient irradiation. To irradiate the reaction mixture, blue LED (100 W) with external fan was set up next to coil, which was wrapped around condenser for additional water cooling. The oxygen was supplied by an external oxygen tank connected to reservoir or by additional mini-peristaltic pump which served as an inlet for atmospheric oxygen. Moreover, efficient mixing of heterogenous catalyst within mobile phase with negligible sedimentation was achieved by maintaining constant flow rate of 30 mL/min. After extensive screening of continuous-flow conditions, the benefit of using oxygen tank instead of atmospheric oxygen was prominent since reaction time was reduced from 9 to 5 days and reaction yield increased. A continuous-flow oxidation of sulfide **96b** into sulfoxide was obtained in gram scale in 94 % yield.

3. HYDROGEN-BONDED CAPSULE COMPRISING CONFORMATIONALLY FLEXIBLE CAVITY

Biological processes inspired chemists to adapt E. Fischer's 'lock-and-key' concept in pursue of synthetic receptors and catalysts based on host-guest chemistry. The current findings emphasize more dynamic models of molecular recognition in nature, such as induced-fit and conformational selection. Both operate in combination of two consecutive reversible steps, binding and conformational change, but in different order.[187] The latter advances stress the necessity to go beyond conventional rigid supramolecular capsules, and challenges to develop biomimetic supramolecular architectures comprising conformationally flexible cavity. Hence, in our case the cavity size of the supramolecular cavitands based on bicyclo[3.3.1]nonane scaffold could be tuned by introducing different types of hydrogen-bonding modes into the system. (Figure **57**).

Figure **57**. Viable self-complementary hydrogen-bonding modes in supramolecular architectures.

In relation to previous studies, we have gained insight that incorporation of substituents by directly modifying ICyt units hinders orthogonal propag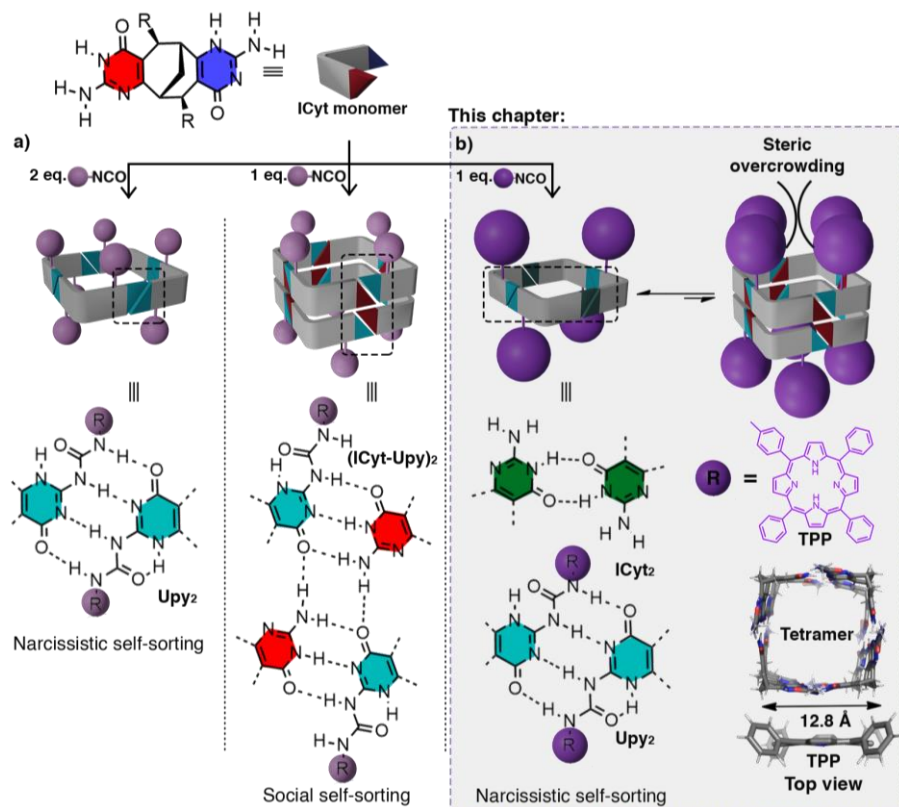ation. Resulting Upy synthons exhibit strong aggregation via quadruple DDAA hydrogen-bonding mode into discrete tetrameric structures (Figure **57a**). However, bicyclo[3.3.1]nonane synthons embedded with ICyt and Upy units on opposite sides tend to assemble into octameric tubes as a result of social self-sorting. Heterodimers are associated via triple hydrogen-bonding pattern, whereas bifurcated hydrogens of ICyt engage in binding two adjacent tetrameric cycles. Hence, the free energy of the entire system is minimized whilst maintaining the highest possible number of hydrogen bonds. However, upon encapsulation of fullerene C_{60}, octamer would rearrange to tetrameric aggregates in order to better fit the guest molecules (Figure **30c**).[124]

We envisioned, that varying the size of urea substituents could be used as a straightforward approach to access different binding properties, without the necessity to redesign the whole hydrogen-bonding motif. It would open doors for easily obtainable supramolecular architecture with desired cavity size for host-guest chemistry whilst comprising orientation, chemical nature and number of substituents for preferred application in functional materials.

3.1 Design and characterization of tetrameric architecture comprising porphyrin moieties

In order to investigate this strategy, it was anticipated that incorporation of four bulky substituents to urea scaffold would hinder orthogonal propagation of tetrameric units, where steric crowding arising from substituents would prohibit their superimposed arrangement on the same side (Figure **57b**). For this reason, tetraphenylporphyrin (TPP) urea substituent was introduced into the monomer. In accordance with molecular modelling, TPP unit is wider than the width of the hollow aggregate. Thus, unfavorable steric interactions ought to impose distribution of substituents over both sides of the tetrameric ring and additionally, promote narcissistic self-sorting of Upy and ICyt fragments.

Monomers **106a-d** were synthesized in few steps starting from easily obtainable enantiopure enone (+)-**87** (Figure **58**). Various linear and branched solubilizing groups were incorporated into 4,8-exo,exo positions of bicyclo[3.3.1]nonane scaffold in order to increase the solubility of the final compound. It was achieved via copper mediated alkylmagnesium bromide

addition to **87** affording bis-β-ketoesters **104a-d** in 76 – 99% yields. The latter intermediates were condensed with guanidinium chloride in presence of strong base KOtBu in methanol to give bisICyt **105** in good yields. In order to attain Upy moiety, 4-nitrophenylformate activated amino-TPP derivative **109** was prepared.
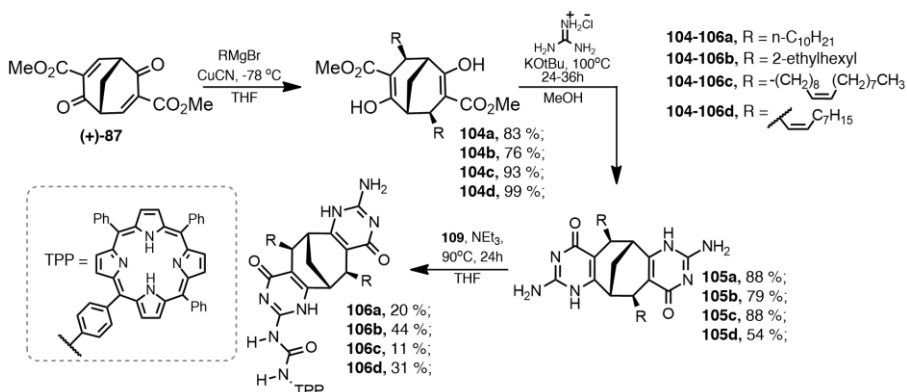
Figure **58**. Synthesis of enantiopure synthons **106a-d** comprising TPP unit.

Synthesis of porphyrin derivative **109** started from commercially available *meso*-tetraphenylporphyrin (H$_2$TPP), which underwent electrophilic regioselective nitration at para position using 1.8 equivalent of NaNO$_2$ in TFA (Figure **59**). Direct substitution at *meso*-(4-phenyl) position is favored since beta-pyrrolic positions are deactivated due to subsequent protonation of porphyrin rings in strongly acidic medium.[188] The crude of mononitroTPP **107** without any prior purification was reduced with SnCl$_2$ in concentrated HCl to afford 5-(p-aminophenyl)-10,15,20-triphenylporphyrin **108** in 32 % overall yield in two steps.
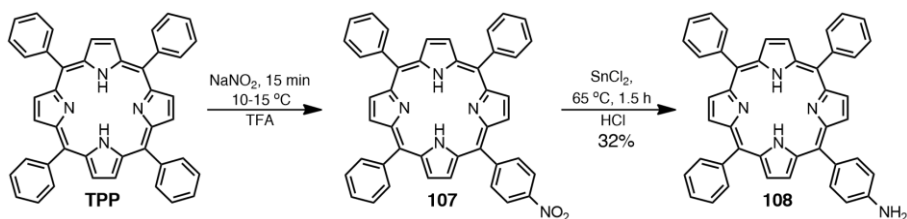
Figure **59**. Synthesis of tetraphenylporphyrin derivative **108**.

The acylation of TPP-amine **108** using 4-nitrophenyl chloroformate resulted in 95 % yield of corresponding TPP carbamate **109** (Figure **60**). The latter derivative was further subjected to coupling with ICyt **105a-d** in the presence of triethylamine. Two reaction pathways are possible: under mildly

basic conditions the corresponding isocyanate can form from the carbamate and react with ICyt *in situ*, or alternatively, the reaction can proceed via direct addition of ICyt to carbamate. In either case, a mixture of mono and bisUpy was obtained with one equivalent of TPP **109**, and the final unsymmetrical monomers **106a-d** were obtained in moderate 11 – 44 % yields.
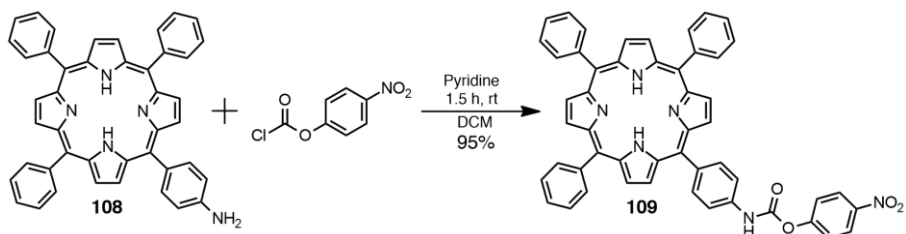
Figure **60**. Acylation of amine **108.**

In addition to its size, tetraphenyl porphyrin fragment was selected as substituent due to its profound importance and versatility in construction of photovoltaic devices[189], application in photodynamic therapy[190] or molecular sensor and recognition systems[191]. In addition, TPP derivatives might be utilized as photocatalysts[192]. Many supramolecular functional devices mainly rely on its strong aggregation mode while retaining its photophysical and redox properties, owing to its intrinsic π-conjugated scaffold. Optoelectronic properties can be easily tailored by incorporation of various metal atoms within porphyrin scaffold.[193] Hence, it has a capacity to serve as a component of various dyad, triad[194] and other multicomponent systems[195] for harvesting solar energy by replicating energy transfer and charge separation processes occurring in natural photosynthesis.

As far as the scope of this work is concerned, the main focus remains on porphyrin's ability to serve as a donor in porphyrin – fullerene dyads. Photoinduced charge separation can take place in discrete 1D nanostructures through covalent linkers, intermolecular noncovalent interactions or host-guest assemblies. However, major drawback of these systems arises from inability to confine donor – acceptor separation and alignment in solutions or solid surfaces.[196] Hence, the most important task is to gain control over dyad geometry in order to be able to pursue more efficient photoinduced electron transfer. For instance, Aida *et al*. have reported amphiphilic zinc porphyrin – fullerene dyads covalently linked via racemic and enantiopure linkers. Chirality of the linker dictate the aggregation mode of dyad wherein racemic mixture produces spherical architectures with poor photoconductivity while

enantiopure dyad assemble into photo-conducting nanofibers.[197] Throughout the years other types of conformations of porphyrin – fullerene dyads have been reported, such as cyclophane[198], parachute[199] or pacman[200].

Subsequently, incorporation of directional noncovalent interactions into the system is an essential tool for constraining spatial separation of dyad components (Figure **61**). For instance, remarkably stable zinc porphyrin – C_{60} complexes **110** encompassing restricted flexibility were achieved through two point binding mode by employing axial metal-ligand coordination and cation-crown ether complexation.[201] Nonetheless, directional Watson-Crick hydrogen-bonding motif was implemented by attaching zinc porphyrin to cytidine unit and fullerene to guanosine . The resulting architecture **111** exhibits long lived through-space charge separation state which is essential for photoactive devices.[202] As a further elaboration, incorporation of complementary Hamilton receptor and cyanuric acid pair comprising six-point hydrogen bonding array has led to successful self-assembly **112** of highly-organized donor – acceptor pair. Through-bond electronic communication between porphyrin and fullerene components was probed by time-resolved fluorescence and transient absorption measurements.[203]
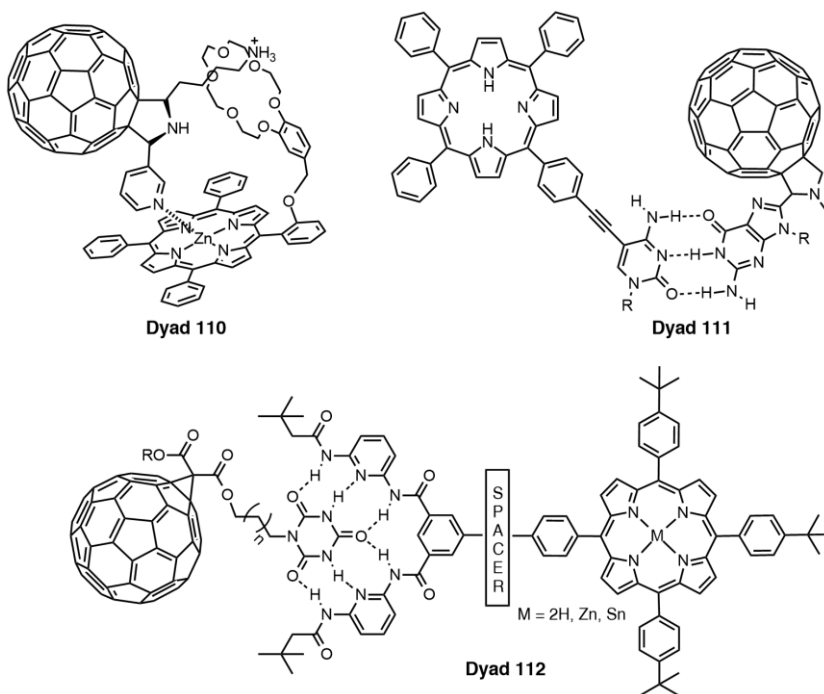
Figure **61**. Noncovalent interaction mediated porphyrin – fullerene dyads.

Another approach was to utilize three-dimensional metal-organic cages possessing internal cavity to enhance host-guest π-interactions between porphyrin units with fullerene inside the inner space. The walls of a synthetic capsule would provide the means to hinder the interference of the external stimuli with guests bound within the cavity. Closed-face $Fe^{II}_8L_6$ cubic cages were built through subcomponent self-assembly employing covalent and coordinative bonds, wherein metalated porphyrin ligands serves as walls and eight octahedral metal ions would be situated in a position of vertices (Figure **62a**).[204] In similar fashion, tetrahedral $Fe^{II}_4L_6$ cage architecture was built from a combination of Ni^{II}-metalloporphyrin with $Fe^{II}(OTf)_2$ and 2-formylpyridine (Figure **62b**). All three diastereomers with a distinctive T, C_3, S_4 symmetry point groups were observed in ^1H NMR spectrum, which is typical for such cages.[205] Both entities demonstrated ability to trap fullerenes C_{60} and C_{70}. However, tetrahedral cage would undergo guest induced rearrangement to $Fe^{II}_3L_4$ cone-shaped complex upon encapsulation of C_{60} or C_{70} to maximize π-π interactions. Additionally, steric constraints imposed by porphyrin scaffold prevent undesired helicate formation which can be often observed with other types of tetrahedral cages.
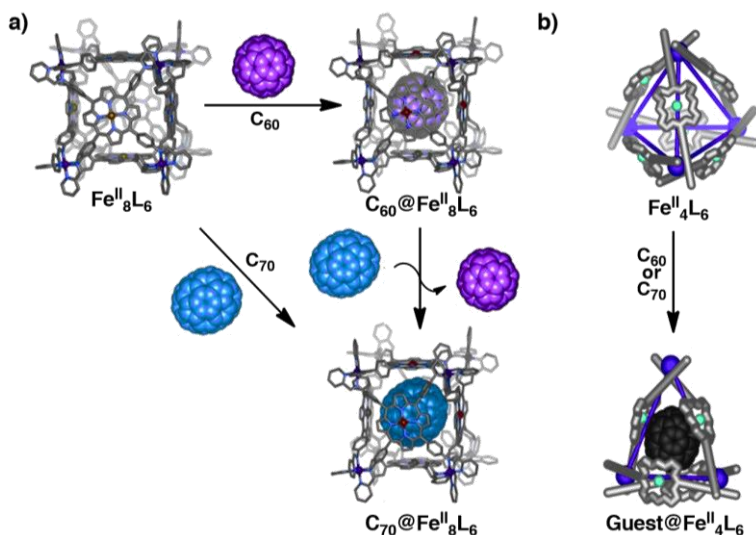
Figure **62**. a) Host-guest chemistry of a) cubic $Fe^{II}_8L_6$ and b) $Fe^{II}_4L_6$ cages. Adapted from ref. 204 and 205 with permission from John Wiley and Sons, 2011 and 2015, respectively.

To implement these design features towards concave capsules with well-defined cavity, aggregation experiments of synthons **106a-e** were first conducted in CDCl$_3$. ^1H NMR spectrum of **106a** revealed the formation of

cyclic tetramer via narcissistic self-sorting of alternating Upy-Upy and ICyt-ICyt homodimeric pairs (Figure **63a,b**). The symmetrical Upy-Upy and ICyt-ICyt association was evident from the set of four downfield resonances attributed to DDAA-AADD and DA-AD binding modes. The resonance at 5.0 ppm assigned to ICyt-NH$_2$ does not participate in hydrogen bonding, thus its involvement in orthogonal stacking of tetrameric units is dismissed.
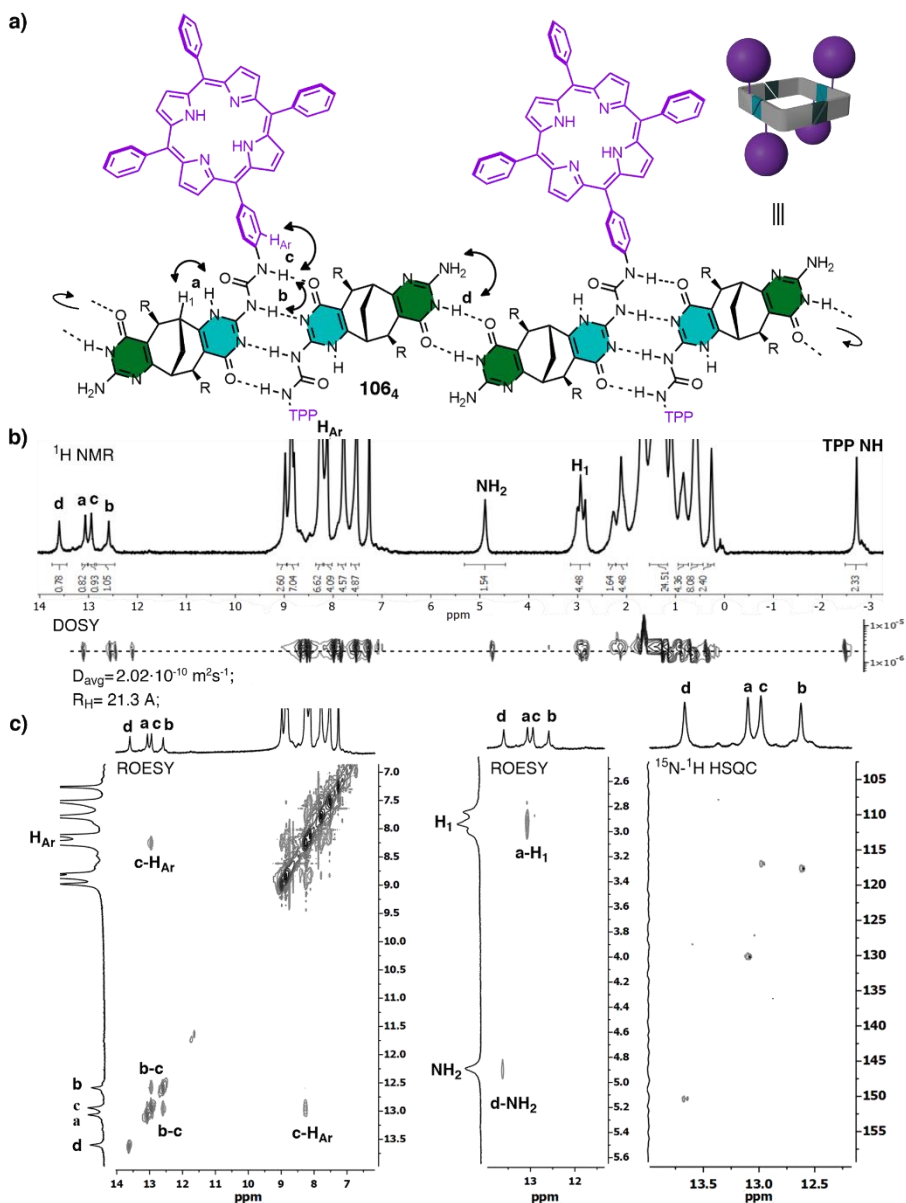
Figure **63**. a) Hydrogen bonding modes Upy-Upy and ICyt-ICyt of enantiopure synthon **106**. Arrows represent through-bond and through-space interactions; b)

H NMR spectrum of tetramer **106a₄** in CDCl₃ with DOSY trace stacked at the bottom; c) main COSY and ROESY cross-peaks used for structural assignment of **106a₄** (left) and ^{1}H-^{15}N HSQC spectrum showing NH resonances (right).

Owing to the fact that the only ROESY correlation observed between proton **d** and ICyt-NH₂, the former must be residing in the isocytosine ring (Figure **63c**). NOE cross-peak with the CH at bridgehead position of bicyclic scaffold allows unambiguous assignment of proton **a.** Correspondingly, COSY and ROESY cross-peaks to TPP aromatic ring revealed proton **c** to reside on nitrogen next to phenyl units, while NOE correlation between the latter proton and the adjacent N-H corresponding to proton **b** further corroborated Upy motif assignments. The ^{15}N-^{1}H heteronuclear single quantum coherence spectroscopy (HSQC) confirmed the involvement of the keto tautomer in dimerization indicating that all four downfield resonances belong to N-H protons. Additionally, diffusion ordered spectroscopy (DOSY) revealed the presence of solely tetrameric species with diffusion coefficient $D = 2.02 \cdot 10^{-10}$ m²s⁻¹ which was translated into hydrodynamic radius $R_H = 21.3$ Å (Figure **63b**).

In accordance with cross-peaks correlations in 2D ^{1}H NMR, same Upy-Upy and ICyt-ICyt hydrogen-bonding pattern was observed in all cases with other monomers **106b-d** (Figure **64**). The aggregates obtained in CDCl₃ were assigned as tetramers based on NMR spectroscopy studies as all proton resonances correlated to a single diffusion coefficient ranging between $D = 2.03 - 2.26 \cdot 10^{-10}$ m²s⁻¹, respectively.
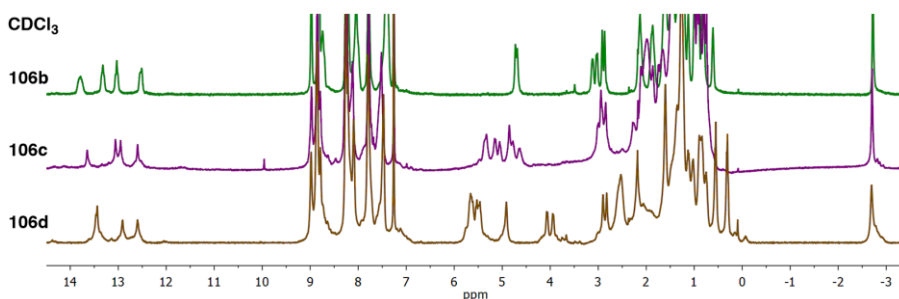
Figure **64**. Stacked ^{1}H NMR spectra in CDCl₃ belonging to enantiopure synthons **106b-d**.

The geometry of molecular model was optimized using MMFF force field method as implemented in Spartan'14 (Figure **65**). The two TPP pairs with parallel arrangement of TPP at both ends of the tetramer are situated

perpendicular to each other while solubilizing decyl chains embedded to bicyclic backbone protrude outwards. Such aggregation mode as opposed to octameric species could be favored due to additional stabilization arising from π-π stacking of well-aligned porphyrin backbones. Additionally, four porphyrins on the same plane would suffer from steric overcrowding by enforcing distorted orientation of TPP scaffolds and resulting in disruption of aromatic stacking. The molecular model of aggregate provided the dimensions of the well-defined cavity with the inner diameter d = 12.6 Å from plane to plane. Likewise, the radius of the molecule from the furthest points was estimated to be around 41.1 Å in accord with an experimentally obtained value from DOSY experiments.
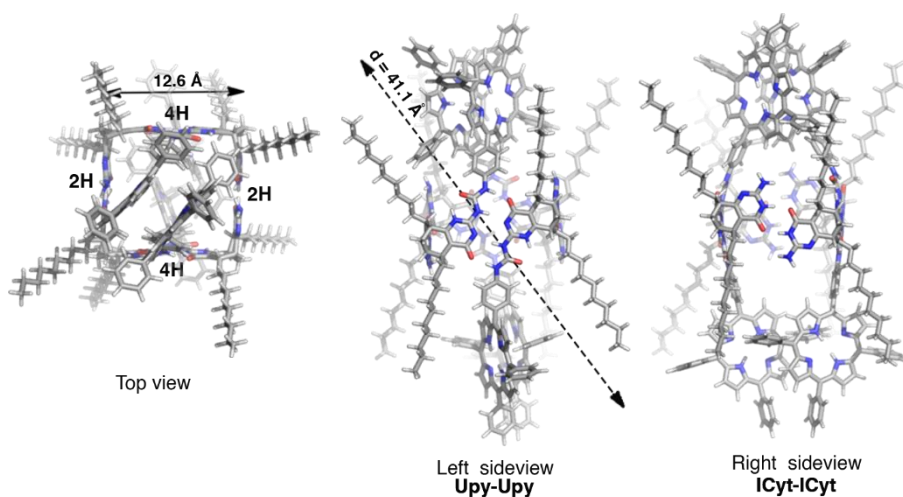
Figure **65**. Top and side views of the optimized molecular models of enantiopure tetramer **106a₄** comprising decyl solubilizing chains.

3.2 Encapsulation-induced conformational changes of dynamic capsule

In order to probe dynamic host properties of a newly obtained concave capsule, fullerene C_{60} was chosen as a model guest because of its important role in functional optoelectronic devices. Heating a mixture of tetramer **106a₄** with 0.25 equiv. of C_{60} in CDCl₃ at 50 °C for 24 hours resulted in a full conversion to inclusion complex **C_{60}@106a₄** (Figure **66**). The complexation was mostly evident from the notable shifting of N-H protons involved in hydrogen bonding. DOSY NMR analysis confirmed the presence of solely tetrameric species since all resonances in the spectrum correlated to the same

value of diffusion coefficient D = 2.07·10⁻¹⁰ m²s⁻¹ which coincide with previously described free tetramer.
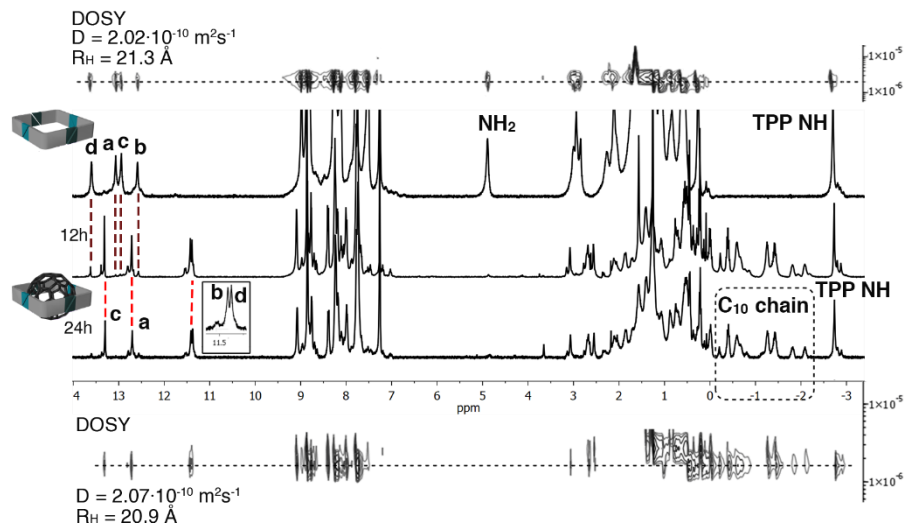
Figure **66**. Stacked ¹H NMR spectra of tetramer **106a₄** (top) complexation experiment with C₆₀ (bottom) in CDCl₃.

The careful analysis of the ¹H NMR spectrum, however, revealed the involvement of Upy enol tautomer in the aggregation process (Figure **67a,b**). Namely, NOE cross-peaks to TPP aromatic ring and to CH next to alkyl substituent in the bicyclic scaffold indicated that the most downfield resonance **c** corresponds to O-H proton. In addition, NOE correlation between the latter proton with proton **b** corroborated ADAD-DADA bonding mode (Figure **67a,c**). The NOE cross-peak with the CH at bridgehead position of bicyclic scaffold and TPP aromatic ring allowed the assignment of the proton **a** to terminal N-H of the urea unit, which forms intramolecular hydrogen bond with pyrimidine nitrogen. The absence of cross-peaks of proton **d** in ROESY spectrum provides evidence for the N-H proton from DA-AD binding mode. The resonances of the free NH₂ group of the isocytosine ring is not seen in the spectrum, most likely due to broadening. Furthermore, the absence of a cross-peak for **c** resonance in ¹⁵N-¹H HSQC spectrum fully corroborated the assignment and the presence of enol tautomeric form of Upy. Such encapsulation-induced tautomeric shift is expected to take place in order to affect structural rearrangements necessary for efficient accommodation of the guest molecule. Most remarkably, however, the resonances of a part of one of the decyl chains were found to be highly shielded and appeared in the region -0.2 – -2.10 ppm. This

observation indicates structural reorganization of the tetramer and possible interaction of the alkyl chain with the aromatic plane of TPP upon complexation.
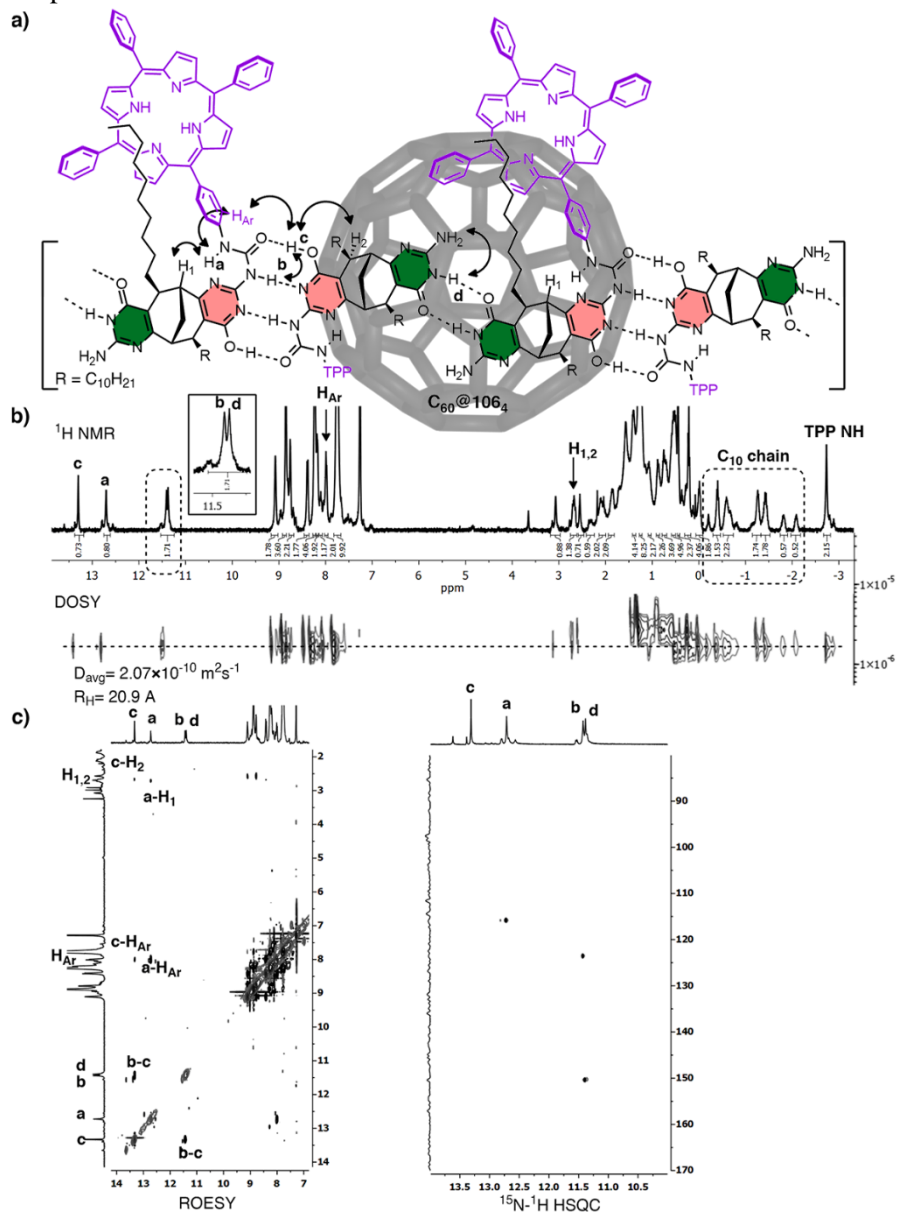
Figure **67**. a) Hydrogen bonding modes of enolic DADA-ADAD and keto DA-AD of inclusion complex **C$_{60}$@106a$_4$**. Arrows represent through-bond and through-space interactions; b) ^{1}H NMR spectrum of tetramer **C$_{60}$@106a$_4$** in CDCl$_3$ with DOSY trace stacked at the bottom; c) main ROESY cross-peaks used for structural assignment of **C$_{60}$@106a$_4$** (left) and ^{1}H-^{15}N HSQC spectrum (right) showing NH resonances.

Based on the molecular model (optimized using MMFF force field method as implemented in Spartan'14), C_{60} locks host's conformation by shifting equilibrium from closed to open-ended form, which offsets TPP units from the center of the tetramer openings (Figure **68**). Such movement of TPP units in response to tautomeric change places one of the alkyl chains in proximity to TPP ring. The conformational plasticity enables additional stabilization from CH-π interactions between peripheral alkyl chains (marked pink in MM models) and TPP backbone. Together with non-covalent interactions between the guest and the host components, it essentially alleviates entropic penalty, which arises from the loss of external degree of freedom upon complexation.

Top view

Left sideview
DADA-ADAD

Right sideview
DA-AD
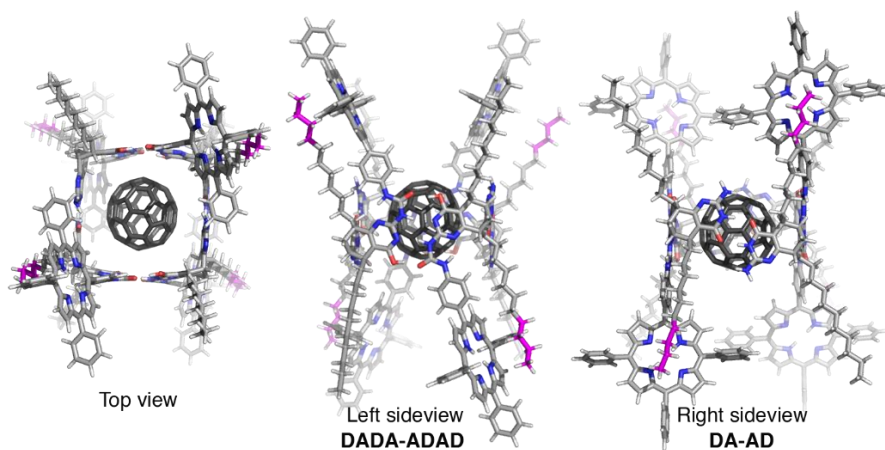
Figure **68**. Top and side views of the optimized molecular models (MMFF) of complex **C_{60}@106a$_4$**. Interacting part of alkyl chain with TPP backbone is marked in pink.

To determine whether the observed CH-π interactions are merely the consequence of the structural reorganization or in fact, are essential for complexation, monomers with solubilizing chains of different length were prepared. Monomer **106b** comprising shorter solubilizing ethylhexyl chain and **106d** containing (Z)-1-nonene chain were subjected to complexation experiment under the same conditions in chloroform. However, no shift or change of resonances in ^{1}H NMR spectrum indicated that encapsulation of C_{60} did not take place. Molecular model of assumed complex **C_{60}@106b$_4$** revealed that alkyl chains are too short to be able to interact with porphyrin (Figure **69**). This confirms that encapsulation of the guest molecule requires a cooperative action of tautomerization to the enol form and establishment of the CH-π interactions. Despite longer (Z)-1-nonene chain, cis double bond

restricts rotation of the alkyl chain and places it outwards from TPP moieties, hence rendering tetramer **106d** unsuitable for induced fit binding.
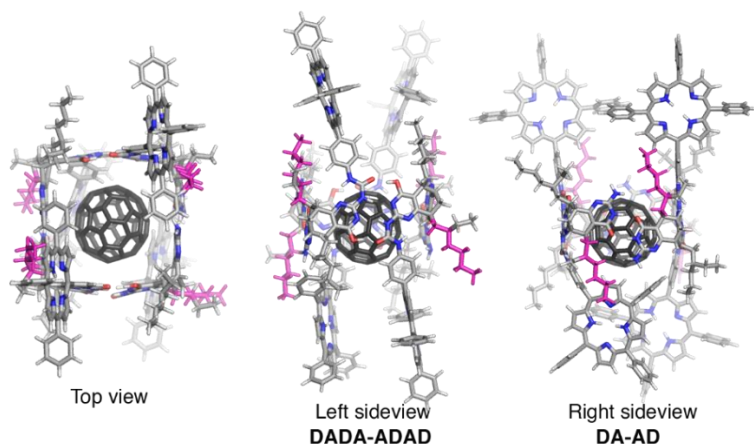
Figure **69**. Top and side views of the optimized molecular models (MMFF) of complex $C_{60}@106b_4$. Solubilizing hexyl chains marked in pink.

On the contrary, ^1H NMR spectrum of $C_{60}@106c_4$ displayed similar set of signals to complex $C_{60}@106a_4$ confirming successful complexation with fullerene (Figure **70**). Diffusion coefficient $D = 2.11 \cdot 10^{-10}$ m^2s^{-1} is in accordance with previously obtained values for similar tetramers. Thus, nine carbon atoms of oleyl chain in **106c** is enough to interact with TPP backbone and to promote C_{60} complexation, wherein double bond of cis configuration situated on 9th carbon. Taking everything into account, combination of efficient CH-π interactions with tautomerization is essential to govern induced-fit encapsulation.
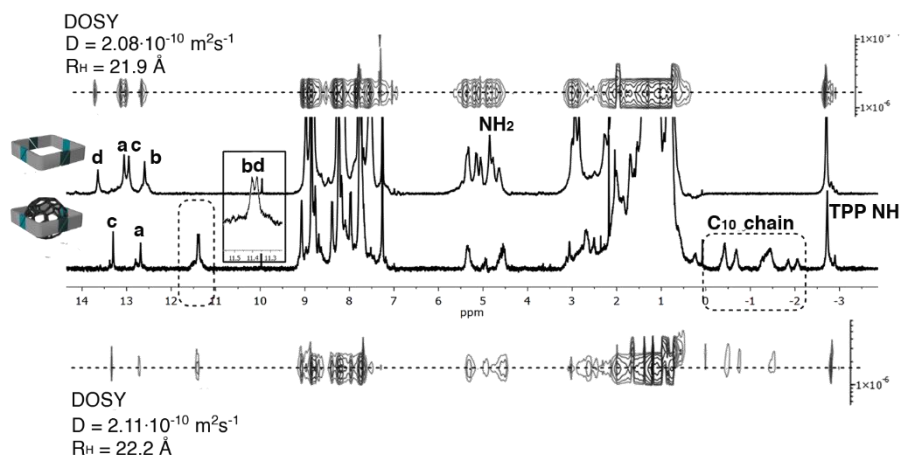
Figure **70**. ^1H NMR spectra with DOSY trace stacked of tetramer **106c₄** (top) and complex $C_{60}@106c_4$ (bottom) in CDCl₃.

Based on the above findings, one may expect that the tetramer with largest number of CH-π interactions should provide the strongest binding to C_{60}. The high integrity recognition was probed by the 0.25 equiv. of fullerene C_{60} addition into the 1:1 mixture consisting of **106a** and **106b** in $CDCl_3$ (Figure **71**). This mixture resulted in scrambled tetrameric aggregates which is suggested by reduced intensity of resonances belonging to initial homo-aggregated tetramers. Self-sorting was observed upon addition of fullerene C_{60} and resulted in the selective formation of the complex **C_{60}@106a$_4$**. Heating the mixture at 40 ºC for 3 days lead exclusively to an inclusion complex **C_{60}@106a$_4$** and free tetramer **106b$_4$**.
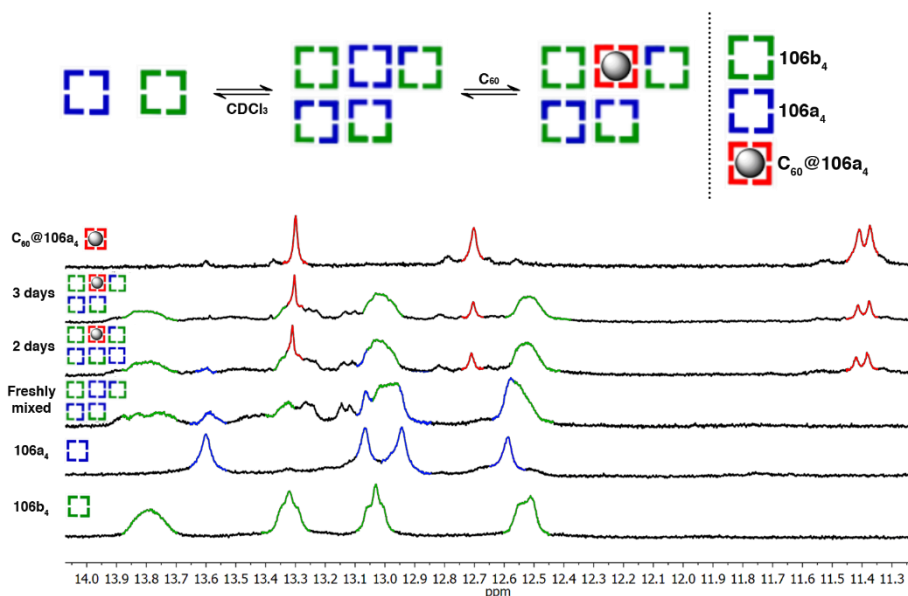
Figure **71**. Self-sorting of synthons **106a** and **106b** in the presence of C_{60} as a guest. In ^{1}H NMR spectra only NH region is shown for the clarity.

Similarly, self-sorting of scrambled **106a** and **106d** mixture took place upon the introduction of fullerene (Figure **72**). This indicated high fidelity of monomer **106a** for homoaggregation as a result of the necessity for CH-π interactions to occur alongside higher order symmetry to provide suitable cavity shape for guest molecule. Such selective molecular recognition in a mixture of similar components is an attractive feature for responsive functional materials.
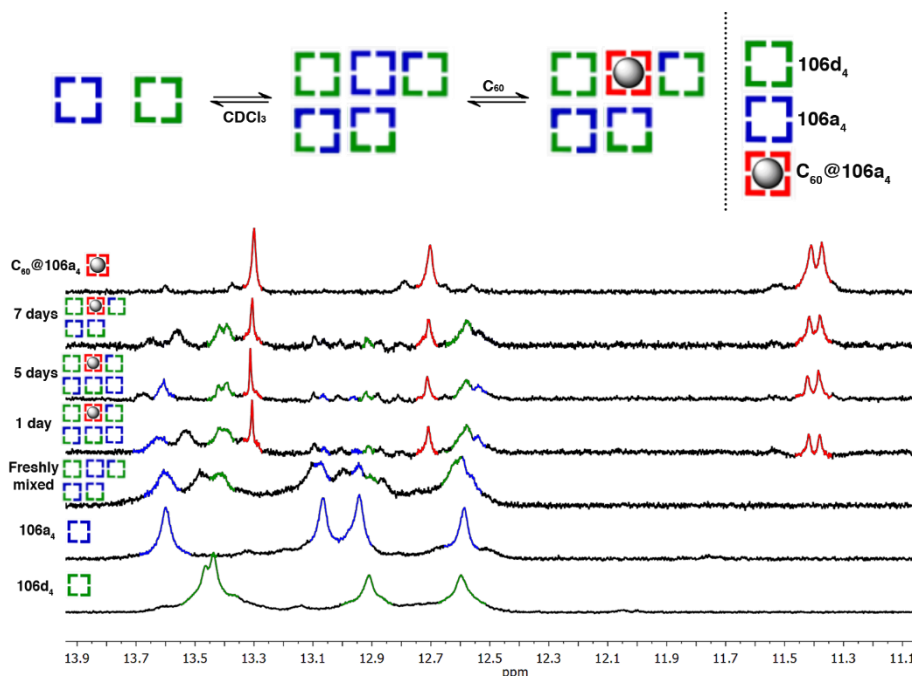
Figure **72**. Self-sorting of synthons **106a** and **106d** in the presence of C_{60} as a guest. In ^{1}H NMR spectra only NH region is shown for the clarity.

Circular dichroism (CD) spectroscopy provides the means to study chirality of the system. Although porphyrin moieties are achiral molecules due to planar backbone but embedded into chiral scaffold, they become intrinsically optically active, thus CD signals can be detected. TPP chromophore has intense absorption in Soret band region at ca. 417 nm (Figure **73**). High $\Delta\varepsilon$ values of bisignate CD signals observed in spectrum of tetramer in chloroform indicate strong exciton coupling which occurs through space between well-aligned TPP chromophores. Two symmetrical Cotton effects of opposite signs correspond to helicity of enantiopure bicyclo[3.3.1]nonane tetrameric cycle, hence no CD signal was detected in DMSO since capsule collapses into monomeric species. Upon C_{60} encapsulation, CD curve is blue shifted with respect to tetramer **106a$_4$** and, surprisingly, its intensity increased which implies a change in the angle or distance between two TPP. Even though, the exact geometry of the TPP moieties cannot be reliably estimated, the increase of interchromophoric distance is compensated by the more twisted geometry. It is known that exciton coupling is enhanced at ca. 55° angle between TPP units.[206] The major spectral features clearly correlate with the induced-fit conformational changes observed in NMR experiments

demonstrating dynamic supramolecular capsule with adaptable cavity for guest molecules.
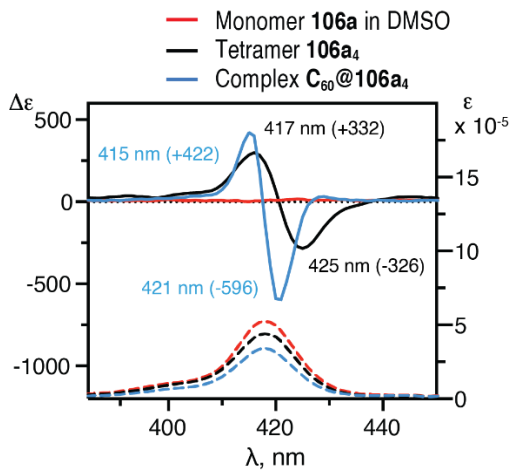
Figure **73**. CD spectra of monomer **106a**, tetramer **106a₄** and complex **C₆₀@106a₄** in chloroform with its UV spectra stacked at the bottom, respectively.

4. π-FUNCTIONAL SUPRAMOLECULAR STRUCTURES COMPRISING 9-AZABICYCLO[3.3.1]NONANE SCAFFOLD

In relation to previous chapter which focused on how varying the spatial arrangement and size of the solubilizing groups influences aggregation modes of supramolecular synthons, the potential of enantiopure 9-azabicyclo[3.3.1]nonane derivatives was utilized. Many natural alkaloids, such as macroline, sarpagine, pavine, ajmaline, etc., contains azabicyclic scaffold which displays a wide array of biological activities making it attractive for synthetic chemists (Figure **74a**).[207,208] In our interest, latter synthon provides access to otherwise inaccessible apex position of bicyclic scaffold, wherein groups attached to nitrogen at 9 position are perpendicular to the monomer backbone and pointing outward (Figure **74b**). Moreover, substituents are placed further away from the hydrogen bonding sites and should not hamper orthogonal propagation of tetrameric cycles into tubular polymers. In fact, further investigation of these derivatives was encouraged by previously reported fruitful polymerization results of azabicyclic hydrogen-bonding monomers bearing large second-generation Fréchet dendron at the equatorial plane.[125]
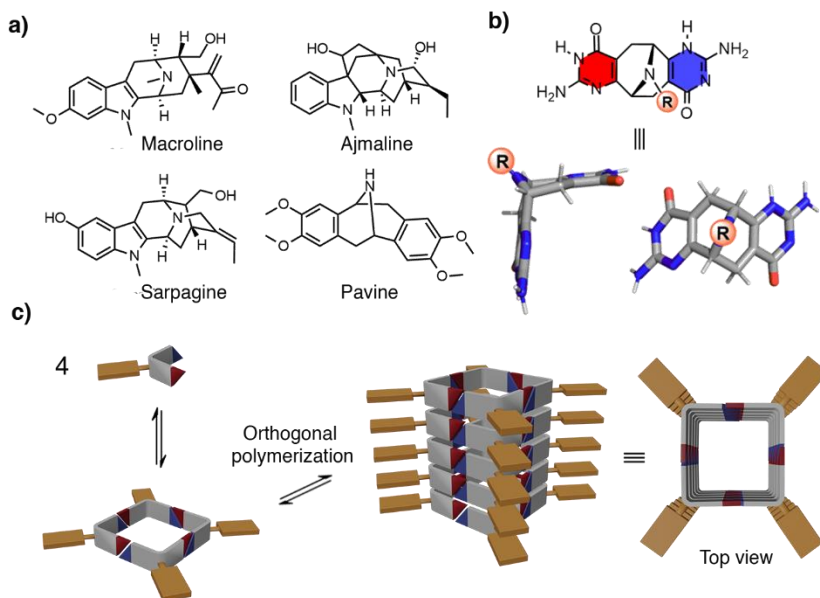
Figure **74**. a) Molecular structure of natural alkaloids; b) structure and molecular model of 9-azabicyclo[3.3.1]nonane bearing substituent to nitrogen at 9 position; c) schematic representation of orthogonal polymerization reinforced by π-π stacking of aromatic substituents.

Additionally, in comparison to monomers **95** comprising flexible linkers, the direct incorporation promotes well-ordered spatial arrangement of the substituents while restricting their movement (Figure **74c**). Cooperative interactions between large π-systems appended at 9 position could potentially come into play and promote the orthogonal stacking of tetrameric units towards tubular polymers via supplementary π-π interactions of planar aromatic substituents.

The simultaneous use of directional and strong hydrogen bonding in conjunction with van der Waals interactions has offered a framework to develop electronically active supramolecular structures possessing high degree of internal order essential for functional materials. π-conjugated systems are the subject of enormous interest as active materials for application in (opto)electronic devices spanning from field-effect transistors (OFETs), solar cells and light-emitting diodes (OLEDs) to photovoltaic devices.[209] Compounds extensively employed for this purpose can be divided into two categories: conjugated polymers, such as polythiophene, poly(phenylenevinylene), polyphenylene and small discrete molecules, such as oligothiophene, pentacene, tetrathiafulvalene, perylene, phthalocyanine, diketopyrrolopyrrole.[209–211] Electrical conductivity is realized by electron delocalization between the overlapping orbitals of the conjugated entities. Organic semiconductors can be labeled as p-type or n-type depending on whether they can transfer holes or electrons, respectively. Ambipolar materials exhibit the ability to transfer both electrons and holes.[212] Charge transfer can be realized either through intramolecular transport over linear π-conjugated backbone or intermolecular hopping between parallel stacked conjugated entities. In the latter case, highly ordered packing systems with planar and rigid backbone in close proximity for strong π-π interactions with overlapping frontier orbitals are necessary to ensure efficient charge carrier mobilities along stacking axis. The spatial arrangement of constituent molecules is typically determined by intermolecular noncovalent forces, such as van der Waals, dipole−dipole, π−π, and hydrogen-bond interactions. Thus, the so-called "bottom-up" strategy provides the means to tailor conducting properties of organic materials by controlling molecular aggregation behavior in multicomponent systems and ensuring well-aligned orientation, crucial to high mobility of charge carrier.

4.1 Recent developments for n/p-heterojunction materials

Materials possessing π-conjugated donor (D) and acceptor (A) arrays are giving rise for high-performance charge transportation in p-type and n-type semiconductors, consequently resulting in an immense interest to D–A heterojunctions. Intrinsic close molecular packing of such systems ensures the modulation of fundamental properties of molecular constituents responsible for efficient charge transfer. Mixing different D–A components opens up possibilities to easily control band gap of overlapping orbitals and to tailor electronic characteristics accordingly. The design of such systems simplifies the manufacturing of complementary integrated circuits by removing additional steps required for coating two separate layers of p-channel and n-channel materials (Figure **75a**).[212,213] For instance, one-step solution processed ambipolar material was produced comprising electron acceptor fullerene C_{60} attached to oligothiophene moiety which is a well-known excellent π-electron donor in semiconductors.[214] Another efficient π-electron donor 9-(1,3-dithiol-2-ylidene)thioxanthene was connected to C_{60} via 1,3-dipolar cycloaddition. Although, they both exhibit ambipolar properties, but separately they suffer from low charge mobilities.[215] Hence, prevention of the interfering charge-transfer interactions between neighboring donor and acceptor channels is essential for suppressing unwanted charge carrier recombination while ensuring efficient electrons and holes movement towards opposing electrodes. Consequently, the development of ambipolar materials is falling behind due to their ambitious architecture since individual n- and p- channels of segregated stacks are hard to achieve.

One of the first instances of segregated heterojunctions was reported by Shmidt-Mende featuring combination of solution processable components like discotic liquid crystals from hexabenzocoronene **HBC** and crystalline network-forming perylene diimide **PDI** (Figure **75b**). In principle, **HBC** discotic liquid crystals tend to spontaneously self-organize into one-dimensional columnar mesophases via mesogenic forces, whereas **PDI** molecules aggregate into micron-scale crystallites scattered across the layer. Spin coating of these components resulted in vertically segregated materials comprising large interfacial area between donor and acceptor units as seen from AFM and SEM images and thus exhibiting good electronical properties for thin-film photovoltaic devices (Figure **75c**).[216]
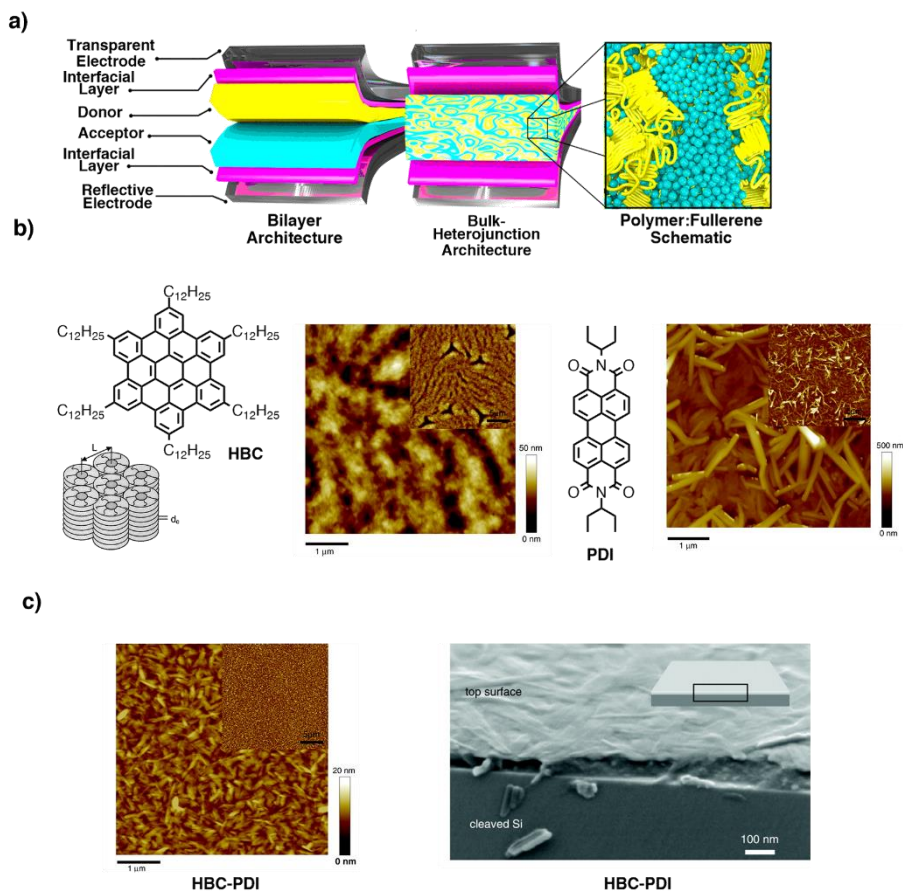
Figure **75**. a) Schematic representation of bilayer (left) and bulk-heterojunction (right) configurations in organic photovoltaic devices; b) tapping-mode AFM images of pure **HBC** and **PDI** surfaces; c) tapping-mode AFM image (left) and field-emission SEM image (right) of **HBC-PDI** mixture. a) and b), c) adapted from ref. 213, 216 with permission from American Chemical Society, 2014 and AAAS, 2001, respectively.

Unfortunately, prevalent interactions in aromatic stacking lack directionality, thus D–A arrangement can adopt multitude of different packing modes ranging from face-to-face parallel, alternating, slipped or face-to-edge. Unfavorable entropic effects hinder segregated arrangement while Coulombic interactions among donor and acceptor promotes heterotopic D–A–D–A stacking. In addition, Hariharan *et al.* investigated total lattice energy of tetrathiafulvalene – tetracyanoquinodimethane stacking mode (Figure **76a**). They stated that higher energy stabilization occurs between D–A components in mixed arrangement.[217] Interaction between frontier molecular orbitals of D–A in a mixed packing can result in decreased energy

difference to a certain extent, although, band gap is not diminished completely. However, extended intermolecular electronic coupling along stacking direction in segregated D-on-D/A-on-A arrangements leads to negligible gap or even overlapping bands which resembles characteristics of metallic bands.[218]
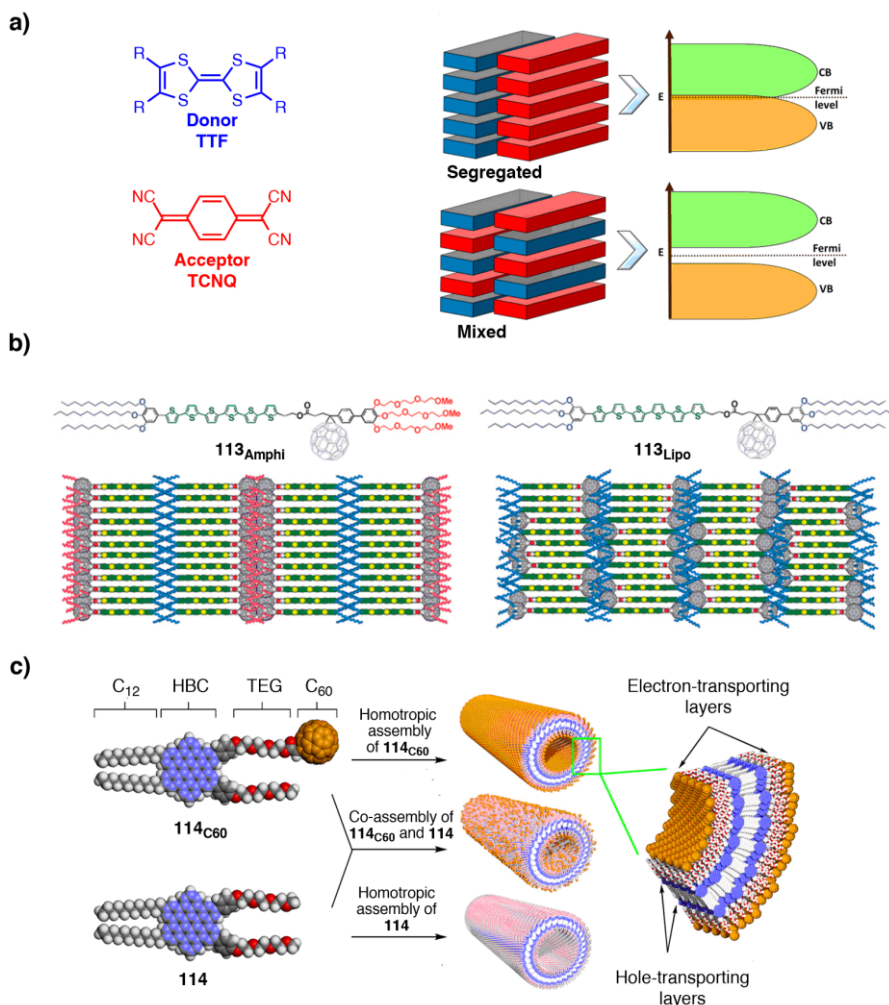
Figure **76**. a) Segregated and mixed stacks of TTF-TCNQ heterojunction architecture; b) molecular orientation of **113**$_{Amphi}$ and **113**$_{Lipo}$ aggregates; c) self-assembly of ambipolar coaxial nanotubes comprising HBC-C$_{60}$ scaffold. Adapted from ref. 218, 219, 220 with permission from American Chemical Society, 2021 (ref. 218), 2008 (ref. 219) and National Academy of Sciences, 2009 (ref. 220).

On the contrary, well-thought-out design of covalently connected donor and acceptor entities ensures improved control over stacking while preventing mixed assemblies. Subsequently, distinct morphologies can be reinforced by additional side chain promoted amphiphilicity[219,220], hydrogen bonding[221–223], metal-coordination[224] or even chiral auxiliaries[197] in conjunction to covalent bonding. For instance, Aida *et al*. developed photoconductive liquid crystals comprising segregated C_{60}–oligothiophene dyad **113$_{Amphi}$** (Figure **76b**). Introduction of incompatible hydrophilic and lipophilic wedges on opposite sides prevented D–A interactions, while promoting spontaneous tail-to-tail arrangement. In comparison, incorporation of lipophilic substituents on both sides resulted in poorly conducting liquid crystals of **113$_{Lipo}$**. The broad absorption band observed at 600 – 800 nm together with synchrotron radiation small angle X-ray scattering (SAXS) profile suggested disordered head-to-tail orientation.[219] In this context, side-chain amphiphilicity induced association of fullerene C_{60} with covalently linked hexabenzocoronene unit **114$_{C60}$** was reported, which co-assembled further into supramolecular nanotubes displaying intrinsic properties of p/n-heterojunction (Figure **76c**). Hole transporting channels are sandwiched between electron transporting C_{60} layers, whereas paraffinic side chains together with phenylene units embedded to hexabenzocoronene direct tubular assembly. Triethylene glycol chains are not essential for the assembly into nanotubes, however, they provide the site for introduction of various functional substituents needed for tuning charge mobility.[220]

An elegant system of zipper assembly mediated through π-π stacking and hydrogen bonding of covalently attached components was designed by Matile *et al*. (Figure **77a**). Highly ordered n/p-heterojunction consisted of alternating building blocks with different naphthalenediimide chromophores linked to rod-like p-oligophenyl or p-oligophenylethynyl h+ transporting backbone, whereas π-acidity and planarity of NDI scaffold in concert with intermolecular hydrogen bonding and ion pairing promoted face-to-face packing of n-channel. Formation of zipper was initiated by deposition of the first component p-quaterphenyl onto gold surface via disulfide linkage. Free anionic ends of the initiator N- stacked with cationic lower half of propagator Y+, whereas upper half would zip up with anionic component Y-. The system was further subjected to dip-wash cycles with cationic R+ and anionic R- components to propagate the architecture to certain length. NDI zipper displayed increased photocurrent generation with smoother surface, essential for solar cells, in comparison to drop casting layer-by-layer assemblies of separated electron or hole-transport materials.[221,222]
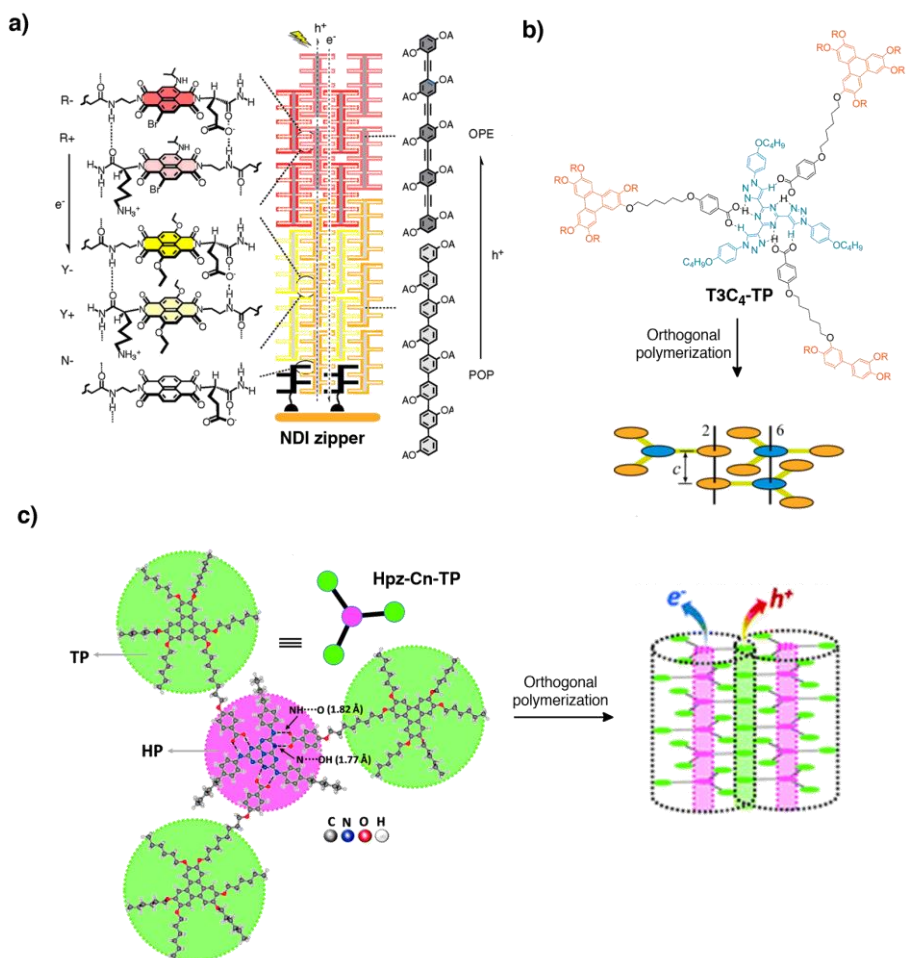
Figure **77**. a) Schematic representation of NDI zipper on gold surface; b) columnar assemblies of b) **T3C₄-TP** and c) **Hpz-Cn-TP**. Adapted from ref. 222, 225, 226 with permission from American Chemical Society, 2010 (ref. 222), 2016 (ref. 225) and the Royal Society of Chemistry, 2021 (ref. 226).

However, such systems require thoroughly designed and structurally complex molecular structures which are usually difficult to achieve. Hence, supramolecular chemistry enables exploitation of smallest possible building blocks of electronically decoupled D and A entities into hierarchical assembly of well-ordered n/p-heterojunctions. In this respect, Giménez and Sierra *et al*. developed hexagonal columnar ambipolar semiconductors **T3C₄-TP** with mesomorphic properties using star-shaped tris(triazolyl)triazine and triphenylene benzoic acids in 1:3 A:D ratio (Figure **77b**). Hydrogen bonding together with mesogenic driving forces directed hexagonal discotic columnar assembly with distinct n- and p-type channels.

Although obtained values for hole and electron mobilities were 1 – 2 folds of magnitude higher, lack of uniform orientation over large area of samples caused the fluctuations of charge mobility in certain sections of the layer. On the other hand, self-error correcting nature of supramolecular architectures resulted in increased charge mobilities over time.[225] Another group utilized heptazine (Hpz) derivatives in similar fashion as an acceptor units for discotic core (Figure **77c**). Its C_3 symmetric core consisting of six nitrogen atoms were embedded with -NH outer groups which ensures hydrogen-bonding with carboxylic groups of triphenylenes (TP). A series of n/p-heterojunctions with varying distance between separated D and A units were synthesized by incorporating different length of methylene spacers. Although **Hpz-C$_n$-TP** complexes with C_8 and C_9 linkers exhibited improved holes and electrons mobility, **Hpz-C$_6$-TP** did not exert ambipolar charge transport behavior. It could be justified by poor alignment of channels based on observations made from images of polarized optical microscopy.[226] Self-assembly of two complementary π-extended tetrathiafulvalene and perylenebisimide fibers, appended with ionic groups of opposite charge, such as carboxylic and guanidinium or quaternary ammonium salt, simplifies a synthetic route for the preparation of building blocks (Figure **78a**). The H-stacking of **PDI-exTTF** complex was corroborated by the appearance of a broad, blue-shifted peak at 500 – 520 nm in the absorption spectrum, whereas well-resolved peak at 400 – 500 nm intrinsic to isolated PDI was not observed unless the assembly was disrupted with MeOH. Well-oriented n/p morphology was further verified using SEM, TEM and SAXS. SEM images displayed vertically aligned fibers with diameters between 10 – 20 nm and with length up to several tens of micrometers. Additionally, AFM images supported formation of fibers with height between 8 – 14 nm, whereas single PDI component afforded structures with height just about 3.0 nm. Electron and hole mobility was examined in films in measurements of flash-photolysis time-resolved microwave conductivity. The obtained values of photo-conductivity transients $(\phi\Sigma\mu)_{max}$ were one order of magnitude higher than values for individual components. Enhancement of charge transport properties was accomplished through parallel long-range n/p-channels in well-ordered fibers.[227]

The work reported so far on segregated D-on-D/A-on-A arrangements is shaping a vision for supramolecular n/p-heterojunction material, however, this concept is still addressed scarcely in the field. Thereby, we propose a rational strategy to create ambipolar supramolecular structures utilizing azabicyclo[3.3.1]nonane scaffold based on its ability to form highly ordered

tubular polymers (Figure **78b**). We envisioned that orthogonal stacking of cyclic tetramers should ensure face-to-face orientation of electron donor appended in a radial position perpendicular to the tetramer. Thus p-type channel would be situated in the outer periphery along the propagation axis, whereas encapsulated fullerene C_{60} inside the cavity potentially would act as a n-type channel. Nitrogen at 9th position of the azabicyclic backbone enables incorporation of various π-conjugated donor units into a scaffold, while facilitating preparation of hybrid architectures with tailored electronic properties.
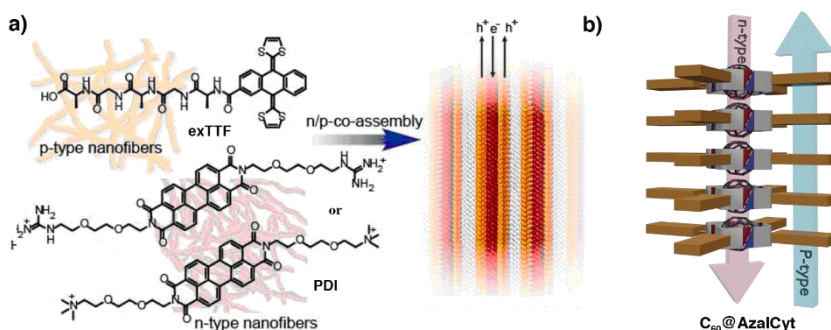
Figure **78**. a) Co-assembly of **exTTF** and **PDI** resulting in segregated n/p-channels in supramolecular polymer; b) orthogonal aggregate **C$_{60}$@AzaICyt** as a potential n/p-heterojunction material for organic semiconductors. a) is adapted from ref. 227 with permission from American Chemical Society, 2015.

4.2 Preparation of building block bearing π-conjugated system

Enantiomerically enriched azabicyclic precursor **(-)-115** was synthesized from commercially available 1,5-cyclooctadiene following previously reported method by Michel and Rassat[228], which was adapted and further developed in Orentas group. The enantiomerically pure diol was obtained through kinetic resolution of the racemic diol utilizing lipase from *Candida rugosa*.[207] N-benzyl protecting group was replaced with 4-bromobenzyl to incorporate an anchor in order to enable straightforward introduction of various functional substituents (Figure **79**). Diol **116** was subjected to catalytic hydrogenation using Pd/C in combination with H_2 in methanol, followed by subsequent nucleophilic substitution reaction with 4-bromobenzyl bromide in acetonitrile. Diol **117** was prepared in 91 % overall yield in two steps. Swern oxidation at -78 °C for 24 hours afforded diketone **118** in high yield. The latter intermediate was treated with lithium bis(trimethylsilyl)amide at -78 °C, and the obtained dienolate was trapped

with ethylcyanoformate in the presence of N,N'-dimethylpropyleneurea giving bis-β-ketoester **119** in 42 % yield.
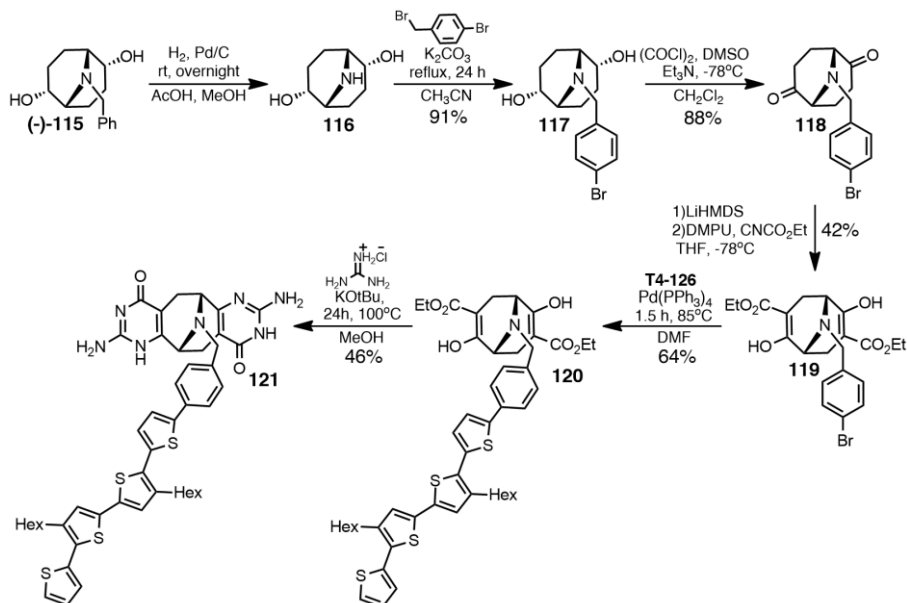
Figure **79**. Synthesis of enantiopure azabicyclo[3.3.1]nonane synthon **121** bearing self-complementary ICyt motif.

In order to incorporate π-conjugated system, tetrathiophene was selected due to its known high potential in application of organic field-effect transistors or photovoltaics devices.[229] To begin with, bromination of 3-hexylthiophene with NBS in acetic acid afforded 2-bromo-3-hexylthiophene **122** in good yield (Figure **80**). Palladium-catalyzed C-H homocoupling of thiophene **122** with AgNO₃/KF system and PdCl₂(PhCN)₂ as a catalyst afforded the corresponding bithiophene **123** in 72 % yield. The conjugated system was extended further by C-C bond formation via Stille cross-coupling reaction in presence of Pd(PPh₃)₄ at 85 °C in a moderate 60 % yield.[230] Tetrathiophene **124** was subjected to regioselective monobromination using NBS. The initial bromination reaction predominantly took place in a more activated α-position, although dibrominated product could not be avoided diminishing the yield of **125**. Lastly, the essential trimethylstannyl- group was incorporated into activated α-position by the use of halogen-lithium exchange with BuLi, followed by a nucleophilic substitution reaction with trimethylstannylchloride in 99 % yield. Although less noxious tributylstannylchloride is more commonly used, trimethylstannylchloride was exploited because of its higher solubility in water. As stannyl-

derivatives tend to decompose on silica gel columns, an excess of unreacted Me₃SnCl was conveniently removed by simple extraction with water resulting in pure compound **T₄-126**.
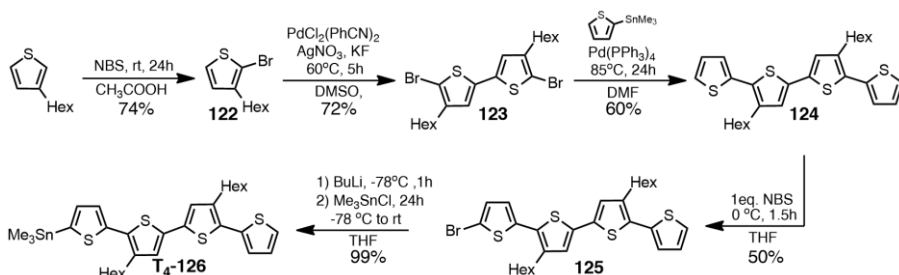
Figure **80**. Synthesis of π-conjugated tetrathiophene derivative **T₄-126**.

The synthesis of 9-azabicyclo[3.3.1]nonane, having π-conjugated tetrathiophene incorporated in the scaffold, was performed utilizing Stille cross-coupling reaction between **119** and organotin **T₄-126** derivatives in DMF at 85 °C for 1.5 hours which resulted in 64 % yield. The monomer **121** was obtained in 39 % yield via condensation of **120** with guanidinium chloride in the presence of KOtBu as a base at 100 °C in MeOH. Unfortunately, close packing enhanced by conjugated system caused poor solubility of the corresponding ICyt **121** in organic solvents and therefore, it could not be used for further association studies in solution. To increase the solubility, various bulky groups had to be incorporated into bicyclic scaffold. For example, incorporation of 3,5-dibromobenzyl instead of 4-bromobenzyl enabled the synthesis of more branched derivative. Regrettably, Stille cross-coupling between 9-(3,5-dibromobenzyl)-9-azabicyclo[3.3.1]nonane and **T₄-126** did not yield the desired product. Additionally, there were attempts to attach tetrathiophene entities through thiol linkers to bicyclo[3.3.1]nonane **90**, however, without any success. Hence, another strategy was utilized in order to add dithiafulvenyl unit bearing decyl chains at the terminal α-position of tetrathiophene (Figure **81**). For this purpose, aldehyde-capped tetrathiophene **130** was prepared by Vilsmeier-Haack formylation reaction according to previously reported procedure.[231] The dithiafulvenyl fragment was obtained in moderate yield from DMF-mediated sodium metal reduction of carbon disulfide. 1,3-dithiole-2-thione-4,5-dithiolate was isolated as zinc-coordinated tetraethylammonium salt **127**. The zinc salt **127** was subjected to nucleophilic substitution reaction with 1-bromodecane in 26 % yield.[232] Resulting dithiafulvenyl derivative **128** was condensed with tetrathiophene **129** in neat P(OEt)₃ in 21 % yield. The decisive step was the incorporation of

101

the solubilizing fragment into azabicyclo[3.3.1]nonane **131a** scaffold. Boc protecting group was removed using TFA and the resulting **131a** salt was directly subjected to reductive amination using sodium triacetoxyborohydride in the presence of triethylamine. However, reaction did not proceed as expected, probably because of electron-donating nature of **130** fragment. Therefore, anticipated product was not obtained.
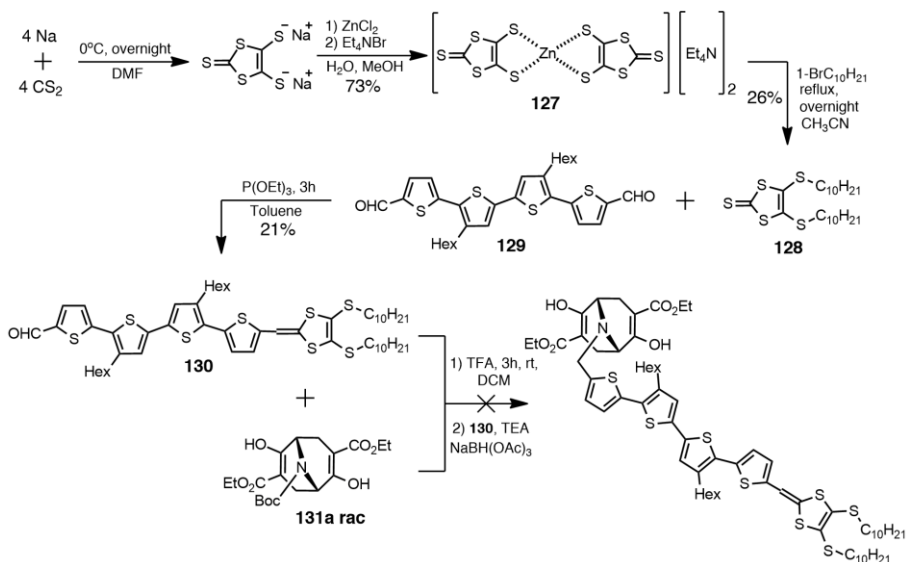
Figure **81**. Synthesis of 9-azabicyclo[3.3.1]nonane synthon comprising π-conjugated substituent.

Instead, it was chosen to incorporate tetrathiafulvalene (TTF) in place of tetrathiophene unit because of its exceptional π-electron donating characteristics. Precursor **134** was synthesized in three steps starting from dibromoethane according to reported procedure (Figure **82**).[233–235] TTF **135** was obtained by using unsymmetrical cross-coupling involving **128** and 2-thioxo-1,3-dithiole **134**. Despite the formation of symmetrical TTF from self-condensation between **128** or **134**, the corresponding product **135** was isolated in 51 % yield. Treatment of the diester **135** with LiBr at 85 °C for 3 hours yielded selective monodecarboxylation in 87 %. However, prolonging reaction time would lead to complete removal of carboxylate groups. Subsequent ester hydrolysis in the presence of LiOH aqueous solution in dioxane afforded monoacid **137** in 98 % yield. The latter intermediate was treated with oxalyl chloride in the presence of a catalytic amount of pyridine to provide the acyl chloride derivative **TTF-138** in surprisingly low yield.
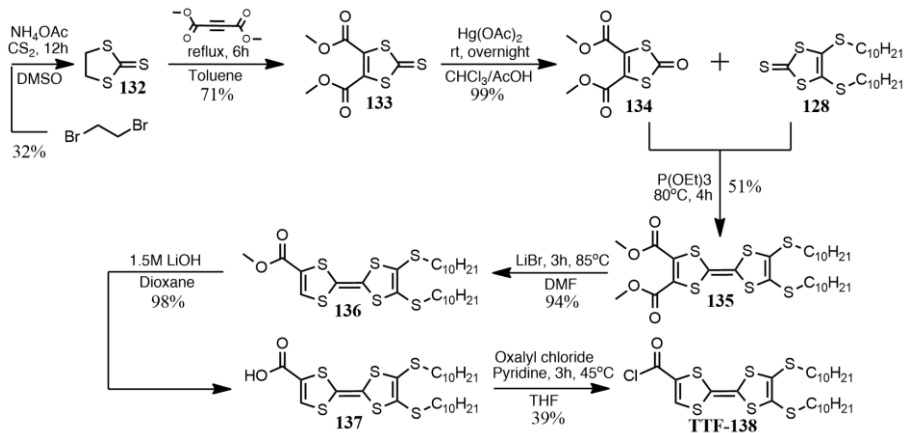
Figure **82**. Synthesis of tetrathiafulvalene derivative **TTF-138**.

Synthetic route for the desired monomer was initially optimized utilizing racemic derivatives and then employed to obtain the final enantiopure ICyt **140b** building block (Figure **83**). Boc group was removed by treating **131** with TFA, followed by acylation using **TTF-138** acylchloride in the presence of TEA as a base. The racemic and enantiopure amides **139a** and **139b** were obtained in 67 % and 80 % yields, respectively. Lastly, condensation with guanidine carbonate at 100 °C in MeOH yielded monomers **140a** and **140b** in 52 % and 61 % yield, respectively. The solubility of the ICyt derivatives **140** was greatly improved in comparison to previously obtained monomer **121**, thus it was subjected further to aggregation studies and host-guest chemistry.
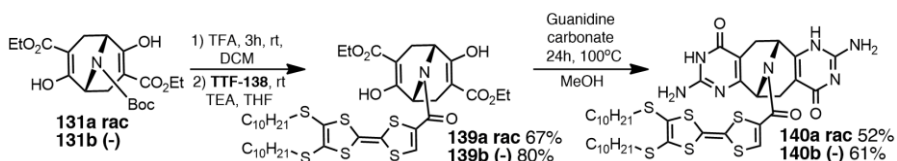
Figure **83**. Synthesis of targeted 9-azabicyclo[3.3.1]nonane synthon comprising TTF scaffold.

4.3 Self-assembly of chiral tubular polymer

Tautoleptic aggregation of novel enantiopure TTF-ICyt synthon **140b** was achieved via self-complementary DDA-AAD hydrogen bonding units between two N^1-H and N^3-H tautomeric forms attached on the opposite edges of bicyclic scaffold (Figure **84a**). Simultaneously orthogonal propagation of newly formed cyclic tetramer was further directed by the

bifurcated hydrogen bonds along the rims of the tetramer. The robustness of the whole supramolecular system benefits from π-π interactions occurring from newly incorporated planar TTF units. Tubular polymeric architecture resulted in gel-like highly viscous solution in either chloroform or toluene. Therefore, it could not be further characterized at the molecular level due to broadened signals in ^{1}H NMR spectrum in chloroform and toluene, however the formation of viscous solution itself is indicative of the formation of polymeric aggregates (Figure **84b**). Highly polar DMSO decreases stability of aggregate by suppressing hydrogen bonding, therefore, sharp resonances were observed in ^{1}H NMR spectrum which could be clearly attributed to monomeric species.
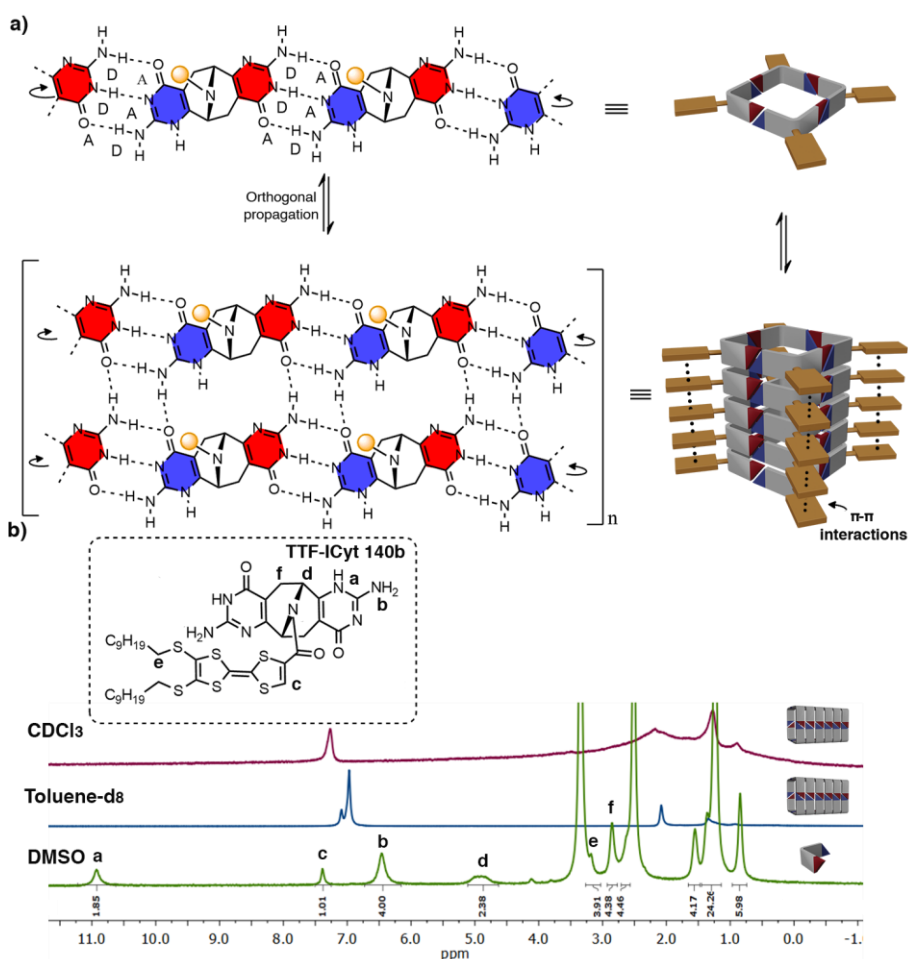
Figure **84**. a) Orthogonal aggregation of TTF-azabicyclo[3.3.1]nonane **131**; b) ^{1}H NMR spectra of synthon **140b** in CDCl$_3$, toluene-d$_8$ and DMSO with assigned proton's resonances.

Additionally, molecular modeling was used to further support aggregation of TTF-ICyt **140b** synthon into tubular polymers. The geometry of tetrameric aggregate was calculated using semi-empirical PM3 as implemented in Spartan'14 (Figure **85a**). As seen from the molecular model, the width of the cavity is 12.3 Å, a perfect fit for fullerene C_{60} as a potential guest in host-guest studies. Molecular electrostatic potential surface of tetramer **140b$_4$** helps to visualize the charge distribution in the corresponding aggregate, where dark blue and deep red corresponds to electron deficient and electron rich regions, respectively (Figure **85b**). Top and bottom rims of the structure have opposing electron density distribution which is one of the driving forces for orthogonal propagation (Figure **86a**).
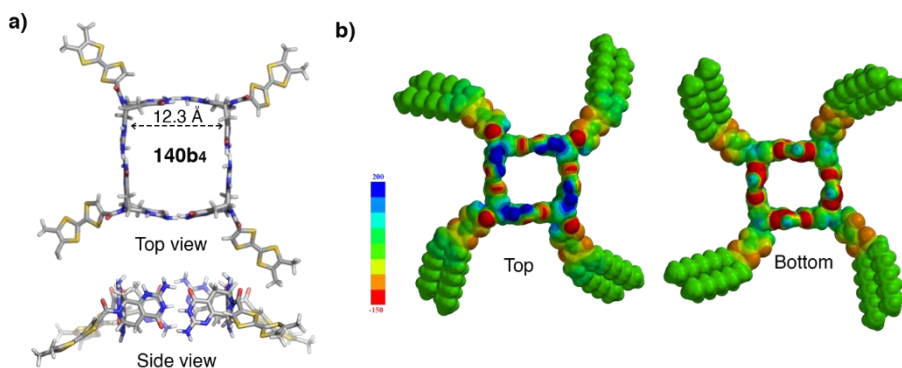
Figure **85**. a) Top and side views of the optimized molecular models of enantiopure TTF-ICyt **140b$_4$**; Alkyl chains were replaced with CH_3 for the clarity; b) Top and bottom view of molecular electrostatic potential map of tetrameric cycle; red color corresponds to electron rich areas, blue – electron deficient.

Furthermore, optimized molecular model of tetrameric species was utilized to assemble a tubular polymer. In this case, molecular mechanics MMFF force field method was used instead to optimize the obtained nanotube due to high number of atoms that increases computation time tremendously. As was anticipated, despite the long alkyl chains, planar TTF moeities are nearly perpendicular to the azabicyclo[3.3.1]nonane scaffold and are able to stack efficiently along propagation axis with 6.3 Å space between the bicyclic backbones (Figure **86b**). Though, TTF units are slightly shifted downwards in the same direction.
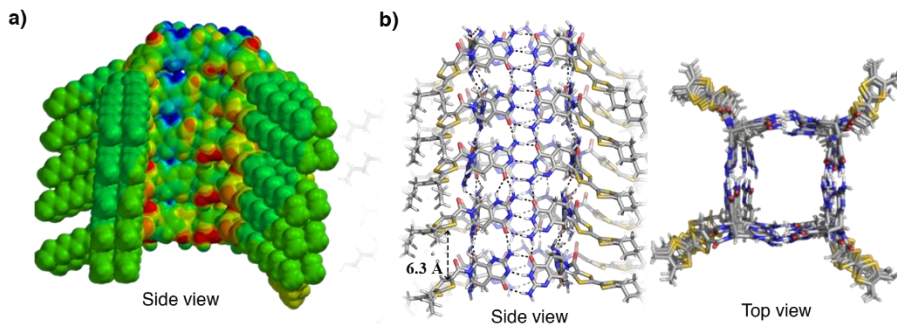
Figure **86**. a) Side view of molecular electrostatic potential map of tubular nanotube; blue color corresponds to electron rich areas, red – electron deficient; b) Top and side views of the optimized molecular models of enantiopure polymer; Alkyl chains were replaced with CH_3 for the clarity; H-bonds are presented by black dashed lines.

Subsequently, as a mean to probe the host-guest chemistry of tubular supramolecule, fullerene C_{60} was complexed within its well-defined inner space (Figure **87a**). We envisioned, that inclusion complexes with fullerene would be energetically favored due to the presence of van der Waals interactions between $-C_{60}-C_{60}-$ inside the cavity. Considering that size of C_{60} matches dimensions of the hollow, in theory, the tetramer could encapsulate guest in 1:1 ratio. However, exact ratio could not be determined. The optimized lowest energy molecular model suggests, however, that terminal guest molecules are glued to the rims of polymer, instead of being fully within cavity (Figure **87b,c**).

Encapsulation experiments were performed by heating enantiopure TTF-ICyt **140b** monomer in toluene at 90 °C until all precipitate dissolved. Allowing the obtained orange solution (c = 11mM) to cool down undisturbed at room temperature would result in the formation of a gel. Then, in respect to the tetramer **140b₄**, 1.0 equivalent of guest C_{60} was added and the mixture was heated at 90 °C until no insoluble residue was left. Successful encapsulation was evident from the change of the color from orange to brown, which is typical for C_{60} complexes (Figure **87d**). The obtained brown solution was left to cool down to room temperature and resulted in the formation of a gel confirming that the polymer was still intact. Additionally, guest complexation was further corroborated by UV-vis spectroscopy. Absorption spectrum in toluene displayed hypsochromic shift of C_{60} absorption band by 3 nm to 333 nm, whereas absorption band of the free guest is at 336 nm (Figure **87e**). No change in band attributed to TTF unit at

300 nm confirms that it does not interact with guest molecule, fullerene being completely entrapped in the cavity.
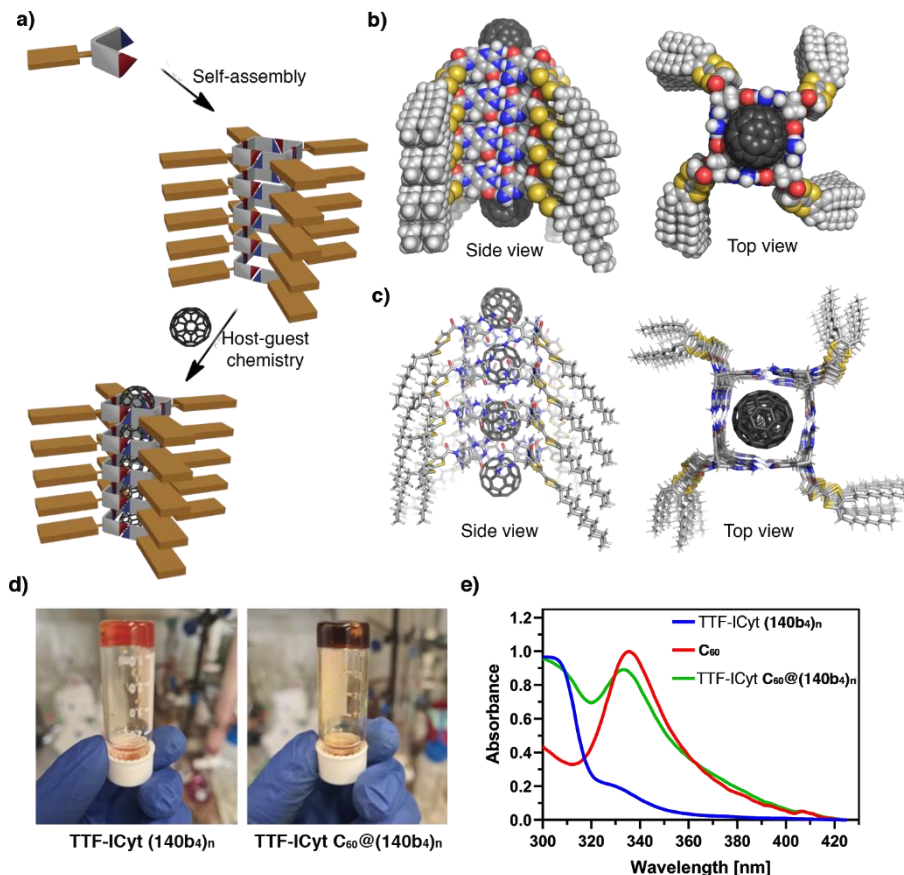
Figure **87**. a) Schematic representation of supramolecular aggregation followed by guest encapsulation; b) Top and side views of space filling model of complex $C_{60}@(140b_4)_n$; c) Top and side views of molecular model of complex $C_{60}@(140b_4)_n$; d) gels of $(140b_4)_n$ (left) and $C_{60}@(140b_4)_n$ (right) in toluene (c = 11mM); e) normalized UV spectra of $(140b_4)_n$, C_{60} and $C_{60}@(140b_4)_n$ (c =1 µM) in toluene.

Control experiments of the complexation were performed with the racemic TTF-ICyt **140a** as well. As anticipated, due to completely different aggregation mode it failed to produce gels in chloroform and toluene, thus resulted in precipitation of the compound. The racemic mixture of synthon **140a** may undergo heterochiral aggregation between two different enantiomers and form zig-zag structures, which could propagate further into

two-dimensional sheets via hydrogen bonding between adjacent isocytosine moieties (Figure **88a**). Moreover, encapsulation of guest molecule did not take place while heating synthon **140a** together with C_{60} in neither toluene nor chloroform .
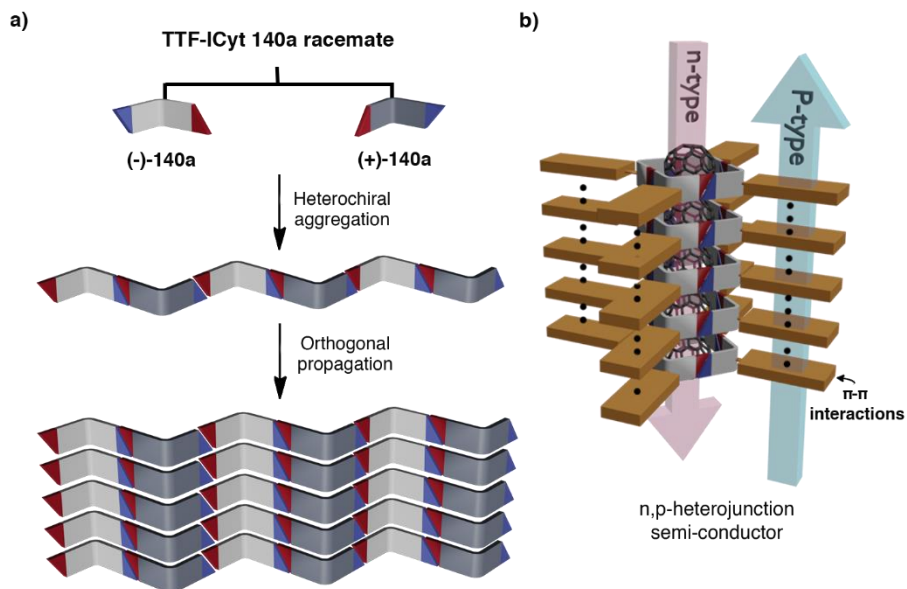
Figure **88**. a) Schematic aggregation of racemic TTF-ICyt **140a** synthon; b) enantiopure complex TTF-ICyt $\mathbf{C_{60}@(140b_4)_n}$ as a synthon for supramolecular n,p-heterojunction material.

The results obtained so far highlight the potential of TTF-ICyt $\mathbf{C_{60}@(140b_4)_n}$ tubular polymer as a candidate for novel supramolecular n,p-heterojunction material comprising electronically decoupled n- and p-type channels (Figure **88b**). Alignment of the channels is ensured by hydrogen bonding in conjunction with favorable π- π interactions between planar TTF entities in radial positions of nanotube. Fullerene entrapped within the cavity is perfectly suitable as an electron transport material since it is well-known for electron acceptor properties, whereas TTF units stacked in face-to-face orientation should potentially exhibit excellent hole mobility.

5. DYNAMIC CHIRAL MOLECULAR TWEEZER

Supramolecular chemistry has grown tremendously by implementing insights acquired from biological processes into state-of-art architectures at the molecular level. The next stage is to introduce function into supramolecular systems; hence it is essential to gain control over dynamicity and reversibility of the system. Host-guest chemistry has made a significant contribution towards fit-induced receptors and recognition systems. However, the construction and use of a recognition element that can reversibly change its geometric form, electronic properties, complementarity, and affinities in response to an external agent is essential for future applications in smart materials, systems chemistry and biology.

Meanwhile various strategies are being employed to utilize tautomerization as a mean to control self-association which would open up a possibility to alter the composition of supramolecular copolymers based on the recognition behavior of the complementary units. Potentially, 2,7-diamino-1,8-naphthyridine (DAN) **142** comprising pre-organized DAAD array disrupts Upy homodimer **141:141** favoring the anticipated DAAD:ADDA heterodimer interaction between DAN and Upy moieties **141:142** (Figure **89a**). The obtained DAN-Upy heterocomplex comprising additional stabilizing intramolecular hydrogen bond in Upy motif has a remarkably high association constant $K_a > 10^4$ M^{-1}.[236,237] Further studies exploiting differing levels of fidelity and association in quadruple hydrogen-bonded systems were carried out. Addition of AUPy **145** into a pre-mixed solution containing DAN-Upy **143:144** led to a disassembly of the former heterocomplex followed by formation of a new dimer DAN-AUPy **143:145** and narcissistic regeneration of Upy-Upy **144:144** (Figure **89b**). The necessity to maximize number of hydrogen bonds to ensure the stability of the entire system promotes a self-sorting network. The challenge here is to imitate transitions occurring between different components of protein assemblies in biological systems.[238] Likewise, self-sorting could be triggered by external stimuli unmasking hydrogen bonding pattern in one of the motifs. A photochromic switch **146** comprising azobenzene unit attached to Upy derivative can be utilized to facilitate assembly of smart supramolecular architectures. Photo-locking strategy is based on ability of azobenzene chromophore to undergo reversible trans – cis isomerization in response to light. The ability to participate in association for Upy moiety in **E-Azo-Upy** is hindered by intramolecular hydrogen bonding with azobenzene unit. UV light-mediated isomerization uncovers complementary hydrogen bonding

site by changing its conformation which results in an enhanced heterodimerization with DAN **147** (Figure **89c**). Upon visible light irradiation, the system switches back to the initial state suppressing any association.[239] Such recognition systems are ought to permit modulation of self-assembly networks in a novel manner for the development of various receptors.
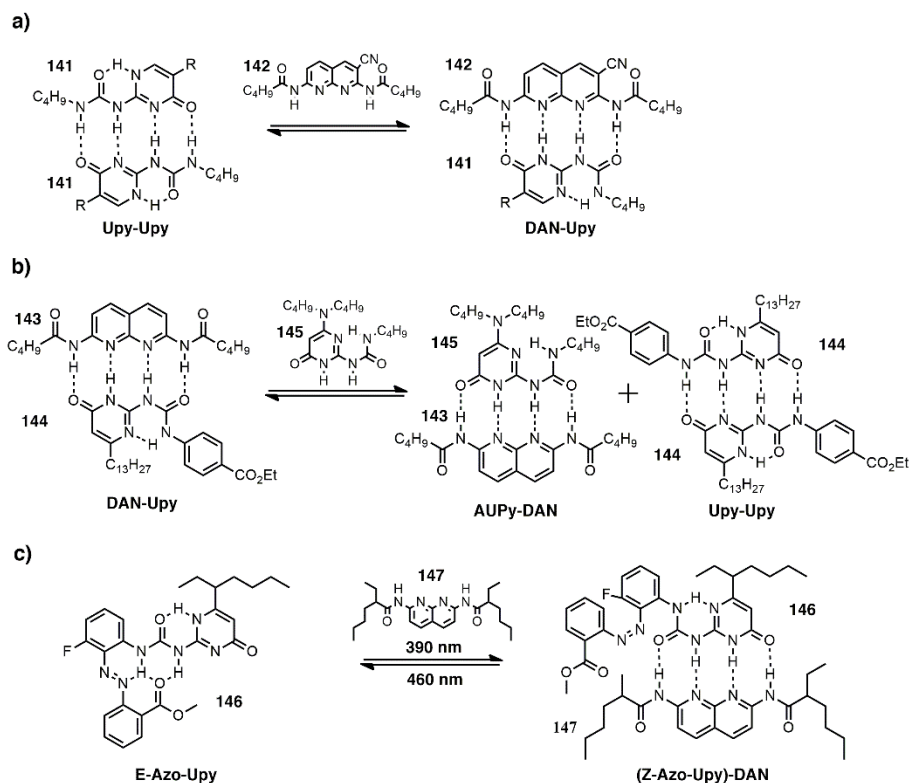
Figure 89. a) Heterodimerization between Upy and DAN units; b) rearrangement of heterodimers driven by self-sorting behavior; c) a photo-switchable heterodimerization comprising photoactive azobenzene unit.

We introduce a strategy solely based on hydrogen-bonding to transform tetrameric aggregates via external stimuli into an open-ended supramolecular construct, the so-called tweezers. Molecular tweezers pioneered by Whitlock are U-shaped tubular architectures with an open cavity between two interaction sites which provide a more facile entry for the guest molecules and can potentially serve as synthetic molecular receptors.[240]

The tetrameric **Upy-Upy₄** components are bound together by strong quadruple hydrogen bonds which are hard to outcompete, especially when the process is entropically unfavored. Thus, for this purpose a C_1-symmetric monomer **Pupy-Upy** was employed. Owing to electronic factors, ureidopyrimidinones fused with electron-rich pyrrole ring favor ADDA over DDAA or DADA hydrogen-bonding arrays. Previously developed in Orentas group, Pupy-Pupy synthon has served as an excellent building block for various supramolecular structures providing 2D H-bonding network between orthogonally located 2H-bonding sites.[241] By introducing the 2H-bonding Pupy unit into the tetrameric aggregate, cooperativity could be potentially disrupted at two point hydrogen-bonding site. DAN ought to primarily prefer heterodimerization with Pupy unit via DAAD – ADDA hydrogen-bonding array leaving Upy unaffected. The propensity of the system to maximize the number of hydrogen bonds could in theory push equilibrium towards the cleft structure. Hence, in our group earlier synthesized monomer **Pupy-Upy 148** was selected as a suitable candidate towards entirely supramolecular hydrogen-bonded tweezer. The synthesis of monomer was presented in recent publication.[242]

Surprisingly, characterization of tetrameric cycle **Pupy-Upy₄** using 1D and 2D NMR spectroscopy revealed the presence of quadruple hydrogen-bonding mode between Pupy units via enolic tautomer instead of the envisioned two hydrogen-bonding (Figure **90**). Enolic form was exposed by the absence of the most downfield shifted cross-peak in $^1H – ^{15}N$ HSQC spectrum. In the ROESY spectrum, the corresponding proton **f** at 14.03 ppm showed through-space interactions with the benzylic proton H_{Ar} and protons H_2 and H_1 residing on the bicyclic backbone. Proton **a** at 13.14 ppm gives correlation to the proton H_{Ar} as well to H_1, H_4 indicating that they are on the same side. Hence, this proton resides on a nitrogen atom. NOE cross-peak of proton **f** with adjacent proton **e** confirms the presence of DADA-ADAD binding mode between Pupy motifs. Proton **d** at 9.86 ppm was assigned to terminal urea on Pupy side due to its interactions with N-methyl from the pyrrole ring and protons H_5 from the butyl chain. Lastly, proton **c** at 10.22 ppm was assigned to NH resonance of terminal urea on Upy side due to its NOE interaction with H_3 from the butyl chain and the neighboring proton **b**. DOSY experiment confirmed the presence of only one type of discrete species with an approximate hydrodynamic radius of 20 Å since all resonances correlated to same value of diffusion coefficient $D = 2.05 \cdot 10^{-10}$ $m^2 s^{-1}$.
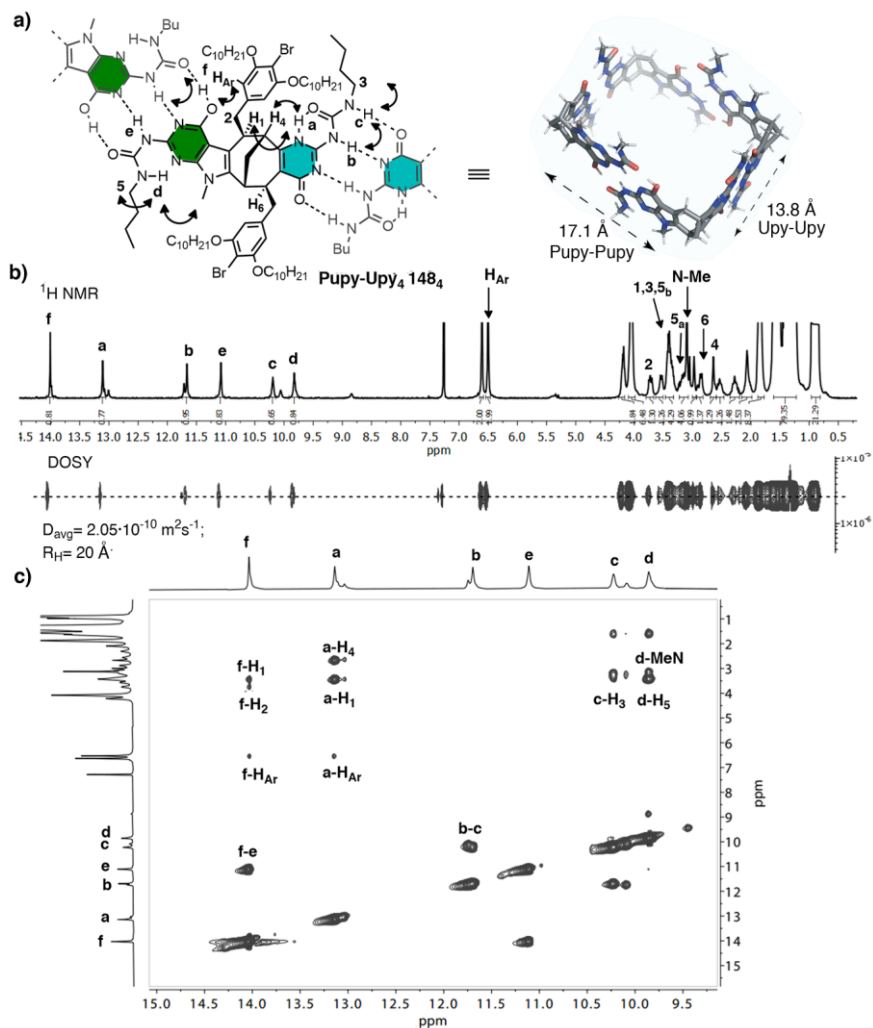
Figure **90**. a) Quadruple hydrogen bonding modes of cyclic **Pupy-Upy₄** with main through-bond and through-space interactions indicated by arrows (left) and its molecular model (semi-empirical, PM3; substituents are removed for clarity); b) ^{1}H NMR spectrum of tetramer **Pupy-Upy₄** in CDCl₃ with DOSY trace stacked at the bottom; c) main ROESY cross-peaks used for structural assignment.

Subsequently, tetrameric aggregate was subjected to selective transformation into a tweezer upon introduction of a rival noncovalent agent. The newly obtained tetramer **Pupy-Upy₄** was mixed with stoichiometric amount of **DAN** in CDCl₃ (Figure **91a**). As anticipated, a new set of eight downfield NH resonances appeared in ^{1}H NMR spectrum which indicated formation of a new species (Figure **91b**). The ^{15}N-^{1}H HSQC further elaborated that all

eight downfield resonances belong to N-H protons, thus enolic binding mode can be dismissed. Alongside ^{15}N-^{1}H HSQC experiment, a newly obtained **Pupy-DAN** dimer in DAAD-ADDA hydrogen bonding arrangement was corroborated by ROESY cross-peaks, where protons **g, h** show correlation with α-protons of amide chain in **DAN** and to adjacent resonances of NH in **Pupy** unit, respectively.
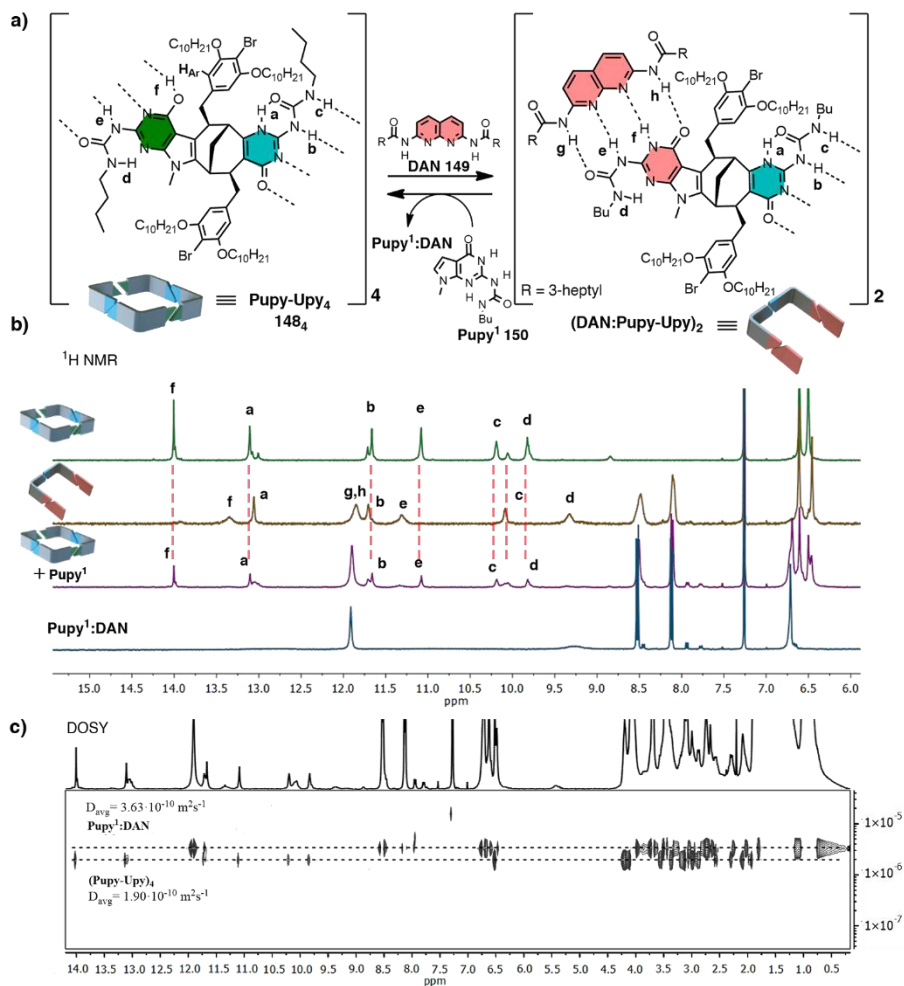
Figure **91**. a) Reversible formation of the so-called tweezer **(DAN:Pupy-Upy)₂** via competitive non-covalent interactions; b) ^{1}H NMR spectra of tetramer **Pupy-Upy₄** (top), tweezer **(DAN:Pupy-Upy)₂** (middle) and a mixture of tetramer **Pupy-Upy₄** with **Pupy¹:DAN** (bottom) in CDCl₃; c) DOSY traces of tetramer **Pupy-Upy₄** with **Pupy¹:DAN** mixture.

The chemical nature of protons **e**, **f** was corroborated by labelling isocytosine ring of **Pupy** unit with ^{15}N isotope. The corresponding protons on labeled nitrogen atoms split into triplets and the chemical shift of ^{15}N attached to proton **e** at 147 ppm coincided with typical shift attributed to H[3] keto form of isocytosine ring. Hydrodynamic radius R_H = 17.3 Å obtained from DOSY experiment revealed the presence of smaller aggregates compared to tetramer, which is in line with the expectations since longer Pupy-Pupy side is dismantled upon DAN induced rearrangement.

Subsequently, addition of excess of competing **Pupy**[1] converted supramolecular tweezer back into cyclic tetramer, thus rendering topology of the system to be fully reversible. Reemergence of signals characteristic to the tetramer **Pupy-Upy$_4$** together with additional peaks attributed to **DAN:Pupy**[1] corroborated high fidelity for homo-aggregation. In DOSY experiment, the presence of both species can be observed with corresponding diffusion coefficient D = $1.90 \cdot 10^{-10}$ $m^2 s^{-1}$ and $3.63 \cdot 10^{-10}$ $m^2 s^{-1}$ for tetramer and **DAN:Pupy**[1], respectively (Figure **91c)**.

Furthermore, topology of the system could be manipulated by external stimuli-induced masking of hydrogen bonding pattern in one of the units. For this purpose, redox-active **DAN** component, pioneered by Zimmerman *et al.*[243] was selected. Quadruple DAAD hydrogen bonding array in **red-DAN** can be transformed to noncomplementary DAA array in iminoquinone (**ox-DAN**) under oxidative conditions in the presence of cobalt salcomine and molecular oxygen in benzene. The broadened resonances in ^{1}H NMR spectrum were observed upon addition of **red-DAN** into a solution of tetramer **Pupy-Upy$_4$** in benzene, as a result of the formation of isomeric tweezers due to nonsymmetric nature of **red-DAN** (Figure **92**). The formation of exclusively tweezer architecture is corroborated by the disappearance of resonances corresponding to tetramer in ^{1}H NMR as well as diffusion coefficient D = $2.30 \cdot 10^{-10}$ $m^2 s^{-1}$ (R_H = 15.7 Å), consistent with previously obtained values for the cleft architecture. Adding stoichiometric amount of Co(salen)$_2$ into oxygen sparged reaction solution resulted in **red-DAN** conversion to **ox-DAN**. As follows, **ox-DAN** is no longer complementary to Pupy moiety and the tweezer is reverted back to the tetramer. Although resonances are broadened in ^{1}H NMR spectrum due to existence of paramagnetic Co^{2+} species in the reaction mixture, characteristic set of signals for tetramer can be clearly observed.
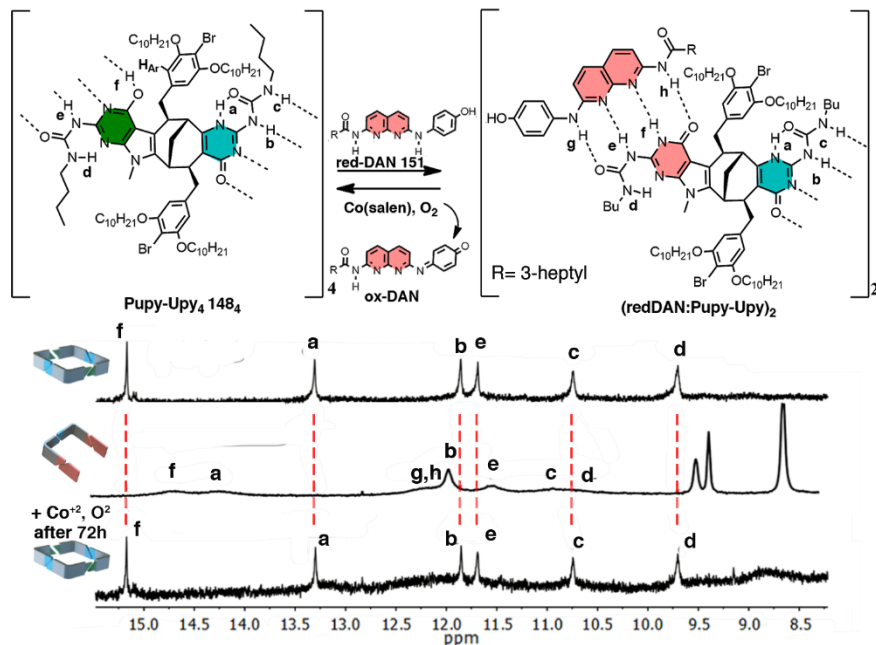
Figure **92**. Reversible formation of tetramer into tweezer and vice versa as a result of chemically induced interconversion of red-DAN and ox-DAN. ^{1}H NMR in C_6D_6 of tetramer **Pupy-Upy$_4$**, tweezer (**red-DAN:Pupy-Upy)$_2$** (middle) and recovered tetramer (bottom).

Both above methods provide the control over the topology by employing chemical stimuli to target selectively DAN:Pupy pair without the necessity to incorporate responsive unit into a scaffold. However, disassociation of Upy-Upy pair needs to be addressed in an effort to fully disrupt the inner cavity within tubular architecture. Hence, we introduce light-modulated proton transfer as an unconventional method to exert control over self-association of Upy motifs in a fully reversible manner. Zwitterionic protonated merocyanine photoacids are known for their ability to release proton upon blue light-mediated nucleophilic cyclization. Resulting cyclic spiropyran thermally recover to the open form by abstracting proton from the protonated species in the dark.[244] Promising results were obtained from initial experiments with dimer **Upy^1:Upy^1**. A mixture of 1.0 equiv. **Upy^1** with 2.0 equiv. **PA** in CDCl$_3$ were irradiated for 1h with 100W blue LED (Figure **93**). Insoluble **PA** dissolved upon photoinduced cyclization while the color of solution changed from colorless to orange. Appearance of a new set of signals corresponds to a newly formed cyclic spiropyran. The disappearance of the downfield NH resonances in ^{1}H NMR spectrum corroborated the protonation of **Upy^1** moiety. Dimer **Upy^1:Upy^1** was

recovered after standing overnight in the dark while protonated **PA** precipitated.
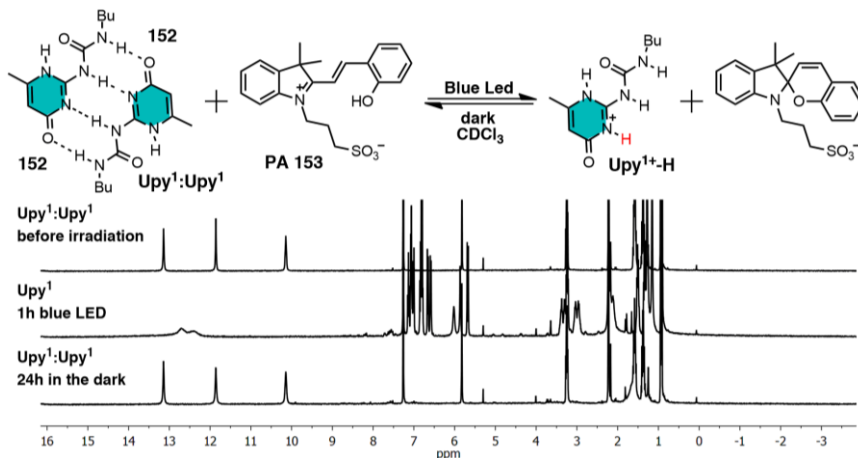
Figure **93**. Blue light-mediated reversible protonation of dimer **Upy¹:Upy¹** in CDCl₃.

In order to probe the selectivity of **PA**, photoinduced protonation was carried out in a mixture of dimers **DAN¹:Pupy¹** and **Upy¹:Upy¹** with 1.0 equiv. **PA** (Figure **94**). According to ¹H NMR spectrum, protonation occurred only on **Upy¹** moiety since no change to resonances assigned to **DAN¹:Pupy¹** was observed. Additional low intensity resonances indicated that small amount of degraded **PA** was left in solution.
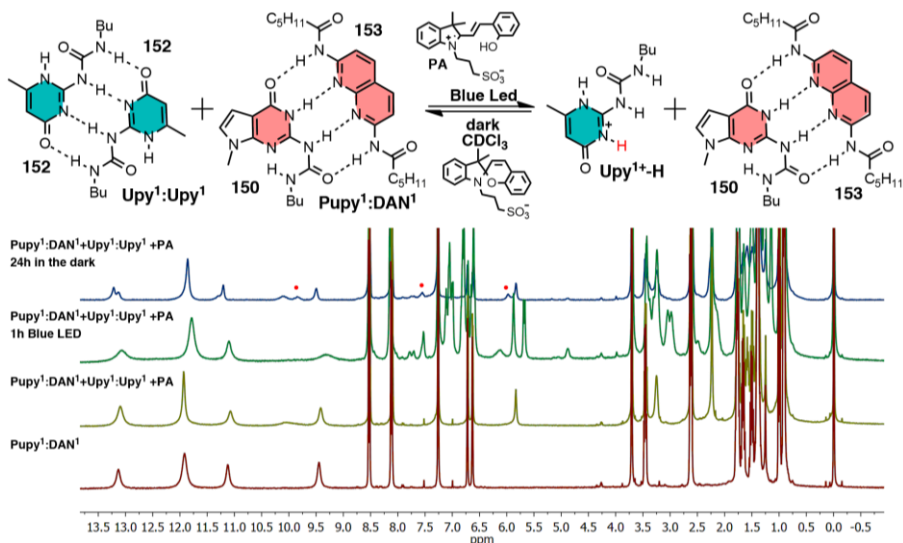
Figure **94**. Blue light-mediated selective protonation of **Upy¹:Upy¹** in a mixture

of dimers **DAN¹:Pupy¹** and **Upy¹:Upy¹** in CDCl₃. **PA** residue marked with red dot.

Subsequently, the application of the photoacid was further extended to our supramolecular architecture. A mixture of tweezer **(DAN¹:Pupy-Upy)₂** with photoacid **PA** were irradiated under blue light in CDCl₃ for 1h (Figure **95a**). Dissociation of **Upy:Upy** motif was apparent from extremely broadened resonances whilst a distinct set of **DAN¹:Pupy** signals remained unaffected (Figure **95b**). In comparison to tweezer, reduced value of hydrodynamic radius (R_H = 11 Å) was obtained from diffusion coefficient (D = 3.70·10⁻¹⁰ m²s⁻¹) which indicated the presence of smaller species. Subsequently, leaving reaction mixture in the dark overnight resulted in completely recovered tweezer.
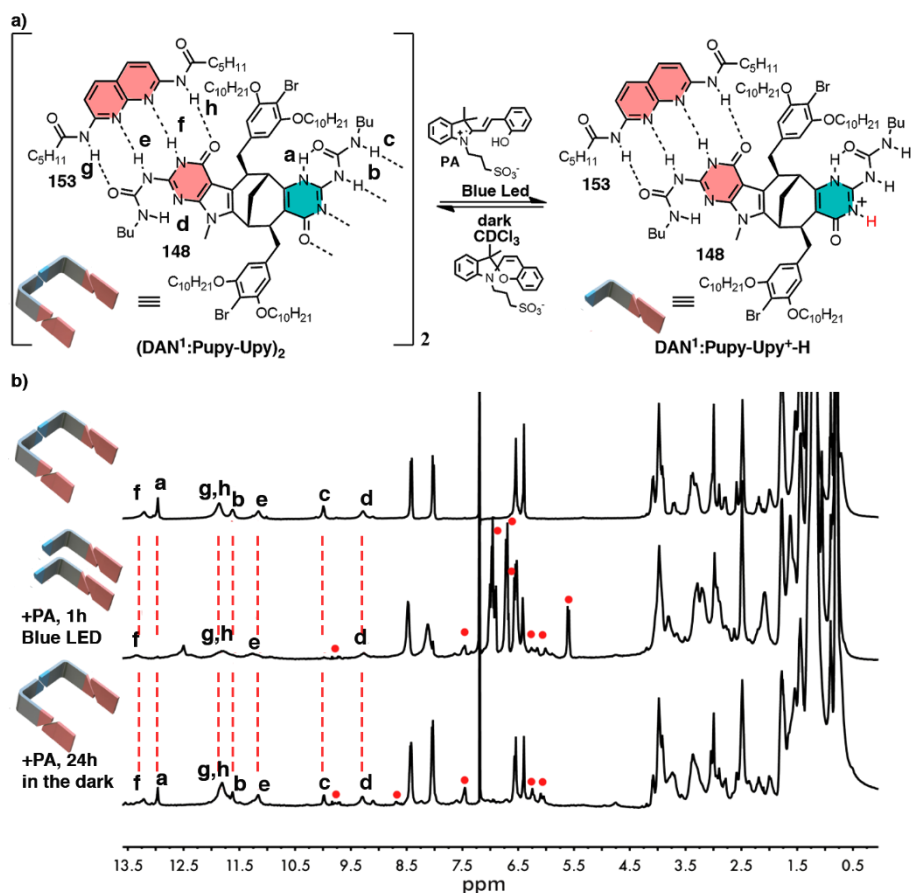
Figure **95**. a) Supramolecular tweezer dissociation via selective protonation of Upy motif; b) stacked ¹H NMR spectrum of reversible dissociation. New resonances emerging from PA marked with red dot.

Taken together, rational strategies were developed to control the topology of supramolecular structures ranging from tetrameric or tweezer to monomeric form without the cavity via chemical or light external stimuli. The development of fully reversible supramolecular aggregates opens the door for their further application in selective binding, guest release or other stimuli-responsive materials.

CONCLUSIONS

1. The strategy to facilitate incorporation of various chromophores into supramolecular scaffold was developed by introduction of nucleophilic thiol anchor via tiol-ene 'click' chemistry. This allowed the extension of the collection of possible supramolecular monomers, including those with bulky substituents.

2. Tubular polymerization of tetrameric aggregates was accomplished by alleviating steric repulsion between peripheral bulky substituents via introduction of flexible linker. Resulting tubular architecture was converted into discrete tetrameric capsules and its capacity to participate in host-guest chemistry was investigated using fullerene C_{60} encapsulation.

3. Fullerene soot and fullerene nanodispersion were successfully employed as a reusable metal-free heterogeneous photocatalysts in blue light-mediated chemoselective oxidation of sulfides to the corresponding sulfoxides in excellent yields. The versatility of this environmentally benign catalyst was effectively demonstrated in radical cyclization, imine formation and boronic acid oxidation reactions. Additionally, its readily implementation in continuous-flow system solved the low scalability issue typical for photochemical reactions, allowing gram scale reactions.

4. Dynamic tetrameric capsule comprising tetraphenyl porphyrin moieties displayed cavity flexibility by induced tautomerization of hydrogen-bonding sites upon fullerene encapsulation. Energetic cost of the rearrangement is fully compensated by CH-π stabilization occurring between peripheral alkyl chains. Fullerene C_{60} promotes high fidelity self-sorting of this novel supramolecular aggregate from a mixture of scrambled similar components.

5. Tubular polymer based on azabicyclo[3.3.1]nonane backbone was synthesized as a novel supramolecular n,p-heterojunction material comprising electronically decoupled n- and p-type channels. Cooperative effect of directional hydrogen bonding between ICyt moieties and π-π stacking between planar tetrathiafulvalenes ensures high degree of internal order with well-aligned n/p channels which is essential for functional materials exhibiting high mobility of charge carriers.

6. The strategy exploiting differing fidelity levels of Upy-Pupy hydrogen bonding modes was introduced as a means to obtain dynamic

supramolecular tweezer. Newly obtained tweezer was assembled solely employing hydrogen bonds. Its reversibility between tetrameric and open-side arrangement was probed using chemical or light external stimuli.

6. EXPERIMENTAL

General. All chemicals were used as received from commercial suppliers. Compounds **83-85**[127], **86**[121], **87-88**[125],5-bis(decyloxy)benzyl bromide[132], bis(MeO-PEG4)benzyl bromide[133], 13-bromo-2,5,8,11-tetraoxatridecane[134], 1-pyrenemethanol[245], **108**[188], **125**[230], **127**[232], **131**[125], **132**[233], **133**[246] were prepared according to reported procedures. All moisture sensitive reactions were carried out under an argon atmosphere using oven-dried glassware. Anhydrous tetrahydrofuran was distilled from benzophenone-sodium. Anhydrous dichloromethane, triethylamine, dimethylformamide, pyridine were distilled from calcium hydride and toluene was distilled from sodium. Yields refer to chromatographically and spectroscopically homogenous material. Reactions were monitored by thin layer chromatography (TLC) carried out on 0.25 mm Merck silica plates ($60F_{254}$), using UV light as the visualizing agent and/or aqueous solutions of vanillin, phosphomolybdic acid, $KMnO_4$ and heat as a developing agent. Flash silica gel chromatography was performed using Fluorochem silica gel (60, particle size 0.043 – 0.063 mm). NMR spectra were recorded at ambient probe temperature on Bruker Avance III 400 MHz (9.0 T) instruments in deuterated solvents and were calibrated using residual undeuterated solvents as an internal reference ($CDCl_3$: ^1H NMR δ = 7.26 ppm, ^{13}C NMR δ = 77.16 ppm, d_6-DMSO ^1H NMR δ = 2.50 ppm, ^{13}C NMR δ = 39.52 ppm, CD_2Cl_2 ^1H NMR δ = 5.32 ppm, ^{13}C NMR δ = 53.84 ppm, CD_3OD ^1H NMR δ = 3.31 ppm, ^{13}C NMR δ = 49.00 ppm). The following abbreviations were used to explain NMR peak multiplicities: s = singlet, d = doublet, t = triplet, q = quartet, p = pentet, m = multiplet, br = broad. ^1H and ^{13}C peaks were assigned with the aid of additional information from 1D and 2D NMR spectra including H,H-COSY, ROESY, HSQC and HMBC. High resolution mass spectra (HRMS) were recorded on an Agilent LC/MSD TOP mass spectrometer by electrospray ionization time-of-flight (ESI-TOF) reflectron experiments or on Thermo Fisher Scientific Q Exactive PLUS hybrid quadrupole-Orbitrap mass spectrometer instrument via direct infusion. Scanning electron microscopy (SEM) images were taken for the morphology characterization with Hitachi SU-70 SEM. Samples for SEM characterization were prepared by dispersing particles on a carbon plate. Melting points were recorded with a Gallenkamp apparatus and are not corrected. The absorption spectra were recorded with a Perkin-Elmer Lambda 35 spectrometer. CD spectra were recorded on Jasco J-810 spectrometer in millidegrees and normalized into $\Delta_{\varepsilon max}$ [L mol^{-1} cm^{-1}]/λ[nm] units.

Diffusion ordered NMR spectroscopy (DOSY). DOSY experiments were performed on a 400 MHz Bruker Avance NMR spectrometer equipped with an Accustar z-axis gradient amplifier and an ATMA BBO probe with a z-axis gradient coil. All experiments were run using insert tubes and without spinning to avoid convection. All calculations were performed using standard applications in Bruker Topspin and MestReNova software. Diffusion was measured at 25 °C using standard Bruker pulse sequence, stegp1s, employing a stimulated echo sequence and 1 spoil gradient with a diffusion gradient, δ, set to 2 ms and the diffusion time, Δ, to 120 ms. The rectangular gradient pulses applied S3 ranged from 2% – 98% of the maximum gradient output of 48.15 Gauss/cm. The number of gradient steps was set to be 32. Individual rows of the quasi-2-D diffusion databases were phased, baseline corrected and aligned. At least three peaks were analyzed for each compound to obtain the average.

6.1 Experimental section for Chapter 2: Hydrogen-Bonded Supramolecular Architectures Possessing Well-Defined Cavity

89
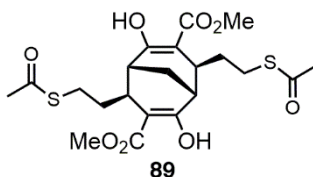
(1R,4S,5R,8S)-dimethyl-*exo,exo*-4,8-bis(2-(acetylthio)ethyl)-2,6-dihydroxybicyclo[3.3.1]nona-2,6-diene-3,7-dicarboxylate 89. Under inert atmosphere a mixture of compound **88** (501 mg, 1.56 mmol, 1.0 equiv) and AIBN (26 mg, 0.15 mmol 0.10 equiv) was dissolved in freshly distilled toluene (5.0 mL). Reaction mixture was sparged with argon for 15 minutes and thioacetic acid (0.66 mL, 9.38 mmol, 6.0 equiv) was added. The reaction was irradiated with UV household lamp (365 nm, 4 x 9 W) with continuous stirring at room temperature. After 4 hours additional 6.0 equiv of thioacetic acid and 0.1 equiv AIBN were added, and the reaction mixture was irradiated with UV lamp for another 4 hours. Then reaction mixture was diluted with water and extracted with EA. Organic phase was washed with water and brine, dried over anhydrous Na_2SO_4 and evaporated to dryness. The crude was purified by column chromatography on silica gel (PE:EA 10:1, R_f = 0.15) to afford 700 mg (95 %) of **89** as a colorless oil.
^{1}H NMR (400 MHz, $CDCl_3$): δ 12.28 (s, 2H), 3.75 (s, 6H), 3.04 (ddd, J = 13.4, 9.7, 4.8 Hz, 2H), 2.85 (ddd, J = 13.4, 9.3, 7.1 Hz, 2H), 2.70 (dt, J = 9.8,

2.3 Hz, 2H), 2.57 – 2.48 (m, 2H), 2.33 (s, 6H), 1.91 (dddd, J = 13.9, 9.9, 7.2, 2.8 Hz, 2H), 1.84 (t, J = 3.1 Hz, 2H), 1.59 (tq, J = 9.5, 4.9 Hz, 2H).

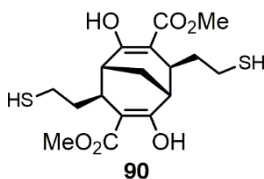**HRMS-ESI⁺**: m/z [M+H]⁺ calcd. for 473.1298; found 473.1298.

90

(1R,4S,5R,8S)-dimethyl-*exo,exo*-4,8-bis(2-mercaptoethyl)-2,6-dihydroxy bicyclo[3.3.1]nona-2,6-diene-3,7-dicarboxylate 90. Under inert atmosphere to a stirred solution of **89** (81.6 mg, 0.17 mmol, 1.0 equiv) in MeOH (5.0 mL) was added dropwise an excess of conc. HCl (0.15 mL). Reaction mixture was heated for 2 hours at 90 °C. Then, the reaction mixture was cooled down to room temperature and the solvent was removed under reduced pressure. The crude was dissolved in EA and washed with sat. NaHCO₃ solution and brine, dried over anhydrous Na₂SO₄ and evaporated to dryness. The crude was purified by column chromatography on silica gel (PE:EA 10:1, R_f = 0.23) to afford 53 mg (79 %) of **90** as a white solid.

¹H NMR (400 MHz, CDCl₃): δ 12.31 (s, 2H), 3.76 (s, 6H), 2.85 – 2.74 (m, 2H), 2.74 – 2.54 (m, 4H), 2.45 (q, J = 2.1, 1.4 Hz, 2H), 1.94 (dddd, J = 14.0, 9.3, 7.3, 2.9 Hz, 2H), 1.81 (t, J = 3.1 Hz, 2H), 1.66 (dddd, J = 13.9, 10.1, 8.7, 5.1 Hz, 2H), 1.46 (t, J = 7.6 Hz, 2H).

¹³C NMR (101 MHz, CDCl₃): δ 173.85, 172.98, 100.18, 51.81, 38.10, 36.73, 36.17, 23.12, 18.59.

HRMS-ESI⁺: m/z [M-H]⁻ calcd. for 387.093; found 387.0942.

General procedure A for 91a-e. Under inert atmosphere a mixture of compound **90** (1.0 equiv), the corresponding RBr (2.2 equiv) and K₂CO₃ (2.2 equiv) in anhydrous DMF was heated at 80 °C for 1-3 hours. Then the reaction mixture was cooled down to room temperature, diluted with 1.0 M HCl solution and extracted with EA. Organic phase was washed with 1.0 M HCl solution, water and brine, dried over anhydrous Na₂SO₄ and evaporated to dryness. The crude was purified by column chromatography on silica gel (CHCl₃:MeOH) to afford product **91a-e**.
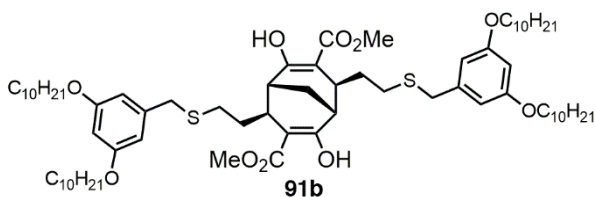
91a
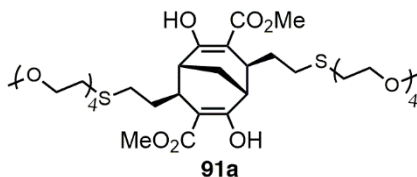
(1R,4S,5R,8S)-dimethyl-*exo,exo*-4,8-di(2,5,8,11-tetraoxa-14-thiahexadecan-16-yl)-2,6-dihydroxybicyclo[3.3.1]nona-2,6-diene-3,7-dicarboxylate 91a. Following general procedure **A**, a mixture of **90** (60 mg, 0.15 mmol, 1.0 equiv), 13-bromo-2,5,8,11-tetraoxatridecane (92 mg, 0.34 mmol, 2.2 equiv), K_2CO_3 (47 mg, 0.34 mmol, 2.2 equiv) in anhydrous DMF (5.0 mL) was heated at 80 °C for 1 hour. The crude was purified by column chromatography on silica gel (CHCl$_3$:MeOH 40:1, R_f = 0.12) to afford 116 mg (98 %) of **91a** as a colorless oil.

^{1}H NMR (400 MHz, CDCl$_3$): δ 12.31 (s, 2H), 3.74 (s, 6H), 3.71 – 3.60 (m, 24H), 3.54 (dd, *J* = 5.7, 3.6 Hz, 4H), 3.37 (s, 6H), 2.79 – 2.66 (m, 8H), 2.59 (ddd, *J* = 12.5, 9.5, 6.9 Hz, 2H), 2.46 (q, *J* = 2.6 Hz, 2H), 1.93 (dddd, *J* = 16.7, 9.6, 6.7, 2.7 Hz, 2H), 1.81 (t, *J* = 3.1 Hz, 2H), 1.58 (dtd, *J* = 14.5, 9.8, 5.0 Hz, 2H).

^{13}C NMR (101 MHz, CDCl$_3$): δ 173.90, 173.00, 100.28, 72.06, 71.06, 70.74, 70.71, 70.65, 70.47, 59.16, 51.76, 37.17, 36.14, 33.76, 31.57, 30.97, 18.52.

HRMS-ESI$^+$: m/z [M+H]$^+$ calcd. for 769.3497; found 769.3499.

91b

(1R,4S,5R,8S)-dimethyl-*exo,exo*-4,8-bis(2-((3,5-bis(decyloxy)benzyl)thio) ethyl)-2,6-dihydroxybicyclo[3.3.1]nona-2,6-diene-3,7-dicarboxylate 91b. Following general procedure **A**, a mixture of **90** (20 mg, 0.052 mmol, 1.0 equiv), 3,5-bis(decyloxy)benzyl bromide (55 mg, 0.11 mmol, 2.2 equiv), K_2CO_3 (16 mg, 0.11 mmol, 2.2 equiv) in anhydrous DMF (2.0 mL) was heated at 80 °C for 2 hours. The crude was purified by column chromatography on silica gel (PE:EA 30:1, R_f = 0.45) to afford 47 mg (76 %) of **91b** as a colorless oil.

^{1}H NMR (400 MHz, CDCl$_3$): δ 12.31 (s, 2H), 6.45 (d, *J* = 2.3 Hz, 4H), 6.33 (t, *J* = 2.3 Hz, 2H), 3.92 (t, *J* = 6.6 Hz, 8H), 3.74 (s, 6H), 3.65 (s, 4H), 2.70 (dt, *J* = 10.1, 2.2 Hz, 2H), 2.51 (qdd, *J* = 12.9, 10.7, 5.9 Hz, 4H), 2.40 (q, *J* = 2.5 Hz, 2H), 1.94 (dtd, *J* = 13.9, 6.8, 3.4 Hz, 2H), 1.75 (dt, *J* = 9.6, 6.7 Hz,

10H), 1.58 – 1.49 (m, 2H), 1.42 (td, J = 8.8, 8.1, 4.7 Hz, 8H), 1.37 – 1.21 (m, 48H), 0.88 (t, J = 6.8 Hz, 12H).

13C NMR (101 MHz, CDCl$_3$): δ 173.99, 173.05, 160.50, 140.53, 107.42, 100.30, 99.95, 68.17, 51.75, 37.14, 36.51, 36.13, 33.43, 32.04, 29.73, 29.71, 29.56, 29.47, 29.44, 26.21, 22.83, 18.48, 14.26.

HRMS-ESI+: m/z [M-H]- calcd. for 1191.7929; found 1191.8160.
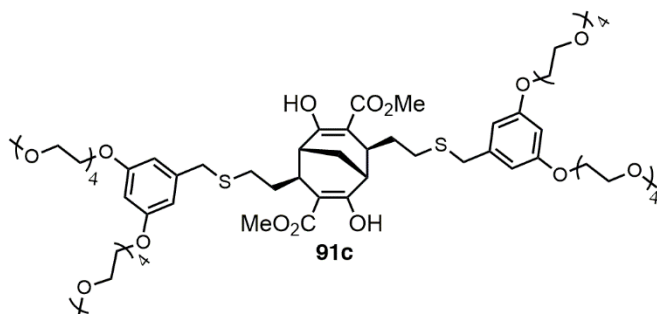
(1R,4S,5R,8S)-dimethyl-*exo*,*exo*-4,8-bis(2-((3,5-bis(2,5,8,11-tetraoxatridecan-13-yloxy)benzyl)thio)ethyl)-2,6-dihydroxy bicyclo[3.3.1]nona-2,6-diene-3,7-dicarboxylate 91c. Following general procedure **A**, a mixture of **90** (61 mg, 0.16 mmol, 1.0 equiv), bis(MeO-PEG4)benzyl bromide (201 mg, 0.35 mmol, 2.2 equiv), K$_2$CO$_3$ (48 mg, 0.35 mmol, 2.2 equiv) in anhydrous DMF (7.0 mL) was heated at 80 °C for 2 hours. The crude was purified by column chromatography on silica gel (CHCl$_3$:MeOH 50:1, R$_f$ = 0.33) to afford 189 mg (87 %) of **91c** as a yellow oil.

1H NMR (400 MHz, CDCl$_3$): δ 12.30 (s, 2H), 6.48 (d, J = 2.3, 4H), 6.37 (t, J = 2.2 Hz, 2H), 4.08 (dd, J = 5.8, 4.0 Hz, 8H), 3.83 (dd, J = 5.7, 4.0, 8H), 3.74 (s, 6H), 3.73 – 3.69 (m, 8H), 3.69 – 3.61 (m, 36H), 3.57 – 3.51 (m, 8H), 3.37 (s, 12H), 2.75 – 2.66 (m, 2H), 2.58 – 2.43 (m, 4H), 2.43 – 2.39 (m, 2H), 1.99 – 1.87 (m, 2H), 1.79 – 1.74 (m, 2H), 1.53 (dtd, J = 14.1, 9.5, 4.9 Hz, 2H),

13C NMR (101 MHz, CDCl$_3$): δ 173.97, 173.03, 160.08, 140.66, 107.83, 100.30, 100.25, 72.08, 70.94, 70.77, 70.76, 70.75, 70.66, 69.82, 67.56, 59.17, 51.79, 37.05, 36.50, 36.11, 33.28, 29.66.

HRMS-ESI+: m/z [M+H]+ calcd. for 1393.6643; found 1393.6665.

91d
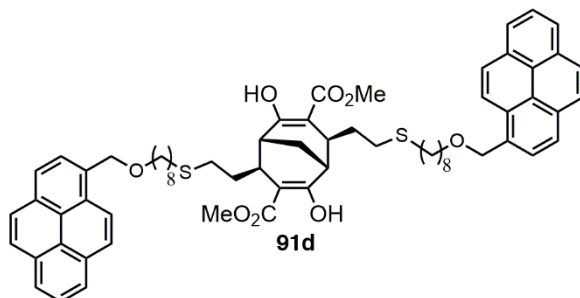
(1R,4S,5R,8S)-dimethyl-*exo,exo*-2,6-dihydroxy-4,8-bis(2-((8-(pyren-1-ylmethoxy)octyl)thio)ethyl)bicyclo[3.3.1]nona-2,6-diene-3,7-dicarboxylate 91d. Following general procedure **A**, a mixture of **90** (47 mg, 0.12 mmol, 1.0 equiv), pyrene bromide **92** (113 mg, 0.27 mmol, 2.2 equiv), K_2CO_3 (37 mg, 0.27 mmol, 2.2 equiv) in anhydrous DMF (5.0 mL) was heated at 80 °C for 3 hours. The crude was purified by column chromatography on silica gel (PE:EA 5:1 → 3:1, R_f = 0.33) to afford 88 mg (67 %) of **91d** as a yellow oil.

^{1}H NMR (400 MHz, $CDCl_3$): δ 12.34 (s, 2H), 8.37 (d, *J* = 9.2 Hz, 2H), 8.28 – 8.10 (m, 8H), 8.09 – 7.96 (m, 8H), 5.21 (s, 4H), 3.73 (s, 6H), 3.60 (t, *J* = 6.5 Hz, 4H), 2.82 – 2.69 (m, 2H), 2.67 – 2.39 (m, 10H), 1.93 (dddd, *J* = 13.1, 9.7, 6.5, 2.6 Hz, 2H), 1.85 – 1.74 (m, 2H), 1.66 (p, *J* = 6.8 Hz, 4H), 1.54 (p, *J* = 7.9, 6.9 Hz, 4H), 1.45 – 1.19 (m, 18H).

^{13}C NMR (101 MHz, $CDCl_3$): δ 173.92, 173.02, 131.93, 131.36, 131.31, 130.95, 129.45, 127.70, 127.54, 127.43, 127.01, 126.01, 125.27, 125.27, 125.05, 124.86, 124.59, 123.65, 100.33, 71.61, 70.61, 51.71, 37.25, 36.12, 33.71, 32.25, 30.49, 29.93, 29.67, 29.41, 29.31, 28.99, 26.29, 18.46.

HRMS-ESI$^+$: m/z [M-H]$^-$ calcd. for 1071.4897; found 1071.5496.

91e
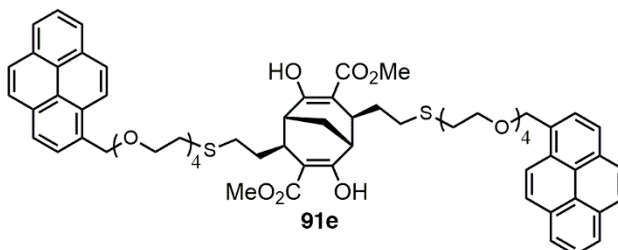
**(1R,4S,5R,8S)-dimethyl-*exo,exo*-2,6-dihydroxy-4,8-bis(2-((8-(pyren-1-ylmethoxy)2,5,8,11-tetraoxatridecan-13-yloxy)thio)ethyl) bicyclo[3.3.1]nona-2,6-diene-3,7-dicarboxylate 91e**. Following general procedure **A**, a mixture of **90** (67 mg, 0.17 mmol, 1.0 equiv), pyrene bromide **93** (180 mg, 0.38 mmol, 2.2 equiv), K_2CO_3 (53 mg, 0.38 mmol, 2.2 equiv) in anhydrous DMF (6.0 mL) was heated at 80 °C for 3 hours. The crude was

purified by column chromatography on silica gel (CHCl$_3$:EA 3:1, R$_f$ = 0.12) to afford 167 mg (82 %) of **91e** as a yellow oil.

^{1}H NMR (400 MHz, CDCl$_3$): δ 12.30 (s, 2H), 8.40 (d, J = 9.2 Hz, 2H), 8.19 (t, J = 6.9 Hz, 4H), 8.14 (dd, J = 8.5, 2.3 Hz, 4H), 8.09 – 7.95 (m, 8H), 5.28 (s, 4H), 3.80 – 3.55 (m, 36H), 2.69 (t, J = 6.9 Hz, 6H), 2.66 – 2.60 (m, 2H), 2.55 (td, J = 12.2, 10.8, 7.1 Hz, 2H), 2.39 (t, J = 2.4 Hz, 2H), 1.95 – 1.79 (m, 2H), 1.50 (dtd, J = 14.5, 9.7, 4.9 Hz, 2H).

^{13}C NMR (101 MHz, CDCl$_3$): δ 173.89, 172.98, 131.54, 131.41, 131.37, 130.95, 129.53, 127.78, 127.55, 127.53, 127.18, 126.06, 125.33, 125.05, 124.84, 124.59, 123.69, 100.25, 71.99, 71.01, 70.89, 70.81, 70.79, 70.73, 70.45, 69.66, 51.76, 37.11, 36.08, 33.66, 31.53, 30.94, 18.42.

HRMS-ESI$^+$: m/z [M-H]$^-$ calcd. for 1167.4592; found 1167.4362.
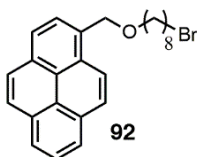
1-(1-Pyrenyl)-2-oxa-10-bromodecane 92. Under inert atmosphere to a stirred suspension of NaH (60% dispersion in mineral oil) (790 mg, 19.80 mmol, 10.0 equiv) in anhydrous THF (30.0 mL) was added 1-pyrenemethanol (460 mg, 1.98 mmol, 1.0 equiv) and 1,8-dibromooctane (1.86 mL, 9.90 mmol, 5.0 equiv). Reaction mixture was heated at 70 °C for 4 hours. The reaction mixture was cooled down to room temperature, quenched with H$_2$O and extracted with DCM. Organic phase was washed with water and brine, dried over anhydrous Na$_2$SO$_4$ and evaporated to dryness. The crude was purified by column chromatography on silica gel (PE) to afford 615 mg (77 %) of **92** as a yellow solid.

Spectral data were in accordance with a literature.[247]
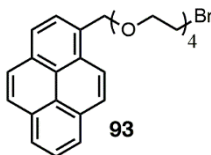
1-(1-Pyrenyl)-13-bromo-2,5,8,11-tetraoxatridecane 93. Under inert atmosphere to a stirred suspension of NaH (60% dispersion in mineral oil) (707 mg, 17.69 mmol, 10.0 equiv) in anhydrous THF (30.0 mL) was added 1-pyrenemethanol (411 mg, 1.77 mmol, 1.0 equiv) and 1,11-dibromo-3,6,9-trioxaundecane (3.11 g, 9.72 mmol, 5.5 equiv). Reaction mixture was heated at 70 °C for 6 hours. The reaction mixture was cooled down to room

temperature, quenched with H_2O and extracted with DCM. Organic phase was washed with brine, dried over anhydrous Na_2SO_4 and evaporated to dryness. The crude was purified by column chromatography on silica gel (PE:EA 2:2→1:1, $R_f = 0.44$) to afford 314 mg (38 %) of **93** as a yellow solid.
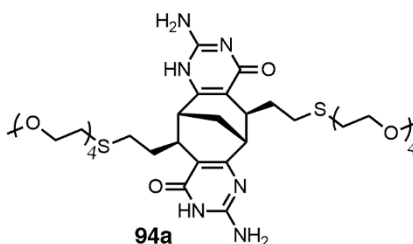
^{1}H NMR (400 MHz, CDCl$_3$): δ 8.41 (d, $J = 9.3$ Hz, 1H), 8.23 – 8.12 (m, 4H), 8.08 – 7.99 (m, 4H), 5.29 (s, 2H), 3.79 – 3.69 (m, 6H), 3.69 – 3.64 (m, 4H), 3.64 – 3.57 (m, 4H), 3.41 (t, $J = 6.3$ Hz, 2H).

^{13}C NMR (101 MHz, CDCl$_3$): δ 131.54, 131.45, 131.39, 130.97, 129.57, 127.81, 127.56, 127.24, 126.09, 125.35, 125.09, 124.87, 124.61, 123.73, 72.02, 71.29, 70.90, 70.83, 70.82, 70.73, 70.64, 69.67, 30.43.

HRMS-ESI$^+$: m/z [M+H]$^+$ calcd. for 471.1165; found 471.1192.

94a

ICyt 94a. A mixture of **91a** (130 mg, 0.17 mmol, 1.0 equiv), guanidinium chloride (81 mg, 0.85 mmol, 5.0 equiv) and KOtBu (95 mg, 0.85 mmol, 5.0 equiv) in MeOH (13.0 mL) was heated at 100 °C for 24 hours. Then the reaction mixture was cooled down to room temperature and the solvent was removed under reduced pressure. The crude was diluted with 1.0 M HCl solution and extracted and washed with DCM. The aqueous phase was basified to 9-11 pH with sat. NaHCO$_3$ solution and extracted with DCM. The crude was precipitated with Et$_2$O, filtered and washed with Et$_2$O to afford 103 mg (77 %) of **94a** as a yellow solid.

^{1}H and ^{13}C NMR could not be acquired due to strong aggregation.

HRMS-ESI$^+$: m/z [M+H]$^+$ calcd. for 787.3729; found 787.3727.

94b
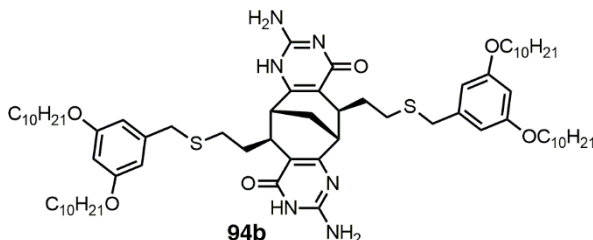
ICyt 94b. A mixture of **91b** (47 mg, 0.039 mmol, 1.0 equiv), guanidinium carbonate (35 mg, 0.20 mmol, 5.0 equiv) in MeOH (5.0 mL) was heated at 100 °C for 24 hours. Then reaction mixture was cooled down to room

temperature and the solvent was removed under reduced pressure. The crude was diluted with 1.0 M HCl solution and extracted with DCM. Organic phase was washed with brine, dried over anhydrous Na_2SO_4 and evaporated to dryness. The crude was precipitated with MeOH, filtered and washed with MeOH to afford 32 mg (68 %) of **94b** as a white solid.

^{1}H and **^{13}C NMR** could not be acquired due to strong aggregation.

HRMS-ESI$^+$: m/z [M+H]$^+$ calcd. for 1211.8314; found 1211.8285.
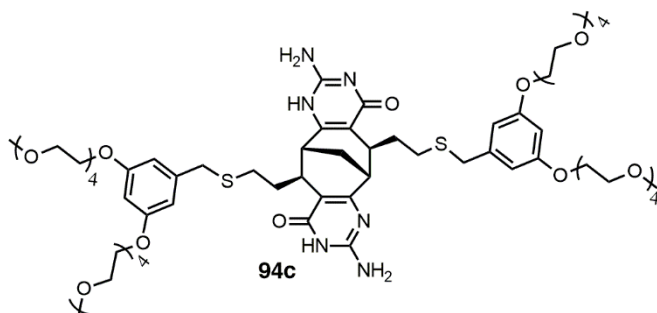
ICyt 94c. A mixture of **91c** (161 mg, 0.12 mmol, 1.0 equiv), guanidinium chloride (110 mg, 1.16 mmol, 10.0 equiv) and KOtBu (114 mg, 1.16 mmol, 10.0 equiv) in MeOH (10.0 mL) was heated at 100 °C for 24 hours. Then the reaction mixture was cooled down to room temperature and the solvent was removed under reduced pressure. The crude was diluted with 1.0 M HCl solution and extracted with CHCl$_3$. Organic phase was washed with brine, dried over anhydrous Na_2SO_4 and evaporated to dryness to afford 160 mg (98 %) of **94c** as a colorless oil. The crude was used without further purification.

^{1}H and **^{13}C NMR** could not be acquired due to strong aggregation.

HRMS-ESI$^+$: m/z [M-H]$^-$ calcd. for 1409.6717; found 1409.6725.
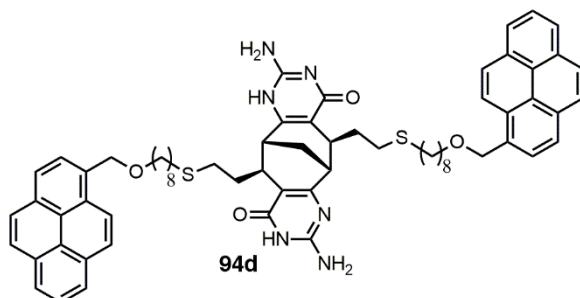
ICyt 94d. A mixture of **91d** (87 mg, 0.081 mmol, 1.0 equiv), guanidinium chloride (78 mg, 0.82 mmol, 10.0 equiv) and KOtBu (92 mg, 0.82 mmol, 10.0 equiv) in MeOH (10.0 mL) was heated at 100 °C for 36 hours. Then

reaction mixture was cooled down to room temperature and the solvent was removed under reduced pressure. The crude was diluted with 1.0 M HCl solution and extracted with CHCl$_3$. Organic phase was washed with brine, dried over anhydrous Na$_2$SO$_4$ and evaporated to dryness to afford 64 mg (72 %) of **94d** as a yellow oil. The crude was used without further purification.

^{1}H and ^{13}C NMR ^{1}H and ^{13}C NMR could not be acquired due to strong aggregation.

HRMS-ESI$^+$: m/z [M+H]$^+$ calcd. for 1091.5286; found 1091.533.

94e
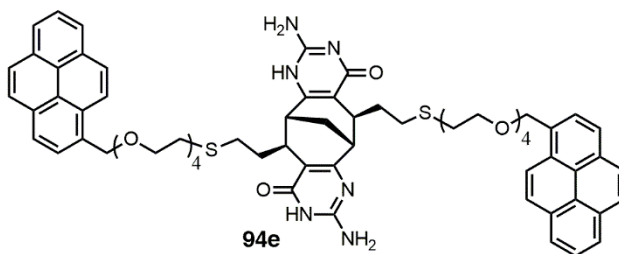
ICyt 94e. A mixture of **91e** (115 mg, 0.098 mmol, 1.0 equiv), guanidinium chloride (66 mg, 0.68 mmol, 7.0 equiv) and KOtBu (77 mg, 0.68 mmol, 7.0 equiv) in MeOH (10.0 mL) was heated at 100 °C for 24 hours. Then reaction mixture was cooled down to room temperature and the solvent was removed under reduced pressure. The crude was diluted with 1.0 M HCl solution and extracted with CHCl$_3$. Organic phase was washed with brine, dried over anhydrous Na$_2$SO$_4$ and evaporated to dryness. The crude was purified by column chromatography on silica gel (CHCl$_3$:MeOH 50:1→20:1→10:1, R$_f$ = 0.35) to afford 65 mg (56 %) of **94e** as a white solid.

^{1}H and ^{13}C NMR could not be acquired due to strong aggregation.

HRMS-ESI$^+$: m/z [M+H]$^+$ calcd. for 1187.4981; found 1187.4980.

General procedure B for 95a-e. Under inert atmosphere a mixture of corresponding **94a-e** (1.0 equiv), BuNCO (4.0 equiv) and freshly distilled anhydrous NEt$_3$ (4.0 equiv) in anhydrous THF was heated at 80 °C for 24 - 72 hours. Then reaction mixture was cooled down to room temperature and the solvent was removed under reduced pressure. The crude was diluted with 1.0 M HCl solution and extracted with CHCl$_3$. Organic phase was washed with brine, dried over anhydrous Na$_2$SO$_4$ and evaporated to dryness. The crude was purified by column chromatography on silica gel (CHCl$_3$:MeOH) to afford product **95a-e**.

95a
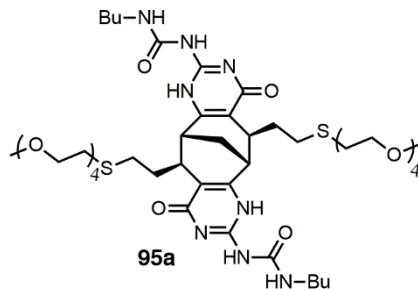
Monomer Upy 95a. Following general procedure **B**, a mixture of **94a** (103 mg, 0.13 mmol, 1.0 equiv), BuNCO (0.06 mL, 0.52 mmol, 4.0 equiv) and freshly distilled anhydrous NEt_3 (0.07 mL, 0.52 mmol, 4.0 equiv) in anhydrous THF (7.0 mL) was heated at 80 °C for 24 hours. The crude was purified by column chromatography on silica gel ($CHCl_3$:MeOH 100:1→50:1, $R_f = 0.44$) to afford 121 mg (93 %) of **95a** as a colorless oil.

^{1}H NMR (400 MHz, $CDCl_3$): δ 12.93 (s, 2N-H), 11.89 (s, 2N-H), 9.63 (d, $J = 5.4$ Hz, 2N-H), 3.77 – 3.60 (m, 24H), 3.60 – 3.51 (m, 4H), 3.37 (s, 6H), 3.31 – 3.11 (m, 4H), 3.00 – 2.73 (m, 12H), 2.48 – 2.28 (m, 2H), 2.01 (s, 2H), 1.64 – 1.50 (m, 6H), 1.44 – 1.32 (m, 4H), 0.93 (t, $J = 7.3$ Hz, 6H).

^{13}C NMR (101 MHz, $CDCl_3$): δ 171.78, 156.34, 153.88, 147.16, 115.69, 72.09, 71.01, 70.76, 70.71, 70.68, 70.46, 59.18, 39.73, 38.07, 34.20, 31.62, 31.42, 31.03, 20.30, 14.01.

HRMS-ESI$^+$: m/z [M+H]$^+$ calcd. for 985.5097; found 985.5146.

95b
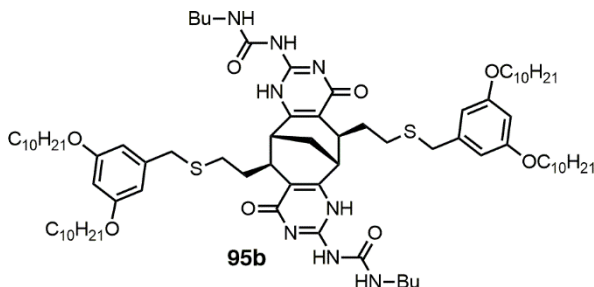
Monomer Upy 95b. Following general procedure **B**, a mixture of **94b** (32 mg, 0.027 mmol, 1.0 equiv), BuNCO (8.0 µL, 0.067 mmol, 2.5 equiv) and freshly distilled anhydrous NEt_3 (9.2 µL, 0.067 mmol, 2.5 equiv) in anhydrous THF (3.0 mL) was heated at 80 °C for 24 hours. The crude was precipitated with MeOH, filtered and washed with MeOH to afford 32 mg (85 %) of **95b** as a white solid.

^{1}H NMR (400 MHz, $CDCl_3$): δ 12.97 (s, 2N-H), 11.88 (s, 2N-H), 9.72 (s, 2N-H), 6.49 (s, 4H), 6.32 (s, 2H), 3.90 (s, 8H), 3.73 (s, 4H), 3.20 (s, 4H),

2.99 – 2.56 (m, 8H), 2.42 (s, 2H), 1.87 (s, 2H), 1.73 (s, 10H), 1.32 (d, J = 58.3 Hz, 64H), 0.87 (s, 18H).

^{13}**C NMR** (101 MHz, CDCl$_3$): δ 171.73, 160.47, 156.33, 153.89, 147.23, 140.70, 115.61, 107.47, 100.00, 68.15, 39.77, 37.87, 36.41, 33.88, 32.04, 31.56, 30.07, 29.73, 29.71, 29.55, 29.47, 29.43, 26.21, 22.82, 20.26, 14.25, 13.94.

**HRMS-ESI$^+$**: m/z [M+H]$^+$ calcd. for 1409.9682; found 1409.9655.

95c
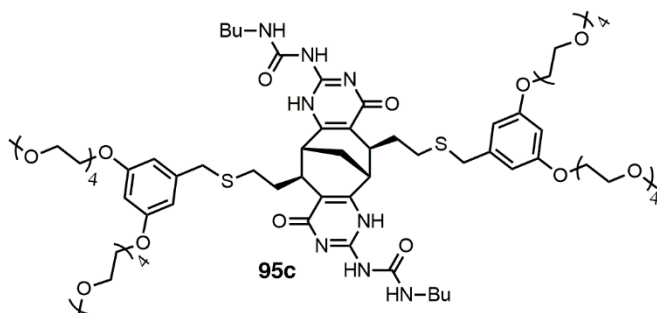
Monomer Upy 95c. Following general procedure **B**, a mixture of **94c** (24 mg, 0.017 mmol, 1.0 equiv), BuNCO (5.0 µL, 0.043 mmol, 2.5 equiv) and freshly distilled anhydrous NEt$_3$ (6.0 µL, 0.043 mmol, 2.5 equiv) in anhydrous THF (3.0 mL) was heated at 80 °C for 24 hours. The crude was purified by column chromatography on silica gel (CHCl$_3$:MeOH 50:1→20:1, R$_f$ = 0.58) to afford 27 mg (98 %) of **95c** as a colorless oil.

^{1}**H NMR** (400 MHz, CDCl$_3$): δ 12.95 (s, 2N-H), 11.88 (s, 2N-H), 9.68 (s, 2N-H), 6.50 (d, J = 2.2 Hz, 4H), 6.36 (t, J = 2.1 Hz, 2H), 4.16 – 3.98 (m, 8H), 3.92 – 3.77 (m, 8H), 3.77 – 3.60 (m, 44H), 3.60 – 3.48 (m, 8H), 3.36 (s, 12H), 3.26 – 3.14 (m, 4H), 2.99 – 2.87 (m, 2H), 2.82 (s, 2H), 2.78 – 2.60 (m, 4H), 2.51 – 2.36 (m, 2H), 1.92 (s, 2H), 1.66 – 1.44 (m, 6H), 1.29 (dt, J = 17.4, 8.7 Hz, 4H), 0.86 (t, J = 7.3 Hz, 6H).

^{13}**C NMR** (101 MHz, CDCl$_3$): δ 171.78, 160.02, 156.30, 153.84, 147.26, 140.79, 115.64, 107.85, 100.22, 72.03, 70.89, 70.71, 70.61, 69.79, 67.51, 59.13, 39.72, 37.74, 36.42, 33.89, 31.50, 30.23, 20.24, 13.96.

**HRMS-ESI$^+$**: m/z [M+H]$^+$ calcd. for 1609.8243; found 1609.8253.

95d
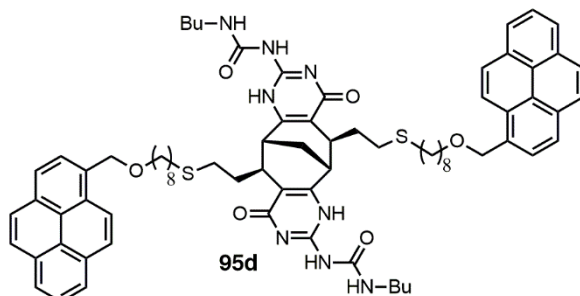
Monomer Upy 95d. Following general procedure **B**, a mixture of **94d** (64 mg, 0.059 mmol, 1.0 equiv), BuNCO (0.02 mL, 0.15 mmol, 2.5 equiv) and freshly distilled anhydrous NEt$_3$ (0.02 mL, 0.15 mmol, 2.5 equiv) in anhydrous THF (10.0 mL) was heated at 80 °C for 24 hours. The crude was precipitated with MeOH, filtered and washed with MeOH to afford 55 mg (73 %) of **95d** as a yellow oil.

¹H NMR (400 MHz, CDCl$_3$): δ 12.82 (s, 2N-H), 11.75 (s, 2N-H), 9.63 (s, 2N-H), 8.31 (d, J = 9.6 Hz, 2H), 8.23 – 8.05 (m, 8H), 8.04 – 7.89 (m, 8H), 5.17 (s, 4H), 3.71 – 3.47 (m, 4H), 3.37 – 3.05 (m, 4H), 2.96 – 2.65 (m, 6H), 2.64 – 2.47 (m, 4H), 2.29 (s, 2H), 2.13 – 1.75 (m, 6H), 1.72 – 1.45 (m, 10H), 1.43 – 1.07 (m, 22H), 1.01 – 0.75 (m, 6H).

¹³C NMR could not be obtained due to high degree of aggregation.

**HRMS-ESI⁺**: m/z [M+H]⁺ calcd. for 1289.6654; found 1289.6638.

95e
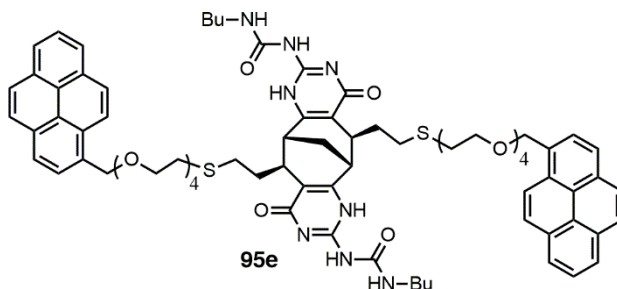
Monomer Upy 95e. Following general procedure **B**, a mixture of **94e** (65 mg, 0.055 mmol, 1.0 equiv), BuNCO (0.015 mL, 0.14 mmol, 2.5 equiv) and freshly distilled anhydrous NEt$_3$ (0.02 mL, 0.14 mmol, 2.5 equiv) in anhydrous THF (10.0 mL) was heated at 80 °C for 72 hours. The crude was precipitated with MeOH, filtered and washed with MeOH to afford 59 mg (78 %) of **95e** as a yellow oil.

¹H NMR (400 MHz, CDCl$_3$): δ 12.70 (s, 2N-H), 11.62 (s, 2N-H), 9.56 (s, 2N-H), 8.34 (d, J = 9.2 Hz, 2H), 8.21 – 8.05 (m, 8H), 8.05 – 7.91 (m, 8H), 5.24 (s, 4H), 3.91 – 3.54 (m, 28H), 3.19 (d, J = 35.9 Hz, 4H), 2.93 – 2.65 (m,

8H), 2.65 – 2.56 (m, 2H), 2.51 (s, 2H), 2.33 – 2.06 (m, 2H), 1.70 – 1.46 (m, 6H), 1.36 (q, J = 7.6 Hz, 6H), 0.93 (t, J = 7.3 Hz, 6H).

^{13}**C NMR** (101 MHz, CDCl$_3$): δ 171.35, 156.08, 153.43, 146.76, 131.48, 131.18, 130.77, 129.28, 127.64, 127.41, 127.35, 126.92, 125.91, 125.18, 125.16, 124.84, 124.65, 124.49, 123.50, 115.17, 71.80, 70.94, 70.78, 70.72, 70.66, 70.38, 69.65, 39.61, 37.72, 33.76, 31.50, 31.30, 30.75, 30.68, 29.72, 20.21, 13.92.

HRMS-ESI$^+$: m/z [M+H]$^+$ calcd. for 1385.6307; found 1385.6308.

6.2 Experimental section for Chapter 2.3: Photooxidation of sulfides to sulfoxides using heterogenous carbon-based catalyst

96a
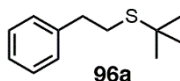
***tert*-Butyl(2-phenylethyl)sulfide 96a.** A mixture of 2-methyl-2-propanethiol (0.4 mL, 3.51 mmol, 1.3 equiv), 2-phenylethylbromide (0.37 mL, 2.70 mmol, 1.0 equiv) and K$_2$CO$_3$ (0.49 g, 3.51 mmol, 1.3 equiv) in DMF (7.0 mL) was stirred at room temperature for 24 hours. The reaction mixture was diluted with 1.0 M HCl solution and extracted with EA. The organic phase was washed with 1.0 M HCl solution and brine, dried over anhydrous Na$_2$SO$_4$ and evaporated to dryness. The crude was purified by column chromatography on silica gel (PE:EA 100:1, R$_f$ = 0.29) to afford 503 mg (96 %) of **96a** as a colorless oil.

Spectral data were in accordance with a literature.[248]

96b
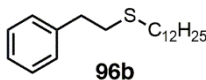
***n*-dodecyl(2-phenylethyl)sulfide 96b.** A mixture of 1-dodecanethiol (0.84 mL, 3.51 mmol, 1.3 equiv), 2-phenylethylbromide (0.37 mL, 2.70 mmol, 1.0 equiv) and K$_2$CO$_3$ (0.49 g, 3.51 mmol, 1.3 equiv) in DMF (7.0 mL) was stirred at room temperature for 24 hours. The reaction mixture was diluted with 1.0 M HCl solution and extracted with EA. The organic phase was washed with 1.0 M HCl solution and brine, dried over anhydrous Na$_2$SO$_4$ and evaporated to dryness. The crude was purified by column chromatography on silica gel (PE:EA 100:1, R$_f$ = 0.30) to afford 760 mg (92 %) of **96b** as a colorless oil.

Spectral data were in accordance with a literature.[249]
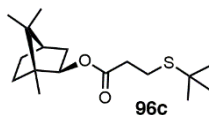
Isobornyl-3-(*tert*-butylthio)propionate 96c. Under inert atmosphere tert-butylthiol (1.1 mL, 9.60 mmol, 2.0 equiv) and catalytic amount of NaOMe (78 mg, 1.44 mmol, 0.3 equiv) were dissolved in anhydrous MeOH (20 mL). The reaction mixture was cooled down to 0 °C and isobornyl acrylate (1.0 mL, 4.80 mmol, 1.0 equiv) was added dropwise over a period of 10 min. The reaction mixture was allowed to warm up to room temperature overnight. The solvent was removed under reduced pressure. The crude was dissolved in CHCl$_3$ and washed with H$_2$O and brine, dried over anhydrous Na$_2$SO$_4$ and evaporated to dryness. The crude was purified by column chromatography on silica gel (PE:EA 100:1, R$_f$ = 0.33) to afford 1.23 g (86 %) of **96c** as a colorless oil.

^{1}H NMR (400 MHz, CDCl$_3$): δ 4.76 – 4.62 (m, 1H), 2.78 (dd, *J* = 8.2, 7.3 Hz, 2H), 2.55 (dd, *J* = 8.2, 7.1 Hz, 2H), 1.90 – 1.62 (m, 4H), 1.62 – 1.49 (m, 1H), 1.32 (s, 9H), 1.21 – 1.02 (m, 2H), 1.02 (s, 3H), 0.83 (s, 3H), 0.82 (s, 3H).

^{13}C NMR (101 MHz, CDCl$_3$): δ 171.58, 81.37, 48.79, 47.03, 45.14, 42.42, 38.90, 35.51, 33.83, 31.02, 27.14, 23.63, 20.22, 20.03, 11.60.

HRMS-ESI$^+$: m/z [M+Na]$^+$ calcd. for C$_{17}$H$_{31}$O$_3$SNa 337.4732; found 337.1809 (only sulfoxide formed during the measurements can be detected with ESI).
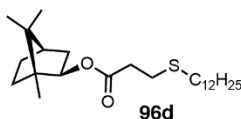
Isobornyl-3-(*n*-dodecylthio)propionate 96d. Under inert atmosphere a mixture of 1-dodecanethiol (0.83 mL, 2.88 mmol, 2.2 equiv), isobornyl acrylate (0.3 mL, 1.44 mmol, 1.0 equiv) and triethylamine (0.48 mL, 2.88 mmol, 2.2 equiv) in anhydrous THF (5.0 mL) was heated at 70 °C for 48 hours. The reaction mixture was cooled down to room temperature and solvent was removed under reduced pressure. The crude was purified by column chromatography on silica gel (PE:EA 100:1, R$_f$ = 0.33) to afford 413 mg (58 %) of **96d** as a colorless oil.

^{1}H NMR (400 MHz, CDCl$_3$): δ 4.74 – 4.64 (m, 1H), 2.76 (t, *J* = 7.5 Hz, 2H), 2.57 (t, J = 7.5 Hz, 2H), 2.51 (t, *J* = 7.4 Hz, 2H), 1.85 – 1.65 (m, 4H), 1.62 – 1.51 (m, 3H), 1.36 (t, *J* = 7.5 Hz, 2H), 1.32 (s, 16H), 1.19 – 1.03 (m, 2H), 0.97 (s, 3H), 0.88 (t, *J* = 6.9 Hz, 3H), 0.84 (s, 3H), 0.83 (s, 3H).

13C NMR (101 MHz, CDCl$_3$): δ 171.59, 81.48, 48.82, 47.08, 45.18, 38.95, 35.48, 33.87, 32.26, 32.06, 29.80, 29.78, 29.75, 29.70, 29.68, 29.50, 29.38, 29.03, 27.29, 27.17, 22.84, 20.25, 20.06, 14.27, 11.63.

HRMS-ESI$^+$: m/z [M+Na]$^+$ calcd. for C$_{25}$H$_{47}$O$_3$SNa 449.6892; found 449.3056 (only sulfoxide formed during the measurements can be detected with ESI).

96e
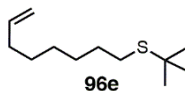
***tert*-butyl(oct-7-en-1-yl)sulfane 96e**. A mixture of 8-bromo-1-octene (0.5 g, 2.62 mmol, 1.0 equiv), 2-methyl-2-propanethiol (0.38 mL, 3.40 mmol, 1.3 equiv) and K$_2$CO$_3$ (0.47 g, 3.40 mmol, 1.3 equiv) in DMF (7.0 mL) was stirred at room temperature for 24 hours. The reaction mixture was diluted with 1.0 M HCl solution and extracted with EA. The organic phase was washed with 1.0 M HCl solution, water and brine, dried over anhydrous Na$_2$SO$_4$ and evaporated to dryness. The crude was purified by column chromatography on silica gel (PE:EA 100:1, R$_f$ = 0.47) to afford 523 mg (99 %) of **96e** as a colorless oil.

Spectral data were in accordance with a literature.[250]

96f
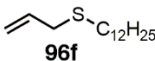
Allyl-*n*-dodecylsulfide 96f. A mixture of allylbromide (0.36 mL, 4.13 mmol, 1.0 equiv), *n*-dodecanethiol (1.29 mL, 5.37 mmol, 1.3 equiv) and K$_2$CO$_3$ (0.742 g, 5.37 mmol, 1.3 equiv) in DMF (7.0 mL) was stirred at room temperature for 24 hours. The reaction mixture was diluted with 1.0 M HCl solution and extracted with EA. The organic phase was washed with 1.0 M HCl solution, water and brine, dried over anhydrous Na$_2$SO$_4$ and evaporated to dryness. The crude was purified by column chromatography on silica gel (PE, R$_f$ = 0.54) to afford 994 mg (99 %) of **96f** as a colorless oil.

1H NMR (400 MHz, CDCl$_3$): δ 5.89 – 5.73 (m, 1H), 5.18 – 5.02 (m, 2H), 3.12 (d, J = 7.2 Hz, 2H), 2.44 (t, J = 7.5 Hz, 2H), 1.54 (q, J = 7.6 Hz, 2H), 1.41 – 1.33 (m, 2H), 1.26 (m, 16H), 0.88 (t, J = 6.7 Hz, 3H).

13C NMR (101 MHz, CDCl$_3$): δ 134.76, 116.80, 34.92, 32.07, 30.88, 29.80, 29.78, 29.75, 29.68, 29.49, 29.49, 29.41, 29.06, 22.84, 14.26.

HRMS-ESI$^+$: m/z [M+H]$^+$ calcd. for C$_{15}$H$_{31}$S 243.2141; found 243.2131.
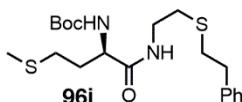
(R)-*tert*-Butyl (1-(methylthio)-4-oxo-6-(phenethylthio)hexan-3-yl)carbamate 96i. A mixture of N-((*tert*-butyloxy)carbonyl)-L-methionine p-nitrophenyl ester (600 mg, 1.622 mmol, 1.0 equiv), 2-(2-phenylethylsulfanyl)ethanamine (300 mg, 1.655 mmol, 1.02 equiv) and TEA (0.24 mL, 1.72 mmol, 1.04 equiv) in DMF (5.0 mL) was stirred at room temperature for 24 hours. The reaction mixture was diluted with water and extracted with EA. The organic phase was washed with water and brine, dried over anhydrous Na_2SO_4 and evaporated to dryness. The crude was purified by column chromatography on silica gel (DCM, $R_f = 0.19$) to afford 530 mg (79 %) of **96i** as a yellow solid. M.p. 48 – 50 °C.

^{1}H NMR (400 MHz, CDCl$_3$): δ 7.33 – 7.27 (m, 2H), 7.24 – 7.18 (m, 3H), 6.51 (s, 1H), 5.17 (s, 1H), 4.35 – 4.16 (m, 1H), 3.59 – 3.27 (m, 2H), 2.92 – 2.84 (m, 2H), 2.83 – 2.74 (m, 2H), 2.65 (t, *J* = 6.5 Hz, 2H), 2.62 – 2.47 (m, 2H), 2.10 (s, 3H), 2.09 – 2.03 (m, 1H), 1.97 – 1.85 (m, 1H), 1.44 (s, 9H)

^{13}C NMR (101 MHz, CDCl$_3$): δ 171.61, 155.67, 140.33, 128.65, 126.59, 80.32, 53.62, 38.48, 36.33, 33.32, 31.95, 31.80, 30.37, 28.46, 15.43.

HRMS-ESI$^+$: m/z [M+Na]$^+$ calcd. for $C_{20}H_{32}N_2O_3S_2Na$ 435.5962; found 435.1741.
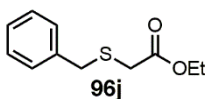
Ethyl(benzylthio)acetate 96j. Under inert atmosphere a mixture of ethyl mercaptoacetate (0.46 mL, 4.16 mmol, 1.0 equiv), benzylbromide (0.49 mL, 4.16 mmol, 1.0 equiv) and K_2CO_3 (0.63 g, 4.16 mmol, 1.0 equiv) in DMF (7.0 mL) was stirred at room temperature for 24 hours. The reaction mixture was diluted with water and extracted with EA. The organic phase was washed with water and brine, dried over anhydrous Na_2SO_4 and evaporated to dryness. The crude was purified by column chromatography on silica gel (PE:EA 50:1, $R_f = 0.29$) to afford 727 mg (83 %) of **96j** as a bluish oil. Spectral data were in accordance with a literature.[251]
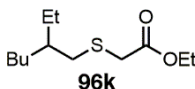

Ethyl(2-ethylhexylthio)acetate 96k. Under inert atmosphere a mixture of ethyl mercaptoacetate (0.46 mL, 4.16 mmol, 1.0 equiv), 2-

ethylhexylbromide (0.74 mL, 4.16 mmol, 1.0 equiv) and K_2CO_3 (633 mg, 4.16 mmol, 1.1 equiv) in DMF (7.0 mL) was stirred at room temperature for 24 hours. The reaction mixture was diluted with water and extracted with EA. The organic phase was washed with water and brine, dried over anhydrous Na_2SO_4 and evaporated to dryness. The crude was purified by column chromatography on silica gel (PE:EA 100:1, R_f = 0.2) to afford 938 mg (91 %) of **96k** as a colorless oil.

^{1}H NMR (400 MHz, CDCl$_3$): δ 4.19 (q, J = 7.2 Hz, 2H), 3.18 (s, 2H), 2.62 (d, J = 6.3 Hz, 2H), 1.58 – 1.46 (m, 1H), 1.45 – 1.17 (m, 11H), 0.99 – 0.82 (m, 6H).

^{13}C NMR (101 MHz, CDCl$_3$): δ 170.81, 61.39, 39.01, 37.34, 34.42, 32.47, 28.94, 25.63, 23.10, 14.33, 14.22, 10.87.

HRMS-ESI$^+$: m/z [M+H]$^+$ calcd. for $C_{12}H_{25}O_2S$ 233,1570; found 233.1556.

96l
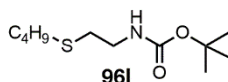
***tert*-Butyl-(2-(butylthio)ethyl)carbamate 96l**. A mixture of 2-[(tert-Butoxycarbonyl)amino]-1-ethanethiol (300 mg, 1.70 mmol, 1.0 equiv), *n*-butylbromide (0.22 mL, 2.03 mmol, 1.2 equiv) and K_2CO_3 (280 mg, 2.03 mmol, 1.2 equiv) in DMF (5.0 mL) was heated at 70 °C for 48 hours. The reaction mixture was cooled down to room temperature and it was diluted with water and extracted with EA. The organic phase was washed with water and brine, dried over anhydrous Na_2SO_4 and evaporated to dryness. The crude was purified by column chromatography on silica gel (PE:EA 30:1, R_f = 0.45) to afford 113 mg (29 %) of **96l** as a colorless oil.

^{1}H NMR (400 MHz, CDCl$_3$): δ 4.92 (s, 1H), 3.31 (q, J = 6.3 Hz, 2H), 2.63 (t, J = 6.5 Hz, 2H), 2.52 (t, J = 7.3 Hz, 2H), 1.61 – 1.50 (m, 2H), 1.45 (s, 9H), 1.44 – 1.34 (m, 2H), 0.91 (t, J = 7.3 Hz, 3H).

^{13}C NMR (101 MHz, CDCl$_3$): δ 155.92, 79.53, 39.86, 32.44, 31.91, 31.65, 28.54, 22.09, 13.80.

HRMS-ESI$^+$: m/z [M+H]$^+$ calcd. for $C_{11}H_{24}NO_2S$ 234.1522; found 234.1524.

96m
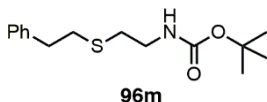
***tert*-Butyl-N-[2-(2-phenylethylthio)ethyl]carbamate 96m**. A mixture of 2-[(tert-Butoxycarbonyl)amino]-1-ethanethiol (237 mg, 1.33 mmol, 1.0 equiv), 2-phenylethylbromide (0.24 mL, 1.74 mmol, 1.3 equiv) and K_2CO_3 (240 mg,

1.74 mmol, 1.3 equiv) in DMF (5.0 mL) was heated at 70 °C for 48 hours. The reaction mixture was cooled down to room temperature and it was diluted with water and extracted with EA. The organic phase was washed with water and brine, dried over anhydrous Na_2SO_4 and evaporated to dryness. The crude was purified by column chromatography on silica gel (PE:EA 30:1, $R_f = 0.12$) to afford 165 mg (44 %) of **96m** as a colorless oil.

^{1}H NMR (400 MHz, CDCl$_3$): δ 7.34 – 7.27 (m, 2H), 7.25 – 7.18 (m, 3H), 4.88 (s, 1H), 3.31 (q, *J* = 8.1, 6.3 Hz, 2H), 2.99 – 2.84 (m, 2H), 2.84 – 2.75 (m, 2H), 2.65 (t, *J* = 6.5 Hz, 2H), 1.44 (s, 9H).

^{13}C NMR (101 MHz, CDCl$_3$): δ 155.85, 140.38, 128.60, 128.59, 126.52, 36.38, 33.42, 32.55, 28.50, 28.48, 28.29.

HRMS-ESI$^+$: m/z [M+H]$^+$ calcd. for $C_{15}H_{24}NO_2S$ 282.1522; found 282.1522.

96n
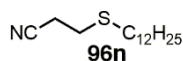
3-(*n*-Dodecylthio)propanenitrile 96n. 1-dodecanethiol (4.5 mL, 18.86 mmol, 2.0 equiv) and NaOMe (146 mg, 2.70 mmol, 0.05 equiv) were dissolved in MeOH (20 mL) and the solution was cooled down to 0 °C in an ice bath. Acrylonitrile (0.61 mL, 9.43 mmol, 1.0 equiv) was added dropwise over a period of approx. 10 min. The reaction was allowed to reach room temperature overnight. The reaction mixture was evaporated to dryness. Then the crude was dissolved in CHCl$_3$ and washed with washed with water and brine. The crude was purified by column chromatography on silica gel (PE:EA 40:1, $R_f = 0.33$) to afford 2.31 g (96 %) of **96n** as a white solid. Spectral data were in accordance with a literature.[252]


96o
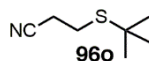
3-(*tert*-Butylthio)propanenitrile 96o. 2-methyl-2-propanethiol (2.1 mL, 18.86 mmol, 2.0 equiv) and NaOMe (146 mg, 2.70 mmol, 0.05 equiv) were dissolved in MeOH (20 mL) and the solution was cooled down to 0 °C in an ice bath. Acrylonitrile (0.61 mL, 9.43 mmol, 1.0 equiv) was added dropwise over a period of approx. 10 min. The reaction was allowed to reach room temperature overnight. The reaction mixture was evaporated to dryness. Then the crude was dissolved in CHCl$_3$ and washed with water and brine. The crude was purified by column chromatography on silica gel (PE:EA 40:1, $R_f = 0.33$) to afford 1.05 g (78 %) of **96o** as a white solid. Spectral data were in accordance with a literature.[253]

96p
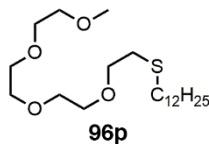
_n_-Dodecylmethyl-2,5,8,11-tetraoxatridecane-13-sulfide 96p. A mixture of 1-dodecanethiol (0.13 mL, 0.538 mmol, 1.0 equiv), 1-bromo-tetraethyleneglycol monomethyl ether (146 mg, 0.538 mmol, 1.0 equiv) and K_2CO_3 (82 mg, 0.592 mmol, 1.1 equiv) in DMF (4.0 mL) was stirred at room temperature for 24 hours. The reaction mixture was diluted with water and extracted with EA. The organic phase was washed with water and brine, dried over anhydrous Na_2SO_4 and evaporated to dryness. The crude was purified by column chromatography on silica gel (PE:EA 1:1, R_f = 0.25) to afford 166 mg (78 %) of **96p** as a colorless oil.

^{1}H NMR (400 MHz, CDCl_3): δ 3.71 – 3.60 (m, 12H), 3.58 – 3.51 (m, 2H), 3.38 (s, 3H), 2.70 (t, _J_ = 7.1 Hz, 2H), 2.53 (t, _J_ = 7.24 Hz, 2H), 1.61 – 1.52 (m, 2H), 1.41 – 1.19 (m, 18H), 0.87 (t, _J_ = 6.64 Hz, 3H).

^{13}C NMR (101 MHz, CDCl_3): δ 72.11, 71.19, 70.79, 70.76, 70.70, 70.46, 59.20, 32.76, 32.07, 31.53, 29.98, 29.81, 29.78, 29.76, 29.69, 29.50, 29.41, 29.04, 22.84, 14.27.

HRMS-ESI[+]: m/z [M+H][+] calcd. for $C_{21}H_{45}O_4S$ 393.3033; found 393.3037.

96q
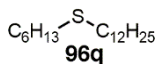
_n_-dodecylhexylsulfide 96q. A mixture of 1-dodecanethiol (0.59 mL, 2.47 mmol, 1.0 equiv), 1-bromohexane (0.35 mL, 2.47 mmol, 1.0 equiv) and K_2CO_3 (0.44 g, 3.21 mmol, 1.3 equiv) in DMF (7.0 mL) was stirred at room temperature for 24 hours. The reaction mixture was diluted with water and extracted with EA. The organic phase was washed with water and brine, dried over anhydrous Na_2SO_4 and evaporated to dryness. The crude was purified by column chromatography on silica gel (PE, R_f = 0.34) to afford 635 mg (90 %) of **96q** as a colorless oil.

^{1}H NMR (400 MHz, CDCl_3): δ 2.50 (t, _J_ = 7.4 Hz, 4H), 1.63 – 1.52 (m, 4H), 1.43 – 1.33 (m, 4H), 1.33 – 1.21 (m, 20H), 0.94 – 0.83 (m, 6H).

^{13}C NMR (101 MHz, CDCl_3): δ 32.36, 32.07, 31.63, 29.91, 29.87, 29.81, 29.79, 29.76, 29.69, 29.50, 29.42, 29.12, 28.80, 22.84, 22.72, 14.27, 14.19.

HRMS-ESI[+]: m/z [M+H][+] calcd. for $C_{18}H_{39}SO$ 303.2716; found 303.2718 (only sulfoxide formed during the measurements can be detected with ESI).
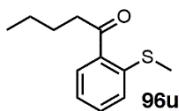
1-(2-(methylthio)phenyl)pentan-1-one 96u. Under inert atmosphere 1-(2-mercaptophenyl)pentan-1-one (300 mg, 1.54 mmol, 1.0 equiv) was added to a suspension of NaH 60 % (62 mg, 1.54 mmol, 1.0 equiv) in anhydrous THF (5.0 mL) and the mixture was stirred for 10 min. Then MeI (0.12 mL, 1.85 mmol, 1.2 equiv) was added and the reaction mixture was stirred at room temperature for 24 hours. The reaction mixture was quenched with H_2O and extracted with DCM. The organic phase was dried over anhydrous Na_2SO_4 and evaporated to dryness. The crude was purified by column chromatography on silica gel (PE:EA 100:1, R_f = 0.22) to afford 267 mg (83 %) of **96u** as a yellow oil.

^{1}H NMR (400 MHz, CDCl$_3$): δ 7.82 (dd, J = 7.8, 1.5 Hz, 1H), 7.46 (td, J = 7.5 Hz, 1.5 Hz, 1H), 7.33 (d, J = 8.0 Hz, 1H), 7.19 (td, J = 7.5, 1.2 Hz, 1H), 2.95 (t, J = 7.4 Hz, 2H), 2.43 (s, 3H), 1.72 (p, J = 7.5 Hz, 2H), 1.46 – 1.35 (m, 2H), 0.94 (t, J = 7.3 Hz, 3H).

^{13}C NMR (101 MHz, CDCl$_3$): δ 202.01, 142.20, 135.06, 132.06, 130.12, 125.37, 123.63, 40.00, 26.70, 22.62, 16.20, 14.09.

HRMS-ESI$^+$: m/z [M+H]$^+$ calcd. for $C_{12}H_{17}OS$ 209.0995; found 209.0994.
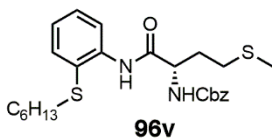
(S)-benzyl (1-((2-(hexylthio)phenyl)amino)-4-(methylthio)-1-oxobutan-2-yl)carbamate 96v. Under inert atmosphere a mixture of 2-(hexylthio)aniline (300 mg, 1.43 mmol, 1.5 equiv), N-Carbobenzyloxy-L-methionine (270 mg, 0.96 mmol, 1.0 equiv), DIPEA (0.18 mL, 1.05 mmol, 1.1 equiv) and HATU (400 mg, 1.05 mmol, 1.1 equiv) in anhydrous DCM (5.0 mL) was stirred at room temperature for 24 hours. The reaction mixture was diluted with water and extracted with DCM. The organic phase was washed with water and brine, dried over anhydrous Na_2SO_4 and evaporated to dryness. The crude was purified by column chromatography on silica gel (CHCl$_3$:MeOH 100:1, R_f = 0.44) to afford 380 mg (56 %) of **96v** as a yellow solid. M.p. 59 – 61 °C.

^{1}H NMR (400 MHz, CDCl$_3$): δ 9.12 (s, 1H), 8.36 (dd, J = 8.0, 1.0 Hz, 1H), 7.50 (dd, J = 7.6, 1.5 Hz, 1H), 7.42 – 7.28 (m, 6H), 7.07 (td, J = 7.6, 1.4 Hz, 1H), 5.63 (d, J = 8.1 Hz, 1H), 5.15 (s, 2H), 4.59 (d, J = 7.2 Hz, 1H), 2.81 – 2.47 (m, 4H), 2.33 – 2.18 (m, 1H), 2.12 (s, 3H), 2.10 – 2.01 (m, 1H), 1.51 (p,

J = 7.4 Hz, 2H), 1.34 (p, J = 9.2, 8.3 Hz, 2H), 1.29 – 1.17 (m, 4H), 0.86 (t, J = 6.9 Hz, 3H).

^{13}C NMR (101 MHz, CDCl$_3$): δ 169.44, 156.17, 138.86, 136.18, 135.14, 129.53, 128.70, 128.40, 128.24, 124.57, 123.95, 120.33, 67.40, 55.22, 36.35, 31.73, 31.43, 30.27, 29.61, 28.46, 22.64, 15.44, 14.13.

HRMS-ESI$^+$: m/z [M+H]$^+$ calcd. for C$_{25}$H$_{35}$N$_2$O$_3$S$_2$ 475.2084; found 475.2086.

General procedure C for photocatalytic oxidation of sulfides:

a) Using **C$_{60}$ solution in toluene** (5.0 mg in 2.0 mL) as a catalyst. The substrate (0.05 – 0.2 mmol) was dissolved in 2.0 mL of the solvent (EtOH or CH$_3$CN) and the solution of C$_{60}$ was added (50 µL). Then the reaction mixture was irradiated with a Blue LED (450 ± 10 nm, 100 W) with continuous stirring at room temperature. The progress of the reaction was monitored by TLC. After the complete conversion was achieved, the solvent was removed under reduced pressure. The crude was purified by column chromatography on silica gel (eluent CHCl$_3$ or CHCl$_3$:MeOH 100:1).

b) Using **C$_{60}$ soot powder** as a catalyst. The substrate (0.05 – 0.2 mmol) was dissolved in 2.0 mL of the solvent (EtOH or CH$_3$CN) and 1.0 mg of C$_{60}$ soot was added. Then the reaction mixture was purged with O$_2$ for 15 minutes and was irradiated with a Blue LED (450 ± 10 nm, 100 W) with continuous stirring at room temperature. The progress of the reaction was monitored by TLC. After the complete conversion was achieved, the solvent was removed under reduced pressure. The crude was purified by column chromatography on silica gel (eluent CHCl$_3$ or CHCl$_3$:MeOH 100:1).

c) Using **C$_{60}$ soot suspension in toluene** (2.0 mg in 4.0 mL) as a catalyst. The substrate (0.05 – 0.2 mmol) was dissolved in 2.0 mL of the solvent (EtOH or CH$_3$CN) and the solution of C$_{60}$ soot was added (100 µL). Then the reaction mixture was purged with O$_2$ for 15 minutes and was irradiated with a Blue LED (450 ± 10 nm, 100 W) with continuous stirring at room temperature. The progress of the reaction was monitored by TLC. After the complete conversion was achieved, the solvent was removed under reduced pressure. The crude was purified by column chromatography on silica gel (eluent CHCl$_3$ or CHCl$_3$:MeOH 100:1).
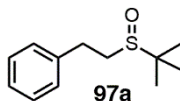
(2-(tert-Butylsulfinyl)ethyl)benzene 97a. The product was obtained as a colorless oil following the general procedure **C**: a) in EtOH irradiated with a

Blue LED for 24 hours (yield 78 %) or in CH$_3$CN irradiated with a Blue LED for 48 hours (yield 48 %); b) in EtOH irradiated with a Blue LED for 96 hours (yield 93 %); c) in EtOH irradiated with a Blue LED for 24 hours (yield 97 %) or in CH$_3$CN irradiated with a Blue LED for 96 hours (yield 81 %).

Spectral data were in accordance with a literature.[254]

97b
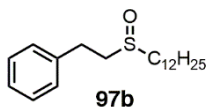
(2-(*n*-Dodecylsulfinyl)ethyl)benzene 97b. The product was obtained as a white solid following the general procedure **C**: a) in EtOH irradiated with a Blue LED for 24 hours (yield 99 %) or in CH$_3$CN irradiated with a Blue LED for 48 hours (yield 60 %); b) in EtOH irradiated with a Blue LED for 5 days (yield 99 %); c) in EtOH irradiated with a Blue LED for 24 hours (yield 93 %) or in CH$_3$CN irradiated with a Blue LED for 48 hours (yield 82 %). M.p. 66 – 68 °C.

^{1}H NMR (400 MHz, CDCl$_3$): δ 7.35 – 7.29 (m, 2H), 7.27 – 7.22 (m, 3H), 3.20 – 3.03 (m, 2H), 3.01 – 2.84 (m, 2H), 2.78 – 2.68 (m, 1H), 2.67 – 2.56 (m, 1H), 1.83 – 1.69 (m, 2H), 1.52 – 1.37 (m, 2H), 1.25 (s, 16H), 0.88 (t, *J* = 6.7 Hz, 3H).

^{13}C NMR (101 MHz, CDCl$_3$): δ 139.17, 128.93, 128.71, 126.90, 53.93, 52.75, 32.05, 29.75, 29.67, 29.49, 29.47, 29.33, 29.02, 22.83, 22.77, 14.26.

HRMS-ESI$^+$: m/z [M+H]$^+$ calcd. for C$_{20}$H$_{35}$OS 323.2403; found 323.2403.

97c

Isobornyl 3-(*tert*-butylsulfinyl)propionate 97c. The product was obtained as a colorless oil following the general procedure **C**: a) in EtOH irradiated with a Blue LED for 48 hours (yield 84 %) or in CH$_3$CN irradiated with a Blue LED for 48 hours (yield 35 %); b) in EtOH irradiated with a Blue LED for 48 hours (yield 74 %); c) in EtOH irradiated with a Blue LED for 48 hours (yield 74 %) or in CH$_3$CN irradiated with a Blue LED for 48 hours (yield 55 %).

^{1}H NMR (400 MHz, CDCl$_3$): δ 4.77 – 4.64 (m, 1H), 2.95 – 2.77 (m, 3H), 2.75 – 2.55 (m, 1H), 1.90 – 1.66 (m, 4H), 1.58 – 1.48 (m, 1H), 1.27 (s, 9H), 1.21 – 1.03 (m, 2H), 0.96 (s, 3H), 0.84 (s, 6H).

¹³C NMR (101 MHz, CDCl₃): δ 171.24, 82.06, 82.01, 53.42, 48.91, 48.89, 47.08, 45.15, 45.14, 40.88, 38.88, 38.86, 33.83, 28.77, 28.75, 27.14, 22.93, 20.21, 20.07, 11.63, 11.62.

HRMS-ESI⁺: m/z [M+Na]⁺ calcd. for $C_{17}H_{31}O_3SNa$ 337.1808; found 337.1812.

97d
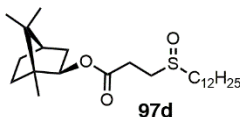
Isobornyl 3-(*n*-dodecylsulfinyl)propionate 97d. The product was obtained as a white solid following the general procedure **C**: a) in EtOH irradiated with a Blue LED for 24 hours (yield 69 %) or in CH₃CN irradiated with a Blue LED for 48 hours (yield 86 %); b) i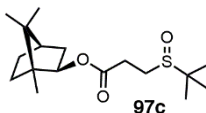n EtOH irradiated with a Blue LED for 48 hours (yield 88 %); c) in EtOH irradiated with a Blue LED for 48 hours (yield 92 %) or in CH₃CN irradiated with a Blue LED for 48 hours (yield 78 %). M.p. 70 – 74 °C.

¹H NMR (400 MHz, CDCl₃): δ 4.70 (dt, *J* = 7.1 Hz, 3.1 Hz, 1H), 3.11 – 2.93 (m, 1H), 2.93 – 2.77 (m, 3H), 2.77 – 2.59 (m, 2H), 1.88 – 1.61 (m, 6H), 1.61 – 1.50 (m, 1H), 1.50 – 1.39 (m, 2H), 1.25 (s, 16H), 1.19 – 1.04 (m, 2H), 0.96 (s, 3H), 0.92 – 0.77 (m, 9H).

¹³C NMR (101 MHz, CDCl₃): δ 170.98, 82.13, 82.10, 52.92, 48.91, 48.89, 47.08, 47.04, 45.13, 38.84, 33.82, 32.04, 29.74, 29.66, 29.48, 29.47, 29.32, 28.98, 27.57, 27.12, 22.82, 22.76, 20.20, 20.06, 14.25, 11.61.

HRMS-ESI⁺: m/z [M+Na]⁺ calcd. for $C_{25}H_{47}O_3SNa$ 449.3060; found 449.3049.

97e

8-(*tert*-Butylsulfinyl)oct-1-ene 97e. The product was obtained as a yellow oil following the general procedure **C**: a) in EtOH irradiated with a Blue LED for 24 hours (yield 92 %) or in CH₃CN irradiated with a Blue LED for 24 hours (yield 59 %); b) in EtOH irradiated with a Blue LED for 72 hours (yield 77 %); c) in EtOH irradiated with a Blue LED for 24 hours (yield 85 %) or in CH₃CN irradiated with a Blue Led for 24 hours (yield 94 %).

¹H NMR (400 MHz, CDCl₃): δ 5.79 (ddt, *J* = 16.9, 10.1, 6.7 Hz, 1H), 5.06 – 4.89 (m, 2H), 2.44 (t, *J* = 7.7 Hz, 2H), 2.04 (q, *J* = 6.8 Hz, 2H), 1.95 – 1.72 (m, 2H), 1.57 – 1.32 (m, 6H), 1.23 (s, 9H).

13C NMR (101 MHz, CDCl₃): δ 138.99, 114.51, 52.81, 45.76, 33.74, 29.01, 28.82, 28.75, 23.85, 23.02.

HRMS-ESI⁺: m/z [M+H]⁺ calcd. for $C_{12}H_{25}OS$ 217.1621; found 217.1621.

97f
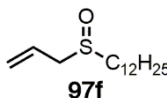
Allyl(*n*-dodecyl)sulfoxide 97f. The product was obtained as a yellow solid following the general procedure **C**: a) in EtOH irradiated with a Blue LED for 24 hours (yield 68 %) or in CH₃CN irradiated with a Blue LED for 72 hours (yield 71 %); c) in EtOH irradiated with a Blue LED for 72 hours (yield 90 %) or in CH₃CN irradiated with a Blue Led for 72 hours (yield 70 %). M.p. 56 – 60 °C.

Using C₆₀/C₇₀ nanodispersion: The substrate (35.4 mg, 0.146 mmol) was dissolved EtOH (2.0 mL) and the solution of C₆₀/C₇₀ (1.0 mg/1.0 mg in 0.8 mL toluene) was added (50 μL). Then the reaction mixture was irradiated with a Blue LED (450 ± 10 nm, 100 W) with continuous stirring at room temperature for 24 hours. The reaction course was monitored by TLC. After the complete conversion was achieved, the solvent was removed under reduced pressure. The crude waas purified by column chromatography on silica gel (CHCl₃:MeOH 100:1) to afford 28.3 mg (75 %) of **97f**.

1H NMR (400 MHz, CDCl₃): δ 5.88 (ddt, *J* = 17.6, 10.2, 7.5 Hz, 1H), 5.47 – 5.32 (m, 2H), 3.55 – 3.34 (m, 2H), 2.75 – 2.60 (m, 2H), 1.82 – 1.68 (m, 2H), 1.52 – 1.37 (m, 2H), 1.25 (s, 16H), 0.86 (t, *J* = 6.7 Hz, 3H).

13C NMR (101 MHz, CDCl₃): δ 126.05, 123.42, 55.94, 51.16, 32.02, 29.71, 29.64, 29.47, 29.44, 29.32, 28.98, 22.79, 22.58, 14.23.

HRMS-ESI⁺: m/z [M+H]⁺ calcd. for $C_{15}H_{31}OS$ 259.2090; found 259.2090.

97g

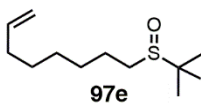**Dibenzylsulfoxide 97g.** The product was obtained as a white solid following the general procedure **C**: a) in EtOH irradiated with a Blue Led for 24 hours (yield 98 %) or in CH₃CN irradiated with a Blue LED for 4 days (yield 69 %); b) in EtOH irradiated with a Blue LED for 6 days (yield 81 %); c) in EtOH irradiated with a Blue LED for 24 hours (yield 94 %).

Spectral data were in accordance with a literature.[255]

97h
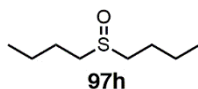
Dibutylsulfoxide 97h. The product was obtained as a colorless crystals following the general procedure **C**: a) in EtOH irradiated with a Blue LED for 24 hours (yield 79 %) or in CH₃CN irradiated with a Blue Led for 24 hours (yield 80 %); b) in EtOH irradiated with a Blue LED for 7 days (yield 82 %); c) in EtOH irradiated with a Blue LED for 24 hours (yield 57 %) or in CH₃CN irradiated with a Blue LED for 72 hours (yield 90 %).

Spectral data were in accordance with a literature.[256]

97i
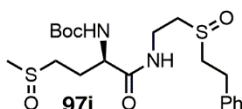
***tert*-Butyl((3R)-1-(methylsulfinyl)-4-oxo-6-(phenethylsulfinyl)hexan-3-yl)carbamate 97i.** The product was obtained as a white solid following the general procedure **C**: a) in EtOH irradiated with a Blue LED for 24 hours (yield 73 %) or in CH₃CN irradiated with a Blue LED for 24 hours (yield 51 %); b) in EtOH irradiated with a Blue LED for 24 hours (yield 35 %); c) in EtOH irradiated with a Blue Led for 24 hours (yield 92 %) or in CH₃CN irradiated with a Blue LED for 24 hours (yield 36 %). M.p. 78 – 86 °C.

¹H NMR (400 MHz, CDCl₃): δ 7.77 (d, *J* = 36.4 Hz, 1H), 7.30 (t, *J* = 7.5 Hz, 2H), 7.25 – 7.20 (m, 3H), 5.82 (d, *J* = 39.8 Hz, 1H), 4.33 (s, 1H), 3.83 – 3.59 (m, 2H), 3.17 – 2.90 (m, 5H), 2.91 – 2.71 (m, 3H), 2.58 (s, 3H), 2.35 – 2.07 (m, 2H), 1.42 (s, 9H).

¹³C NMR (101 MHz, CDCl₃): δ 171.77, 155.76, 138.65, 128.94, 128.68, 126.98, 80.25, 53.99, 52.99, 51.57, 34.29, 34.20, 28.85, 28.46, 27.18, 26.21.

HRMS-ESI⁺: m/z [M+H]⁺ calcd. for C₂₅H₃₅N₂O₅S₂ 507.1982; found 507.1982.

97j
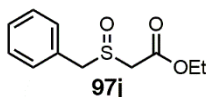
Ethylbenzylsulfinylacetate 97j. The product was obtained as a white solid following the general procedure **C**: a) in EtOH irradiated with a Blue LED for 24 hours (yield 59 %) or in CH₃CN irradiated with a Blue LED for 24 hours (yield 21 %); b) in EtOH irradiated with a Blue LED for 48 hours (yield 58 %); c) in EtOH irradiated with a Blue LED for 48 hours (yield 44 %) or in CH₃CN irradiated with a Blue LED for 48 hours (yield 18 %).

Spectral data were in accordance with a literature.[251]

Et   O   O
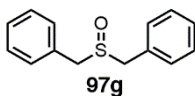Bu   S   OEt
                97k
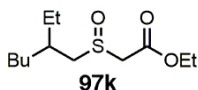
2-Ethylhexylethoxycarbonylmethylsulfoxide 97k. The product was obtained as a colorless oil following the general procedure **C**: a) in EtOH irradiated with a Blue LED for 24 hours (yield 56 %) or in CH$_3$CN irradiated with a Blue LED for 72 hours (yield 36 %); b) in EtOH irradiated with a Blue LED for 72 hours (yield 47 %); c) in EtOH irradiated with a Blue LED for 24 hours (yield 53 %) or in CH$_3$CN irradiated with a Blue LED for 72 hours (yield 16 %).

^{1}H NMR (400 MHz, CDCl$_3$): δ 4.25 (q, J = 7.1 Hz, 2H), 3.68 (d, J = 1.2 Hz, 2H), 2.86 (dt, J = 13.0, 4.3 Hz, 1H), 2.73 (ddd, J = 13.0, 9.1, 6.9 Hz, 1H), 2.02 – 1.90 (m, 1H), 1.57 – 1.37 (m, 4H), 1.31 (t, J = 7.1 Hz, 7H), 0.97 – 0.87 (m, 6H).

^{13}C NMR (101 MHz, CDCl$_3$): δ 165.34, 62.25, 58.87, 58.73, 56.87, 56.84, 34.55, 34.29, 32.85, 32.20, 28.64, 28.37, 26.32, 25.32, 23.01, 22.94, 14.28, 14.15, 10.71, 10.27.

HRMS-ESI$^+$: m/z [M+H]$^+$ calcd. for C$_{12}$H$_{25}$O$_3$S 249.1519; found 249.1519.

C$_4$H$_9$ S   N   O
                O   97l   O
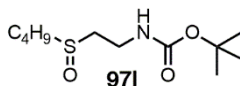
***tert*-Butyl(2-(butylsulfinyl)ethyl)carbamate 97l.** The product was obtained as a white solid following the general procedure **C**: a) in EtOH irradiated with a Blue LED for 24 hours (yield 96 %) or in CH$_3$CN irradiated with a Blue LED for 24 hours (yield 97 %); b) in EtOH irradiated with a Blue LED for 5 days (yield 72 %); c) in EtOH irradiated with a Blue LED for 24 hours (yield 98 %) or in CH$_3$CN irradiated with a Blue LED for 24 hours (yield 65 %). M.p. 48 – 52 °C.

^{1}H NMR (400 MHz, CDCl$_3$): δ 5.29 (s, 1H), 3.62 (q, J = 6.0 Hz, 2H), 2.96 (dt, J = 12.9 Hz, 1H), 2.85 – 2.73 (m, 2H), 2.73 – 2.60 (m, 1H), 1.83 – 1.67 (m, 2H), 1.57 – 1.36 (m, 11H), 0.95 (t, J = 7.3 Hz, 3H).

**^{13}C NMR** (101 MHz, CDCl$_3$): δ 156.04, 79.83, 52.55, 51.77, 35.41, 28.47, 24.71, 22.13, 13.78.

HRMS-ESI$^+$: m/z [M+H]$^+$ calcd. for C$_{11}$H$_{24}$NO$_3$S 250.1471; found 250.1465.
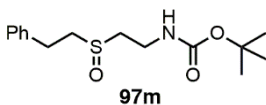
tert-Butyl(2-(phenethylsulfinyl)ethyl)carbamate 97m. The product was obtained as a white solid following the general procedure **C**: a) in EtOH irradiated with a Blue LED for 24 hours (yield 82 %) or in CH$_3$CN irradiated with a Blue LED for 24 hours (yield 60 %); b) in EtOH irradiated with a Blue LED for 24 hours (yield 98 %); c) in EtOH irradiated with a Blue LED for 48 hours (yield 42 %) or in CH$_3$CN irradiated with a Blue LED for 24 hours (yield 78 %). M.p. 58 – 60 °C.

^{1}H NMR (400 MHz, CDCl$_3$): δ 7.36 – 7.29 (m, 2H), 7.25 (dd, J = 7.5 Hz, 5.7 Hz, 3H), 5.23 (s, 1H), 3.64 (q, J = 6.1 Hz, 2H), 3.17 – 3.02 (m, 3H), 3.02 – 2.91 (m, 2H), 2.80 (dt, J = 13.1 Hz, 5.4 Hz, 1H), 1.43 (s, 9H).

^{13}C NMR (101 MHz, CDCl$_3$): δ 156.01, 138.75, 128.97, 128.70, 127.01, 79.94, 54.21, 51.96, 35.45, 28.97, 28.49.

HRMS-ESI$^+$: m/z [M+H]$^+$ calcd. for C$_{15}$H$_{24}$NO$_3$S 298.1471; found 298.1469.
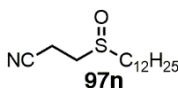
(n-Dodecylsulfinyl)propanenitrile 97n. The product was obtained as a white solid following the general procedure **C**: a) in EtOH irradiated with a Blue LED for 48 hours (yield 92 %) or in CH$_3$CN irradiated with a Blue LED for 24 hours (yield 61 %); b) in EtOH irradiated with a Blue LED for 48 hours (yield 67 %); c) in EtOH irradiated with a Blue LED for 24 hours (yield 96 %) or in CH$_3$CN irradiated with a Blue LED for 48 hours (yield 80 %). M.p. 72 – 74 °C.

^{1}H NMR (400 MHz, CDCl$_3$): δ 3.04 – 2.93 (m, 1H), 2.93 – 2.84 (m, 3H), 2.84 – 2.75 (m, 1H), 2.74 – 2.62 (m, 1H), 1.87 – 1.68 (m, 2H), 1.56 – 1.38 (m, 2H), 1.25 (s, 16H), 0.86 (t, J = 6.7 Hz, 3H).

^{13}C NMR (101 MHz, CDCl$_3$): δ 117.60, 52.76, 46.56, 31.98, 29.67, 29.58, 29.40, 29.23, 28.82, 22.76, 22.67, 14.20, 11.10.

HRMS-ESI$^+$: m/z [M+H]$^+$ calcd. for C$_{15}$H$_{30}$NOS 272.2043; found 272.2043.
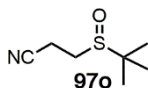
(tert-Butylsulfinyl)propanenitrile 97o. The product was obtained as a yellow oil following the general procedure **C**: a) in EtOH irradiated with a

Blue LED for 48 hours (yield 72 %) or in CH$_3$CN irradiated with a Blue LED for 48 hours (yield 89 %); b) in EtOH irradiated with a Blue LED for 72 hours (yield 70 %); c) in EtOH irradiated with a Blue LED for 48 hours (yield 53 %) or in CH$_3$CN irradiated with a Blue LED for 72 hours (yield 59 %).

^{1}H NMR (400 MHz, CDCl$_3$): δ 2.96 – 2.61 (m, 4H), 1.25 (s, 9H).

^{13}C NMR (101 MHz, CDCl$_3$): δ 117.67, 54.00, 40.97, 22.73, 12.56.

HRMS-ESI$^+$: m/z [M+H]$^+$ calcd. for C$_7$H$_{14}$NOS 160.0791; found 160.0783.

97p
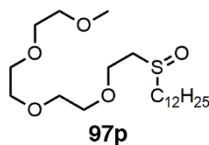
***n*-Dodecyl-2,5,8,11-tetraoxatridecane-13-sulfoxide 97p.** The product was obtained as a yellow solid following the general procedure **C**: a) in EtOH irradiated with a Blue LED for 24 hours (yield 99 %) or in CH$_3$CN irradiated with a Blue LED for 24 hours (yield 80 %); b) in EtOH irradiated with a Blue LED for 72 hours (yield 88 %) or in CH$_3$CN irradiated with a Blue LED for 9 days (yield 79 %); c) in EtOH irradiated with a Blue LED for 72 hours (yield 97 %) or in CH$_3$CN irradiated with a Blue LED for 72 hours (yield 82 %). M.p. 38 – 40 °C.

^{1}H NMR (400 MHz, CDCl$_3$): δ 3.90 (dd, *J* = 7.0, 4.3 Hz, 2H), 3.73 – 3.59 (m, 10H), 3.57 – 3.51 (m, 2H), 3.36 (s, 3H), 2.97 (dt, *J* = 13.7, 7.0 Hz, 1H), 2.83 (dt, *J* = 13.3, 4.3 Hz, 1H), 2.78 – 2.63 (m, 2H), 1.85 – 1.67 (m, 2H), 1.53 – 1.37 (m, 2H), 1.25 (s, 16H), 0.86 (t, *J* = 6.7 Hz, 3H).

^{13}C NMR (101 MHz, CDCl$_3$): δ 72.07, 70.80, 70.75, 70.73, 70.66, 70.57, 63.85, 59.15, 53.09, 52.79, 32.01, 29.72, 29.66, 29.48, 29.44, 29.34, 28.97, 22.79, 22.78, 14.22.

HRMS-ESI$^+$: m/z [M+H]$^+$ calcd. for C$_{21}$H$_{45}$O$_5$S 409.2982; found 409.2983.

97q
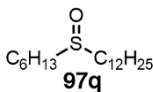
***n*-Dodecylhexylsulfoxide 97q.** The product was obtained as a white solid following the general procedure **C**: a) in EtOH irradiated with a Blue LED for 24 hours (yield 95 %) or in CH$_3$CN irradiated with a Blue LED for 48 hours (yield 93 %); b) in EtOH irradiated with a Blue LED for 96 hours (yield 98 %) or in CH$_3$CN irradiated with a Blue LED for 72 hours (yield 85 %); c) in EtOH irradiated with a Blue LED for 48 hours (yield 92 %) or in

CH$_3$CN irradiated with a Blue LED for 48 hours (yield 82 %). M.p. 63 – 64 °C.

^{1}H NMR (400 MHz, CDCl$_3$): δ 2.81 – 2.70 (m, 2H), 2.70 – 2.59 (m, 2H), 1.85 – 1.68 (m, 4H), 1.55 – 1.38 (m, 4H), 1.37 – 1.20 (m, 20H), 0.95 – 0.83 (m, 6H).

^{13}C NMR (101 MHz, CDCl$_3$): δ 52.38, 32.05, 31.51, 29.75, 29.68, 29.51, 29.48, 29.35, 29.02, 28.69, 22.83, 22.78, 22.74, 22.55, 14.26, 14.11.

HRMS-ESI$^+$: m/z [M+H]$^+$ calcd. for C$_{18}$H$_{39}$OS 303.2716; found 303.2716.

97r
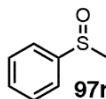
Methyl phenyl sulfoxide 97r. Solvent in the reaction vial was purged with O$_2$ for 15 minutes. Thioanisole (45.4 mg, 0.37 mmol, 1.0 equiv) and TEA (10 µL, 0.073 mmol, 0.2 equiv) was dissolved in 2.0 mL of the solvent. Then solution of C$_{60}$ in toluene was added (50 µL) and the reaction mixture was irradiated with a Blue LED (450 ± 10nm, 100W) with continuous stirring at room temperature for 5 days. The reaction course was monitored by TLC. After the complete conversion was achieved, the solvent was removed under reduced pressure. The crudes were purified by column chromatography on silica gel (CHCl$_3$:MeOH 100:1, R$_f$ = 0.1) to afford 49 mg (95 %) of **97r** as a yellow oil.

Spectral data were in accordance with a literature.[257]

97s
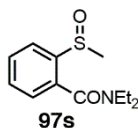
_N_,_N_-diethyl-2-(methylsulfinyl)benzamide 97s. Solvent in the reaction vial was purged with O$_2$ for 15 minutes. N,N-diethyl-2-(methylthio)benzamide (36 mg, 0.16 mmol, 1.0 equiv) and TEA (3.2 mg, 0.032 mmol, 0.2 equiv) was dissolved in EtOH (2.0 mL). Then solution of C$_{60}$ in toluene was added (50 µL) and the reaction mixture was irradiated with a Blue LED (450 ± 10nm, 100W) with continuous stirring at room temperature for 7 days. The reaction course was monitored by TLC. After the complete conversion was achieved, the solvent was removed under reduced pressure. The crudes were purified by column chromatography on silica gel (CHCl$_3$:MeOH 100:1, R$_f$ = 0.1) to afford 34 mg (89 %) of **97s** as a yellow oil.

^{1}H NMR (400 MHz, CDCl$_3$): δ 8.12 (dd, _J_ = 7.9, 1.3 Hz, 1H), 7.64 (td, _J_ = 7.7, 1.3 Hz, 1H), 7.51 (td, _J_ = 7.5, 1.3 Hz, 1H), 7.29 (dd, _J_ = 7.5, 1.3 Hz,

1H), 3.64 (dq, J = 14.2, 7.1 Hz, 1H), 3.44 (dq, J = 14.0, 7.1 Hz, 1H), 3.21 (qd, J = 7.2, 4.5 Hz, 2H), 2.85 (s, 3H), 1.25 (t, J = 7.1 Hz, 3H), 1.11 (t, J = 7.1 Hz, 3H).

^{13}C NMR (101 MHz, CDCl$_3$): δ 167.63, 144.09, 134.07, 130.81, 130.43, 125.79, 123.84, 44.37, 43.38, 39.37, 14.14, 12.63.

HRMS-ESI$^+$: m/z [M+H]$^+$ calcd. for C$_{12}$H$_{18}$NO$_2$S 240.1053; found 240.1053.
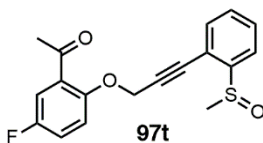
1-(5-fluoro-2-((3-(2-(methylsulfinyl)phenyl)prop-2-yn-1-yl)oxy)phenyl)ethenone 97t. Solvent in the reaction vial was purged with O$_2$ for 15 minutes. 1-(5-fluoro-2-((3-(2-(methylthio)phenyl)prop-2-yn-1-yl)oxy)phenyl)ethenone (37 mg, 0.12 mmol, 1.0 equiv) and TEA (2.4 mg, 0.024 mmol, 0.2 equiv) was dissolved in EtOH (2.0 mL). Then solution of C$_{60}$ in toluene was added (50 µL) and the reaction mixture was irradiated with a Blue LED (450 ± 10 nm, 100 W) with continuous stirring at room temperature for 8 days. The progress of the reaction was monitored by TLC. After the complete conversion was achieved, the solvent was removed under reduced pressure. The crudes were purified by column chromatography on silica gel (CHCl$_3$:MeOH 100:1, R$_f$ = 0.1) to afford 33 mg (85 %) of **97t** as a yellow oil.

^{1}H NMR (400 MHz, CDCl$_3$): δ 7.94 (d, J = 7.7 Hz, 1H), 7.66 – 7.54 (m, 1H), 7.52 – 7.40 (m, 3H), 7.25 – 7.16 (m, 1H), 7.09 (dd, J = 9.1, 4.1 Hz, 1H), 5.05 (s, 2H), 2.65 (s, 3H), 2.62 (s7, 3H).

^{13}C NMR (101 MHz, CDCl$_3$): δ 198.01, 198.00, 158.73, 156.32, 152.81, 152.79, 147.91, 133.07, 130.63, 130.50, 123.51, 120.12, 119.89, 117.85, 117.11, 116.87, 115.10, 115.02, 91.51, 82.98, 57.48, 42.32, 31.88.

HRMS-ESI$^+$: m/z [M+H]$^+$ calcd. for C$_{18}$H$_{16}$FO$_3$S 331.0799; found 331.0798.
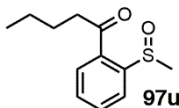
1-(2-(methylsulfinyl)phenyl)pentan-1-one 97u. Solvent in the reaction vial was purged with O$_2$ for 15 minutes. 1-(2-(methylthio)phenyl)pentan-1-one (33 mg, 0.16 mmol, 1.0 equiv) and TEA (3.2 mg, 0.032 mmol, 0.2 equiv) was dissolved in EtOH (2.0 mL). Then solution of C$_{60}$ in toluene was added

(50 µL) and the reaction mixture was irradiated with a Blue LED (450 ± 10 nm, 100 W) with continuous stirring at room temperature for 4 days. The progress of the reaction was monitored by TLC. After the complete conversion was achieved, the solvent was removed under reduced pressure. The crudes were purified by column chromatography on silica gel (CHCl$_3$:MeOH 100:1, R$_f$ = 0.1) to afford 32 mg (90 %) of **97u** as a yellow oil.

^{1}H NMR (400 MHz, CDCl$_3$): δ 8.36 (d, *J* = 7.8 Hz, 1H), 7.97 (dd, *J* = 7.8, 1.3 Hz, 1H), 7.80 (td, *J* = 7.6, 1.3 Hz, 1H), 7.59 (td, *J* = 7.6, 1.3 Hz, 1H), 2.99 (td, *J* = 7.3, 4.0 Hz, 2H), 2.81 (s, 3H), 1.73 – 1.62 (m, 2H), 1.38 (h, *J* = 7.4 Hz, 2H), 0.92 (t, *J* = 7.3 Hz, 3H).

^{13}C NMR (101 MHz, CDCl$_3$): δ 201.14, 150.29, 134.00, 133.76, 130.29, 129.73, 124.65, 44.46, 38.77, 26.28, 22.41, 13.96.

HRMS-ESI$^+$: m/z [M+H]$^+$ calcd. for C$_{12}$H$_{17}$O$_2$S 225.0944; found 225.0944.
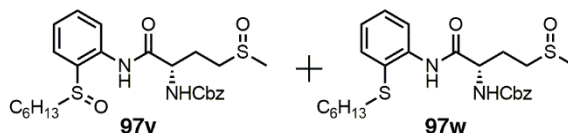
Bisulfoxide 97w and 97v. a) Using **C$_{60}$ solution in toluene** (5.0 mg in 2.0 mL) as a catalyst. The substrate **96v** (0.08 mmol) was dissolved in 2.0 mL of the solvent (EtOH or CH$_3$CN) and solution of C$_{60}$ was added (50 µL). Then the reaction mixture was irradiated with a Blue LED (450 ± 10 nm, 100 W) with continuous stirring at room temperature for 24 hours. The progress of the reaction was monitored by TLC. After the complete conversion was achieved, the solvent was removed under reduced pressure. The crudes were purified by column chromatography on silica gel (CHCl$_3$:MeOH 50:1 to 40:1, R$_f$ = 0.13 and 0.2) to afford **97v** (yield 81 % in EtOH; 46 % in CH$_3$CN) and **97w** (yield 14 % in EtOH; 28 % in CH$_3$CN) as yellow oils.

b) Using **C$_{60}$ soot powder as a catalyst**. The substrate **96v** (0.08 mmol) was dissolved in 2.0 mL of the solvent (EtOH or CH$_3$CN) and 1.0 mg of C$_{60}$ soot was added. Then the reaction mixture was purged with O$_2$ for 15 minutes and was irradiated with a Blue LED (450 ± 10 nm, 100 W) with continuous stirring at room temperature for 5 days in EtOH and 9 days in CH$_3$CN. The progress of the reaction was monitored by TLC. After the complete conversion was achieved, the solvent was removed under reduced pressure. The crudes were purified by column chromatography on silica gel (CHCl$_3$:MeOH 50:1 to 40:1, R$_f$ = 0.13 and 0.2) to afford **97v** (yield 72 % in EtOH; 31 % in CH$_3$CN) and 2w (yield 28 % in EtOH; 22 % in CH$_3$CN) as yellow oils.

c) Using **C$_{60}$ soot suspension in toluene** (2.0 mg in 4.0 mL) as a catalyst. The substrate **96v** (0.08 mmol) was dissolved in 2.0 mL of the solvent (EtOH or CH$_3$CN) and the suspension of C$_{60}$ soot was added (100 μL). Then the reaction mixture was purged with O$_2$ for 15 minutes and was irradiated with a Blue LED (450 ± 10 nm, 100 W) with continuous stirring at room temperature for 3 days. The progress of the reaction was monitored by TLC. After the complete conversion was achieved, the solvent was removed under reduced pressure. The crudes were purified by column chromatography on silica gel (CHCl$_3$:MeOH 50:1 to 40:1, R$_f$ = 0.13 and 0.2) to afford **97v** (yield 68 % in EtOH; 61 % in CH$_3$CN) and 2w (yield 15 % in EtOH; 39 % in CH$_3$CN) as yellow oils.

^{1}H NMR of 97v (400 MHz, CDCl$_3$): δ 11.17 (d, J = 51.6 Hz, 1H), 8.53 – 8.29 (m, 1H), 7.47 (t, J = 7.9 Hz, 1H), 7.43 – 7.23 (m, 6H), 7.20 – 7.12 (m, 1H), 6.56 – 6.18 (m, 1H), 5.33 – 5.00 (m, 2H), 4.46 (s, 1H), 3.30 – 3.01 (m, 1H), 2.99 – 2.69 (m, 3H), 2.55 (s, 3H), 2.48 – 2.22 (m, 2H), 2.06 (s, 2H), 1.39 (q, J = 7.5 Hz, 2H), 1.34 – 1.10 (m, 4H), 0.97 – 0.80 (m, 3H).

^{13}C NMR of 97v (101 MHz, CDCl$_3$): δ 170.03, 169.88, 169.70, 169.67, 156.52, 156.31, 139.75, 139.69, 136.35, 132.44, 128.62, 128.60, 128.29, 128.26, 128.24, 128.22, 127.44, 126.54, 126.41, 124.22, 124.17, 124.08, 124.06, 123.02, 122.93, 67.31, 67.29, 55.20, 55.00, 54.80, 50.11, 38.69, 38.60, 38.45, 38.36, 31.44, 31.42, 28.27, 28.24, 26.19, 25.79, 25.48, 23.21, 23.14, 22.49, 22.47, 14.06.

HRMS-ESI$^+$ of 97v: m/z [M+H]$^+$ calcd. for C$_{25}$H$_{35}$N$_2$O$_5$S$_2$ 507.1982; found 507.1982.

^{1}H NMR of 97w (400 MHz, CDCl$_3$): δ 10.33 (d, J = 17.1 Hz, 1H), 8.44 (t, J = 8.6 Hz, 1H), 7.87 (d, J = 7.9 Hz, 1H), 7.63 (t, J = 7.9 Hz, 1H), 7.44 – 7.27 (m, 6H), 6.53 (dd, J = 29.0, 7.3 Hz, 1H), 5.36 – 5.01 (m, 2H), 4.61 – 4.36 (m, 1H), 3.05 (q, J = 9.7, 9.2 Hz, 2H), 2.98 – 2.71 (m, 2H), 2.56 (s, 3H), 2.51 – 2.33 (m, 2H), 1.70 – 1.53 (m, 2H), 1.38 – 1.13 (m, 6H), 0.83 (t, J = 6.8 Hz, 3H).

^{13}C NMR of 97w (101 MHz, CDCl$_3$): δ 169.98, 169.90, 169.07, 156.77, 136.70, 136.68, 136.19, 136.17, 135.24, 130.46, 130.45, 129.34, 128.87, 128.85, 128.68, 128.66, 128.40, 128.38, 128.35, 128.24, 128.23, 126.62, 124.81, 124.76, 124.62, 124.61, 122.91, 122.82, 120.72, 120.61, 67.62, 67.59, 67.39, 55.99, 55.32, 55.22, 50.12, 38.44, 38.32, 36.06, 31.44, 31.27, 29.83, 29.58, 28.47, 27.91, 26.00, 25.48, 25.28, 22.64, 22.44, 22.40, 14.14, 14.03.

HRMS-ESI+ of 97w: m/z [M+H]+ calcd. for $C_{25}H_{35}N_2O_4S_2$ 491.2033; found 491.2033.

99
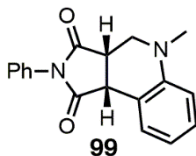
(3aS*,9bR*)-5-Methyl-2-phenyl-3a,4,5,9b-tetrahydro-1H-pyrrolo[3,4-c]quinoline-1,3(2H)-dione 99. **a)** Using **C₆₀ solution in toluene (5.0 mg in 2.0 mL)** as a catalyst. N-Phenylmaleimide (0.2 mmol, 1.0 equiv) and *N,N*-dimethylaniline (2.0 equiv) was dissolved in 3.0 mL of the solvent (EtOH, CH₃CN or CHCl₃). Then solution of C₆₀ was added (50 µL) and the reaction mixture was irradiated with a Blue LED (450 ± 10 nm, 100 W) with continuous stirring at room temperature for 5 days in EtOH, 2 days in CH₃CN or 12 days in CHCl₃. The progress of the reaction was monitored by TLC. After the complete conversion was achieved, the solvent was removed under reduced pressure. The crudes were purified by column chromatography on silica gel (CHCl₃, R_f = 0.22) to afford **99** (yield 75 % in EtOH; 56 % in CH₃CN; 73 % in CHCl₃) as a yellow solid.

b) Using **C₆₀ soot powder** as a catalyst. *N*-Phenylmaleimide (0.2 mmol, 1.0 equiv) and N,N-dimethylaniline (2.0 equiv) was dissolved in 3.0 mL of the solvent (EtOH, CH₃CN or CHCl₃). Then 1.0 mg of C₆₀ soot was added and the reaction mixture was irradiated with a Blue LED (450 ± 10 nm, 100 W) with continuous stirring at room temperature for 5 days in EtOH, 15 days in CH₃CN or 12 days in CHCl₃. The progress of the reaction was monitored by TLC. After the complete conversion was achieved, the solvent was removed under reduced pressure. The crudes were purified by column chromatography on silica gel (CHCl₃, R_f = 0.22) to afford **99** (yield 71 % in EtOH; 68 % in CH₃CN; 45 % in CHCl₃) as a yellow solid.

c) Using **C₆₀ soot suspension in toluene (2.0 mg in 4.0 mL)** as a catalyst N-Phenylmaleimide (0.2 mmol, 1.0 equiv) and *N,N*-dimethylaniline (2.0 equiv) was dissolved in 3.0 mL of the solvent (EtOH, CH₃CN or CHCl₃). Then suspension of C₆₀ soot was added (100 µL) and the reaction mixture was irradiated with a Blue LED (450 ± 10 nm, 100 W) with continuous stirring at room temperature for 4 days in EtOH, 3 days in CH₃CN or 12 days in CHCl₃. The progress of the reaction was monitored by TLC. After the complete conversion was achieved, the solvent was removed under reduced pressure. The crudes were purified by column chromatography on silica gel

(CHCl$_3$, R$_f$ = 0.22) to afford **99** (yield 68 % in EtOH; 51 % in CH$_3$CN; 46 % in CHCl$_3$) as a yellow solid.

Spectral data were in accordance with a literature.[176]
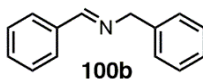
100b

N-Benzylidenebenzylamine 100b. **a)** Using **C$_{60}$ solution in toluene** (5.0 mg in 2.0 mL) as a catalyst. Dibenzylamine (0.16 mmol) was dissolved in 3.0 mL of the solvent (EtOH, CH$_3$CN or CHCl$_3$). Then activated molecular sieves 4 Å and the solution of C$_{60}$ (50 µL) was added. The reaction mixture was purged with O$_2$ for 15 minutes and was irradiated with a Blue LED (450 ± 10 nm, 100 W) with continuous stirring at room temperature for 3 days in EtOH or CH$_3$CN and 1 day in CHCl$_3$. The progress of the reaction was monitored by TLC. After the complete conversion was achieved, the solvent was removed under reduced pressure to afford **100b** (yield 88 % in EtOH; 86 % in CH$_3$CN; 100 % in CHCl$_3$) as a yellow oil.

b) Using **C$_{60}$ soot powder** as a catalyst. Dibenzylamine (0.16 mmol) was dissolved in 3.0 mL of the solvent (EtOH, CH$_3$CN or CHCl$_3$). Then activated molecular sieves 4 Å and the C$_{60}$ soot (1.0 mg) was added. The reaction mixture was purged with O$_2$ for 15 minutes and was irradiated with a Blue LED (450 ± 10 nm, 100 W) with continuous stirring at room temperature for 4 days. The progress of the reaction was monitored by TLC. After the complete conversion was achieved, the solvent was removed under reduced pressure to afford **100b** (yield 0 % in EtOH; 0 % in CH$_3$CN; 78 % in CHCl$_3$) as a yellow oil.

c) Using **C$_{60}$ soot suspension in toluene** (2.0 mg in 4.0 mL) as a catalyst Dibenzylamine (0.16 mmol) was dissolved in 3.0 mL of the solvent (EtOH, CH$_3$CN or CHCl$_3$). Then activated molecular sieves 4 Å and the suspension of C$_{60}$ soot (100 µL) was added. The reaction mixture was purged with O$_2$ for 15 minutes and was irradiated with a Blue LED (450 ± 10 nm, 100 W) with continuous stirring at room temperature for 17 days in CH$_3$CN or 8 days in CHCl$_3$. The progress of the reaction was monitored by TLC. After the complete conversion was achieved, the solvent was removed under reduced pressure to afford **100b** (yield 0 % in EtOH; 85 % in CH$_3$CN; 91 % in CHCl$_3$) as a yellow oil.

Spectral data were in accordance with a literature.[178]
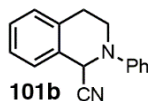
2-phenyl-1,2,3,4-tetrahydroisoquinoline-1-carbonitrile 101b. **a)** Using **C$_{60}$ solution in toluene** (5.0 mg in 2.0 mL) as a catalyst. 2-phenyl-1,2,3,4-tetrahydroisoquinoline (0.16 mmol, 1.0 equiv) and TMSCN (2.5 equiv) was dissolved in 3.0 mL of the solvent (EtOH, CH$_3$CN or CHCl$_3$). Then activated molecular sieves 4 Å and the solution of C$_{60}$ (50 µL) was added. The reaction mixture was purged with O$_2$ for 15 minutes and was irradiated with a Blue LED (450 ± 10 nm, 100 W) with continuous stirring at room temperature for 1 day in EtOH or 2 days in CH$_3$CN. The progress of the reaction was monitored by TLC. After the complete conversion was achieved, the solvent was removed under reduced pressure. The crudes were purified by column chromatography on silica gel (PE:EA 40:1, R$_f$ = 0.17) to afford **101b** (yield 70 % in EtOH; 63 % in CH$_3$CN; 0 % in CHCl$_3$) as a yellow oil.

b) Using **C$_{60}$ soot powder** as a catalyst. 2-phenyl-1,2,3,4-tetrahydroisoquinoline (0.16 mmol, 1.0 equiv) and TMSCN (2.5 equiv) was dissolved in 3.0 mL of the solvent (EtOH, CH$_3$CN or CHCl$_3$). Then activated molecular sieves 4 Å and the C$_{60}$ soot (1 mg) was added. The reaction mixture was purged with O$_2$ for 15 minutes and was irradiated with a Blue LED (450 ± 10 nm, 100 W) with continuous stirring at room temperature for 17 days in EtOH or 7 days in CHCl$_3$. The progress of the reaction was monitored by TLC. After the complete conversion was achieved, the solvent was removed under reduced pressure. The crudes were purified by column chromatography on silica gel (PE:EA 40:1, R$_f$ =0.17) to afford **101b** (yield 86 % in EtOH; 0 % in CH$_3$CN; 84 % in CHCl$_3$) as a yellow oil.

c) Using **C$_{60}$ soot suspension in toluene** (2.0 mg in 4.0 mL) as a catalyst 2-phenyl-1,2,3,4-tetrahydroisoquinoline (0.16 mmol, 1.0 equiv) and TMSCN (2.5 equiv) was dissolved in 3.0 mL of the solvent (EtOH, CH$_3$CN or CHCl$_3$). Then activated molecular sieves 4 Å and the suspension of C$_{60}$ soot (100 µL) was added. The reaction mixture was purged with O$_2$ for 15 minutes and was irradiated with a Blue LED (450 ± 10 nm, 100 W) with continuous stirring at room temperature for 17 days in EtOH, 6 days in CH$_3$CN or 2 days in CHCl$_3$. The progress of the reaction was monitored by TLC. After the complete conversion was achieved, the solvent was removed under reduced pressure. The crudes were purified by column chromatography on silica gel (PE:EA 40:1, R$_f$ = 0.17) to afford **101b** (yield 74 % in EtOH; 52 % in CH$_3$CN; 65 % in CHCl$_3$) as a yellow oil.

Spectral data were in accordance with a literature.[258]

General procedure D for photoinduced hydroxylation of arylboronic acids:

a) Using **C_{60} solution in toluene** (5.0 mg in 2.0 mL) as a catalyst. The substrate (0.1 – 0.25 mmol) was dissolved in 2.0 mL of the solvent (EtOH or CHCl$_3$), then DIPEA (2.0 equiv) and the solution of C_{60} was added (50 µL). The reaction mixture was purged with O$_2$ for 15 minutes and was irradiated with a Blue LED (450 ± 10 nm, 100 W) with continuous stirring at room temperature. The progress of the reaction was monitored by TLC. After the complete conversion was achieved, the solvent was removed under reduced pressure. The crude was purified by column chromatography on silica gel.

b) Using **C_{60} soot powder** as a catalyst. The substrate (0.1 – 0.25 mmol) was dissolved in 2.0 mL of the solvent (EtOH or CHCl$_3$), then DIPEA (2.0 equiv) and 1.0 mg of C_{60} soot was added. The reaction mixture was purged with O$_2$ for 15 minutes and was irradiated with a Blue LED (450 ± 10 nm, 100 W) with continuous stirring at room temperature. The progress of the reaction was monitored by TLC. After the complete conversion was achieved, the solvent was removed under reduced pressure. The crude was purified by column chromatography on silica gel.

c) Using **C_{60} soot suspension in toluene** (2.0 mg in 4.0 mL) as a catalyst. The substrate (0.1 – 0.25 mmol) was dissolved in 2.0 mL of the solvent (EtOH or CHCl$_3$)), then DIPEA (2.0 equiv) and the suspension of C_{60} soot was added (100 µL). The reaction mixture was purged with O$_2$ for 15 minutes and was irradiated with a Blue LED (450 ± 10nm, 100W) with continuous stirring at room temperature. The progress of the reaction was monitored by TLC. After the complete conversion was achieved, the solvent was removed under reduced pressure. The crude was purified by column chromatography on silica gel.
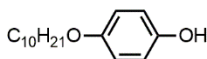
102b

4-Decyloxyphenol 102ba. The product was obtained following the general procedure **D** for photoinduced hydroxylation of arylboronic acids: a) in EtOH irradiated with a Blue LED for 4 days (yield 96 %) or in CHCl$_3$ irradiated with a Blue LED for 48 hours (yield 48 %); b) in EtOH irradiated with a Blue LED for 13 days (yield 99 %) or in CHCl$_3$ irradiated with a Blue LED for 48 hours (yield 93 %); c) in EtOH irradiated with a Blue LED for 10 days (yield 89 %) or in CHCl$_3$ irradiated with a Blue LED for 24 hours (yield 59 %). The crudes were purified by column chromatography on silica

gel (CHCl$_3$ to CHCl$_3$:MeOH 100:1, R$_f$ = 0.45) to afford **102b** as a white solid.

Spectral data were in accordance with a literature.[259]
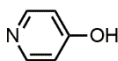
103b

Pyridin-4-ol 103b. The product was obtained following the general procedure **D** for photoinduced hydroxylation of arylboronic acids: a) in EtOH irradiated with a Blue LED for 48 hours (yield 100 %); b) in EtOH irradiated with a Blue LED for 9 days (yield 63 %); c) in EtOH irradiated with a Blue LED for 9 days (yield 67 %). The crudes were purified by column chromatography on silica gel (CHCl$_3$:MeOH 5:1, R$_f$ = 0.09) to afford **103b** as a white solid.

Spectral data were in accordance with a literature.[260]

6.3 Experimental for Chapter 3: Hydrogen-Bonded Capsule Comprising Conformationally Flexible Cavity

General procedure E for 1,4-addition of RMgBr to enones. Under inert atmosphere Mg turnings (1.05 equiv) in anhydrous THF were activated by addition of I$_2$ crystal and refluxing for 30 min until brown color of iodine faded away. A solution of RBr (1.0 equiv) in THF was added dropwise over 15 min at room temperature and reaction mixture was refluxed for 30 min until Mg dissolved. After cooling down to room temperature, the mixture was diluted with anhydrous THF to afford 0.5 M RMgBr solution.

Under inert atmosphere to a suspension of CuCN (4.2 equiv) in anhydrous THF 0.5 M RMgBr solution (4.0 equiv) was added dropwise over 10 min at -30°C. The mixture was stirred for 10 min at -30°C and 15 min at room temperature resulting in deep brown solution. The mixture was cooled to -78°C and a solution of bicyclo[3.3.1]nona-3,7-diene-2,6-dione (+)-**87** (1.0 equiv) in anhydrous THF was added dropwise. After 10 min, cooling bath was removed, and the reaction mixture was quenched with 1.0 M HCl solution. The mixture was diluted with H$_2$O and extracted with EA. Combined organic phase was diluted with H$_2$O (100 mL) and white precipitate was removed by filtration through CELITE. Organic phase was washed with sat. NaHCO$_3$ solution and brine, dried over anhydrous Na$_2$SO$_4$ and evaporated to dryness. The crude was purified by column chromatography on silica gel (PE:EA) to afford **104a-d** as a white solid.
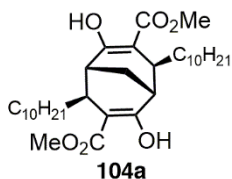
104a

(1R,4S,5R,8S)-dimethyl-*exo,exo*-4,8-didecyl-2,6-dihydroxy bicyclo[3.3.1]nona-2,6-diene-3,7-dicarboxylate 104a. Following general procedure **E**, under inert atmosphere Mg turnings (153 mg, 6.28 mmol, 1.05 equiv) in anhydrous THF (0.7 mL) were activated by addition of I_2 crystal. A solution of decyl bromide (1.24 mL, 5.98 mmol, 1.0 equiv) in THF (4.0 mL) was added dropwise over 15 min at room temperature and reaction mixture was refluxed for 30 min until Mg dissolved. The mixture was diluted with anhydrous THF (7.3 mL) prior next step to afford 0.5 M fresh solution of decylmagnesium bromide.

To a suspension of CuCN (527 mg, 5.88 mmol 4.2 equiv) in anhydrous THF (3.5 mL), 0.5 M decylmagnesium bromide solution (11.2 mL, 5.60 mmol, 4.0 equiv) was added dropwise over 10 min at -30°C. A solution of bicyclo[3.3.1]nona-3,7-diene-2,6-dione **(+)-87** (370 mg, 1.40 mmol, 1.0 equiv) in anhydrous THF (3.5 mL) was added dropwise. The crude was purified by column chromatography on silica gel (PE:EA 100:1 , R_f = 0.31) to afford 641 mg (83 %) of **104a** as a white solid.

¹H NMR (400 MHz, CDCl₃): δ 12.28 (s, 2H), 3.74 (s, 6H), 2.60 (d, J = 10.1 Hz, 2H), 2.50 – 2.43 (m, 2H), 1.79 (t, J = 2.8 Hz, 2H), 1.69 – 1.58 (m, 2H), 1.49 – 140 (m, 2H), 1.27 (s, 32H), 0.88 (t, J = 6.8 Hz, 6H).

¹³C NMR (101 MHz, CDCl₃): δ 174.28, 173.43, 100.98, 51.54, 37.59, 36.10, 33.78, 32.07, 29.82, 29.78, 29.69, 29.51, 28.07, 22.84, 18.27, 14.26.

HRMS-ESI⁺: m/z [M-H]⁻ calcd. for 547.4004; found 547.4021.
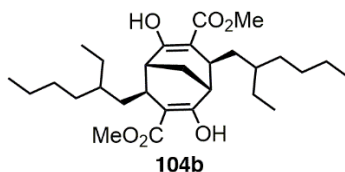
104b

(1R,4S,5R,8S)-dimethyl-*exo,exo*-4,8-bis(2-ethylhexyl)-2,6-dihydroxy bicyclo[3.3.1]nona-2,6-diene-3,7-dicarboxylate 104b. Following general procedure **E**, under inert atmosphere Mg turnings (174 mg, 7.15 mmol, 1.05 equiv) in anhydrous THF (0.7 mL) were activated by addition of I_2 crystal. A solution of 2-ethylhexylbromide (1.2 mL, 6.81 mmol, 1.0 equiv) in THF (4.0 mL) was added dropwise over 15 min at room temperature and reaction

mixture was refluxed for 30 min until Mg dissolved. The mixture was diluted with anhydrous THF (8.9 mL) prior next step to afford 0.5 M fresh solution of 2-ethylhexylmagnesium bromide.

To a suspension of CuCN (427 mg, 4.77 mmol 4.2 equiv) in anhydrous THF (3.5 mL), 0.5 M 2-ethylhexylmagnesium bromide solution (9.1 mL, 4.54 mmol, 4.0 equiv) was added dropwise over 10 min at -30°C. A solution of bicyclo[3.3.1]nona-3,7-diene-2,6-dione (+)-**87** (300 mg, 1.13 mmol, 1.0 equiv) in anhydrous THF (3.5 mL) was added dropwise. The crude was purified by column chromatography on silica gel (PE:EA 100:1 , R_f = 0.11) to afford 424 mg (76 %) of **104b** as a white solid.

^{1}H NMR (400 MHz, CDCl$_3$): δ 12.28 (s, 1H), 12.25 (s, 1H), 3.73 (s, 6H), 2.71 (dt, J = 10.9, 2.1 Hz, 2H), 2.45 (d, J = 3.6 Hz, 2H), 1.82 (t, J = 3.1 Hz, 2H), 1.54 – 1.08 (m, 22H), 0.95 – 0.81 (m, 12H).

^{13}C NMR (101 MHz, CDCl$_3$): δ 174.49, 174.46, 173.36, 173.35, 101.03, 100.99, 51.41, 51.36, 37.53, 37.52, 37.35, 37.21, 37.21, 36.63, 36.06, 35.93, 35.50, 35.36, 33.62, 31.63, 29.45, 27.84, 27.07, 24.29, 24.27, 23.39, 23.21, 17.93, 14.36, 14.30, 11.52, 9.56.

HRMS-ESI$^+$: m/z [M-H]$^-$ calcd. for 491.3378; found 491.3386.

104c

(1R,4S,5R,8S)-dimethyl-*exo*,*exo*-4,8-di((Z)-octadec-9-en-1-yl)-2,6-dihydroxybicyclo[3.3.1]nona-2,6-diene-3,7-dicarboxylate 104c. Following general procedure **E**, under inert atmosphere Mg turnings (111 mg, 4.56 mmol, 1.05 equiv) in anhydrous THF (0.7 mL) were activated by addition of I$_2$ crystal. A solution of oleyl bromide (1.44 g, 4.35 mmol, 1.0 equiv) in THF (5.0 mL) was added dropwise over 15 min at room temperature and reaction mixture was refluxed for 30 min until Mg dissolved. The mixture was diluted with anhydrous THF (4.0 mL) prior next step to afford 0.5 M fresh solution of oleylmagnesium bromide.

To a suspension of CuCN (409 mg, 4.56 mmol 4.2 equiv) in anhydrous THF (3.5 mL), 0.5 M oleylmagnesium bromide solution (8.7 mL, 4.35 mmol, 4.0 equiv) was added dropwise over 10 min at -30°C. A solution of bicyclo[3.3.1]nona-3,7-diene-2,6-dione (+)-**87** (287 mg, 1.09 mmol, 1.0 equiv) in anhydrous THF (3.5 mL) was added dropwise. The crude was

purified by column chromatography on silica gel (PE:EA 60:1 , R_f = 0.18) to afford 779 mg (93 %) of **104c** as a white solid.

¹H NMR (400 MHz, CDCl₃): δ 12.28 (s, 2H), 5.35 (t, *J* = 4.9 Hz, 4H), 3.74 (s. 6H), 2.61 (dt, *J* = 10.0, 2.1 Hz, 2H), 2.46 (q, *J* = 2.6 Hz, 2H), 2.02 (q, *J* = 7.1, 6.6 Hz, 8H), 1.79 (t, *J* = 3.1 Hz, 2H), 1.68 – 1.58 (m, 2H), 1.50 – 1.39 (m, 2H), 1.38 – 1.20 (m, 48H), 0.88 (t, *J* = 6.7 Hz, 6H).

¹³C NMR (101 MHz, CDCl₃): δ 174.28, 173.42, 130.10, 130.00, 100.97, 51.54, 37.59, 36.11, 33.79, 32.76, 32.06, 29.95, 29.93, 29.86, 29.82, 29.68, 29.50, 29.48, 29.34, 28.07, 27.38, 22.84, 18.27, 14.26.

HRMS-ESI⁺: m/z [M-H]⁻ calcd. for 767.6184; found 767.6211.
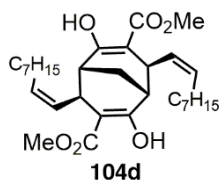
104d

(1R,4S,5R,8S)-dimethyl-*exo*,*exo*-4,8-di((Z)-non-1-en-1-yl)-2,6-dihydroxy bicyclo[3.3.1]nona-2,6-diene-3,7-dicarboxylate 104d. Following general procedure **E**, under inert atmosphere Mg turnings (153 mg, 6.28 mmol, 1.05 equiv) in anhydrous THF (0.7 mL) were activated by addition of I₂ crystal. A solution of (Z)-1-bromo-1-nonene (1.22 g, 5.98 mmol, 1.0 equiv) in THF (4.0 mL) was added dropwise over 15 m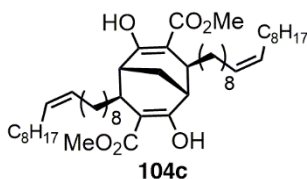in at room temperature and reaction mixture was refluxed for 30 min until Mg dissolved. The mixture was diluted with anhydrous THF (7.3 mL) prior next step to afford 0.5 M fresh solution of (Z)-1-nonene magnesium bromide.

To a suspension of CuCN (527 mg, 5.88 mmol 4.2 equiv) in anhydrous THF (3.5 mL), 0.5 M (Z)-1-nonene magnesium bromide solution (11.2 mL, 5.60 mmol, 4.0 equiv) was added dropwise over 10 min at -30°C. A solution of bicyclo[3.3.1]nona-3,7-diene-2,6-dione **(+)-87** (370 mg, 1.40 mmol, 1.0 equiv) in anhydrous THF (4.0 mL) was added dropwise. The crude was purified by column chromatography on silica gel (PE:EA 100:1 , R_f = 0.37) to afford 721 mg (99 %) of **104d** as a white solid.

¹H NMR (400 MHz, CDCl₃): δ 12.28 (s, 2H), 5.46 – 5.29 (m, 4H), 3.69 (s, 6H), 3.65 (dd, *J* = 8.7, 1.8 Hz, 2H), 2.42 (q, *J* = 2.5 Hz, 2H), 2.27 – 2.16 (m, 4H), 1.88 (t, *J* = 3.1 Hz, 2H), 1.47 – 1.21 (m, 20H), 0.95 – 0.85 (m, 6H).

¹³C NMR (101 MHz, CDCl₃): δ 173.51, 173.37, 131.86, 131.42, 99.69, 51.56, 40.54, 35.54, 32.03, 29.70, 29.51, 29.43, 27.44, 22.84, 19.39, 14.26.

HRMS-ESI⁺: m/z [M-H]⁻ calcd. for 515.3367; found 515.3394.
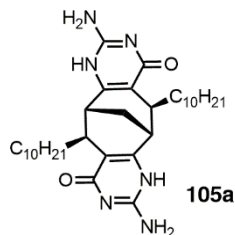
ICyt 105a. A mixture of **104a** (610 mg, 1.11 mmol, 1.0 equiv), guanidinium chloride (531 mg, 5.56 mmol, 5.0 equiv) and KOtBu (623 mg, 5.56 mmol, 5.0 equiv) in MeOH (10 mL) was heated at 100 °C for 24 hours. The reaction mixture was diluted with 1.0 M HCl solution. The resulting white precipitate was filtered and washed with 1.0 M HCl solution, water and MeOH to afford 552 mg (88 %) of **105a** as a white solid. The crude was used without any further purification.

HRMS-ESI⁺: m/z [M+H]⁺ calcd. for 567.4381; found 567.4388.
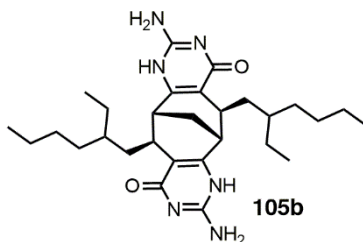
ICyt 105b. A mixture of **104b** (390 mg, 0.79 mmol, 1.0 equiv), guanidinium chloride (378 mg, 3.96 mmol, 5.0 equiv) and KOtBu (444 mg, 3.96 mmol, 5.0 equiv) in MeOH (5.0 mL) was heated at 100 °C for 36 hours. Then reaction mixture was diluted with 1.0 M HCl solution and extracted with CHCl₃. Organic phase was washed with water and brine, dried over anhydrous Na₂SO₄, and evaporated to dryness. The crude was triturated in MeOH, filtered and washed with MeOH to afford 319 mg (79 %) of **105b** as a white solid. The crude was used without any further purification.

HRMS-ESI⁺: m/z [M+H]⁺ calcd. for 511.3755; found 511.3753.
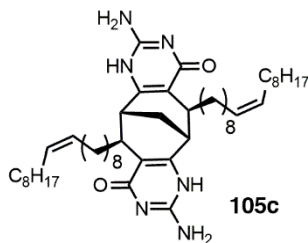
105c

ICyt 105c. A mixture of **104c** (760 mg, 0.988 mmol, 1.0 equiv), guanidinium chloride (472 mg, 4.94 mmol, 5.0 equiv) and KOtBu (554 mg, 4.94 mmol, 5.0 equiv) in MeOH (8.0 mL) was heated at 100 °C for 24 hours. The reaction mixture was diluted with 1.0 M HCl solution. The resulting white precipitate was filtered and washed with 1.0 M HCl solution, water and MeOH to afford 686 mg (88 %) of **105c** as a white solid. The crude was used without any further purification.

HRMS-ESI$^+$: m/z [M+H]$^+$ calcd. for 787.6572; found 787.6570.
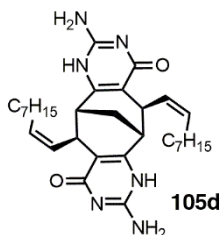
105d

ICyt 105d. A mixture of **104d** (715 mg, 1.39 mmol, 1.0 equiv), guanidinium chloride (662 mg, 6.93 mmol, 5.0 equiv) and KOtBu (777 mg, 6.93 mmol, 5.0 equiv) in MeOH (8.0 mL) was heated at 100 °C for 24 hours. The reaction mixture was diluted with 1.0 M HCl solution. The resulting white precipitate was filtered and washed with 1.0 M HCl solution, water and minimum amount of MeOH to afford 401 mg (54 %) of **105d** as a white solid. The crude was used without any further purification.

HRMS-ESI$^+$: m/z [M+H]$^+$ calcd. for 535.3755; found 535.3765.

109
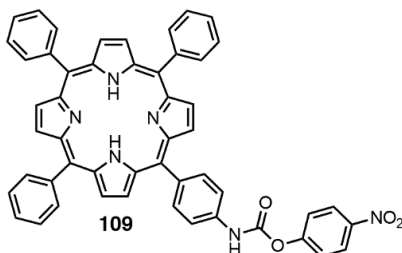
4-nitrophenyl N-[4-(10,15,20-triphenylporphyrin-5-yl)phenyl] carbamate 109. A mixture of TPP amine **108** (400 mg, 0.635 mmol, 1.0

equiv), 4-nitrophenylchloroformate (192 mg, 0.953 mmol, 1.50 equiv) and pyridine (0.1 mL, 1.27 mmol, 2.0 equiv) in DCM (10 mL) was stirred at room temperature for 1.5 hours. The reaction mixture was diluted with water and extracted with DCM. The organic phase was washed with water and brine, dried over anhydrous Na_2SO_4, and evaporated to dryness. The crude was purified by column chromatography on silica gel (PE:CHCl$_3$ 1:1 , R$_f$ = 0.25) to afford 477 mg (95 %) of **109** as a purple glass.

Spectral data were in accordance with a literature.[261]

General procedure F for monoUpy 106a-d. Under inert atmosphere a mixture of corresponding **105a-d** (1.0 equiv) and freshly distilled anhydrous NEt$_3$ (10.0 equiv) in anhydrous THF was heated at 90 °C for 10 minutes until ICyt **105** dissolved. Then reaction mixture was cooled down to room temperature and TPP **109** (1.10 equiv) was added. Reaction was heated at 90 °C for 24 hours. After cooling down to room temperature, the solvent was removed under reduced pressure. The crude was dissolved in toluene and filtered through CELITE. Then subjected to size-exclusion column (Bio Beads SX-3) using toluene as an eluent. Subsequently, the crude was purified by column chromatography on silica gel (CHCl$_3$:MeOH) to afford product **106a-e** as a purple solid.
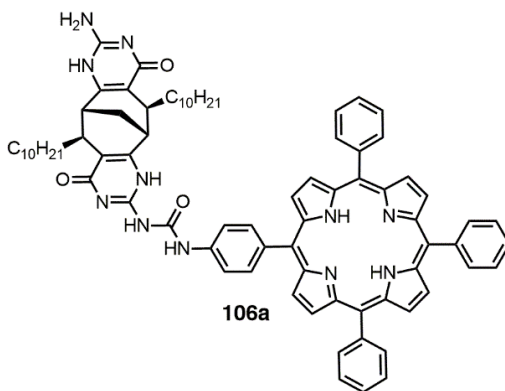

106a

Mono Upy 106a. Following general procedure **F**, under inert atmosphere a mixture of **105a** (55 mg, 0.097 mmol, 1.0 equiv), freshly distilled anhydrous NEt$_3$ (0.14 mL, 0.97 mmol, 10.0 equiv) and TPP **109** (85 mg, 0.11 mmol, 1.10 equiv) in anhydrous THF (7.0 mL) was heated at 90 °C for 24 hours. Then subjected to size-exclusion column using toluene as an eluent and subsequently was purified by column chromatography on silica gel (CHCl$_3$:MeOH 70:1→50:1→30:1→20:1, R$_f$ = 0.08) to afford 102 mg (44 %) of **106a** as a purple solid.

¹H NMR (400 MHz, CDCl₃): δ 13.60 (s, 1N-H), 13.07 (s, 1N-H), 12.94 (s, 1N-H), 12.59 (s, 1N-H), 8.98 (s, 2H), 8.92 – 8.76 (m, 7H), 8.24 (br. s, 6H), 8.12 (br. s, 4H), 7.79 (s, 4H), 7.52 (s, 4H), 4.89 (s, 2N-H), 3.16 – 2.72 (m, 4H), 2.27 (br. s, 2H), 2.11 (br. s, 4H), 1.56 – 1.01 (m, 24H), 0.94 – 0.73 (m, 4H), 0.70 – 0.40 (m, 8H), 0.26 (s, 2H), -2.71 (s, TPP 2N-H).

¹³C NMR (101 MHz, CDCl₃) could not be acquired due to low solubility and strong aggregation.

HRMS-ESI⁺: m/z [M+H]⁺ calcd. for 1222.6753; found 1222.6777.

106b

Mono Upy 106b. Following general procedure **F**, under inert atmosphere a mixture of **105b** (100 mg, 0.20 mmol, 1.0 equiv), freshly distilled anhydrous NEt₃ (0.27 mL, 1.96 mmol, 10.0 equiv) and TPP **109** (171.2 mg, 0.22 mmol, 1.10 equiv) in anhydrous THF (10 mL) was heated at 90 °C for 24 hours. Then subjected to size-exclusion column using toluene as an eluent and subsequently was purified by column chromatography on silica gel (CHCl₃:MeOH 100:1→50:1, R$_f$ = 0.15) to afford 102 mg (44 %) of **106b** as a purple solid.

¹H NMR (400 MHz, CDCl₃): δ 13.79 (s, 1N-H), 13.32 (s, 1N-H), 13.03 (s, 1N-H), 12.52 (s, 1N-H), 8.97 (s, 2H), 8.87 – 8.63 (m, 6H), 8.33 – 8.16 (m, 6H), 8.12 – 7.93 (m, 4H), 7.88 – 7.71 (m, 4H), 7.59 – 7.31 (m, 5H), 4.71 (d, J = 15.9 Hz, 2N-H), 3.12 (s, 1H), 3.03 (d, J = 10.1 Hz, 1H), 2.89 (d, J = 20.6 Hz, 2H), 2.24 – 2.05 (m, 3H), 1.97 – 1.78 (m, 3H), 1.54 – 1.37 (m, 6H), 1.37 – 1.16 (m, 10H), 1.12 (s, 2H), 1.05 – 0.70 (m, 10H), 0.61 (s, 2H), -2.72 (s, TPP 2N-H).

¹³C NMR (101 MHz, DMSO-d₆): δ 164.92, 164.86, 162.79, 162.74, 154.09, 154.05, 154.01, 141.68, 135.26, 135.20, 134.67, 131.59, 128.54, 127.45, 120.47, 120.42, 120.21, 120.19, 118.67, 118.64, 118.56, 118.53, 118.48, 111.46, 111.22, 37.01, 36.13, 33.73, 33.55, 32.07, 31.69, 29.26, 27.47,

27.22, 26.95, 24.31, 23.45, 23.29, 22.98, 18.58, 14.62, 14.50, 14.42, 11.79, 11.71, 9.62.

HRMS-ESI$^+$: m/z [M+H]$^+$ calcd. for 1166.6127; found 1166.6189.
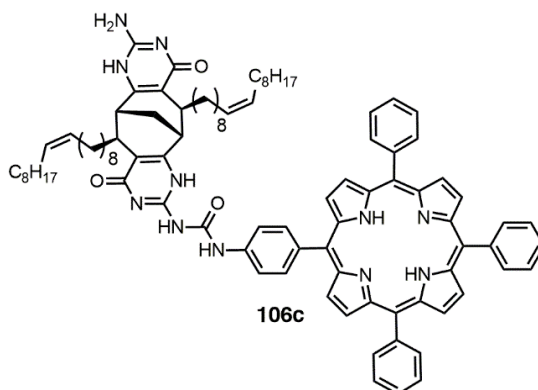
Mono Upy 106c. Following general procedure **F**, under inert atmosphere a mixture of **105c** (70 mg, 0.089 mmol, 1.0 equiv), freshly distilled anhydrous NEt$_3$ (0.12 mL, 0.89 mmol, 10.0 equiv) and TPP **109** (78 mg, 0.098 mmol, 1.10 equiv) in anhydrous THF (7.0 mL) was heated at 90 °C for 24 hours. Then subjected to size-exclusion column using toluene as an eluent and subsequently was purified by column chromatography on silica gel (CHCl$_3$:MeOH 100:1→70:1→50:1→20:1, R$_f$ = 0.12) to afford 14 mg (11 %) of **106c** as a dark red solid.

^{1}H NMR (400 MHz, CDCl$_3$): δ 13.65 (s, 1N-H), 13.06 (s, 1N-H), 12.95 (s, 1N-H), 12.60 (s, 1N-H), 9.06 – 8.94 (m, 2H), 8.92 – 8.73 (m, 6H), 8.37 – 8.06 (m, 10H), 7.89 – 7.72 (m, 5H), 7.64 – 7.44 (m, 4H), 5.43 – 5.26 (m, 1H), 5.22 – 4.99 (m, 2H), 4.86 (s, 2N-H), 4.82 – 4.58 (m, 1H), 3.09 – 2.77 (m, 5H), 2.18 – 1.82 (m, 14H), 1.80 – 1.58 (m, 9H), 1.53 – 1.33 (m, 14H), 1.18 – 0.98 (m, 18H), 0.91 – 0.86 (m, 6H), 0.86 – 0.67 (m, 6H), -2.70 (s, TPP 2N-H).

^{13}C NMR (101 MHz, CDCl$_3$) could not be acquired due to low solubility and strong aggregation.

HRMS-ESI$^+$: m/z [M+H]$^+$ calcd. for 1442.8944; found 1442.8833.

106d

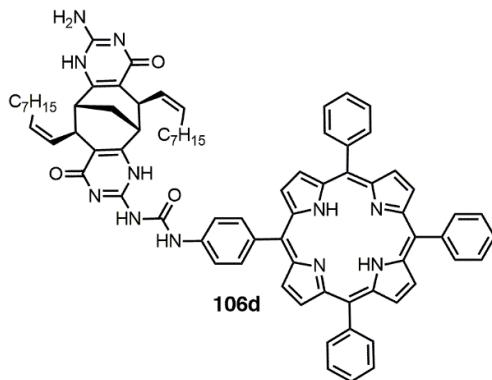**Mono Upy 106d.** Following general procedure **F**, under inert atmosphere a mixture of **105d** (100 mg, 0.19 mmol, 1.0 equiv), freshly distilled anhydrous NEt$_3$ (0.26 mL, 1.87 mmol, 10.0 equiv) and TPP **109** (164 mg, 0.21 mmol, 1.10 equiv) in anhydrous THF (10 mL) was heated at 90 °C for 24 hours. Then subjected to size-exclusion column using toluene as an eluent and subsequently was purified by column chromatography on silica gel (CHCl$_3$:MeOH 100:1→70:1→50:1→20:1, R$_f$ = 0.12) to afford 68 mg (31 %) of **106d** as a dark red solid.

^{1}H NMR (400 MHz, CDCl$_3$): δ 13.46 (s, 1N-H), 13.44 (s, 1N-H), 12.91 (s, 1N-H), 12.60 (s, 1N-H), 9.04 – 8.92 (m, 2H), 8.92 – 8.74 (m, 6H), 8.34 – 8.12 (m, 8H), 8.14 – 8.01 (m, 2H), 7.89 – 7.69 (m, 5H), 7.59 – 7.41 (m, 4H), 5.86 – 5.35 (m, 4H), 4.91 (s, 2N-H), 4.06 (d, J = 8.5 Hz, 1H), 3.94 (d, J = 8.5 Hz, 1H), 2.90 (s, 1H), 2.82 (s, 1H), 2.69 – 2.39 (m, 4H), 2.30 – 1.93 (m, 4H), 1.30 – 1.19 (m, 6H), 1.15 – 0.96 (m, 8H), 0.95 – 0.70 (m, 4H), 0.65 – 0.47 (m, 4H), 0.39 – 0.22 (m, 2H), -2.70 (s, TPP 2N-H).

^{13}C NMR (101 MHz, CDCl$_3$) could not be acquired due to low solubility and strong aggregation.

HRMS-ESI$^+$: m/z [M+H]$^+$ calcd. for 1190.6127; found 1190.6156.

6.4 Experimental for Chapter 4: π-Functional Supramolecular Structures Comprising 9-Azabicyclo[3.3.1]nonane Scaffold

116
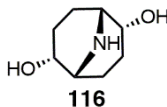
(1R,2R,5R,6R)-9-azabicyclo[3.3.1]nonane-2,6-diol 116. A solution of diol **115** (1.0 g, 4.05 mmol, 1.0 equiv) in MeOH (50 mL) and acetic acid (0.70 mL, 12.16 mmol, 3.0 equiv) was vacuumed and flushed with argon several times. Then 10% Pd/C (80 mg, 10% w/w) was added, and reaction mixture was vacuumed and flushed with H$_2$ several times. The resultant suspension

was stirred overnight at room temperature under an atmosphere of hydrogen. After filtration through CELITE, the solvent was removed under reduced pressure and dried under vacuum. The crude was used without any further purification.

117
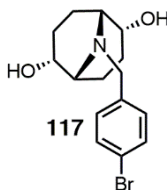
(1R,2R,5R,6R)-9-(4-bromobenzyl)-9-azabicyclo[3.3.1]nonane-2,6-diol

117. A mixture of diol **116** (4.05 mmol, 1.0 equiv), 4-bromobenzyl bromide (1.21 g, 4.86 mmol, 1.20 equiv), K_2CO_3 (1.11 g, 8.09 mmol, 2.0 equiv) in CH_3CN (100 mL) was refluxed for 24 hours. After cooling down to room temperature, the solvent was removed under reduced pressure. Resulting crude was diluted with water and extracted with DCM. Organic phase was washed with water, dried over anhydrous Na_2SO_4 and evaporated to dryness. The crude was purified by column chromatography on silica gel (EA, R_f = 0.36) to afford 1.20 g (91 %) of **117** as a white solid.

¹H NMR (400 MHz, $CDCl_3$): δ 7.43 (d, J = 8.1 Hz, 2H), 7.24 (d, J = 9.1 Hz, 2H), 4.18 – 4.08 (m, 2H), 3.91 (s, 2H), 2.72 (s, 2H), 1.98 (tt, J = 12.8, 6.6 Hz, 4H), 1.87 (td, J = 14.1, 13.2, 6.3 Hz, 2H), 1.71 (qd, J = 12.4, 6.7 Hz, 2H).

¹³C NMR (101 MHz, $CDCl_3$): δ 132.61, 131.58, 131.13, 130.08, 68.13, 55.91, 54.98, 30.23, 20.22.

HRMS-ESI⁺: m/z [M+H]⁺ calcd. for 326.0750; found 326.0747.

118
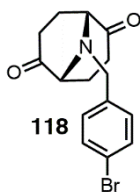
(1R,5R)-9-(4-bromobenzyl)-9-azabicyclo[3.3.1]nonane-2,6-dione 118. To a solution of oxalyl chloride (0.79 mL, 9.19 mmol, 2.5 equiv) in anhydrous DCM (30 mL) was added a solution of anhydrous DMSO (1.18 mL, 16.55 mmol, 4.5 equiv) in anhydrous DCM (2.6 mL) at -78 °C under inert atmosphere. After stirring for 30 min at the same temperature, a solution of diol **117** (1.2 g, 3.68 mmol, 1.0 equiv) in anhydrous DMSO/DCM (5.7 mL, 1:2 v:v) was added. After stirring for 45 min at -78 °C, Et_3N (5.4 mL, 38.62 mmol, 10.5 equiv) was added. Reaction mixture was stirred for 1 hour at the

same temperature and slowly reached room temperature while stirring for another 1 hour. After diluting with water, the resultant mixture was extracted with CHCl$_3$. Combined organic phase was washed with brine, dried over anhydrous Na$_2$SO$_4$ and evaporated to dryness. The crude was purified by column chromatography on silica gel (PE:EA 2:1, R$_f$ = 0.68) to afford 1.04 g (88 %) of **118** as a white solid.

^{1}H NMR (400 MHz, CDCl$_3$): δ 7.46 (d, J = 8.1 Hz, 2H), 7.19 (d, *J* = 7.9 Hz, 2H), 3.77 (d, *J* = 4.1 Hz, 2H), 3.36 (d, *J* = 6.7 Hz, 2H), 2.82 – 2.64 (m, 2H), 2.56 – 2.38 (m, 4H), 2.01 (t, *J* = 10.1 Hz, 2H).

^{13}C NMR (101 MHz, CDCl$_3$): δ 211.67, 136.08, 131.87, 130.39, 121.70, 63.07, 55.89, 35.39, 24.19.

HRMS-ESI$^+$: m/z [M+H]$^+$ calcd. for 322.0437; found 322.0435.

119
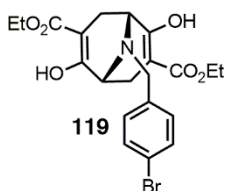
(1R,5R)-diethyl9-(4-bromobenzyl)-2,6-dihydroxy-9-azabicyclo[3.3.1]nona-2,6-diene-3,7-dicarboxylate **119**. Under inert atmosphere, to a solution of LiHMDS (7.9 ml, 7.99 mmol, 1.0 M, 2.5 equiv) in anhydrous THF (40 ml) diketone **118** (1.03 g, 3.19 mmol, 1.0 equiv) in anhydrous THF (10 ml) was added dropwise at -78°C. Some white precipitate of dienolate of **118** formed shortly after addition and the viscosity of the solution markedly increased. To complete enolization, the mixture was allowed to warm to RT for 15 min and then brought back to -78°C. DMPU (0.96 ml, 7.99 mmol, 2.5 equiv) was added followed by ethyl cyanoformate (0.79 ml, 7.99 mmol, 2.5 equiv). Reaction mixture was stirred for 30 min at -78°C and quenched by adding sat. NH$_4$Cl aqueous solution into reaction mixture. Crude product was extracted with DCM, dried over anhydrous Na$_2$SO$_4$ and evaporated to dryness. The crude was purified by column chromatography on silica gel (PE:EA 15:1, R$_f$ = 0.40) to afford 0.64 g (42 %) of **119** as a white solid.

^{1}H NMR (400 MHz, CDCl$_3$): δ 12.02 (s, 2H), 7.44 (d, *J* = 8.3 Hz, 2H), 7.23 (d, *J* = 8.3 Hz, 2H), 4.21 (qd, *J* = 7.2, 1.2 Hz, 4H), 3.66 (dd, *J* = 16.3, 13.5 Hz, 2H), 3.39 (d, *J* = 6.0 Hz, 2H), 2.66 (d, *J* = 6.3 Hz, 1H), 2.62 (d, *J* = 6.4 Hz, 1H), 2.44 (s, 1H), 2.40 (s, 1H), 1.31 (t, *J* = 7.1 Hz, 6H).

^{13}C NMR (101 MHz, CDCl$_3$): δ 171.85, 168.09, 135.82, 132.00, 131.96, 130.39, 94.92, 61.06, 55.39, 53.95, 24.66, 14.32.

HRMS-ESI$^+$: m/z [M-H]$^-$ calcd. for 464.0703; found 464.0721.
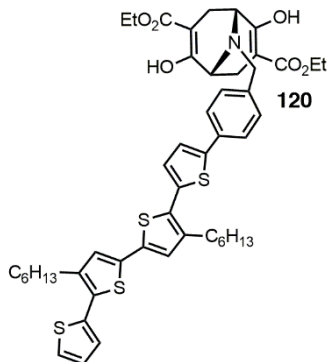
(1R,5R)-diethyl-9-(4-(3',4''-dihexyl-[2,2':5',2'':5'',2'''-quaterthiophen]-5-yl)benzyl)-2,6-dihydroxy-9-azabicyclo[3.3.1]nona-2,6-diene-3,7 dicarboxylate 120. A mixture of compound **119** (60.7 mg, 0.13 mmol, 1.0 equiv), 5-trimethylstannyl quaterthiophene **126** (128 mg; 0.19 mmol, 1.5 equiv) was dissolved in anhydrous DMF (4.0 mL) under argon atmosphere. The mixture was sparged with argon for 15 min and Pd(PPh₃)₄ (15 mg, 0.013 mmol, 0.10 equiv) was added. Then reaction mixture was heated at 85ºC for 1.5 hours. The reaction was allowed to reach room temperature and then diluted with water and extracted with EA. Combined organic phase was washed with brine, dried over anhydrous Na₂SO₄ and evaporated to dryness. The crude was purified by column chromatography on silica gel (PE:EA 10:1, R_f = 0.35) to afford 73.7 mg (64 %) of **120** as an orange solid.

¹H NMR (400 MHz, CDCl₃): δ 12.05 (s, 2H), 7.61 – 7.54 (m, 2H), 7.38 (d, *J* = 8.2 Hz, 2H), 7.31 (dd, *J* = 5.1, 1.2 Hz, 1H), 7.28 – 7.25 (m, 1H), 7.14 (tt, *J* = 4.1, 2.2 Hz, 1H), 7.12 – 7.05 (m, 2H), 7.04 – 6.99 (m, 2H), 4.23 (qd, *J* = 7.1, 1.4 Hz, 4H), 3.73 (q, *J* = 13.3 Hz, 2H), 3.46 (d, *J* = 6.0 Hz, 2H), 2.90 – 2.62 (m, 6H), 2.47 (s, 1H), 2.43 (s, 1H), 1.68 (tdd, *J* = 10.7, 9.0, 7.9, 4.7 Hz, 4H), 1.46 – 1.39 (m, 4H), 1.32 (td, *J* = 7.2, 3.5 Hz, 14H), 1.01 – 0.82 (m, 6H).

¹³C NMR (101 MHz, CDCl₃): δ 172.28, 170.53, 143.78, 140.52, 140.50, 137.25, 136.09, 135.50, 134.97, 134.96, 133.44, 129.80, 129.75, 129.47, 127.58, 126.71, 126.64, 126.54, 125.93, 125.83, 125.46, 123.55, 94.94, 60.76, 55.79, 54.09, 31.81, 31.79, 30.66, 30.61, 29.65, 29.50, 29.39, 29.37, 24.92, 22.77, 22.76, 14.37, 14.26, 14.24.

HRMS-ESI⁺: m/z [M-H]⁻ calcd. for 882.2996; found 882.3023.

121
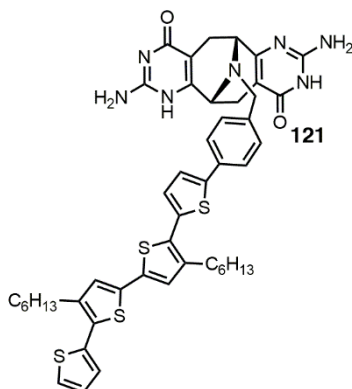
Monomer 121. Under inert atmosphere a mixture of **120** (19 mg, 0.021 mmol, 1.0 equiv), guanidinium chloride (10.2 mg, 0.11 mmol, 5.0 equiv) and KOtBu (12 mg, 0.11 mmol, 5.0 equiv) in MeOH (3.0 mL) was heated at 100 °C for 24 hours. The solvent was removed under reduced pressure. The crude was diluted with water and pH was adjusted to 7 using AcOH. The resulting orange precipitate was filtered, washed with MeOH, and subsequently was purified by column chromatography on silica gel (CHCl$_3$:MeOH:AcOH 50:1:1, R_f = 0.65) to afford 8.6 mg (46 %) of **121** as an orange solid.

^{1}H NMR (400 MHz, CDCl$_3$ + AcOH): δ 7.57 (d, J = 7.7 Hz, 1H), 7.36 – 7.28 (m, 3H), 7.15 – 7.08 (m, 3H), 7.06 (d, J = 4.6 Hz, 1H), 6.99 (s, 1H), 6.79 (d, J = 8.3 Hz, 2H), 4.17 (dd, J = 10.9, 2.1 Hz, 1H), 4.08 – 4.02 (m, 1H), 3.93 (dd, J = 10.8, 5.6 Hz, 1H), 3.84 – 3.72 (m, 2H), 3.72 – 3.61 (m, 1H), 3.39 – 3.29 (m, 1H), 2.95 – 2.65 (m, 4H), 2.57 – 2.52 (m, 1H), 1.72 – 1.63 (m, 2H), 1.49 – 1.15 (m, 14H), 0.95 – 0.76 (m, 6H).

^{13}C NMR could not be obtained due to its poor solubility and high aggregation.

HRMS-ESI$^+$: m/z [M+H]$^+$ calcd. for 874.3060; found 874.3044.

T$_4$-126
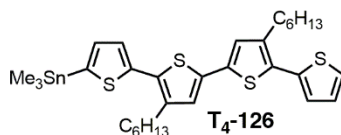
(3',4''-dihexyl-[2,2':5',2'':5,2'''-quaterthiophen]-5-yl)trimethylstannane 126. Under inert atmosphere 5-bromo quaterthiophene 1**25** (203 mg, 0.35 mmol, 1.0 equiv) was dissolved in anhydrous THF (5.0 mL). The mixture was cooled to – 78°C and 2.5 M butyllithium solution in hexane (0.16 mL, 0.40 mmol, 1.15 equiv) was added dropwise. After stirring the mixture for 1.5 hours at – 78°C, the solution of trimethyltin chloride (80.5 mg, 0.40 mmol, 1.15 equiv) in anhydrous THF (2.0 mL) was added in one portion at –

78°C. The mixture was slowly warmed up to room temperature. After stirring overnight at room temperature, the mixture was diluted with sat. NH$_4$Cl solution and extracted with ethyl acetate, then washed with water and brine. Combined organic phase was washed with brine, dried over anhydrous Na$_2$SO$_4$ and evaporated to dryness to afford 229 mg (99 %) of **126** as a brown oil. The crude was used without any further purification.

128
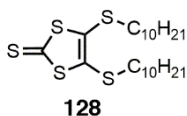
4,5-bis(decylthio)-1,3-dithiole-2-thione 128. A mixture of **127** (3.0 g, 4.19 mmol, 1.0 equiv), 1-bromodecane (4.34 mL, 20.99 mmol, 5.0 equiv) in CH$_3$CN (40 mL) was refluxed overnight. After cooling down to room temperature, the reaction mixture was filtered through CELITE and evaporated to dryness. The crude was purified by column chromatography on silica gel (PE:EA 100:1, R$_f$ = 0.41) to afford 1.06 g (26 %) of **128** as a yellow oil.

Spectral data were in accordance with a literature.[262]

134
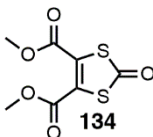
4,5-bis(methoxycarbonyl)-1,3-dithiole-2-one 134. Hg(OAc)$_2$ (1.15 g, 3.62 mmol, 2.0 equiv) was added to a solution of **133** (453 mg, 1.81 mmol, 1.0 equiv) in CHCl$_3$/AcOH 20 mL/7.0 mL mixture. The resulting suspension was stirred at room temperature overnight. Afterwards the mixture was filtered through CELITE and evaporated to dryness. The crude was purified by column chromatography on silica gel (PE:EA 10:1, R$_f$ = 0.40) to afford 417 mg (99 %) of **134** as a white solid.

Spectral data were in accordance with a literature.[263]

135
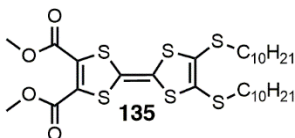
4,5-bis(thiodecyl)-4',5'-bis(methoxycarbonyl)tetrathiafulvalene 135. Under inert atmosphere a mixture of **128** (1.03 g, 2.16 mmol, 1.0 equiv) and **134** (0.66 g, 2.80 mmol, 1.3 equiv) in P(OEt)$_3$ (15 mL) were heated at 80 °C for 4 hours. After cooling down to room temperature, the solvent was

removed under reduced pressure. The crude was purified by column chromatography on silica gel (PE:EA 60:1→20:1, R_f = 0.25) to afford 0.73 g (51 %) of **135** as an orange solid.

¹H NMR (400 MHz, CDCl₃): δ 3.85 (s, 6H), 2.79 (br.s, 4H), 1.64 (s, 4H), 1.48 – 1.36 (m, 4H), 1.32 – 1.17 (m, 24H), 0.88 (t, *J* = 6.7 Hz, 6H).

¹³C NMR (101 MHz, CDCl₃): δ 199.35, 160.12, 132.16, 128.11, 113.16, 53.51, 36.59, 32.04, 29.89, 29.70, 29.67, 29.46, 29.26, 28.65, 22.83, 14.26.

HRMS-ESI⁺: m/z [M+H]⁺ calcd. for 665.1949; found 665.1912.

136
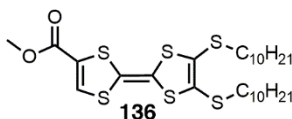
4,5-bis(thiodecyl)-4'-(methoxycarbonyl)tetrathiafulvalene 136. Under inert atmosphere a mixture of **135** (463 mg, 0.70 mmol, 1.0 equiv), LiBr (605 mg, 6.96 mmol, 10.0 equiv) in anhydrous DMF (9.0 mL) was heated at 85 °C for 3 hours. The reaction was cooled down to room temperature and then diluted with water and extracted with EA. Combined organic phase was washed with water and brine, dried over anhydrous Na₂SO₄ and evaporated to dryness. The crude was purified by column chromatography on silica gel (PE:EA 60:1, R_f = 0.17) to afford 395 mg (94 %) of **136** as an orange oil.

¹H NMR (400 MHz, CD₂Cl₂): δ 7.35 (s, 1H), 3.79 (s, 3H), 2.81 (td, *J* = 7.3, 3.0 Hz, 4H), 1.61 (p, *J* = 7.3 Hz, 4H), 1.39 (p, *J* = 6.8 Hz, 4H), 1.33 – 1.21 (m, 24H), 0.87 (t, *J* = 6.7 Hz, 6H).

¹³C NMR (101 MHz, CD₂Cl₂): δ 160.07, 132.20, 128.71, 128.57, 128.05, 112.30, 110.14, 36.73, 32.33, 30.21, 30.18, 29.98, 29.94, 29.74, 29.52, 28.88, 23.10, 14.29.

HRMS-ESI⁺: m/z [M+H]⁺ calcd. for 607.1895; found 607.1885.

137
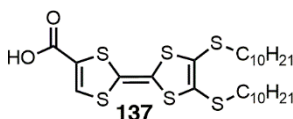
4,5-bis(thiodecyl)-4'-carboxytetrathiafulvalene 137. Aqueous solution of 1.5M LiOH (3.5 mL, 5.21 mmol, 5.0 equiv) was added into a mixture of **136** (632 mg, 1.04 mmol, 1.0 equiv) in 1,4-dioxane (20 mL). Reaction mixture was stirred at room temperature for 15 hours. Then 5.0 M HCl aqueous solution (1.2 mL) was added, and the solution was stirred for 15 min. Reaction mixture was diluted with water and EA and the pH of solution was adjusted to pH = 1-2 with solution of 5.0 M HCl. The mixture was extracted

with EA. Combined organic phase was washed with 1.0 M HCl and water, dried over anhydrous Na$_2$SO$_4$ and evaporated to dryness. The crude was precipitated with water, filtered and washed to afford 603 mg (98 %) of **137** as an orange solid.

^{1}H NMR (400 MHz, CD$_2$Cl$_2$): δ 7.49 (s, 1H), 4.15 (br.s, 1H), 2.83 (s, 4H), 1.62 (dd, J = 13.9, 7.2 Hz, 4H), 1.49 – 1.16 (m, 28H), 0.89 (t, J = 6.6 Hz, 6H).

^{13}C NMR (101 MHz, CD$_2$Cl$_2$): δ 138.08, 129.20, 128.95, 128.73, 128.31, 128.05, 127.81, 32.35, 30.01, 29.97, 29.77, 29.55, 28.95, 28.93, 23.13, 14.32.

HRMS-ESI$^+$: m/z [M-H]$^-$ calcd. for 591.1593; found 591.1597.
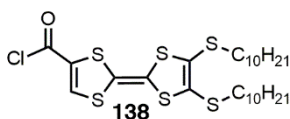
4,5-bis(thiodecyl)-4'-(carbonylchloride)tetrathiafulvalene 138. Under inert atmosphere **137** (603 mg, 1.02 mmol, 1.0 equiv) was dissolved in anhydrous DCM (50 mL) and anhydrous DMF (seven drops). Then oxalyl chloride (0.17 mL, 2.03 mmol, 2.0 equiv) was added dropwise and the mixture was stirred at room temperature overnight. Then reaction mixture was filtered, and the collected filtrate was evaporated to dryness. The crude was purified by column chromatography on silica gel (PE:EA 80:1, R$_f$ = 0.20) to afford 244 mg (39 %) of **138** as a purple solid.

^{1}H NMR (400 MHz, CD$_2$Cl$_2$): δ 7.82 (s, 1H), 2.83 (td, J = 7.3, 3.2 Hz, 4H), 1.63 (p, J = 7.3 Hz, 4H), 1.41 (p, J = 7.0, 6.2 Hz, 4H), 1.34 – 1.21 (m, 24H), 0.88 (t, J = 7.0 Hz, 6H).

^{13}C NMR (101 MHz, CD$_2$Cl$_2$): δ 138.09, 129.20, 128.96, 128.72, 128.30, 128.06, 127.82, 36.81, 32.34, 30.21, 29.99, 29.94, 29.76, 29.52, 28.87, 23.12, 14.30.

HRMS-ESI$^+$: m/z [M+H]$^+$ calcd. for 611.1399; found 611.0568.
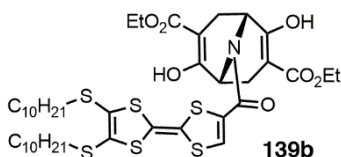
(1R,5R)-diethyl 9-(4,5-bis(thiodecyl)tetrathiafulvalene carbonyl)-2,6-dihydroxy-9-azabicyclo[3.3.1]nona-2,6-diene-3,7-dicarboxylate 139b.

Under inert atmosphere to a solution of **(-)-131b** (71 mg, 0.18 mmol, 1.0 equiv) in anhydrous DCM (3.0 mL) was added TFA (0.68 mL, 8.93 mmol,

50 equiv) dropwise. The mixture was stirred at room temperature for 3 hours and then evaporated to dryness. Under inert atmosphere the solid residue was dissolved in anhydrous THF (3.0 mL) followed by the addition of Et$_3$N (0.02 mL, 0.18 mmol, 1.0 equiv) and a solution of TTF-carbonylchloride **138** (131 mg, 0.21 mmol, 1.2 equiv) in anhydrous THF (3.0 mL). The reaction mixture was stirred at room temperature for 4 hours and then evaporated to dryness. The crude was purified by column chromatography on silica gel (PE:DCM 1:1→DCM, R$_f$ = 0.23) to afford 225 mg (80 %) of (-)-**139b** as an orange solid. Racemic **139a** was synthesized using same method in 67 % yield.

^{1}H NMR (400 MHz, CD$_2$Cl$_2$): δ 12.12 (s, 2H), 6.73 (s, 1H), 4.93 (br. s, 2H), 4.23 (qt, J = 7.1, 3.3 Hz, 4H), 2.90 (m, 6H), 2.68 (s, 1H), 2.64 (s, 1H), 1.63 (p, J = 7.4 Hz, 4H), 1.40 (q, J = 7.2 Hz, 4H), 1.35 – 1.18 (m, 30H), 0.89 (t, J = 6.6 Hz, 6H).

^{13}C NMR (101 MHz, CD$_2$Cl$_2$): δ 172.21, 168.27, 138.09, 129.20, 128.96, 128.73, 128.29, 128.06, 127.82, 95.96, 61.53, 36.78, 32.34, 30.21, 29.99, 29.96, 29.76, 29.55, 28.91, 23.12, 14.36, 14.31.

HRMS-ESI$^+$: m/z [M+H]$^+$ calcd. for 872.2845; found 872.2815.
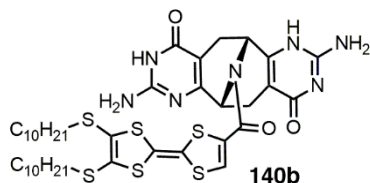
140b

Monomer ICyt 140b. A mixture of **139b** (103 mg, 0.12 mmol, 1.0 equiv), guanidinium carbonate (106 mg, 0.59 mmol, 5.0 equiv) in MeOH (8.0 mL) was heated at 100 °C for 24 hours. Then reaction mixture was cooled down to room temperature and was diluted with water. The resulting orange and washed with water and methanol. Additionally, the crude was precipitated with MeOH, filtered and washed with MeOH to afford 62 mg (61 %) of **140b** as an orange solid. Racemic **140a** was synthesized using same method in 52 % yield.

^{1}H NMR (400 MHz, DMSO-d$_6$): δ 10.99 (s, 2H), 7.37 (s, 1H), 6.47 (s, 4H), 5.18 – 4.67 (m, 2H), 2.84 (q, J = 6.7 Hz, 4H), 2.61 (d, J = 14.7 Hz, 4H), 1.73 – 1.47 (m, 4H), 1.40 – 1.29 (m, 4H), 1.28 – 1.07 (m, 24H), 0.83 (t, J = 6.6 Hz, 6H).

^{13}C NMR (101 MHz, DMSO-d$_6$): δ 160.01, 158.78, 157.06, 154.49, 128.16, 127.48, 126.99, 125.15, 112.40, 106.93, 104.27, 35.34, 31.26, 31.24, 29.14, 28.89, 28.86, 28.81, 28.70, 28.63, 28.36, 28.33, 27.52, 22.04, 13.89.

HRMS-ESI$^+$: m/z [M+H]$^+$ calcd. for 862.2763; found 862.2739.

REFERENCES

(1) Whitesides, G. M.; Mathias, J. P.; Seto, C. T. Molecular Self-Assembly and Nanochemistry: A Chemical Strategy for the Synthesis of Nanostructures. *Science* **1991**, *254* (5036), 1312–1319. https://doi.org/10.1126/science.1962191.

(2) Elemans, J. A. A. W.; Rowan, A. E.; Nolte, R. J. M. Mastering Molecular Matter. Supramolecular Architectures by Hierarchical Self-Assembly. *J Mater Chem* **2003**, *13* (11), 2661–2670. https://doi.org/10.1039/B304972H.

(3) Philp, D.; Stoddart, J. F. Self-Assembly in Natural and Unnatural Systems. *Angew. Chem. Int. Ed. Engl.* **1996**, *35* (11), 1154–1196. https://doi.org/10.1002/anie.199611541.

(4) Whitesides, G. M.; Grzybowski, B. Self-Assembly at All Scales. *Science* **2002**, *295* (5564), 2418–2421. https://doi.org/10.1126/science.1070821.

(5) Feynman, R. P. There's Plenty of Room at the Bottom. *J. Microelectromechanical Syst.* **1992**, *1* (1), 60–66. https://doi.org/10.1109/84.128057.

(6) Stoddart, J. F. From Supramolecular to Systems Chemistry: Complexity Emerging out of Simplicity. *Angew. Chem. Int. Ed.* **2012**, *51* (52), 12902–12903. https://doi.org/10.1002/anie.201209124.

(7) Whitesides, G. M.; Boncheva, M. Beyond Molecules: Self-Assembly of Mesoscopic and Macroscopic Components. *Proc. Natl. Acad. Sci.* **2002**, *99* (8), 4769–4774. https://doi.org/10.1073/pnas.082065899.

(8) Watson, J. D.; Crick, F. H. C. Molecular Structure of Nucleic Acids: A Structure for Deoxyribose Nucleic Acid. *Nature* **1953**, *171* (4356), 737–738. https://doi.org/10.1038/171737a0.

(9) Koch, C.; Eber, F. J.; Azucena, C.; Förste, A.; Walheim, S.; Schimmel, T.; Bittner, A. M.; Jeske, H.; Gliemann, H.; Eiben, S.; Geiger, F. C.; Wege, C. Novel Roles for Well-Known Players: From Tobacco Mosaic Virus Pests to Enzymatically Active Assemblies. *Beilstein J. Nanotechnol.* **2016**, *7*, 613–629. https://doi.org/10.3762/bjnano.7.54.

(10) Percec, V.; Glodde, M.; Bera, T. K.; Miura, Y.; Shiyanovskaya, I.; Singer, K. D.; Balagurusamy, V. S. K.; Heiney, P. A.; Schnell, I.; Rapp, A.; Spiess, H.-W.; Hudson, S. D.; Duan, H. Self-Organization of Supramolecular Helical Dendrimers into Complex Electronic Materials. *Nature* **2002**, *419* (6905), 384–387. https://doi.org/10.1038/nature01072.

(11) Goujon, A.; Mariani, G.; Lang, T.; Moulin, E.; Rawiso, M.; Buhler, E.; Giuseppone, N. Controlled Sol–Gel Transitions by Actuating Molecular Machine Based Supramolecular Polymers. *J. Am. Chem. Soc.* **2017**, *139* (13), 4923–4928. https://doi.org/10.1021/jacs.7b00983.

(12) Welte, L.; Calzolari, A.; Di Felice, R.; Zamora, F.; Gómez-Herrero, J. Highly Conductive Self-Assembled Nanoribbons of Coordination Polymers. *Nat. Nanotechnol.* **2010**, *5* (2), 110–115. https://doi.org/10.1038/nnano.2009.354.

(13) Zhang, L.; Zhong, X.; Pavlica, E.; Li, S.; Klekachev, A.; Bratina, G.; Ebbesen, T. W.; Orgiu, E.; Samorì, P. A Nanomesh Scaffold for Supramolecular Nanowire Optoelectronic Devices. *Nat. Nanotechnol.* **2016**, *11* (10), 900–906. https://doi.org/10.1038/nnano.2016.125.

(14) Chwastek, M.; Cmoch, P.; Szumna, A. Dodecameric Anion-Sealed Capsules Based on Pyrogallol[5]Arenes and Resorcin[5]Arenes. *Angew. Chem.* **2021**, *133* (9), 4590–4594. https://doi.org/10.1002/ange.202013105.

(15) Chamorro, P. B.; Aparicio, F. Chiral Nanotubes Self-Assembled from Discrete Non-Covalent Macrocycles. *Chem. Commun.* **2021**, *57*, 12712–12724. https://doi.org/10.1039/D1CC04968B.

(16) Chen, H.; Zhang, W.; Ren, S.; Zhao, X.; Jiao, Y.; Wang, Y.; Stoddart, J. F.; Guo, X. Temperature-Triggered Supramolecular Assembly of Organic Semiconductors. *Adv. Mater.* **2021**, 2101487. https://doi.org/10.1002/adma.202101487.

(17) Cheng, C.-C.; Chang, F.-C.; Kao, W.-Y.; Hwang, S.-M.; Liao, L.-C.; Chang, Y.-J.; Liang, M.-C.; Chen, J.-K.; Lee, D.-J. Highly Efficient Drug Delivery Systems Based on Functional Supramolecular Polymers: In Vitro Evaluation. *Acta Biomater.* **2016**, *33*, 194–202. https://doi.org/10.1016/j.actbio.2016.01.018.

(18) James Clare Speakman - The Hydrogen Bond and Other Intermolecular Forces. ISBN 9780851869193, The Chemical Society, **1975**, 33 p.

(19) van der Lubbe, S. C. C.; Haim, A.; van Heesch, T.; Fonseca Guerra, C. Tuning the Binding Strength of Even and Uneven Hydrogen-Bonded Arrays with Remote Substituents. *J. Phys. Chem. A* **2020**, *124* (45), 9451–9463. https://doi.org/10.1021/acs.jpca.0c07815.

(20) Zhang, D.-W.; Wang, H.; Li, Z.-T. Hydrogen Bonding Motifs: New Progresses. In Hydrogen Bonded Supramolecular Structures. ISBN 978366245755-9, Springer, Berlin, Heidelberg, **2015**, *87*, 1–36. https://doi.org/10.1007/978-3-662-45756-6_1.

(21) Herbst, F.; Binder, W. H. Comparing Solution and Melt-State Association of Hydrogen Bonds in Supramolecular Polymers. *Polym. Chem.* **2013**, *4* (12), 3602–3609. https://doi.org/10.1039/c3py00362k.

(22) Coubrough, H. M.; Balonova, B.; Pask, C. M.; Blight, B. A.; Wilson, A. J. A pH-Switchable Triple Hydrogen-Bonding Motif. *ChemistryOpen* **2020**, *9* (1), 40–44. https://doi.org/10.1002/open.201900338.

(23) Wood, J. L. pH-Controlled Hydrogen-Bonding. *Biochem. J.* **1974**, *143* (3), 775–777. https://doi.org/10.1042/bj1430775.

(24) Street, D. P.; Ledford, W. K.; Allison, A. A.; Patterson, S.; Pickel, D. L.; Lokitz, B. S.; Messman, J. M.; Kilbey, S. M. Self-Complementary Multiple Hydrogen-Bonding Additives Enhance Thermomechanical Properties of 3D-Printed PMMA Structures. *Macromolecules* **2019**, *52* (15), 5574–5582. https://doi.org/10.1021/acs.macromol.9b00546.

(25) Lavrenova, A.; Balkenende, D. W. R.; Sagara, Y.; Schrettl, S.; Simon, Y. C.; Weder, C. Mechano- and Thermoresponsive Photoluminescent Supramolecular Polymer. *J. Am. Chem. Soc.* **2017**, *139* (12), 4302–4305. https://doi.org/10.1021/jacs.7b00342.

(26) Gilli, G.; Gilli, P. The Nature of the Hydrogen Bond: Outline of a Comprehensive Hydrogen Bond Theory. ISBN 9780191720949, Oxford University Press: Oxford , UK, 2009.

(27) Isaacs, E. D.; Shukla, A.; Platzman, P. M.; Hamann, D. R.; Barbiellini, B.; Tulk, C. A. Covalency of the Hydrogen Bond in Ice: A Direct X-Ray Measurement. *Phys. Rev. Lett.* **1999**, *82* (3), 600–603. https://doi.org/10.1103/PhysRevLett.82.600.

(28) Zarycz, M. N. C.; Schiel, M. A.; Angelina, E.; Enriz, R. D. Covalence and π-Electron Delocalization Influence on Hydrogen Bonds in Proton Transfer Process of *o*-Hydroxy Aryl Schiff Bases: A Combined NMR and QTAIM Analysis. *J. Chem. Phys.* **2021**, *155* (5), 054307. https://doi.org/10.1063/5.0058422.

(29) Shahi, A.; Arunan, E. Hydrogen Bonding, Halogen Bonding and Lithium Bonding: An Atoms in Molecules and Natural Bond Orbital Perspective towards Conservation of Total Bond Order, Inter- and Intra-Molecular Bonding. *Phys Chem Chem Phys* **2014**, *16* (42), 22935–22952. https://doi.org/10.1039/C4CP02585G.

(30) Zubatyuk, R. I.; Volovenko, Y. M.; Shishkin, O. V.; Gorb, L.; Leszczynski, J. Aromaticity-Controlled Tautomerism and Resonance-Assisted Hydrogen Bonding in Heterocyclic

Enaminone−Iminoenol Systems. *J. Org. Chem.* **2007**, *72* (3), 725–735. https://doi.org/10.1021/jo0616411.

(31) Tan, K. P.; Singh, K.; Hazra, A.; Madhusudhan, M. S. Peptide Bond Planarity Constrains Hydrogen Bond Geometry and Influences Secondary Structure Conformations. *Curr. Res. Struct. Biol.* **2021**, *3*, 1–8. https://doi.org/10.1016/j.crstbi.2020.11.002.

(32) Sartorius, J.; Schneider, H.-J. A General Scheme Based on Empirical Increments for the Prediction of Hydrogen-Bond Associations of Nucleobases and of Synthetic Host–Guest complexes. *Chem. Eur. J.* **1996**, *2* (11), 1446–1452. https://doi.org/10.1002/chem.19960021118.

(33) Wilson, A. J. Non-Covalent Polymer Assembly Using Arrays of Hydrogen-Bonds. *Soft Matter* **2007**, *3* (4), 409–425. https://doi.org/10.1039/b612566b.

(34) Pranata, J.; Wierschke, S. G.; Jorgensen, W. L. OPLS Potential Functions for Nucleotide Bases. Relative Association Constants of Hydrogen-Bonded Base Pairs in Chloroform. *J. Am. Chem. Soc.* **1991**, *113* (8), 2810–2819. https://doi.org/10.1021/ja00008a002.

(35) Jorgensen, W. L.; Pranata, J. Importance of Secondary Interactions in Triply Hydrogen Bonded Complexes: Guanine-Cytosine vs Uracil-2,6-Diaminopyridine. *J. Am. Chem. Soc.* **1990**, *112* (5), 2008–2010. https://doi.org/10.1021/ja00161a061.

(36) Karas, L. J.; Wu, C.; Das, R.; Wu, J. I. Hydrogen Bond Design Principles. *WIREs Comput. Mol. Sci.* **2020**, *10* (6). https://doi.org/10.1002/wcms.1477.

(37) Ośmiałowski, B.; Kolehmainen, E.; Kowalska, M. 2-Acylamino-6-Pyridones: Breaking of an Intramolecular Hydrogen Bond by Self-Association and Complexation with Double and Triple Hydrogen Bonding Counterparts. Uncommon Steric Effect on Intermolecular Interactions. *J. Org. Chem.* **2012**, *77* (4), 1653–1662. https://doi.org/10.1021/jo201800u.

(38) Sijbesma, R. P.; Meijer, E. W. Quadruple Hydrogen Bonded Systems. *Chem. Commun.* **2003**, *1*, 5–16. https://doi.org/10.1039/b205873c.

(39) Murray, T. J.; Zimmerman, S. C. New Triply Hydrogen Bonded Complexes with Highly Variable Stabilities. *J. Am. Chem. Soc.* **1992**, *114* (10), 4010–4011. https://doi.org/10.1021/ja00036a079.

(40) Djurdjevic, S.; Leigh, D. A.; McNab, H.; Parsons, S.; Teobaldi, G.; Zerbetto, F. Extremely Strong and Readily Accessible

AAA−DDD Triple Hydrogen Bond Complexes. *J. Am. Chem. Soc.* **2007**, *129* (3), 476–477. https://doi.org/10.1021/ja067410t.

(41) Beijer, F. H.; Kooijman, H.; Spek, A. L.; Sijbesma, R. P.; Meijer, E. W. Self-Complementarity Achieved through Quadruple Hydrogen Bonding. *Angew. Chem. Int. Ed.* **1998**, *37* (1–2), 75–78. https://doi.org/10.1002/(SICI)1521-3773(19980202)37:1/2<75::AID-ANIE75>3.0.CO;2-R.

(42) Beijer, F. H.; Sijbesma, R. P.; Kooijman, H.; Spek, A. L.; Meijer, E. W. Strong Dimerization of Ureidopyrimidones via Quadruple Hydrogen Bonding. *J. Am. Chem. Soc.* **1998**, *120* (27), 6761–6769. https://doi.org/10.1021/ja974112a.

(43) Baruah, P. K.; Khan, S. Self-Complementary Quadruple Hydrogen Bonding Motifs: From Design to Function. *RSC Adv.* **2013**, *3* (44), 21202–21217. https://doi.org/10.1039/c3ra43814g.

(44) Corbin, P. S.; Zimmerman, S. C. Self-Association without Regard to Prototropy. A Heterocycle That Forms Extremely Stable Quadruply Hydrogen-Bonded Dimers. *J. Am. Chem. Soc.* **1998**, *120* (37), 9710–9711. https://doi.org/10.1021/ja981884d.

(45) Gong, B. Molecular Duplexes with Encoded Sequences and Stabilities. *Acc. Chem. Res.* **2012**, *45* (12), 2077–2087. https://doi.org/10.1021/ar300007k.

(46) Zhang, Y.; Cao, R.; Shen, J.; Detchou, C. S. F.; Zhong, Y.; Wang, H.; Zou, S.; Huang, Q.; Lian, C.; Wang, Q.; Zhu, J.; Gong, B. Hydrogen-Bonded Duplexes with Lengthened Linkers. *Org. Lett.* **2018**, *20* (6), 1555–1558. https://doi.org/10.1021/acs.orglett.8b00283.

(47) Zhang, P.; Chu, H.; Li, X.; Feng, W.; Deng, P.; Yuan, L.; Gong, B. Alternative Strategy for Adjusting the Association Specificity of Hydrogen-Bonded Duplexes. *Org. Lett.* **2011**, *13* (1), 54–57. https://doi.org/10.1021/ol102522m.

(48) Liu, R.; Cheng, S.; Baker, E. S.; Smith, R. D.; Zeng, X. C.; Gong, B. Surprising Impact of Remote Groups on the Folding–Unfolding and Dimer-Chain Equilibria of Bifunctional H-Bonding Unimers. *Chem. Commun.* **2016**, *52* (19), 3773–3776. https://doi.org/10.1039/C6CC00224B.

(49) Bisson, A. P.; Carver, F. J.; Eggleston, D. S.; Haltiwanger, R. C.; Hunter, C. A.; Livingstone, D. L.; McCabe, J. F.; Rotger, C.; Rowan, A. E. Synthesis and Recognition Properties of Aromatic Amide Oligomers: Molecular Zippers. *J. Am. Chem. Soc.* **2000**, *122* (37), 8856–8868. https://doi.org/10.1021/ja0012671.

(50) Blight, B. A.; Camara-Campos, A.; Djurdjevic, S.; Kaller, M.; Leigh, D. A.; McMillan, F. M.; McNab, H.; Slawin, A. M. Z.

AAA−DDD Triple Hydrogen Bond Complexes. *J. Am. Chem. Soc.* **2009**, *131* (39), 14116–14122. https://doi.org/10.1021/ja906061v.

(51) Bell, D. A.; Anslyn, E. V. Establishing a Cationic AAA-DDD Hydrogen Bonding Complex. *Tetrahedron* **1995**, *51* (26), 7161–7172. https://doi.org/10.1016/0040-4020(95)00381-H.

(52) Taubitz, J.; Lüning, U. The AAAA·DDDD Hydrogen Bond Dimer. Synthesis of a Soluble Sulfurane as AAAA Domain and Generation of a DDDD Counterpart. *Aust. J. Chem.* **2009**, *62* (11), 1550–1555. https://doi.org/10.1071/CH09113.

(53) Blight, B. A.; Hunter, C. A.; Leigh, D. A.; McNab, H.; Thomson, P. I. T. An AAAA–DDDD Quadruple Hydrogen-Bond Array. *Nat. Chem.* **2011**, *3* (3), 244–248. https://doi.org/10.1038/nchem.987.

(54) Leigh, D. A.; Robertson, C. C.; Slawin, A. M. Z.; Thomson, P. I. T. AAAA-DDDD Quadruple Hydrogen-Bond Arrays Featuring NH···N and CH···N Hydrogen Bonds. *J. Am. Chem. Soc.* **2013**, *135* (26), 9939–9943. https://doi.org/10.1021/ja404504m.

(55) van der Lubbe, S. C. C.; Zaccaria, F.; Sun, X.; Fonseca Guerra, C. Secondary Electrostatic Interaction Model Revised: Prediction Comes Mainly from Measuring Charge Accumulation in Hydrogen-Bonded Monomers. *J. Am. Chem. Soc.* **2019**, *141* (12), 4878–4885. https://doi.org/10.1021/jacs.8b13358.

(56) Lin, X.; Wu, W.; Mo, Y. How Resonance Modulates Multiple Hydrogen Bonding in Self-Assembled Systems. *J. Org. Chem.* **2019**, *84* (22), 14805–14815. https://doi.org/10.1021/acs.joc.9b02381.

(57) Zhou, F.; Wang, J.; Zhang, Y.; Wang, Q.; Guo, C.; Wang, F.; Zheng, X.; Zhang, H. Theoretical Studies on the Bond Strength and Electron Density Characteristics in Multiple Hydrogen Bonded Arrays. *J. Mol. Graph. Model.* **2019**, *93*, 107439. https://doi.org/10.1016/j.jmgm.2019.107439.

(58) Vallejo Narváez, W. E.; Jiménez, E. I.; Cantú-Reyes, M.; Yatsimirsky, A. K.; Hernández-Rodríguez, M.; Rocha-Rinza, T. Stability of Doubly and Triply H-Bonded Complexes Governed by Acidity–Basicity Relationships. *Chem. Commun.* **2019**, *55* (11), 1556–1559. https://doi.org/10.1039/C8CC06967K.

(59) Vallejo Narváez, W. E.; Jiménez, E. I.; Romero-Montalvo, E.; Sauza-de la Vega, A.; Quiroz-García, B.; Hernández-Rodríguez, M.; Rocha-Rinza, T. Acidity and Basicity Interplay in Amide and Imide Self-Association. *Chem. Sci.* **2018**, *9* (19), 4402–4413. https://doi.org/10.1039/C8SC01020J.

(60) Wu, J. I.; Jackson, J. E. Reciprocal Hydrogen Bonding–Aromaticity Relationships. *J. Am. Chem. Soc.* **2014**, *136* (39), 13526–13529. https://doi.org/10.1021/ja507202f.

(61) Wu, C.-H.; Zhang, Y.; van Rickley, K.; Wu, J. I. Aromaticity Gain Increases the Inherent Association Strengths of Multipoint Hydrogen-Bonded Arrays. *Chem. Commun.* **2018**, *54* (28), 3512–3515. https://doi.org/10.1039/C8CC00422F.

(62) Taubitz, J.; Lüning, U. On the Importance of the Nature of Hydrogen Bond Donors in Multiple Hydrogen Bond Systems. *Eur. J. Org. Chem.* **2008**, 5922–5927. https://doi.org/10.1002/ejoc.200800589.

(63) Lukin, O.; Leszczynski, J. Rationalizing the Strength of Hydrogen-Bonded Complexes. Ab Initio HF and DFT Studies. *J. Phys. Chem. A* **2002**, *106* (29), 6775–6782. https://doi.org/10.1021/jp0145154.

(64) Chapman, K. T.; Still, W. C. A Remarkable Effect of Solvent Size on the Stability of a Molecular Complex. *J. Am. Chem. Soc.* **1989**, *111* (8), 3075–3077. https://doi.org/10.1021/ja00190a058.

(65) Mabesoone, M. F. J.; Palmans, A. R. A.; Meijer, E. W. Solute–Solvent Interactions in Modern Physical Organic Chemistry: Supramolecular Polymers as a Muse. *J. Am. Chem. Soc.* **2020**, *142* (47), 19781–19798. https://doi.org/10.1021/jacs.0c09293.

(66) Würthner, F. Solvent Effects in Supramolecular Chemistry: Linear Free Energy Relationships for Common Intermolecular Interactions. *J. Org. Chem.* **2022**, *87*, 3, 1602–1615. https://doi.org/10.1021/acs.joc.1c00625.

(67) Park, T.; Zimmerman, S. C.; Nakashima, S. A Highly Stable Quadruply Hydrogen-Bonded Heterocomplex Useful for Supramolecular Polymer Blends. *J. Am. Chem. Soc.* **2005**, *127* (18), 6520–6521. https://doi.org/10.1021/ja050996j.

(68) Hisamatsu, Y.; Shirai, N.; Ikeda, S.; Odashima, K. A New Quadruple Hydrogen-Bonding Module with a DDAA Array: Formation of a Stable Homodimer without Competition from Undesired Hydrogen-Bonded Dimers. *Org. Lett.* **2009**, *11* (19), 4342–4345. https://doi.org/10.1021/ol9017084.

(69) Park, T.; Todd, E. M.; Nakashima, S.; Zimmerman, S. C. A Quadruply Hydrogen Bonded Heterocomplex Displaying High-Fidelity Recognition. *J. Am. Chem. Soc.* **2005**, *127* (51), 18133–18142. https://doi.org/10.1021/ja0545517.

(70) Sun, H.; Lee, H. H.; Blakey, I.; Dargaville, B.; Chirila, T. V.; Whittaker, A. K.; Smith, S. C. Multiple Hydrogen-Bonded Complexes Based on 2-Ureido-4[1H]-Pyrimidinone: A

Theoretical Study. *J. Phys. Chem. B* **2011**, *115* (38), 11053–11062. https://doi.org/10.1021/jp2061305.

(71) Wang, S.; Wu, L.; Zhang, L.; Tung, C. Supramolecular Assemblies Based on 2-Ureido-4[1H]-Pyrimidinone Building Block. *Chin. Sci. Bull.* **2006**, *51* (2), 129–138. https://doi.org/10.1007/s11434-005-1118-5.

(72) Appavoo, D.; Carnevale, D.; Deschenaux, R.; Therrien, B. Combining Coordination and Hydrogen-Bonds to Form Arene Ruthenium Metalla-Assemblies. *J. Organomet. Chem.* **2016**, *824*, 80–87. https://doi.org/10.1016/j.jorganchem.2016.10.011.

(73) Zhang, J.; Qi, S.; Zhang, C.; Fan, Z.; Ding, Q.; Mao, S.; Dong, Z. Controlling Keto–Enol Tautomerism of Ureidopyrimidinone to Generate a Single-Quadruple AADD-DDAA Dimeric Array. *Org. Lett.* **2020**, *22* (18), 7305–7309. https://doi.org/10.1021/acs.orglett.0c02644.

(74) Raczyńska, E. D.; Kosińska, W.; Ośmiałowski, B.; Gawinecki, R. Tautomeric Equilibria in Relation to π-Electron Delocalization. *Chem. Rev.* **2005**, *105* (10), 3561–3612. https://doi.org/10.1021/cr030087h.

(75) Xiao, T.; Xu, L.; Wang, J.; Li, Z.-Y.; Sun, X.-Q.; Wang, L. Biomimetic Folding of Small Organic Molecules Driven by Multiple Non-Covalent Interactions. *Org. Chem. Front.* **2019**, *6* (7), 936–941. https://doi.org/10.1039/C9QO00089E.

(76) Lafitte, V. G. H.; Aliev, A. E.; Hailes, H. C.; Bala, K.; Golding, P. Ureidopyrimidinones Incorporating a Functionalizable *p*-Aminophenyl Electron-Donating Group at C-6. *J. Org. Chem.* **2005**, *70* (7), 2701–2707. https://doi.org/10.1021/jo048223l.

(77) Kheria, S.; Rayavarapu, S.; Kotmale, A. S.; Sanjayan, G. J. Three in One: Prototropy-Free Highly Stable AADD-Type Self-Complementary Quadruple Hydrogen-Bonded Molecular Duplexes with a Built-in Fluorophore. *Chem. Commun.* **2017**, *53* (18), 2689–2692. https://doi.org/10.1039/C6CC09478C.

(78) Lafitte, V. G. H.; Aliev, A. E.; Horton, P. N.; Hursthouse, M. B.; Bala, K.; Golding, P.; Hailes, H. C. Quadruply Hydrogen Bonded Cytosine Modules for Supramolecular Applications. *J. Am. Chem. Soc.* **2006**, *128* (20), 6544–6545. https://doi.org/10.1021/ja0587289.

(79) Folmer, B. J. B.; Sijbesma, R. P.; Kooijman, H.; Spek, A. L.; Meijer, E. W. Cooperative Dynamics in Duplexes of Stacked Hydrogen-Bonded Moieties. *J. Am. Chem. Soc.* **1999**, *121* (39), 9001–9007. https://doi.org/10.1021/ja991409v.

(80) Aparicio, F.; Mayoral, M. J.; Montoro-García, C.; González-Rodríguez, D. Guidelines for the Assembly of Hydrogen-Bonded Macrocycles. *Chem. Commun.* **2019**, *55* (51), 7277–7299. https://doi.org/10.1039/C9CC03166A.

(81) Lehn, J.-M.; Mascal, M.; DeCian, A.; Fischer, J. Molecular Ribbons from Molecular Recognition Directed Self-Assembly of Self-Complementary Molecular Components. *J. Chem. Soc. Perkin Trans. 2.* **1992**, 461–467. https://doi.org/10.1039/p29920000461.

(82) Marsh, A.; Silvestri, M.; Lehn, J.-M. Self-Complementary Hydrogen Bonding Heterocycles Designed for the Enforced Self-Assembly into Supramolecular Macrocycles. *Chem. Commun.* **1996**, 1527–1528. https://doi.org/10.1039/cc9960001527.

(83) Mascal, M.; Hext, N. M.; Warmuth, R.; Moore, M. H.; Turkenburg, J. P. Programming a Hydrogen-Bonding Code for the Specific Generation of a Supermacrocycle. *Angew. Chem. Int. Ed. Engl.* **1996**, *35* (19), 2204–2206. https://doi.org/10.1002/anie.199622041.

(84) Mascal, M.; Hext, N. M.; Warmuth, R.; Arnall-Culliford, J. R.; Moore, M. H.; Turkenburg, J. P. The G−C DNA Base Hybrid: Synthesis, Self-Organization and Structural Analysis. *J. Org. Chem.* **1999**, *64* (23), 8479–8484. https://doi.org/10.1021/jo990719t.

(85) Zerkowski, J. A.; Seto, C. T.; Whitesides, G. M. Solid-State Structures of Rosette and Crinkled Tape Motifs Derived from the Cyanuric Acid Melamine Lattice. *J. Am. Chem. Soc.* **1992**, *114* (13), 5473–5475. https://doi.org/10.1021/ja00039a096.

(86) Choi, I. S.; Li, X.; Simanek, E. E.; Akaba, R.; Whitesides, G. M. Self-Assembly of Hydrogen-Bonded Polymeric Rods Based on the Cyanuric Acid·Melamine Lattice. *Chem. Mater.* **1999**, *11* (3), 684–690. https://doi.org/10.1021/cm980540j.

(87) Fenniri, H.; Mathivanan, P.; Vidale, K. L.; Sherman, D. M.; Hallenga, K.; Wood, K. V.; Stowell, J. G. Helical Rosette Nanotubes: Design, Self-Assembly, and Characterization. *J. Am. Chem. Soc.* **2001**, *123* (16), 3854–3855. https://doi.org/10.1021/ja005886l.

(88) Beingessner, R. L.; Fan, Y.; Fenniri, H. Molecular and Supramolecular Chemistry of Rosette Nanotubes. *RSC Adv.* **2016**, *6* (79), 75820–75838. https://doi.org/10.1039/C6RA16315G.

(89) Fenniri, H.; Deng, B.-L.; Ribbe, A. E. Helical Rosette Nanotubes with Tunable Chiroptical Properties. *J. Am. Chem. Soc.* **2002**, *124* (37), 11064–11072. https://doi.org/10.1021/ja026164s.

(90) Yagai, S.; Kitamoto, Y.; Datta, S.; Adhikari, B. Supramolecular Polymers Capable of Controlling Their Topology. *Acc. Chem. Res.* **2019**, *52* (5), 1325–1335. https://doi.org/10.1021/acs.accounts.8b00660.

(91) Kitamoto, Y.; Pan, Z.; Prabhu, D. D.; Isobe, A.; Ohba, T.; Shimizu, N.; Takagi, H.; Haruki, R.; Adachi, S.; Yagai, S. One-Shot Preparation of Topologically Chimeric Nanofibers via a Gradient Supramolecular Copolymerization. *Nat. Commun.* **2019**, *10*, 4578. https://doi.org/10.1038/s41467-019-12654-z.

(92) Asadi, A.; Patrick, B. O.; Perrin, D. M. G^C Quartet — A DNA-Inspired Janus-GC Heterocycle: Synthesis, Structural Analysis, and Self-Organization. *J. Am. Chem. Soc.* **2008**, *130* (39), 12860–12861. https://doi.org/10.1021/ja8047128.

(93) Yang, Y.; Xue, M.; Marshall, L. J.; de Mendoza, J. Hydrogen-Bonded Cyclic Tetramers Based on Ureidopyrimidinones Attached to a 3,6-Carbazolyl Spacer. *Org. Lett.* **2011**, *13* (12), 3186–3189. https://doi.org/10.1021/ol200946b.

(94) Montoro-García, C.; Camacho-García, J.; López-Pérez, A. M.; Bilbao, N.; Romero-Pérez, S.; Mayoral, M. J.; González-Rodríguez, D. High-Fidelity Noncovalent Synthesis of Hydrogen-Bonded Macrocyclic Assemblies. *Angew. Chem. Int. Ed.* **2015**, *54* (23), 6780–6784. https://doi.org/10.1002/anie.201501321.

(95) Montoro-García, C.; Camacho-García, J.; López-Pérez, A. M.; Mayoral, M. J.; Bilbao, N.; González-Rodríguez, D. Role of the Symmetry of Multipoint Hydrogen Bonding on Chelate Cooperativity in Supramolecular Macrocyclization Processes. *Angew. Chem. Int. Ed.* **2016**, *55* (1), 223–227. https://doi.org/10.1002/anie.201508854.

(96) Romero-Pérez, S.; Camacho-García, J.; Montoro-García, C.; López-Pérez, A. M.; Sanz, A.; Mayoral, M. J.; González-Rodríguez, D. G-Arylated Hydrogen-Bonded Cyclic Tetramer Assemblies with Remarkable Thermodynamic and Kinetic Stability. *Org. Lett.* **2015**, *17* (11), 2664–2667. https://doi.org/10.1021/acs.orglett.5b01042.

(97) Wyler, R.; de Mendoza, J.; Rebek, J. A Synthetic Cavity Assembles Through Self-Complementary Hydrogen Bonds. *Angew. Chem. Int. Ed. Engl.* **1993**, *32* (12), 1699–1701. https://doi.org/10.1002/anie.199316991.

(98) Meissner, R. S.; Rebek, J.; de Mendoza, J. Autoencapsulation Through Intermolecular Forces: A Synthetic Self-Assembling Spherical Complex. *Science* **1995**, *270* (5241), 1485–1488. https://doi.org/10.1126/science.270.5241.1485.

(99) Heinz, T.; Rudkevich, D. M.; Rebek, J. Pairwise Selection of Guests in a Cylindrical Molecular Capsule of Nanometre Dimensions. *Nature* **1998**, *394* (6695), 764–766. https://doi.org/10.1038/29501.

(100) Barrett, E. S.; Dale, T. J.; Rebek, J. Stability, Dynamics, and Selectivity in the Assembly of Hydrogen-Bonded Hexameric Capsules. *J. Am. Chem. Soc.* **2008**, *130* (7), 2344–2350. https://doi.org/10.1021/ja078009p.

(101) Avram, L.; Cohen, Y.; Rebek Jr., J. Recent Advances in Hydrogen-Bonded Hexameric Encapsulation Complexes. *Chem. Commun.* **2011**, *47* (19), 5368–5375. https://doi.org/10.1039/C1CC10150A.

(102) Beaudoin, D.; Rominger, F.; Mastalerz, M. Chirality-Assisted Synthesis of a Very Large Octameric Hydrogen-Bonded Capsule. *Angew. Chem. Int. Ed.* **2016**, *55* (50), 15599–15603. https://doi.org/10.1002/anie.201609073.

(103) Merget, S.; Catti, L.; Zev, S.; Major, D. T.; Trapp, N.; Tiefenbacher, K. Concentration-Dependent Self-Assembly of an Unusually Large Hexameric Hydrogen-Bonded Molecular Cage. *Chem. Eur. J.* **2021**, *27* (13), 4447–4453. https://doi.org/10.1002/chem.202005046.

(104) Nelson, J. C.; Saven, J. G.; Moore, J. S.; Wolynes, P. G. Solvophobically Driven Folding of Nonbiological Oligomers. *Science* **1997**, *277* (5333), 1793–1796. https://doi.org/10.1126/science.277.5333.1793.

(105) Prince, R. B.; Barnes, S. A.; Moore, J. S. Foldamer-Based Molecular Recognition. *J. Am. Chem. Soc.* **2000**, *122* (12), 2758–2762. https://doi.org/10.1021/ja993830p.

(106) Ronan, D.; Jeannerat, D.; Pinto, A.; Sakai, N.; Matile, S. New Staves for Old Barrels: Regioisomeric $(1^2,2^2,3^3,4^2,5^3,6^2,7^3,8^2)$-p-Octiphenyl Rods with an NMR Tag. *New J Chem* **2006**, *30* (2), 168–176. https://doi.org/10.1039/B512276G.

(107) Ghadiri, M. R.; Granja, J. R.; Milligan, R. A.; McRee, D. E.; Khazanovich, N. Self-Assembling Organic Nanotubes Based on a Cyclic Peptide Architecture. *Nature* **1993**, *366* (6453), 324–327. https://doi.org/10.1038/366324a0.

(108) Appella, D. H.; Christianson, L. A.; Karle, I. L.; Powell, D. R.; Gellman, S. H. β-Peptide Foldamers: Robust Helix Formation in

a New Family of β-Amino Acid Oligomers. *J. Am. Chem. Soc.* **1996**, *118* (51), 13071–13072. https://doi.org/10.1021/ja963290l.

(109) Gellman, S. H. Foldamers: A Manifesto. *Acc. Chem. Res.* **1998**, *31* (4), 173–180. https://doi.org/10.1021/ar960298r.

(110) Appella, D. H.; Christianson, L. A.; Klein, D. A.; Powell, D. R.; Huang, X.; Barchi, J. J.; Gellman, S. H. Residue-Based Control of Helix Shape in β-Peptide Oligomers. *Nature* **1997**, *387* (6631), 381–384. https://doi.org/10.1038/387381a0.

(111) Rodríguez-Vázquez, N.; García-Fandiño, R.; Amorín, M.; Granja, J. R. Self-Assembling α,γ-Cyclic Peptides That Generate Cavities with Tunable Properties. *Chem. Sci.* **2016**, *7* (1), 183–187. https://doi.org/10.1039/C5SC03187G.

(112) Horne, W. S.; Ashkenasy, N.; Ghadiri, M. R. Modulating Charge Transfer through CyclicD,L-α-Peptide Self-Assembly. *Chem. Eur. J.* **2005**, *11* (4), 1137–1144. https://doi.org/10.1002/chem.200400923.

(113) Ashkenasy, N.; Horne, W. S.; Ghadiri, M. R. Design of Self-Assembling Peptide Nanotubes with Delocalized Electronic States. *Small* **2006**, *2* (1), 99–102. https://doi.org/10.1002/smll.200500252.

(114) Insua, I.; Montenegro, J. 1D to 2D Self Assembly of Cyclic Peptides. *J. Am. Chem. Soc.* **2020**, *142* (1), 300–307. https://doi.org/10.1021/jacs.9b10582.

(115) Pantoş, G. D.; Pengo, P.; Sanders, J. K. M. Hydrogen-Bonded Helical Organic Nanotubes. *Angew. Chem. Int. Ed.* **2007**, *46* (1–2), 194–197. https://doi.org/10.1002/anie.200603348.

(116) Ponnuswamy, N.; Pantoş, G. D.; Smulders, M. M. J.; Sanders, J. K. M. Thermodynamics of Supramolecular Naphthalenediimide Nanotube Formation: The Influence of Solvents, Side Chains, and Guest Templates. *J. Am. Chem. Soc.* **2012**, *134* (1), 566–573. https://doi.org/10.1021/ja2088647.

(117) Pantoş, G. D.; Wietor, J.-L.; Sanders, J. K. M. Filling Helical Nanotubes with C_{60}. *Angew. Chem. Int. Ed.* **2007**, *46* (13), 2238–2240. https://doi.org/10.1002/anie.200604891.

(118) Vázquez-González, V.; Mayoral, M. J.; Chamorro, R.; Hendrix, M. M. R. M.; Voets, I. K.; González-Rodríguez, D. Noncovalent Synthesis of Self-Assembled Nanotubes through Decoupled Hierarchical Cooperative Processes. *J. Am. Chem. Soc.* **2019**, *141* (41), 16432–16438. https://doi.org/10.1021/jacs.9b07868.

(119) Vázquez-González, V.; Mayoral, M. J.; Aparicio, F.; Martínez-Arjona, P.; González-Rodríguez, D. The Role of

Peripheral Amide Groups as Hydrogen-Bonding Directors in the Tubular Self-Assembly of Dinucleobase Monomers. *ChemPlusChem* **2021**, *86* (8), 1087–1096. https://doi.org/10.1002/cplu.202100255.

(120) Yagai, S.; Yamauchi, M.; Kobayashi, A.; Karatsu, T.; Kitamura, A.; Ohba, T.; Kikkawa, Y. Control over Hierarchy Levels in the Self-Assembly of Stackable Nanotoroids. *J. Am. Chem. Soc.* **2012**, *134* (44), 18205–18208. https://doi.org/10.1021/ja308519b.

(121) Orentas, E.; Wallentin, C.-J.; Bergquist, K.-E.; Lund, M.; Butkus, E.; Wärnmark, K. Topology Selection and Tautoleptic Aggregation: Formation of an Enantiomerically Pure Supramolecular Belt over a Helix. *Angew. Chem. Int. Ed.* **2011**, *50* (9), 2071–2074. https://doi.org/10.1002/anie.201002665.

(122) Račkauskaitė, D.; Bergquist, K.-E.; Shi, Q.; Sundin, A.; Butkus, E.; Wärnmark, K.; Orentas, E. A Remarkably Complex Supramolecular Hydrogen-Bonded Decameric Capsule Formed from an Enantiopure C_2-Symmetric Monomer by Solvent-Responsive Aggregation. *J. Am. Chem. Soc.* **2015**, *137* (33), 10536–10546. https://doi.org/10.1021/jacs.5b03160.

(123) Shi, Q.; Bergquist, K.-E.; Huo, R.; Li, J.; Lund, M.; Vácha, R.; Sundin, A.; Butkus, E.; Orentas, E.; Wärnmark, K. Composition- and Size-Controlled Cyclic Self-Assembly by Solvent- and C_{60}-Responsive Self-Sorting. *J. Am. Chem. Soc.* **2013**, *135* (40), 15263–15268. https://doi.org/10.1021/ja408582w.

(124) Račkauskaitė, D.; Gegevičius, R.; Matsuo, Y.; Wärnmark, K.; Orentas, E. An Enantiopure Hydrogen-Bonded Octameric Tube: Self-Sorting and Guest-Induced Rearrangement. *Angew. Chem. Int. Ed.* **2016**, *55*, 208–212. https://doi.org/10.1002/anie.201508362.

(125) Neniškis, A.; Račkauskaitė, D.; Shi, Q.; Robertson, A. J.; Marsh, A.; Ulčinas, A.; Valiokas, R.; Brown, S. P.; Wärnmark, K.; Orentas, E. A Tautoleptic Approach to Chiral Hydrogen-Bonded Supramolecular Tubular Polymers with Large Cavity. *Chem. Eur. J.* **2018**, *24* (53), 14028–14033. https://doi.org/10.1002/chem.201803701.

(126) Orentas, E. Design of Supramolecular Tubular Structures Based on Bicyclo[3.3.1]Nonane Framework. Doctoral dissertation, Vilnius University, 2009, 195p.

(127) Wallentin, C.; Orentas, E.; Butkus, E.; Wärnmark, K. Baker's Yeast for Sweet Dough Enables Large-Scale Synthesis of Enantiomerically Pure Bicyclo[3.3.1]Nonane-2,6-Dione.

Synthesis **2009**, *5*, 864–867. https://doi.org/10.1055/s-0028-1083364.

(128) Kade, M. J.; Burke, D. J.; Hawker, C. J. The Power of Thiol-Ene Chemistry: Highlight. *J. Polym. Sci. Part Polym. Chem.* **2010**, *48* (4), 743–750. https://doi.org/10.1002/pola.23824.

(129) Dondoni, A.; Massi, A.; Nanni, P.; Roda, A. A New Ligation Strategy for Peptide and Protein Glycosylation: Photoinduced Thiol-Ene Coupling. *Chem. Eur. J.* **2009**, *15* (43), 11444–11449. https://doi.org/10.1002/chem.200901746.

(130) Fiore, M.; Marra, A.; Dondoni, A. Photoinduced Thiol−Ene Coupling as a Click Ligation Tool for Thiodisaccharide Synthesis. *J. Org. Chem.* **2009**, *74* (11), 4422–4425. https://doi.org/10.1021/jo900514w.

(131) Motesharei, K.; Myles, D. C. Multistep Synthesis on the Surface of Self-Assembled Thiolate Monolayers on Gold: Probing the Mechanism of the Thiazolium-Promoted Acyloin Condensation. *J. Am. Chem. Soc.* **1997**, *119* (28), 6674–6675. https://doi.org/10.1021/ja970627q.

(132) Mahmud, I. M.; Zhou, N.; Wang, L.; Zhao, Y. Triazole-Linked Dendro[60]Fullerenes: Modular Synthesis via a 'Click' Reaction and Acidity-Dependent Self-Assembly on the Surface. *Tetrahedron* **2008**, *64* (50), 11420–11432. https://doi.org/10.1016/j.tet.2008.08.083.

(133) Tang, D.-H.; Fan, Q.-H. Convergent Synthesis of AB2-AB3 Hybrid-Type of Amphiphilic Oligoethyleneoxy-Modified Poly(Benzyl Ether) Dendrons. *J. Chem. Res.* **2003**, *11*, 698–699. https://doi.org/10.3184/030823403322862978.

(134) Kramer, J. R.; Deming, T. J. Multimodal Switching of Conformation and Solubility in Homocysteine Derived Polypeptides. *J. Am. Chem. Soc.* **2014**, *136* (15), 5547–5550. https://doi.org/10.1021/ja500372u.

(135) Timmerman, P.; Weidmann, J.-L.; Jolliffe, K. A.; Prins, L. J.; Reinhoudt, D. N.; Shinkai, S.; Frish, L.; Cohen, Y. NMR Diffusion Spectroscopy for the Characterization of Multicomponent Hydrogen-Bonded Assemblies in Solution. *J. Chem. Soc. Perkin Trans. 2* **2000**, 2077–2089. https://doi.org/10.1039/b003968n.

(136) Yamakoshi, Y.; Umezawa, N.; Ryu, A.; Arakane, K.; Miyata, N.; Goda, Y.; Masumizu, T.; Nagano, T. Active Oxygen Species Generated from Photoexcited Fullerene (C_{60}) as Potential Medicines: $O_2^{-\bullet}$ versus $^1O_2$. *J. Am. Chem. Soc.* **2003**, *125* (42), 12803–12809. https://doi.org/10.1021/ja0355574.

(137) Arbogast, J. W.; Foote, C. S.; Kao, M. Electron Transfer to Triplet Fullerene C60. *J. Am. Chem. Soc.* **1992**, *114* (6), 2277–2279. https://doi.org/10.1021/ja00032a063.

(138) Sermon, P. A., H., R. C. The Fullerenes: Powerful Carbon-Based Electron Acceptors. *Philos. Trans. R. Soc. Lond. Ser. Phys. Eng. Sci.* **1993**, *343* (1667), 53–62. https://doi.org/10.1098/rsta.1993.0040.

(139) Baciocchi, E.; Crescenzi, C.; Lanzalunga, O. Photoinduced Electron Transfer Reactions of Benzyl Phenyl Sulfides Promoted by 9,10-Dicyanoanthracene. *Tetrahedron* **1997**, *53* (12), 4469–4478. https://doi.org/10.1016/S0040-4020(97)00119-1.

(140) Clarke, A. K.; Parkin, A.; Taylor, R. J. K.; Unsworth, W. P.; Rossi-Ashton, J. A. Photocatalytic Deoxygenation of Sulfoxides Using Visible Light: Mechanistic Investigations and Synthetic Applications. *ACS Catal.* **2020**, *10*, 5814–5820. https://doi.org/10.1021/acscatal.0c00690.

(141) Ohkubo, K.; Nanjo, T.; Fukuzumi, S. Photocatalytic Electron-Transfer Oxidation of Triphenylphosphine and Benzylamine with Molecular Oxygen via Formation of Radical Cations and Superoxide Ion. *Bull. Chem. Soc. Jpn.* **2006**, *79* (10), 1489–1500. https://doi.org/10.1246/bcsj.79.1489.

(142) Yasui, S.; Tojo, S.; Majima, T. Reaction of Triarylphosphine Radical Cations Generated from Photoinduced Electron Transfer in the Presence of Oxygen. *J. Org. Chem.* **2005**, *70* (4), 1276–1280. https://doi.org/10.1021/jo049032l.

(143) Lang, X.; Chen, X.; Zhao, J. Heterogeneous Visible Light Photocatalysis for Selective Organic Transformations. *Chem Soc Rev* **2014**, *43* (1), 473–486. https://doi.org/10.1039/C3CS60188A.

(144) Jia, J.-G.; Zheng, L.-M. Metal-Organic Nanotubes: Designs, Structures and Functions. *Coord. Chem. Rev.* **2020**, *403*, 213083. https://doi.org/10.1016/j.ccr.2019.213083.

(145) Romero, N. A.; Nicewicz, D. A. Organic Photoredox Catalysis. *Chem. Rev.* **2016**, *116* (17), 10075–10166. https://doi.org/10.1021/acs.chemrev.6b00057.

(146) Mizuno, N.; Misono, M. Heterogeneous Catalysis. *Chem. Rev.* **1998**, *98* (1), 199–218. https://doi.org/10.1021/cr960401q.

(147) Zheng, D.-Y.; Chen, E.-X.; Ye, C.-R.; Huang, X.-C. High-Efficiency Photo-Oxidation of Thioethers over C_{60}@PCN-222 under Air. *J. Mater. Chem. A* **2019**, *7* (38), 22084–22091. https://doi.org/10.1039/C9TA07965C.

(148) Casado-Sánchez, A.; Gómez-Ballesteros, R.; Tato, F.; Soriano, F. J.; Pascual-Coca, G.; Cabrera, S.; Alemán, J. Pt(II) Coordination Complexes as Visible Light Photocatalysts for the Oxidation of Sulfides Using Batch and Flow Processes. *Chem. Commun.* **2016**, *52* (58), 9137–9140. https://doi.org/10.1039/C6CC02452A.

(149) Gao, Y.; Xu, H.; Zhang, S.; Zhang, Y.; Tang, C.; Fan, W. Visible-Light Photocatalytic Aerobic Oxidation of Sulfides to Sulfoxides with a Perylene Diimide Photocatalyst. *Org. Biomol. Chem.* **2019**, *17* (30), 7144–7149. https://doi.org/10.1039/C9OB00945K.

(150) Zen, J.-M.; Liou, S.-L.; Kumar, A. S.; Hsia, M.-S. An Efficient and Selective Photocatalytic System for the Oxidation of Sulfides to Sulfoxides. *Angew. Chem.* **2003**, *115* (5), 597–599. https://doi.org/10.1002/ange.200390134.

(151) Lang, X.; Zhao, J.; Chen, X. Visible-Light-Induced Photoredox Catalysis of Dye-Sensitized Titanium Dioxide: Selective Aerobic Oxidation of Organic Sulfides. *Angew. Chem. Int. Ed.* **2016**, *55* (15), 4697–4700. https://doi.org/10.1002/anie.201600405.

(152) Jiang, J.; Luo, R.; Zhou, X.; Chen, Y.; Ji, H. Photocatalytic Properties and Mechanistic Insights into Visible Light-Promoted Aerobic Oxidation of Sulfides to Sulfoxides via Tin Porphyrin-Based Porous Aromatic Frameworks. *Adv. Synth. Catal.* **2018**, *360* (22), 4402–4411. https://doi.org/10.1002/adsc.201800730.

(153) Gu, X.; Li, X.; Chai, Y.; Yang, Q.; Li, P.; Yao, Y. A Simple Metal-Free Catalytic Sulfoxidation under Visible Light and Air. *Green Chem.* **2013**, *15* (2), 357–361. https://doi.org/10.1039/c2gc36683e.

(154) Sridhar, A.; Rangasamy, R.; Selvaraj, M. Polymer-Supported Eosin Y as a Reusable Photocatalyst for Visible Light Mediated Organic Transformations. *New J. Chem.* **2019**, *43* (46), 17974–17979. https://doi.org/10.1039/C9NJ04064A.

(155) Li, W.; Xie, Z.; Jing, X. BODIPY Photocatalyzed Oxidation of Thioanisole under Visible Light. *Catal. Commun.* **2011**, *16* (1), 94–97. https://doi.org/10.1016/j.catcom.2011.09.007.

(156) Takaguchi, Y.; Yanagimoto, Y.; Fujima, S.; Tsuboi, S. Photooxygenation of Olefins, Phenol, and Sulfide Using Fullerodendrimer as Catalyst. *Chem. Lett.* **2004**, *33* (9), 1142–1143. https://doi.org/10.1246/cl.2004.1142.

(157) Hungerbuehler, H.; Guldi, D. M.; Asmus, K. D. Incorporation of C_{60} into Artificial Lipid Membranes. *J. Am. Chem. Soc.* **1993**, *115* (8), 3386–3387. https://doi.org/10.1021/ja00061a070.

(158) Moor, K. J.; Kim, J.-H. Simple Synthetic Method Toward Solid Supported C_{60} Visible Light-Activated Photocatalysts. *Environ. Sci. Technol.* **2014**, *48* (5), 2785–2791. https://doi.org/10.1021/es405283w.

(159) Alargova, R. G.; Deguchi, S.; Tsujii, K. Stable Colloidal Dispersions of Fullerenes in Polar Organic Solvents. *J. Am. Chem. Soc.* **2001**, *123* (43), 10460–10467. https://doi.org/10.1021/ja010202a.

(160) Jozeliūnaitė, A.; Valčeckas, D.; Orentas, E. Fullerene Soot and a Fullerene Nanodispersion as Recyclable Heterogeneous Off-the-Shelf Photocatalysts. *RSC Adv.* **2021**, *11* (7), 4104–4111. https://doi.org/10.1039/D0RA10147H.

(161) Keypour, H.; Noroozi, M.; Rashidi, A. An Improved Method for the Purification of Fullerene from Fullerene Soot with Activated Carbon, Celite, and Silica Gel Stationary Phases. *J. Nanostructure Chem.* **2013**, *3* (1), 45. https://doi.org/10.1186/2193-8865-3-45.

(162) Liang, J. J.; Gu, C. L.; Kacher, M. L.; Foote, C. S. Chemistry of Singlet Oxygen. 45. Mechanism of the Photooxidation of Sulfides. *J. Am. Chem. Soc.* **1983**, *105* (14), 4717–4721. https://doi.org/10.1021/ja00352a033.

(163) Jensen, F.; Greer, A.; Clennan, E. L. Reaction of Organic Sulfides with Singlet Oxygen. A Revised Mechanism. *J. Am. Chem. Soc.* **1998**, *120* (18), 4439–4449. https://doi.org/10.1021/ja973782d.

(164) Bonesi, S. M.; Albini, A. Effect of Protic Cosolvents on the Photooxygenation of Diethyl Sulfide. *J. Org. Chem.* **2000**, *65* (15), 4532–4536. https://doi.org/10.1021/jo000069p.

(165) Bonesi, S. M.; Fagnoni, M.; Albini, A. Photosensitized Electron Transfer Oxidation of Sulfides: A Steady-State Study. *Eur. J. Org. Chem.* **2008**, 2612–2620. https://doi.org/10.1002/ejoc.200800048.

(166) Bonesi, S. M.; Manet, I.; Freccero, M.; Fagnoni, M.; Albini, A. Photosensitized Oxidation of Sulfides: Discriminating between the Singlet-Oxygen Mechanism and Electron Transfer Involving Superoxide Anion or Molecular Oxygen. *Chem. Eur. J.* **2006**, *12*, 4844–4857. https://doi.org/10.1002/chem.200501144.

(167) Arbogast, J. W.; Darmanyan, A. P.; Foote, C. S.; Diederich, F. N.; Whetten, R. L.; Rubin, Y.; Alvarez, M. M.; Anz, S. J. Photophysical Properties of Sixty Atom Carbon Molecule (C_{60}). *J. Phys. Chem.* **1991**, *95* (1), 11–12. https://doi.org/10.1021/j100154a006.

(168) Nahm, K.; Foote, C. S. Trimethyl Phosphite Traps Intermediates in the Reaction of Singlet Oxygen ($^1O_2$) and Diethyl Sulfide. *J. Am. Chem. Soc.* **1989**, *111* (5), 1909–1910. https://doi.org/10.1021/ja00187a071.

(169) Akasaka, T.; Sakurai, A.; Ando, W. Cooxidation Reaction in the Singlet Oxygenation of Cyclic and Benzylic Sulfides: S-Hydroperoxysulfonium Ylide Intermediate as a New Epoxidizing Species. *J. Am. Chem. Soc.* **1991**, *113* (7), 2696–2701. https://doi.org/10.1021/ja00007a051.

(170) Baciocchi, E.; Giacco, T. D.; Elisei, F.; Gerini, M. F.; Guerra, M.; Lapi, A.; Liberali, P. Electron Transfer and Singlet Oxygen Mechanisms in the Photooxygenation of Dibutyl Sulfide and Thioanisole in MeCN Sensitized by *N*-Methylquinolinium Tetrafluoborate and 9,10-Dicyanoanthracene. The Probable Involvement of a Thiadioxirane Intermediate in Electron Transfer Photooxygenations. *J. Am. Chem. Soc.* **2003**, *125* (52), 16444–16454. https://doi.org/10.1021/ja037591o.

(171) Baciocchi, E.; Del Giacco, T.; Lanzalunga, O.; Lapi, A. Singlet Oxygen Promoted Carbon−Heteroatom Bond Cleavage in Dibenzyl Sulfides and Tertiary Dibenzylamines. Structural Effects and the Role of Exciplexes. *J. Org. Chem.* **2007**, *72* (25), 9582–9589. https://doi.org/10.1021/jo701641b.

(172) Murahashi, S.-I.; Zhang, D.; Iida, H.; Miyawaki, T.; Uenaka, M.; Murano, K.; Meguro, K. Flavin-Catalyzed Aerobic Oxidation of Sulfides and Thiols with Formic Acid/Triethylamine. *Chem Commun* **2014**, *50* (71), 10295–10298. https://doi.org/10.1039/C4CC05216A.

(173) Zou, M.; Feng, L.; Thomas, T.; Yang, M. Amine Coupled Ordered Mesoporous (Co–N) Co-Doped TiO_2 : A Green Photocatalyst for the Selective Aerobic Oxidation of Thioether. *Catal. Sci. Technol.* **2017**, *7*, 4182–4192. https://doi.org/10.1039/C7CY00946A.

(174) Mittal, J. P. Excited States and Electron Transfer Reactions of Fullerenes. *Pure Appl. Chem.* **1995**, *67* (1), 103–110. https://doi.org/10.1351/pac199567010103.

(175) Sun, Y.-P.; Ma, B.; Lawson, G. E. Electron Donor-Acceptor Interactions of Fullerenes C_{60} and C_{70} with Triethylamine. *Chem. Phys. Lett.* **1995**, 233, 75–62. https://doi.org/10.1016/0009-2614(94)01436-Y.

(176) Liang, Z.; Xu, S.; Tian, W.; Zhang, R. Eosin Y-Catalyzed Visible-Light-Mediated Aerobic Oxidative Cyclization of *N* , *N* -

Dimethylanilines with Maleimides. *Beilstein J. Org. Chem.* **2015**, *11*, 425–430. https://doi.org/10.3762/bjoc.11.48.

(177) Ju, X.; Li, D.; Li, W.; Yu, W.; Bian, F. The Reaction of Tertiary Anilines with Maleimides under Visible Light Redox Catalysis. *Adv. Synth. Catal.* **2012**, *354* (18), 3561–3567. https://doi.org/10.1002/adsc.201200608.

(178) Kumar, R.; Gleißner, E. H.; Tiu, E. G. V.; Yamakoshi, Y. C_{70} as a Photocatalyst for Oxidation of Secondary Benzylamines to Imines. *Org. Lett.* **2016**, *18* (2), 184–187. https://doi.org/10.1021/acs.orglett.5b03194.

(179) Stanek, F.; Pawlowski, R.; Morawska, P.; Bujok, R.; Stodulski, M. Dehydrogenation and α-Functionalization of Secondary Amines by Visible-Light-Mediated Catalysis. *Org. Biomol. Chem.* **2020**, *18* (11), 2103–2112. https://doi.org/10.1039/C9OB02699A.

(180) Suzuki, K.; Tang, F.; Kikukawa, Y.; Yamaguchi, K.; Mizuno, N. Visible-Light-Induced Photoredox Catalysis with a Tetracerium-Containing Silicotungstate. *Angew. Chem. Int. Ed.* **2014**, *53* (21), 5356–5360. https://doi.org/10.1002/anie.201403215.

(181) Kumar, P.; Varma, S.; Jain, S. L. A TiO_2 Immobilized Ru(II) Polyazine Complex: A Visible-Light Active Photoredox Catalyst for Oxidative Cyanation of Tertiary Amines. *J. Mater. Chem. A* **2014**, *2* (13), 4514. https://doi.org/10.1039/c3ta14783e.

(182) Ide, T.; Shimizu, K.; Egami, H.; Hamashima, Y. Redox-Neutral C–H Cyanation of Tetrahydroisoquinolines under Photoredox Catalysis. *Tetrahedron Lett.* **2018**, *59* (34), 3258–3261. https://doi.org/10.1016/j.tetlet.2018.07.030.

(183) Kumar, I.; Sharma, R.; Kumar, R.; Kumar, R.; Sharma, U. C_{70} Fullerene-Catalyzed Metal-Free Photocatalytic *Ipso*-Hydroxylation of Aryl Boronic Acids: Synthesis of Phenols. *Adv. Synth. Catal.* **2018**, *360* (10), 2013–2019. https://doi.org/10.1002/adsc.201701573.

(184) Huang, L.; Cui, X.; Therrien, B.; Zhao, J. Energy-Funneling-Based Broadband Visible-Light-Absorbing Bodipy–C_{60} Triads and Tetrads as Dual Functional Heavy-Atom-Free Organic Triplet Photosensitizers for Photocatalytic Organic Reactions. *Chem. Eur. J.* **2013**, *19* (51), 17472–17482. https://doi.org/10.1002/chem.201302492.

(185) Colomer, J. P.; Traverssi, M.; Oksdath-Mansilla, G. Oxidation of Organosulfur Compounds Promoted by Continuous-Flow

Chemistry. *J. Flow Chem.* **2020**, *10* (1), 123–138. https://doi.org/10.1007/s41981-019-00066-5.

(186) Bottecchia, C.; Erdmann, N.; Tijssen, P. M. A.; Milroy, L.-G.; Brunsveld, L.; Hessel, V.; Noël, T. Batch and Flow Synthesis of Disulfides by Visible-Light-Induced TiO_2 Photocatalysis. *ChemSusChem* **2016**, *9* (14), 1781–1785. https://doi.org/10.1002/cssc.201600602.

(187) Boehr, D. D.; Nussinov, R.; Wright, P. E. The Role of Dynamic Conformational Ensembles in Biomolecular Recognition. *Nat. Chem. Biol.* **2009**, *5* (11), 789–796. https://doi.org/10.1038/nchembio.232.

(188) Iglesias, B. A.; Hörner, M.; Toma, H. E.; Araki, K. 5-(1-(4-Phenyl)-3-(4-Nitrophenyl)Triazene)-10,15,20-Triphenylporphyrin: A New Triazene-Porphyrin Dye and Its Spectroelectrochemical Properties. *J. Porphyr. Phthalocyanines* **2012**, *16* (02), 200–209. https://doi.org/10.1142/S1088424612004501.

(189) Mao, B.; Hodges, B.; Franklin, C.; Calatayud, D. G. Self-Assembled Materials Incorporating Functional Porphyrins and Carbon Nanoplatforms as Building Blocks for Photovoltaic Energy Applications. *Front. Chem.* **2021**, *9*, 36, 727574. https://doi.org/10.3389/fchem.2021.727574.

(190) Wang, X.; Wang, P.; Xue, S.; Zheng, X.; Xie, Z.; Chen, G.; Sun, T. Nanoparticles Based on Glycyrrhetinic Acid Modified Porphyrin for Photodynamic Therapy of Cancer. *Org. Biomol. Chem.* **2018**, *16* (9), 1591–1597. https://doi.org/10.1039/C7OB03108D.

(191) Park, J. M.; Hong, K.-I.; Lee, H.; Jang, W.-D. Bioinspired Applications of Porphyrin Derivatives. *Acc. Chem. Res.* **2021**, *54* (9), 2249–2260. https://doi.org/10.1021/acs.accounts.1c00114.

(192) Alemohammad, T.; Rayati, S.; Safari, N. Highly Selective and Efficient Oxidation of Sulfide to Sulfoxide Catalyzed by Platinum Porphyrins. *J. Porphyr. Phthalocyanines* **2015**, *19* (12), 1279–1283. https://doi.org/10.1142/S1088424615501126.

(193) Lu, H.; Kobayashi, N. Optically Active Porphyrin and Phthalocyanine Systems. *Chem. Rev.* **2016**, *116* (10), 6184–6261. https://doi.org/10.1021/acs.chemrev.5b00588.

(194) Gust, D.; Moore, T. A. A Synthetic System Mimicking the Energy Transfer and Charge Separation of Natural Photosynthesis. *J. Photochem.* **1985**, *29* (1–2), 173–184. https://doi.org/10.1016/0047-2670(85)87069-6.

(195) El-Khouly, M. E.; Wijesinghe, C. A.; Nesterov, V. N.; Zandler, M. E.; Fukuzumi, S.; D'Souza, F. Ultrafast Photoinduced Energy and Electron Transfer in Multi-Modular Donor-Acceptor Conjugates. *Chem. Eur. J.* **2012**, *18* (43), 13844–13853. https://doi.org/10.1002/chem.201202265.

(196) Schuster, D. I.; Cheng, P.; Jarowski, P. D.; Guldi, D. M.; Luo, C.; Echegoyen, L.; Pyo, S.; Holzwarth, A. R.; Braslavsky, S. E.; Williams, R. M.; Klihm, G. Design, Synthesis, and Photophysical Studies of a Porphyrin-Fullerene Dyad with Parachute Topology; Charge Recombination in the Marcus Inverted Region. *J. Am. Chem. Soc.* **2004**, *126*, (23), 7257–7270. https://doi.org/10.1021/ja038676s.

(197) Hizume, Y.; Tashiro, K.; Charvet, R.; Yamamoto, Y.; Saeki, A.; Seki, S.; Aida, T. Chiroselective Assembly of a Chiral Porphyrin−Fullerene Dyad: Photoconductive Nanofiber with a Top-Class Ambipolar Charge-Carrier Mobility. *J. Am. Chem. Soc.* **2010**, *132*, (19), 6628–6629. https://doi.org/10.1021/ja1014713.

(198) Bourgeois, J.-P.; Diederich, F.; Echegoyen, L.; Nierengarten, J.-F. Synthesis, and Optical and Electrochemical Properties of Cyclophane-Type Molecular Dyads Containing a Porphyrin in Close, Tangential Orientation Relative to the Surface Oftrans-1 Functionalized C_{60}. Preliminary Communication. *Helv. Chim. Acta* **1998**, *81* (10), 1835–1844. https://doi.org/10.1002/(SICI)1522-2675(19981007)81:10<1835::AID-HLCA1835>3.0.CO;2-N.

(199) Galili, T.; Regev, A.; Levanon, H.; Schuster, D. I.; Guldi, D. M. Spin Dynamics of a "Parachute" Shaped Fullerene−Porphyrin Dyad. *J. Phys. Chem. A* **2004**, *108* (48), 10632–10639. https://doi.org/10.1021/jp0462310.

(200) D'Souza, F.; Maligaspe, E.; Karr, P. A.; Schumacher, A. L.; El Ojaimi, M.; Gros, C. P.; Barbe, J.-M.; Ohkubo, K.; Fukuzumi, S. Face-to-Face Pacman-Type Porphyrin–Fullerene Dyads: Design, Synthesis, Charge-Transfer Interactions, and Photophysical Studies. *Chem. Eur. J.* **2008**, *14* (2), 674–681. https://doi.org/10.1002/chem.200700936.

(201) D'Souza, F.; Chitta, R.; Gadde, S.; Zandler, M. E.; Sandanayaka, A. S. D.; Araki, Y.; Ito, O. Supramolecular Porphyrin–Fullerene via 'Two-Point' Binding Strategy: Axial-Coordination and Cation–Crown Ether Complexation. *Chem Commun*. **2005**, 1279–1281. https://doi.org/10.1039/B416736H.

(202) Sessler, J. L.; Jayawickramarajah, J.; Gouloumis, A.; Torres, T.; Guldi, D. M.; Maldonado, S.; Stevenson, K. J. Synthesis and Photophysics of a Porphyrin–Fullerene Dyad Assembled through Watson–Crick Hydrogen Bonding. *Chem Commun.* **2005**, *14*, 1892–1894. https://doi.org/10.1039/B418345B.

(203) Wessendorf, F.; Gnichwitz, J.-F.; Sarova, G. H.; Hager, K.; Hartnagel, U.; Guldi, D. M.; Hirsch, A. Implementation of a Hamiliton-Receptor-Based Hydrogen-Bonding Motif toward a New Electron Donor−Acceptor Prototype: Electron versus Energy Transfer. *J. Am. Chem. Soc.* **2007**, *129* (51), 16057–16071. https://doi.org/10.1021/ja075751g.

(204) Meng, W.; Breiner, B.; Rissanen, K.; Thoburn, J. D.; Clegg, J. K.; Nitschke, J. R. A Self-Assembled M_8L_6 Cubic Cage That Selectively Encapsulates Large Aromatic Guests. *Angew. Chem. Int. Ed.* **2011**, *50* (15), 3479–3483. https://doi.org/10.1002/anie.201100193.

(205) Wood, D. M.; Meng, W.; Ronson, T. K.; Stefankiewicz, A. R.; Sanders, J. K. M.; Nitschke, J. R. Guest-Induced Transformation of a Porphyrin-Edged $Fe^{II}_4L_6$ Capsule into a $Cu^IFe^{II}_2L_4$ Fullerene Receptor. *Angew. Chem. Int. Ed.* **2015**, *54* (13), 3988–3992. https://doi.org/10.1002/anie.201411985.

(206) Berova, N.; Bari, L. D.; Pescitelli, G. Application of Electronic Circular Dichroism in Configurational and Conformational Analysis of Organic Compounds. *Chem. Soc. Rev.* **2007**, *36* (6), 914–931. https://doi.org/10.1039/b515476f.

(207) Bieliūnas, V.; Račkauskaitė, D.; Orentas, E.; Stončius, S. Synthesis, Enantiomer Separation, and Absolute Configuration of 2,6-Oxygenated 9-Azabicyclo[3.3.1]Nonanes. *J. Org. Chem.* **2013**, *78* (11), 5339–5348. https://doi.org/10.1021/jo400506h.

(208) Lewis, S. E. Recent Advances in the Chemistry of Macroline, Sarpagine and Ajmaline-Related Indole Alkaloids. *Tetrahedron* **2006**, *62* (37), 8655–8681. https://doi.org/10.1016/j.tet.2006.06.017.

(209) Guo, X.; Facchetti, A.; Marks, T. J. Imide- and Amide-Functionalized Polymer Semiconductors. *Chem. Rev.* **2014**, *114* (18), 8943–9021. https://doi.org/10.1021/cr500225d.

(210) Janzen, D. E.; Burand, M. W.; Ewbank, P. C.; Pappenfus, T. M.; Higuchi, H.; da Silva Filho, D. A.; Young, V. G.; Brédas, J.-L.; Mann, K. R. Preparation and Characterization of π-Stacking Quinodimethane Oligothiophenes. Predicting Semiconductor Behavior and Bandwidths from Crystal Structures and Molecular

Orbital Calculations. *J. Am. Chem. Soc.* **2004**, *126* (46), 15295–15308. https://doi.org/10.1021/ja0484597.

(211) Nakano, T. Synthesis, Structure and Function of π-Stacked Polymers. *Polym. J.* **2010**, *42* (2), 103–123. https://doi.org/10.1038/pj.2009.332.

(212) Zaumseil, J.; Sirringhaus, H. Electron and Ambipolar Transport in Organic Field-Effect Transistors. *Chem. Rev.* **2007**, *107* (4), 1296–1323. https://doi.org/10.1021/cr0501543.

(213) Savoie, B. M.; Jackson, N. E.; Chen, L. X.; Marks, T. J.; Ratner, M. A. Mesoscopic Features of Charge Generation in Organic Semiconductors. *Acc. Chem. Res.* **2014**, *47* (11), 3385–3394. https://doi.org/10.1021/ar5000852.

(214) Kunugi, Y.; Takimiya, K.; Negishi, N.; Otsubo, T.; Aso, Y. An Ambipolar Organic Field-Effect Transistor Using Oligothiophene Incorporated with Two [60]Fullerenes. *J. Mater. Chem.* **2004**, *14*, 2840–2841. https://doi.org/10.1039/b412177e.

(215) Amriou, S.; Mehta, A.; Bryce, M. R. Functionalised 9-(1,3-Dithiol-2-Ylidene)Thioxanthene Derivatives: A C_{60} Conjugate as an Ambipolar Organic Field Effect Transistor (OFET). *J. Mater. Chem.* **2005**, *15*, 1232–1234. https://doi.org/10.1039/b500500k.

(216) Schmidt-Mende, L.; Fechtenkötter, A.; Müllen, K.; Moons, E.; Friend, R. H.; MacKenzie, J. D. Self-Organized Discotic Liquid Crystals for High-Efficiency Organic Photovoltaics. *Science* **2001**, *293* (5532), 1119–1122. https://doi.org/10.1126/science.293.5532.1119.

(217) Niyas, M. A.; Ramakrishnan, R.; Vijay, V.; Hariharan, M. Structure-Packing-Property Correlation of Self-Sorted Versus Interdigitated Assembly in TTF·TCNQ-Based Charge-Transport Materials. *Chem. Eur. J.* **2018**, *24* (47), 12318–12329. https://doi.org/10.1002/chem.201705537.

(218) Madhu, M.; Ramakrishnan, R.; Vijay, V.; Hariharan, M. Free Charge Carriers in Homo-Sorted π-Stacks of Donor–Acceptor Conjugates. *Chem. Rev.* **2021**, *121* (13), 8234–8284. https://doi.org/10.1021/acs.chemrev.1c00078.

(219) Li, W.-S.; Yamamoto, Y.; Fukushima, T.; Saeki, A.; Seki, S.; Tagawa, S.; Masunaga, H.; Sasaki, S.; Takata, M.; Aida, T. Amphiphilic Molecular Design as a Rational Strategy for Tailoring Bicontinuous Electron Donor and Acceptor Arrays: Photoconductive Liquid Crystalline Oligothiophene−C_{60} Dyads. *J. Am. Chem. Soc.* **2008**, *130* (28), 8886–8887. https://doi.org/10.1021/ja802757w.

(220) Yamamoto, Y.; Zhang, G.; Jin, W.; Fukushima, T.; Ishii, N.; Saeki, A.; Seki, S.; Tagawa, S.; Minari, T.; Tsukagoshi, K.; Aida, T. Ambipolar-Transporting Coaxial Nanotubes with a Tailored Molecular Graphene–Fullerene Heterojunction. *Proc. Natl. Acad. Sci.* **2009**, *106* (50), 21051–21056. https://doi.org/10.1073/pnas.0905655106.

(221) Sakai, N.; Bhosale, R.; Emery, D.; Mareda, J.; Matile, S. Supramolecular n/p-Heterojunction Photosystems with Antiparallel Redox Gradients in Electron- and Hole-Transporting Pathways. *J. Am. Chem. Soc.* **2010**, *132* (20), 6923–6925. https://doi.org/10.1021/ja101944r.

(222) Sisson, A. L.; Sakai, N.; Banerji, N.; Fürstenberg, A.; Vauthey, E.; Matile, S. Zipper Assembly of Vectorial Rigid-Rod π-Stack Architectures with Red and Blue Naphthalenediimides: Toward Supramolecular Cascade n/p-Heterojunctions. *Angew. Chem. Int. Ed.* **2008**, *47* (20), 3727–3729. https://doi.org/10.1002/anie.200800203.

(223) Hafner, R. J.; Görl, D.; Sienkiewicz, A.; Balog, S.; Frauenrath, H. Long-Lived Photocharges in Supramolecular Polymers of Low-Band-Gap Chromophores. *Chem. Eur. J.* **2020**, *26* (43), 9506–9517. https://doi.org/10.1002/chem.201904561.

(224) Wu, Y.-L.; Brown, K. E.; Wasielewski, M. R. Extending Photoinduced Charge Separation Lifetimes by Using Supramolecular Design: Guanine–Perylenediimide G-Quadruplex. *J. Am. Chem. Soc.* **2013**, *135* (36), 13322–13325. https://doi.org/10.1021/ja407648d.

(225) Feringán, B.; Romero, P.; Serrano, J. L.; Folcia, C. L.; Etxebarria, J.; Ortega, J.; Termine, R.; Golemme, A.; Giménez, R.; Sierra, T. H-Bonded Donor–Acceptor Units Segregated in Coaxial Columnar Assemblies: Toward High Mobility Ambipolar Organic Semiconductors. *J. Am. Chem. Soc.* **2016**, *138* (38), 12511–12518. https://doi.org/10.1021/jacs.6b06792.

(226) Bala, I.; De, J.; Gupta, S. P.; Pandey, U. K.; Pal, S. K. Enabling Efficient Ambipolar Charge Carrier Mobility in a H-Bonded Heptazine–Triphenylene System Forming Segregated Donor–Acceptor Columnar Assemblies. *J. Mater. Chem. C.* **2021**, *9* (27), 8552–8561. https://doi.org/10.1039/D1TC01898A.

(227) López-Andarias, J.; Rodriguez, M. J.; Atienza, C.; López, J. L.; Mikie, T.; Casado, S.; Seki, S.; Carrascosa, J. L.; Martín, N. Highly Ordered *n/p*-Co-Assembled Materials with Remarkable Charge Mobilities. *J. Am. Chem. Soc.* **2015**, *137* (2), 893–897. https://doi.org/10.1021/ja510946c.

(228) Michel, P.; Rassat, A. An Easy Access to 2,6-Dihydroxy-9-Azabicyclo[3.3.1]Nonane, a Versatile Synthon. *J. Org. Chem.* **2000**, *65* (8), 2572–2573. https://doi.org/10.1021/jo991333l.

(229) Beaujuge, P. M.; Fréchet, J. M. J. Molecular Design and Ordering Effects in π-Functional Materials for Transistor and Solar Cell Applications. *J. Am. Chem. Soc.* **2011**, *133* (50), 20009–20029. https://doi.org/10.1021/ja2073643.

(230) Takahashi, M.; Masui, K.; Sekiguchi, H.; Kobayashi, N.; Mori, A.; Funahashi, M.; Tamaoki, N. Palladium-Catalyzed C−H Homocoupling of Bromothiophene Derivatives and Synthetic Application to Well-Defined Oligothiophenes. *J. Am. Chem. Soc.* **2006**, *128* (33), 10930–10933. https://doi.org/10.1021/ja060749v.

(231) Kanato, H.; Takimiya, K.; Otsubo, T.; Aso, Y.; Nakamura, T.; Araki, Y.; Ito, O. Synthesis and Photophysical Properties of Ferrocene−Oligothiophene−Fullerene Triads. *J. Org. Chem.* **2004**, *69* (21), 7183–7189. https://doi.org/10.1021/jo049137o.

(232) Guo, K.; Yan, K.; Lu, X.; Qiu, Y.; Liu, Z.; Sun, J.; Yan, F.; Guo, W.; Yang, S. Dithiafulvenyl Unit as a New Donor for High-Efficiency Dye-Sensitized Solar Cells: Synthesis and Demonstration of a Family of Metal-Free Organic Sensitizers. *Org. Lett.* **2012**, *14* (9), 2214–2217. https://doi.org/10.1021/ol300477b.

(233) Arzehgar, Z.; Ahmadi, H. A Convenient One-Pot Method for the Synthesis of Symmetrical Dialkyl Trithiocarbonates Using NH$_4$OAc under Mild Neutral Conditions. *J. Chin. Chem. Soc.* **2019**, *66* (3), 303–306. https://doi.org/10.1002/jccs.201800062.

(234) O'Connor, B. R.; Jones, F. N. Reactions of Ethylene Di- and Trithiocarbonates with Acetylenes. Anomalous Reaction with Bromocyanoacetylene to Give a Thioacyl Bromide. *J. Org. Chem.* **1970**, *35* (6), 2002–2005. https://doi.org/10.1021/jo00831a062.

(235) Baffreau, J.; Dumur, F.; Hudhomme, P. New Versatile Building Block for the Construction of Tetrathiafulvalene-Based Donor−Acceptor Systems. *Org. Lett.* **2006**, *8* (7), 1307–1310. https://doi.org/10.1021/ol060011i.

(236) Otte, P.; Taubitz, J.; Lüning, U. Lipophilicity Enhancing Substituents for ADDA Recognition Domains of DAAD·ADDA Heterodimers with Quadruple Hydrogen Bonds: Lipophilic Substituents for DAAD·ADDA Heterodimers. *Eur. J. Org. Chem.* **2013**, *2013* (11), 2130–2139. https://doi.org/10.1002/ejoc.201201450.

(237) Felder, T.; de Greef, T. F. A.; Nieuwenhuizen, M. M. L.; Sijbesma, R. P. Alternation and Tunable Composition in Hydrogen Bonded Supramolecular Copolymers. *Chem Commun,* **2014**, *50* (19), 2455–2457. https://doi.org/10.1039/C3CC46611F.

(238) Coubrough, H. M.; van der Lubbe, S. C. C.; Hetherington, K.; Minard, A.; Pask, C.; Howard, M. J.; Fonseca Guerra, C.; Wilson, A. J. Supramolecular Self-Sorting Networks Using Hydrogen-Bonding Motifs. *Chem. Eur. J.* **2019**, *25* (3), 785–795. https://doi.org/10.1002/chem.201804791.

(239) Han, S.; Duan, H.; Chen, L.; Zhan, T.; Liu, L.; Kong, L.; Zhang, K. Photo-Controlled Macroscopic Self-Assembly Based on Photo-Switchable Hetero-Complementary Quadruple Hydrogen Bonds. *Chem. Asian J.* **2021**, *16*, 23, 3886–3889. https://doi.org/10.1002/asia.202101076.

(240) Chen, C. W.; Whitlock, H. W. Molecular Tweezers: A Simple Model of Bifunctional Intercalation. *J. Am. Chem. Soc.* **1978**, *100* (15), 4921–4922. https://doi.org/10.1021/ja00483a063.

(241) Shi, Q.; Javorskis, T.; Bergquist, K.-E.; Ulčinas, A.; Niaura, G.; Matulaitienė, I.; Orentas, E.; Wärnmark, K. Stimuli-Controlled Self-Assembly of Diverse Tubular Aggregates from One Single Small Monomer. *Nat. Commun.* **2017**, *8* (1), 14943. https://doi.org/10.1038/ncomms14943.

(242) Jozeliūnaitė, A.; Javorskis, T.; Vaitkevičius, V.; Klimavičius, V.; Orentas, E. Fully Supramolecular Chiral Hydrogen-Bonded Molecular Tweezer. *J. Am. Chem. Soc.* **2022**, *144* (18), 8231–8241. https://doi.org/10.1021/jacs.2c01455.

(243) Li, Y.; Park, T.; Quansah, J. K.; Zimmerman, S. C. Synthesis of a Redox-Responsive Quadruple Hydrogen-Bonding Unit for Applications in Supramolecular Chemistry. *J. Am. Chem. Soc.* **2011**, *133* (43), 17118–17121. https://doi.org/10.1021/ja2069278.

(244) Liao, Y. Design and Applications of Metastable-State Photoacids. *Acc. Chem. Res.* **2017**, *50* (8), 1956–1964. https://doi.org/10.1021/acs.accounts.7b00190.

(245) Garoni, E.; Nisic, F.; Colombo, A.; Fantacci, S.; Griffini, G.; Kamada, K.; Roberto, D.; Dragonetti, C. Perylenetetracarboxy-3,4:9,10-Diimide Derivatives with Large Two-Photon Absorption Activity. *New J. Chem.* **2019**, *43* (4), 1885–1893. https://doi.org/10.1039/C8NJ03216E.

(246) Liu, B.; Wu, B.; Xu, J.; Wu, Z.; Zhao, Y.; Zheng, X.; Wang, H. Resonance Raman Intensity Analysisof the Excited-State Photochemical Dynamicsof Dimethyl 1,3-Dithiole-2-Thione-4,5-

Dicarboxylate in the A-Band Absorption. *J. Raman Spectrosc.* **2010**, *41* (10), 1185–1193. https://doi.org/10.1002/jrs.2580.

(247) Sun, Y.; Huang, Q.; Zhang, X.; Ding, X.; Han, P.; Lin, B.; Yang, H.; Guo, L. Functionalization of Side Chain Terminals with Fused Aromatic Rings in Carbazole–Diketopyrrolopyrrole Based Conjugated Polymers for Improved Charge Transport Properties. *RSC Adv.* **2016**, *6* (100), 97783–97790. https://doi.org/10.1039/C6RA19914C.

(248) Guo, S.; Kumar, P. S.; Yang, M. Recent Advances of Oxidative Radical Cross-Coupling Reactions: Direct α-C(Sp^3)-H Bond Functionalization of Ethers and Alcohols. *Adv. Synth. Catal.* **2017**, *359* (1), 2–25. https://doi.org/10.1002/adsc.201600467.

(249) Biermann, U.; Metzger, J. O. Regioselectivity of Radical Addition of Thiols to 1-Alkenes: Regioselectivity of Radical Addition of Thiols to 1-Alkenes. *Eur. J. Org. Chem.* **2018**, 730–734. https://doi.org/10.1002/ejoc.201701692.

(250) Ruwwe, J.; Martín-Alvarez, J. M.; Horn, C. R.; Bauer, E. B.; Szafert, S.; Lis, T.; Hampel, F.; Cagle, P. C.; Gladysz, J. A. Olefin Metatheses in Metal Coordination Spheres: Versatile New Strategies for the Construction of Novel Monohapto or Polyhapto Cyclic, Macrocyclic, Polymacrocyclic, and Bridging Ligands. *Chem. Eur. J.* **2001**, *7* (18), 3931–3950. https://doi.org/10.1002/1521-3765(20010917)7:18<3931::AID-CHEM3931>3.0.CO;2-Y.

(251) Wang, X.; Xue, Z.; Ma, Y.; Yang, F. Facile Synthesis of 3-Benzylsulfinyl- and 3-Benzylsulfonyl-7-Diethylaminocoumarins. *J. Chem. Res.* **2014**, *38* (8), 493–495. https://doi.org/10.3184/174751914X14054403315001.

(252) Hussain, S.; Bharadwaj, S. K.; Chaudhuri, M. K.; Kalita, H. Borax as an Efficient Metal-Free Catalyst for Hetero-Michael Reactions in an Aqueous Medium. *Eur. J. Org. Chem.* **2007**, 374–378. https://doi.org/10.1002/ejoc.200600691.

(253) Göschke, R.; Stutz, S.; Rasetti, V.; Cohen, N.-C.; Rahuel, J.; Rigollier, P.; Baum, H.-P.; Forgiarini, P.; Schnell, C. R.; Wagner, T.; Gruetter, M. G.; Fuhrer, W.; Schilling, W.; Cumin, F.; Wood, J. M.; Maibaum, J. Novel 2,7-Dialkyl-Substituted 5(*S*)-Amino-4(*S*)-Hydroxy-8-Phenyl-Octanecarboxamide Transition State Peptidomimetics Are Potent and Orally Active Inhibitors of Human Renin. *J. Med. Chem.* **2007**, *50* (20), 4818–4831. https://doi.org/10.1021/jm070314y.

(254) Guerrero-Corella, A.; María Martinez-Gualda, A.; Ahmadi, F.; Ming, E.; Fraile, A.; Alemán, J. Thiol–Ene/Oxidation Tandem Reaction under Visible Light Photocatalysis: Synthesis of Alkyl Sulfoxides. *Chem. Commun.* **2017**, *53* (75), 10463–10466. https://doi.org/10.1039/C7CC05672A.

(255) Li, J.; Bao, W.; Tang, Z.; Guo, B.; Zhang, S.; Liu, H.; Huang, S.; Zhang, Y.; Rao, Y. Cercosporin-Bioinspired Selective Photooxidation Reactions under Mild Conditions. *Green Chem.* **2019**, *21* (22), 6073–6081. https://doi.org/10.1039/C9GC02270H.

(256) Saikia, G.; Ahmed, K.; Rajkhowa, C.; Sharma, M.; Talukdar, H.; Islam, N. S. Polymer Immobilized Tantalum(V)–Amino Acid Complexes as Selective and Recyclable Heterogeneous Catalysts for Oxidation of Olefins and Sulfides with Aqueous H_2O_2. *New J. Chem.* **2019**, *43* (44), 17251–17266. https://doi.org/10.1039/C9NJ04180J.

(257) Yu, B.; Liu, A.-H.; He, L.-N.; Li, B.; Diao, Z.-F.; Li, Y.-N. Catalyst-Free Approach for Solvent-Dependent Selective Oxidation of Organic Sulfides with Oxone. *Green Chem.* **2012**, *14* (4), 957–962. https://doi.org/10.1039/c2gc00027j.

(258) Patil, M. R.; Dedhia, N. P.; Kapdi, A. R.; Kumar, A. V. Cobalt(II)/*N*-Hydroxyphthalimide-Catalyzed Cross-Dehydrogenative Coupling Reaction at Room Temperature under Aerobic Condition. *J. Org. Chem.* **2018**, *83* (8), 4477–4490. https://doi.org/10.1021/acs.joc.8b00203.

(259) Senthilkumar, N.; Raghavan, A.; Narasimhaswamy, T.; Kim, I.-J. Novel Macro Metallomesogens Derived from Simple Dihydroxy Benzenes. *Inorganica Chim. Acta* **2013**, *397*, 129–139. https://doi.org/10.1016/j.ica.2012.12.001.

(260) Castro-Godoy, W. D.; Schmidt, L. C.; Argüello, J. E. A Green Alternative for the Conversion of Arylboronic Acids/Esters into Phenols Promoted by a Reducing Agent, Sodium Sulfite. *Eur. J. Org. Chem.* **2019**, 3035–3039. https://doi.org/10.1002/ejoc.201900311.

(261) Matthews, S. E.; Pouton, C. W.; Threadgill, M. D. Monofunctional Electrophilic and Nucleophilic Derivatives of Meso-Tetraphenylporphyrin for Attachment to Peptides. *J. Chem. Soc. Chem. Commun.* **1995**, *17*, 1809–1811. https://doi.org/10.1039/c39950001809.

(262) Donders, C. A.; Liu, S.-X.; Loosli, C.; Sanguinet, L.; Neels, A.; Decurtins, S. Synthesis of Tetrathiafulvalene-Annulated

Phthalocyanines. *Tetrahedron* **2006**, *62* (15), 3543–3549. https://doi.org/10.1016/j.tet.2006.01.098.

(263) Parg, R. P.; Kilburn, J. D.; Petty, M. C.; Pearson, C.; Ryan, T. G. Synthesis of Novel Bis- and Tris(Tetrathiafulvalene) Amphiphiles for Use in Langmuir-Blodgett Film Deposition. *Synthesis* **1994**, *6*, 613–618. https://doi.org/10.1055/s-1994-25534.

SANTRAUKA

ĮVADAS

Supramolekulinė chemija yra puikus įrankis kuriant sudėtingas funkcionalias medžiagas molekuliniame lygmenyje. Gamtoje gausu tokių supramolekulinių struktūrų, pavyzdžiui, virusai, ląstelės membranos, fermentai ar DNR gradinės.[1,2] Susidomėjimas tokiomis sistemomis atsirado dėl mažų molekulių gebėjimo spontaniškai sudaryti tvarkias struktūras sujungtas nekovalentinėmis sąveikomis, tokiomis kaip vandenilinis ryšys, dipolio – dipolio, elektrostatinė, π-π sąveika ar metalo – ligando koordinacija.[15,18] Vandenilinis ryšys yra dažniausiai naudojamas dėl savo stiprumo[19], grįžtamumo, kryptingumo[18] ir galimybės valdyti išoriniais dirgikliais, pvz. keičiant tirpiklio poliškumą[20,21], pH[22,23] ar temperatūrą[24,25]. Sukurti tokio pat sudėtingumo nanostruktūras kaip, kad randamos biologinėse sistemose, chemikams yra vis dar iššūkis.

Įvairios supramolekulinės kapsulės ir tuščiaviudurės polimerinės struktūros yra patrauklios dėl galimybės jas pritaikyti „šeimininko-svečio" kompleksų formavimui, katalizėje, bei vaistų ir žymeklių pernašai organizme. Kapsulė, suteikdama mechaninį barjerą, apsaugo viduje esančias molekules nuo neigiamų aplinkos veiksnių. Daugumos tokių kapsulių karkasą sudaro kovalentiniais ryšiais sujungti makrociklai, pvz. ciklodekstrinai, kukurbiturilai, kaliksarenai ar pilarenai, kurie užtikrina vidinės ertmės tvirtumą. Tačiau tai riboja kapsulės galimybes erdviškai prisitaikyti prie svečio molekulės, kad galėtų jį efektyviai sukompleksuoti ir po to reikiamu momentu išlaisvinti. Todėl yra ypač svarbu sukurti dinamines struktūras, sudarytas pilnai iš nekovalentinių sąveikų, kurių forma galėtų kisti priklausomai nuo svečio ar aplinkos veiksnių. Visa reikalinga informacija sėkmingai agregacijai turi būti iš anksto užprogramuota supramolekulinių sistemų komponentuose, todėl tokių monomerų sintezė yra komplikuota.

Siekiant sukurti dinamines supramolekulines sistemas buvo pasirinktas enantiomeriškai grynas V formos biciklo[3.3.1]nonano monomeras, turintis komplementarius izocitozino (ICyt) ir/ar ureidopirimidinono (Upy) fragmentus. Susidarant vandeniliniams ryšiams tarp komplementarių DAA-ADD tautomerinių formų yra gaunami cikliniai tetramerai, kurie toliau agreguojasi į supramolekulinius vamzdelius dėl papildomų ortogonalių vandenilinių ryšių tarp gretimų tetramerų. Manipuliavimas pakaitų prigimtimi, dydžiu ar erdviniu išsidėstymu leidžia ne tik kontroliuoti

agregacijos laipsnį ar darinio topologiją, tačiau ir pačios sistemos elektronines savybes kuriant išmaniąsias supramolekulines medžiagas.

Pagrindinis šio darbo tikslas yra sukurti supramolekulines dinamines kapsules ir vamzdelinius polimerus, sudarytus iš biciklo[3.3.1]nonano karkaso, kurie galėtų būti ateityje pritaikyti organinėje elektronikoje kuriant funkcionalias medžiagas.

Tikslui įgyvendinti buvo suformuluoti šie uždaviniai:

1. Susintetinti monomerus, turinčius komplementarius izocitozino ir/ar ureidopirimidinono fragmentus bei lanksčių jungtuką, kuris leistų lengvai inkorporuoti įvairius chromoforus ar kitus funkcinius elementus į sistemą.
2. Susintetinti asimetrinius monomerus, funkcionalizuojant vieną iš izocitozino fragmentų, prijungiant didelį tetrafenilporfirino pakaitą, kurie būtų pritaikyti kuriant dinamines kapsules.
3. Pademonstruoti, kad tuščiaviduėrės kapsulės gali į vidų įterpti fulereno C_{60} molekulę.
4. Sukonstruoti vamzdelinius supramolekulinius agregatus turinčius π-konjuguotą sistemą ir pasižyminčius aukštu savitvarkos laipsniu.
5. Pademonstruoti galimybę grįžtamai valdyti agregato virtimą tarp ciklinio tetramero, dimerinių žnyplių ar pavienio monomero naudojant cheminį ar šviesos stimulą.

Mokslinis naujumas:

Šiame darbe sukonstruoti nauji supramolekuliniai nanovamzdeliai ir diskretiškos kapsulės, turinčios lanksčius jungtukus, kurie leidžia lengvai įvesti įvarius chromoforus reikalingus kuriant funkcionalias medžiagas. Atrasta šeimininko-svečio komplekse unikali tamsoje vykstanti elektronų pernaša tarp artimai erdvėje išsidėsčiusių jungtukų turinčių sulfidines grupes ir svečio – fulereno C_{60} molekulę. Šiame kontekste pademonstruota galimybė fullereną C_{60} ir jo pigią žaliavą – fulereno suodžius pritaikyti žalioje chemijoje kaip tvarų heterogeninį katalizatorių atliekant chemoselektyvią sulfidų oksidaciją iki sulfoksidų naudojant molekulinį deguonį. Taip pat buvo sėkmingai sukonstruota dinaminė supramolekulinė kapsulė funkcionalizuota tetrafenilporfirinais, kurios ertmė atitinkamai persigrupuoja tautomerizacijos proceso metu, kad galėtų efektyviai sukompleksuoti svečio molekulę. Vamzdeliniai polimerai azabiciklo[3.3.1]nonano pagrindu, turintys π-konjuguotus tetratiafulvaleno fragmentus, buvo pritaikyti kuriant

potencialius organinius puslaidininkius. Tokia savitvarkė sistema užtikrina n ir p tipo kanalų atskyrimą, kuris yra reikalingas efektyviai skirtingų krūvių pernašai organinėje elektronikoje. Galiausiai, pirmą kartą pademonstruota galimybė grįžtamai manipuliuoti supramolekulinio biciklo[3.3.1]nonano agregato asociaciją tarp ciklinio tetramero, dimerinių žnyplių ar pavienio monomero naudojant cheminį ar šviesos stimulą.

TYRIMŲ REZULTATAI

1. Diskrečios vandeniliniais ryšiais sudarytos kapsulės enantiomeriškai gryno biciklo[3.3.1]nonano pagrindu

Supramolekulinėms struktūroms sukurti buvo pasirinktas enantiomeriškai grynas V formos biciklo[3.3.1]nonano monomeras, turintis komplementarius izocitozino (ICyt) ar ureidopirimidinono (Upy) fragmentus. Susidarant vandeniliniams ryšiams tarp komplementarių tautomerinių formų yra gaunami cikliniai tetramerai, kurie toliau agreguojasi į supramolekulinius vamzdelius dėl papildomų ortogonalių vandenilinių ryšių tarp gretimų tetramerų. Modifikuojant ICyt fragmentą galima užblokuoti ortogonalią agregaciją, ir tokiu būdu yra gaunami diskretūs cikliniai tetramerai turintys Upy fragmentus. Šiam tikslui buvo susintetinti biciklo[3.3.1]nonano monomerai, remiantis sintezės metodika, kuri buvo sukurta ir optimizuota E. Orento grupėje.[126,127] Iš ankstesnių darbų yra žinoma, kad dideli pakaitai prijungti tiesiogiai prie monomero karkaso neleidžia susidaryti vamzdelinėms struktūroms dėl atsirandančių sterinių trukdžių. Manipuliavimas pakaitų dydžiu, lankstumu ar erdviniu išsidėstymu galėtų leisti selektyviai kontroliuoti tetramerų agregaciją į sudėtingesnius darinius, todėl buvo nuspręsta tarp didelio pakaito ir biciklo[3.3.1]nonano pagrindo įvesti lankstų jungtuką, kuris leistų palankiai išsidėstyti šoninėms grupėms erdvėje (1 pav.).
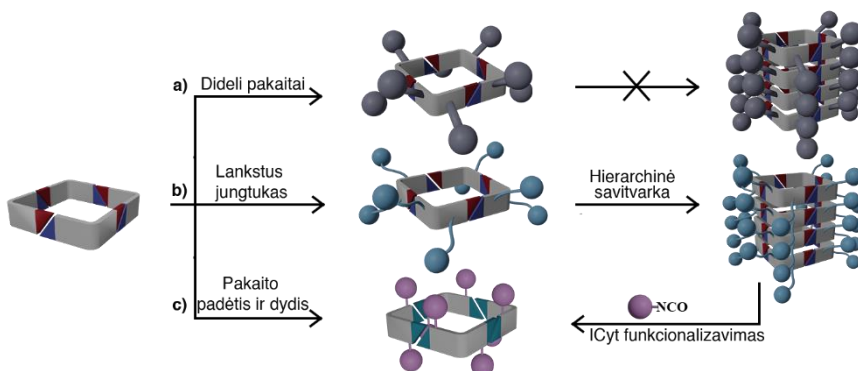
1 pav. Pavyzdžiai kaip keičiant pakaitų dydį (a), lankstumą (b) ar erdvinį išsidėstymą (c) galima kontroliuoti supramolekulinio darinio agregacijos laipsnį.

Tiolo grupę turintis jungtukas įvestas geromis išeigomis (90 – 99%) atliekant fotocheminę „click" reakciją tarp neaktyvuoto dvigubo ryšio ir tioacto rūgšties (2 pav.). Gautas tioacetatas gali būti suhidrolizuotas tiek rūgštinėje

tiek bazinėje terpėje, tačiau atliekant hidrolizę rūgštinėmis sąlygomis yra gaunama didesnė išeiga (79 %).
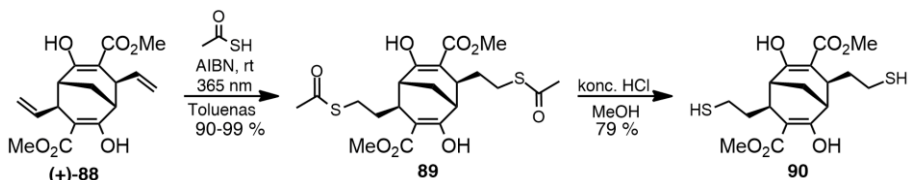
2 pav. Monomero **90** turinčio nukleofilinį jungtuką sintezė.

Gautas nukleofilinis jungtukas įgalina supaprastintą įvairaus dydžio pakaitų įvedimą į sistemą atliekant nukleofilinio pakeitimo reakcijas su atitinkamais bromidais (3 pav.). Buvo prijungti įvairūs pakaitai, nuo linijinių tetraetilenglikol- iki šakotų 3,5-bis(deciloksi)benzil-, kad įvertinti jų daromą įtaką ciklinių tetramerų hierarchinei agregacijai į supramolekulinius vamzdelius.
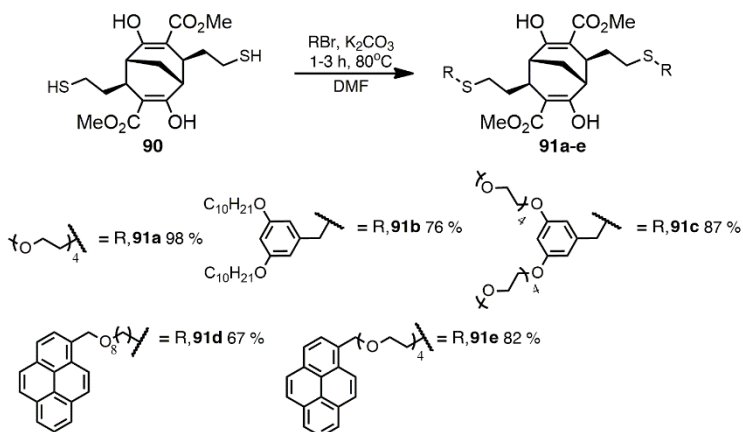
3 pav. Nukleofilinio pakeitimo reakcijos tarp monomero **90** ir atitinkamų bromidų **91a-e**.

Tiksliniai monomerai, turintys komplementarius izocitozino fragmentus, buvo susintetinti kondensuojant atitinkamus ketoesterius **91a-e** su guanidino chloridu bazinėje terpėje (4 pav.).

209
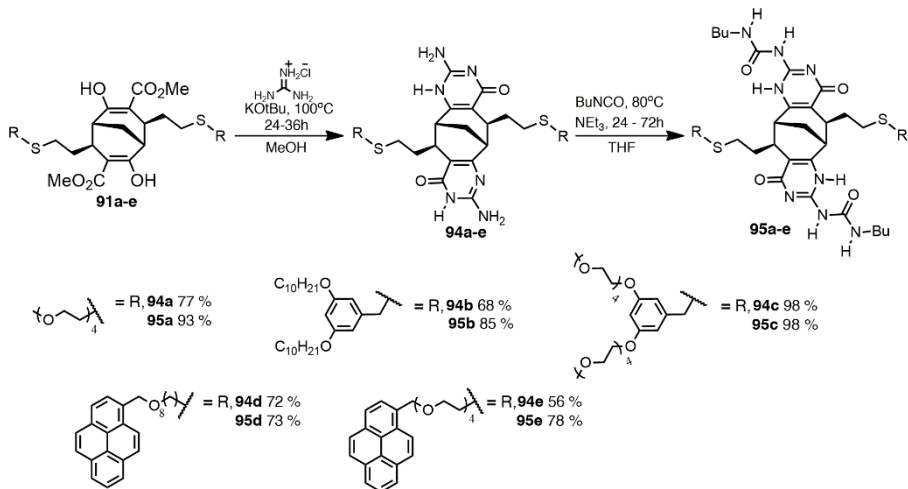
4 pav. Komplementarius vandenilinius ryšius sudarančių enantiomeriškai grynų monomerų **95a-e** sintezė.

Monomerai **94a-e** nepoliniuose organiniuose tirpikliuose asocijuojasi į tetramerinius darinius dėl susidariusių DDA-AAD vandenilinių ryšių tarp komplementarių izocitozino tautomerinių formų (5 pav.). Tolimesnės agregacijos metu gaunamos vamzdelinės struktūros susidarant papildomiems ortogonaliems vandeniliniams ryšiams tarp gretimų tetramerų. Polimerinių struktūrų susidarymas dažnai stebimas plika akimi, susidarant geliams.
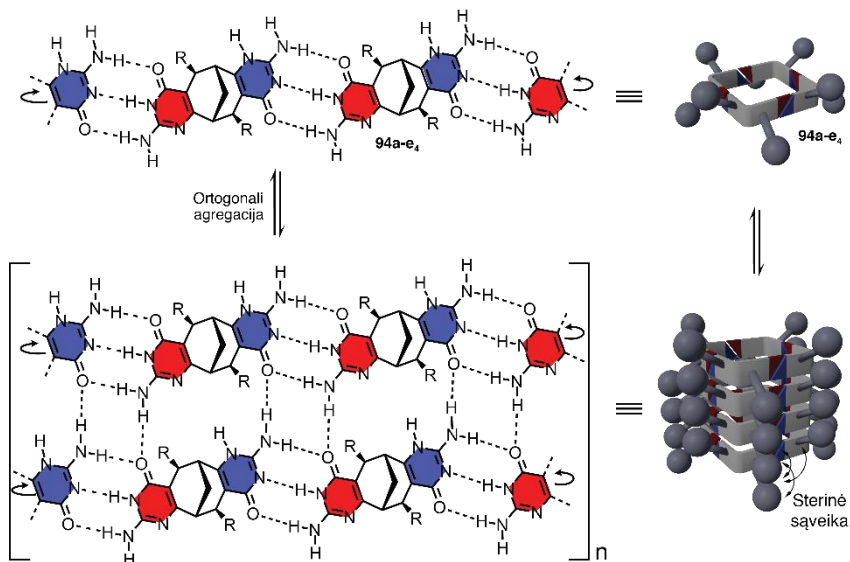
5 pav. Ciklinių tetramerų **94a-e₄** ortogonali agregacija į vamzdelinius polimerus.

Tolimesnis polimerų charakterizavimas nebuvo įmanomas dėl didelio tirpalų klampumo ir taip pat išplitusių signalų BMR spektruose. Polimerai buvo paversti į diskrečius tetramerinius kavitandus blokuojant vandenilius esančius ICyt fragmente, kurie dalyvauja vandenilinių ryšių susidaryme tarp gretimų tetramerų (1c pav). Nauji monomerai **95a-e**, turintys ureidopirimidinono fragmentą, buvo gauti geromis išeigomis (73 – 97 %) veikiant ICyt **94a-e** n-butilo izocianatu ir trietilaminu THF tirpiklyje. Šių monomerų agregacijos procesai toliau buvo tyrinėti organiniuose nepoliniuose tirpikliuose.

1.1 Tuščiavidurių kapsulių pritaikymas svečio-šeimininko kompleksams

Tuščiaviduriai cikliniai tetramerai buvo gauti susidarant DDAA-AADD keturgubiems vandeniliniams ryšiams tarp sau komplementarių Upy fragmentų esančių monomeruose **95a-e** (6a pav.). [1]H BMR spektrai chloroforme patvirtina tetramerinių agregatų **95₄** susidarymą (6b pav.). Signalų rinkinys (12,93, 11,89, 9,64 m.d.) silpnuose laukuose junginio **95a** spektre priskirtas atitinkamiems NH protonams, kurie dalyvauja susidarant vandeniliniams ryšiams tarp ureidopirimidinono fragmentų. DOSY spektre visi signalai yra priskiriami tokiam pačiam difuzijos koeficientui – $D = 2,44 \cdot 10^{-10}$ m^{2}s^{-1}, kuris atitinka 16 Å hidrodinaminį spindulį sferinės dalelės. Tai patvirtina vienos rūšies agregato egzistavimą chloroforme. Taip pat, gauta vertė atitinka anksčiau aprašytų supramolekulinių tetramerų spindulio vertę.[121,123] Kitų tetramerų **95b-e₄** [1]H BMR spektruose chloroforme stebimi analogiški signalų rinkiniai, kurių difuzijos koeficientai yra tarp 2,12 – 2,17 m^{2}s^{-1} (6c pav.). Remiantis erdvinėmis sąveikomis stebimomis 2D COSY ir ROESY spektruose, nustatyta, kad monomeras egzistuoja keto tautomerinėje formoje, kuris sudaro DDAA-AADD vandenilinius ryšius dimerizuojantis komplementariems Upy fragmentams.
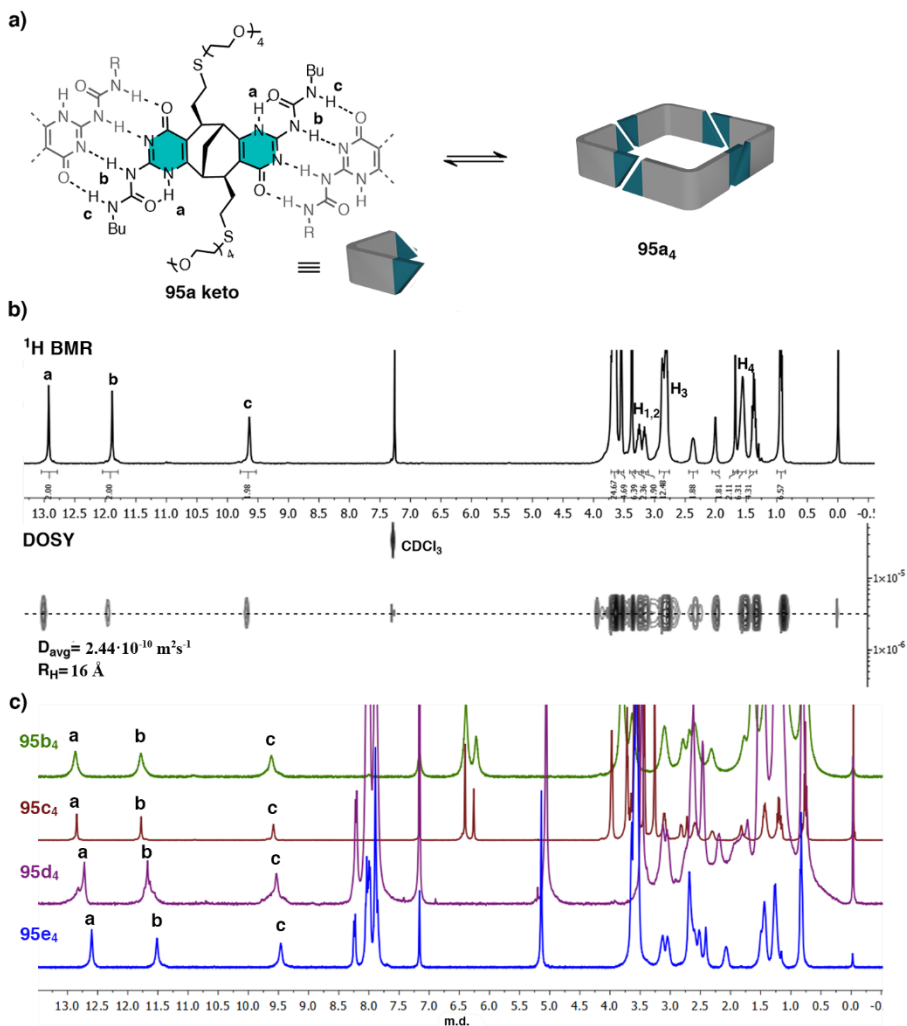
6 pav. a) monomero **95a** asociacija į tetramerines kapsules; b) tetramero **95a₄** (10 mM) ^{1}H BMR ir DOSY spektrai CDCl₃; c) tetramerų **95b-e₄** ^{1}H BMR spektrai CDCl₃.

Supramolekulinių ciklinių tetramerų susidarymas net tokiuose poliniuose tirpikliuose kaip acetonitrilas patvirtina didelį tokių struktūrų stabilumą. Benzene monomeras **95a** sudaro du skirtingo dydžio agregatus – tetramerą ir pentamerą, kurių hidrodinaminiai spinduliai atitinkamai yra 15,8 Å (D = $2{,}09 \cdot 10^{-10}$ m²s⁻¹) ir 17,52 Å (D = $1{,}89 \cdot 10^{-10}$ m²s⁻¹) (7a,b pav.).
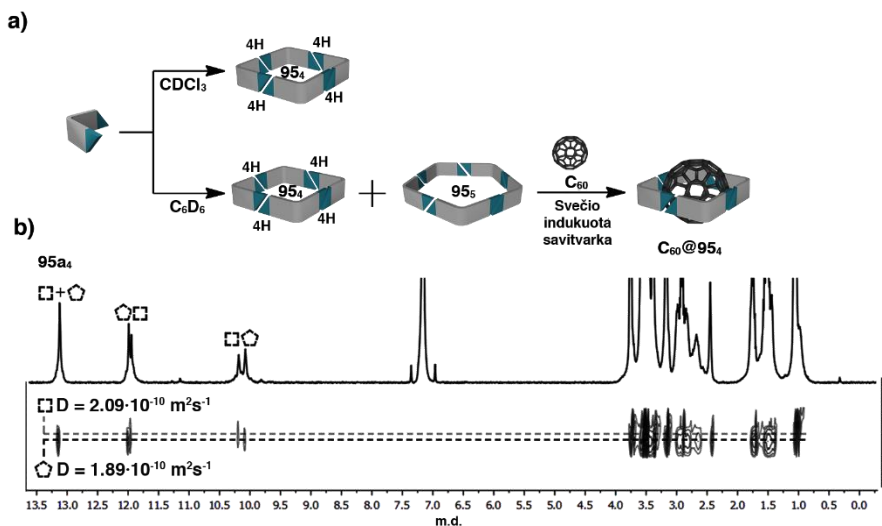
7 pav. a) Monomero asociacija į ciklinius tetramerus ir pentamerus nepoliniuose tirpikliuose; b) **95a₄** (15 mM) ¹H BMR ir DOSY spektrai C_6D_6.

Iš molekulinio modelio (optimizuoto PM3 metodu naudojant Spartan'14 programą) buvo nustatyta, kad kapsulės ertmės diametras yra 13,4 Å (8a pav.), pakankamo dydžio fulereno C_{60} svečio kompleksavimui. Inertinėje atmosferoje visi monomerai **95a-e** sėkmingai sudarė įterpimo kompleksus C_{60}@**95₄** d_6-benzene ir d_3-acetonitrile. Komplekso C_{60}@**95a₄** difuzijos koeficientas ($D = 2,08 \cdot 10^{-10}$ m²s⁻¹) parodo, kad gautas vienos rūšies agregatas, kurio matmenys yra identiški laisvam tetramerui (8b pav.). Įdomu tai, kad vyksta fulereno indukuota savaiminė saviatranka, kuri yra pagrįsta ertmės dydžiu. Tai rodo, kad proceso metu parazitiniai pentamerai yra linkę persitvarkyti į termodinamiškai stabilesnius tetramerus ir yra pašalinami. Tačiau buvo pastebėta, kad laikui bėgant vyksta šeimininko-svečio komplekso degradacija, jeigu nėra pašalinamas deguonis iš atmosferos.
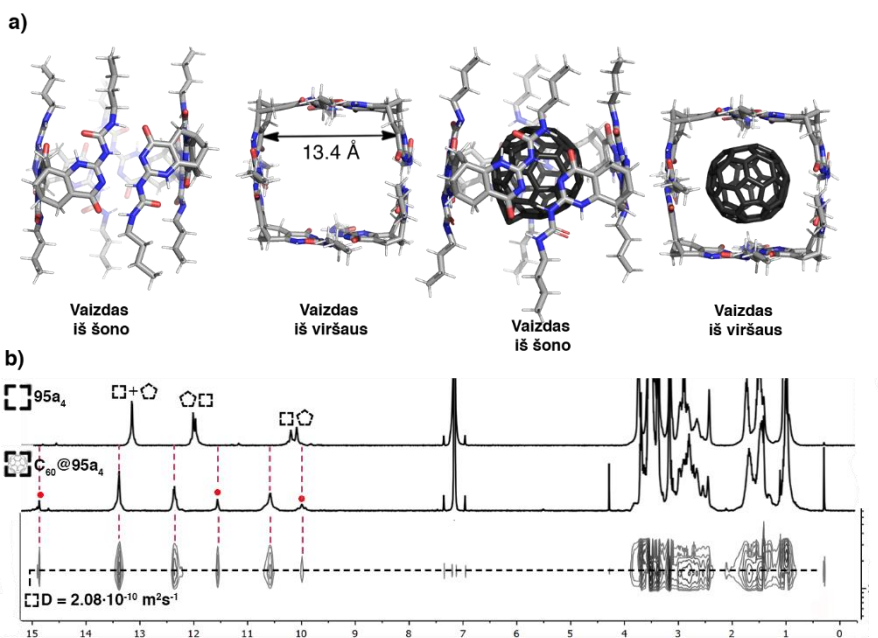
8 pav. a) Tetramero **95₄** ir komplekso **C₆₀@95₄** molekuliniai modeliai; b) laisvo tetramero ir komplekso **C₆₀@95₄** ¹H BMR ir DOSY spektrai C₆D₆. Raudonais taškais pažymėti signalai yra priskiriami enolinei formai.

Kadangi sukompleksuota fulereno molekulė pozicionuojama arti sulfidinių grupių, tai įgalina elektrono pernašą iš sulfido donoro į fulereno akceptorių, netgi nenaudojant šviesos šaltinio (9a pav.). Tamsoje susidaręs sulfido katijono radikalas **A** gali toliau reaguoti su molekuliniu deguonimi. Rūgštinis α-protonas persulfokside **B** lengvai atskyla, todėl tarpinis junginys persitvarko į hidroperoksisulfidą **D**. Jis toliau hidrolizuojasi suyrant anglies-sulfido ryšiui, atskylant benzaldehidui bei susidarant įvairiems sulfidų dariniams.

Trifenilfosfinas yra geras elektronų donoras, todėl buvo nuspręsta jį pritaikyti kaip inhibitorių. Sulfido katijono radikalas yra suredukuojamas vykstant elektrono pernašai iš PPh₃ (9b pav.). Gautas fosfino katijono radikalas toliau reaguoja su molekuliniu deguonimi. Susidaręs aduktas, perduodant vieną deguonies atomą, suoksiduoja kitą PPh₃ molekulę. ¹H BMR protonų spektre matome, kad acetonitrile buvo sėkmingai pasiekta pilna PPh₃ konversija į trifenilfosnino oksidą (9c pav.). Ši tamsoje vykstanti elektronų pernaša yra unikali, kadangi pagrįsta erdviniu C₆₀ ir sulfido grupių artumu ir jai nėra reikalingas joks šviesos šaltinis.
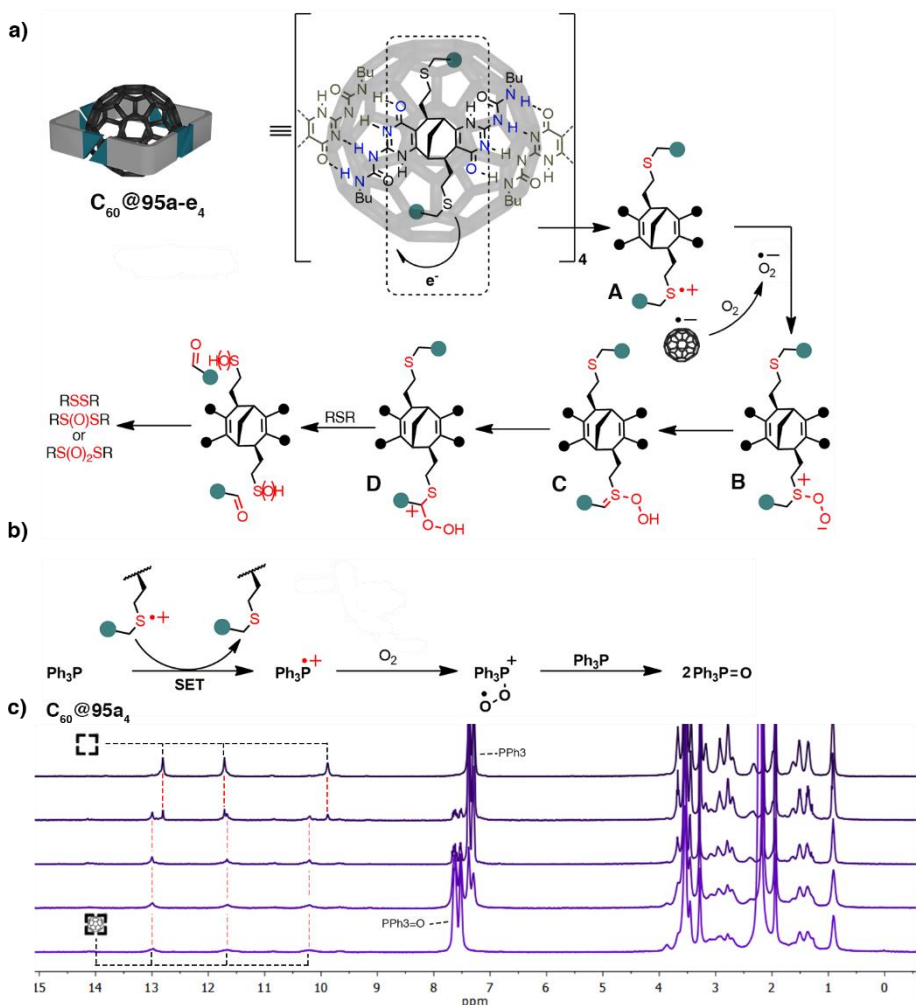
9 pav. a) Spekuliatyvus mechanizmas pagal kurį vyksta tetramero degradacija; b) PPh₃ oksidacija esant kompleksui **C₆₀@95a₄** ir molekuliniam deguoniui; c) PPh₃ oksidacija stebima ¹H BMR spektruose CD₃CN.
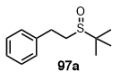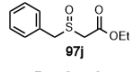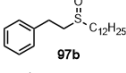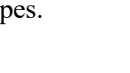
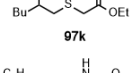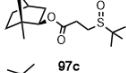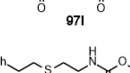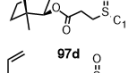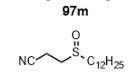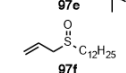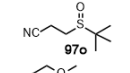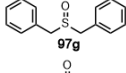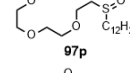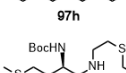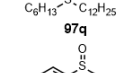## 1.2 Chemoselektyvi sulfidų fotooksidacija iki sulfoksidų naudojant heterogeninius fulereno pagrindu katalizatorius

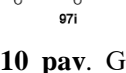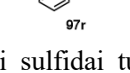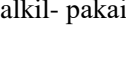Nors keli bandymai panaudoti fulereną kaip katalizatorių oksidacijos reakcijose yra aprašyti, dažnu atveju reikalingas papildomas fulereno darinio paruošimas, pvz. funkcionalizavimas[156], įvedimas į miceles[157] ar imobilizacija ant kietos fazės[158]. Dėl šios priežasties buvo nuspręsta pademonstruoti nemodifikuoto fulereno potencialą kaip heterogeninio katalizatoriaus selektyvioje sulfidų oksidacijoje iki sulfoksidų naudojant molekulinį deguonį. Fulerenas yra ganėtinai brangus, todėl tuo pačiu buvo

pasirinkta ištirti pigios fulereno žaliavos fulerenų suodžių (FS) aktyvumą sulfidų oksidacijoje. Šiame kontekste parodyta galimybė fulereną C_{60} ir FS pritaikyti žalioje chemijoje kaip tvarų heterogeninį katalizatorių. Fulereno suodžiai buvo naudojami kietoje būsenoje arba kaip suspensija toluene. Toluene ištirpintą fulereną supylus į polinį reakcijos tirpiklį buvo gauta stabili koloidinė nanodispersija. Naudojant mėlyną šviesą (100 W 450 nm) buvo sėkmingai suoksiduoti įvairūs sulfidai turintys linijinius ar šakotus alkil- pakaitus, taip pat įvairias funkcines grupes, pvz. esterius, amidus, nitrilus ar net alkenus (10 pav.). Sulfidų fotooksidacija gali vykti dviem skirtingais mechanizmais: elektronų pernašos mechanizmu arba energijos perdavimo mechanizmu, kuris generuoja singletinį deguonį.[162-166] Dažnai abu šie mechanizmai operuoja vienu metu.

Junginys	[FS] EtOH	[FS] CH3CN	[FS in Tol] EtOH	[FS in Tol] CH3CN	[C60 in Tol] EtOH	[C60 in Tol] CH3CN
97a	93%	0%	97%	81%	78%	48%
97b	99%	0%	93%	82%	99%	60%
97c	74%	0%	74%	55%	84%	35%
97d	88%	0%	92%	78%	69%	86%
97e	77%	0%	85%	94%	92%	59%
97f	81%	0%	90%	70%	68%	71%
97g	81%	0%	94%	0%b	98%	69%
97h	82%	0%	57%	90%	79%	93%
97i	35%	0%	92%	36%	73%	51%
97j	58%	0%	44%	18%	56%	21%
97k	47%	0%	53%	16%	56%	36%
97l	72%	0%	98%	65%	95%	97%
97m	98%	0%	42%	78%	82%	60%
97n	67%	0%	96%	80%	92%	61%
97o	70%	0%	53%	59%	72%	89%
97p	88%	79%	97%	82%	99%	80%
97q	98%	85%	92%	82%	95%	80%
97r	<5%	0%	<5%	<5%	<5%	<5%

10 pav. Geromis išeigomis suoksiduoti sulfidai turintys linijinius ar šakotus alkil- pakaitus, bei įvairias funkcines grupes.

Deja, dialkilsulfidams optimizuotomis sąlygomis tioanizolo dariniai pasirodė esą neaktyvūs, dėl per aukšto jų oksidacijos potencialo. Ši problema buvo išspręsta panaudojant tretinio amino mediatorius, kurie įgalina ypač sparčią

elektrono pernašą į fullereną. Tioanizolo dariniai buvo suoksiduoti puikiomis išeigomis (>85 %) naudojant katalitinį kiekį TEA (11a pav.). Fullereno potencialas kaip heterogeninio katalizatoriaus buvo taip pat pademonstruotas chemoselektyviai oksiduojant bisulfidą **96v**, turintį dialkil- ir arilalkil-sulfido grupes (11b pav.). Disulfoksidai buvo sėkmingai gauti gera išeiga (68 – 81 %) etanolyje. Nors be trietilamino arilsulfidų oksidacija nevyksta, tačiau chemoselektyvi oksidacija įvyko netiesiogiai dėl deguonies atomo vidujmolekulinės pernašos nuo dialkilpersulfoksido tarpinio junginio į arilalkilsulfidą.
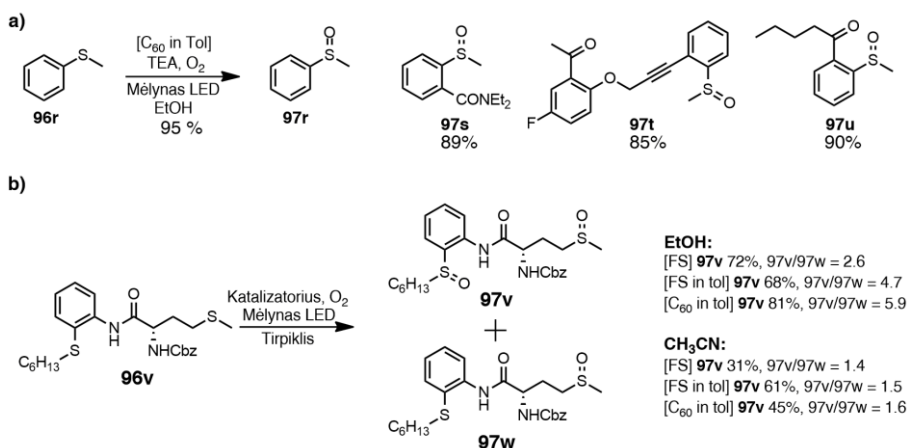
11 pav. a) Suoksiduoti tioanizolo dariniai naudojant katalitinį kiekį TEA kaip elektronų mediatorių; b) oksidacija bisulfido **96v**, turinčio dialkil- ir arilalkil-sulfidines grupes.

Norint pademonstruoti fullereno kaip heterogeninio katalizatoriaus universalumą, jis buvo pritaikytas fotooksidacinėje prisijungimo-ciklizacijos reakcijoje tarp N,N-dimetilanilino ir maleimido (12 pav.). Tetrahidrochinolino darinys **99** buvo gautas 68 – 75 % išeigomis etanolyje.
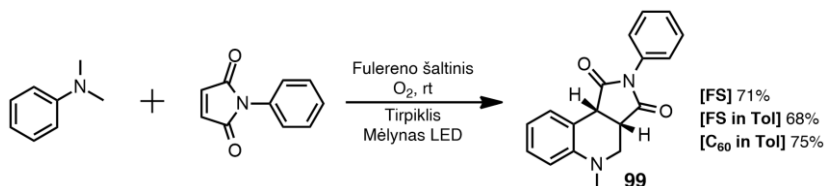
12 pav. Fotooksidacinė ciklizacijos-prisijungimo reakcija tarp N,N-dimetilanilino ir maleimido.

Taip pat, veikiant mėlyna šviesa N-benzilaminai buvo lengvai paversti į atitinkamus iminus, susidariusiame amino katijono radikale pirmiausiai vykstant α-deprotonizacija ir po to sekančiai oksidacijai (13a pav.). Atlikus reakciją EtOH, CH₃CN ir CHCl₃ tirpikliuose buvo pastebėta, kad efektyviausiai reakcija vyksta chloroforme 78 – 100 % išeigomis. Manoma tai susiję su tuo, kad šiame tirpiklyje singletinio deguonies $^1O_2$ gyvavimo trukmė yra ilgiausia. Analogiškai buvo įvesta nitrilo grupė į tretinį aminą 2-fenil-1,2,3,4-tetrahidroizochinoliną naudojant TMSCN (13b pav.). Tokia vieno indo reakcija leidžia efektyviai ir selektyviai sintetinti α-aminonitrilus, kurie naudojami kaip universalūs prekursoriai įvairių bioaktyvių produktų gamybai.[180-182]
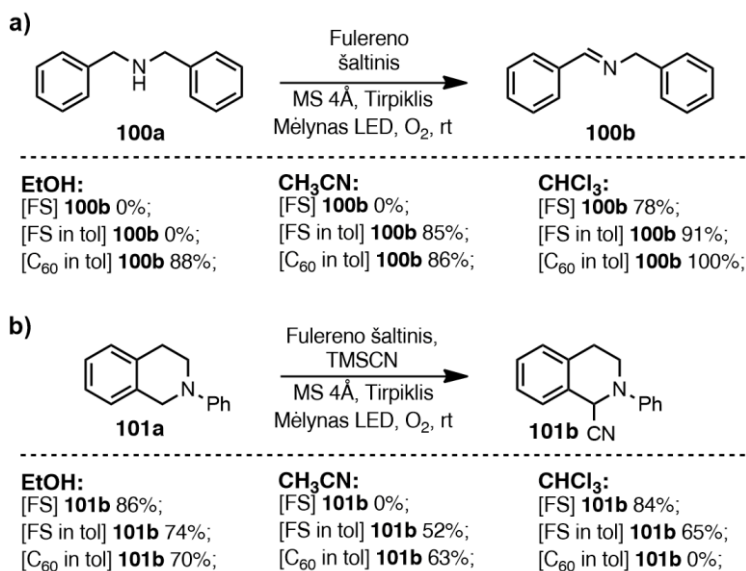
13 pav. a) N-benzilamino fotooksidacija į iminą; b) ciano grupės fotooksidacinis įvedimas į tretinį aminą 2-fenil-1,2,3,4-tetrahidroizochinoliną naudojant TMSCN.

Galiausiai, veikiant mėlyna šviesa atliktas arilboronio rūgščių ipso-hidroksilinimas, esant DIPEA elektronų donorui (14 pav.). Fotooksidacinio hidroksilinimo metu 4-deciloksifenolis sėkmingai gautas geromis išeigomis EtOH ir CHCl₃ tirpikliuose, tačiau dėl prasto piridilboronio rūgšies tirpumo, tikslinis produktas piridin-4-olis buvo gautas tik etanolyje.
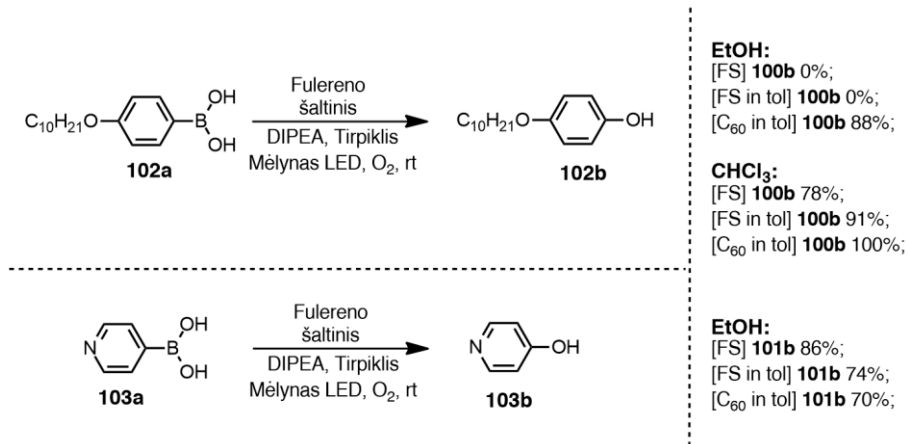
14 pav. Arilboronio rūgščių ipso-hidroksilinimas naudojant DIPEA kaip elektronų donorą.

## 2. Dinaminė supramolekulinė kapsulė gebanti konformaciškai prisitaikyti prie svečio molekulės

Biologiniuose atpažinimo procesuose veikiantis "spynos – rakto" modelis buvo plačiai pritaikytas siekiant sukurti sintetinius receptorius ir katalizatorius, kurie būtų pagrįsti šeimininko ir svečio komplekso susidarymu. Tačiau pastaruoju metu didelis dėmesys skiriamas dinaminiams molekulinio atpažinimo modeliams biologinėse sistemose, kurie yra pagrįsti indukuoto atitikimo (angl. induced-fit) ar konformacinės atrankos mechanizmais (angl. conformational selection).[187] Todėl, norint sukurti panašias biomimetines sistemas, reikia susintetinti lanksčias supramolekulines sistemas, kurios įterpiant svečio molekulę galėtų konformaciškai pasiekti optimalią geometriją.

Šiam tikslui buvo susintetinti asimetriniai enantiomeriškai gryni monomerai **106a–d**, turintys šonuose prijungtus komplementarius izocitozino ir ureidopirimidinono motyvus (15 pav.). Pirmiausiai, naudojant atitinkamus alkilmagniobromidus ir vario cianidą, prie ketoesterio buvo prijungti įvairaus ilgio tirpumą gerinantys alkil- pakaitai. Alkil- pakeisti ketoesteriai buvo kondensuojami su guanidino hidrochloridu. Galiausiai selektyviai modifikuojant izocitoziną, buvo suformuotas urėjos fragmentas turintis didelį tetrafenilporfirino (TPP) chromoforą.

15 pav. Asimetrinio monomero, turinčio ICyt ir Upy fragmentus, sintezė.

Iš ankstesnių darbų žinome, kad ureidopirimidinono grupė nesudaro ortogonalių vandenilinių ryšių ir negali polimerizuotis. Tačiau asimetrinis monomeras, turintis Upy ir ICyt fragmentus, gali sudaryti oktamerinius darinius, nes heteroasociacijos metu susidaro papildomi tarpmolekuliniai ortogonalūs vandeniliniai ryšiai tarp izocitozino grupių (16a pav.)[124].

16 pav. Galimos supramolekulinio agregato struktūros priklausomai nuo pakaito dydžio prijungto prie ICyt fragmento.

Buvo nuspręsta patikrinti, ar galima kontroliuoti šį agregacijos procesą, įvedant erdviškai ekranuojančius pakaitus į Upy fragmentą. Siekiant ištirti šią strategiją buvo inkorporuoti tetrafenilporfirinai, kurie yra didesni net už patį tetramerą (16b pav.). Cikliniuose tetrameruose **106a**–**d₄** porfirinai pasiskirstė skirtingose kapsulės pusėse dėl atsiradusios nepalankios erdvinės sąveikos tarp didelių pakaitų, ir neleido susidaryti oktamerinėms struktūroms (17a pav.). Gautas diskretiškas tetrameras yra papildomai stabilizuojamas atsiradusių π-π sąveikų tarp TPP aromatinių žiedų. Kapsulių ^{1}H BMR spektruose matome 4 signalų rinkinius silpnesniuose laukuose, kurie yra priskiriami protonams esantiems Upy ir ICyt fragmentuose, dalyvaujančiuose homoasociacijoje susidarant DDAA-AADD ir DA-AD vandeniliniams ryšiams (18a pav.). Vienas signalas ties 5,0 m.d., kuris priskirtas izocitozino NH_2 protonams, rodo, kad ICyt žiedo aminogrupė nedalyvauja susidarant vandeniliniams ryšiams ir oktameras nesusidaro. Iš tetramero **106a₄** eksperimentiškai gauto difuzijos koeficiento $D = 2{,}02 \cdot 10^{-10}$ m^2s^{-1}, pagal Stokso-Einšteino lygtį paskaičiuotas hidrodinaminis spindulys $R_H = 21{,}3$ Å, kuris atitinka teorinį diametrą $d = 41{,}1$ Å, gautą remiantis optimizuotu molekuliniu modeliu.
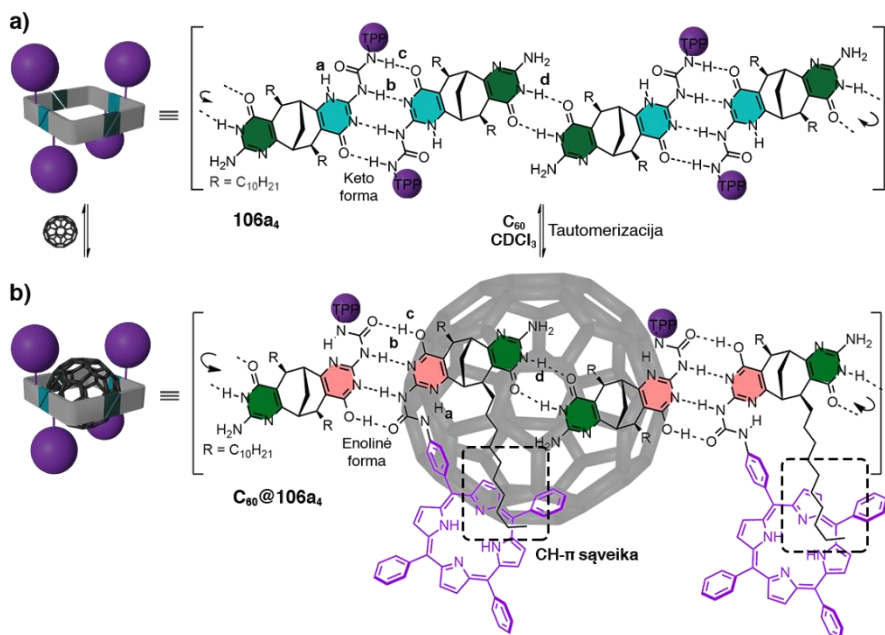

17 pav. Tetramero **106a₄** (a) kompleksacija su svečio C_{60} molekule susidarant kompleksui **C₆₀@106a₄** (b) CDCl₃.
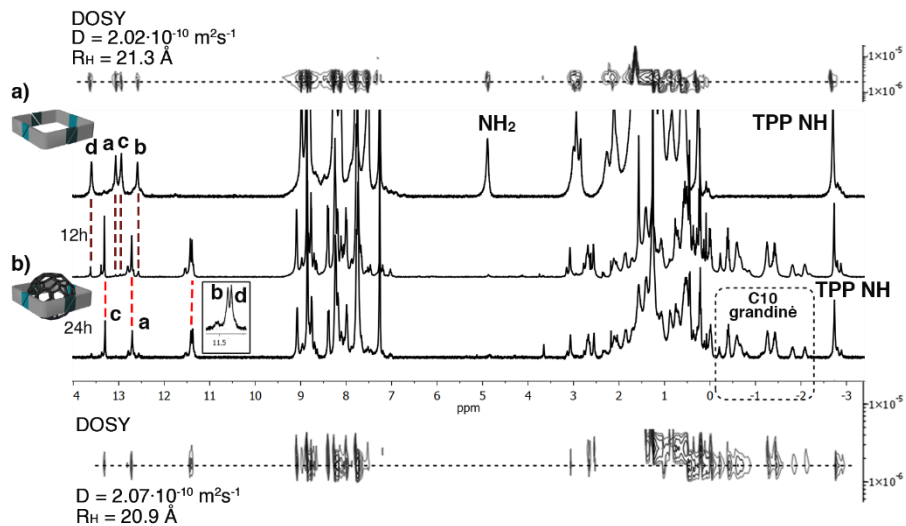
18 pav. Tetramero **106a₄** (a) ir komplekso **C₆₀@106a₄** (b) ^{1}H BMR ir DOSY spektrai CDCl₃.

Tetramerai **106a₄** ir **106c₄** chloroforme su svečio C_{60} molekulėmis sėkmingai sudarė įterpimo kompleksus **C₆₀@106₄**, kurių difuzijos koeficientai sutampa su laisvų tetramerų vertėmis (17b, 18b pav.). Tačiau buvo pastebėta, kad svečio kompleksacija sukelia konformacijos pokyčius, kuomet tautomerizacijos metu keto forma Upy fragmente virsta į enolinę. Iš ^{1}H-^{15}N HSQC spektro matyti, kad nebeliko sąveikos tarp vieno vandenilio ir azoto, kuri buvo stebima laisvame tetramere esant keto formai. [1]H BMR spektre taip pat stebima naujai atsiradusi sąveika tarp porfirino ir alkil- pakaitų, nes dėl stipraus ekranavimo matomas CH_2 grupių poslinkis į stipresnius laukus (-0,2 – -2,10 m.d) (18b pav.). Tokie patys rezultatai gauti su ilgus decil- ir oleil- pakaitus turinčiais monomerais **106a** ir **106c**, tačiau monomeras **106b** su trumpesne 2-etilheksil- grandine nekompleksavo fulereno. Remiantis molekuliniu modeliu, porfirino fragmentai tautomerizacijos metu yra priversti išsisukti iš plokštumos, kad fulerenas galėtų būti inkorporuotas į vidinę ertmę (19a pav.). Tačiau vien tautomerizacijos neužtenka komplekso stabilumui užtikrinti ir yra reikalinga papildoma stabilizuojanti π-CH sąveika tarp porfirino žiedo ir alkilo grupių. Ši papildoma sąveika taip pat kompensuoja ir entropijos sumažėjimą, susijusį su kompleksavimo procesu. Kadangi, 2-etilheksil- pakaitas yra per trumpas, kad galėtų sąveikauti su porfirino fragmentu, todėl nėra galimybės papildomai stabilizuoti komplekso ir kompleksacija neįvyksta (19b pav.). Nors monomeras **106d** turi pakankamai ilgą (Z)-1-noneno pakaitą, tačiau cis dvigubas ryšys neleidžia alkilo grandinei laisvai suktis ir užrakina ją padėtyje nukreiptoje į išorę nuo

TPP fragmentų. Sąveika tarp alkilo pakaito su TPP nėra galima, todėl monomeras **106d** kompleksacijoje taip pat nedalyvauja. Taigi, su monomerais **106a** ir **106c** buvo sėkmingai gauti dinaminiai supramolekuliniai kavitandai, kurių ertmės atitinkamai persigrupuoja, kad galėtų efektyviai sukompleksuoti svečio molekulę.
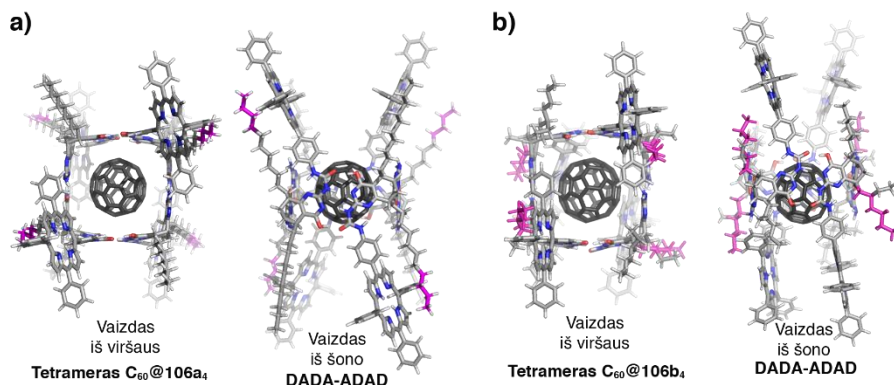
19 pav. Molekuliniai modeliai kompleksų a) $C_{60}@106a_4$ ir b) $C_{60}@106b_4$. Rausva spalva pažymėtos atitinkamai C_{10} ir 2-etilheksil alkilų grandinės.

3. π-Konjunguotos supramolekulinės struktūros 9-azabiciklo[3.3.1]nonano pagrindu

Ankstesniuose skyriuose įsitikinome, kad manipuliavimas pakaitų dydžiu, lankstumu ar erdviniu išsidėstymu leidžia selektyviai kontroliuoti tetramerų agregacijos laipsnį ir darinių topologiją, todėl šiame kontekste buvo pasirinktas enantiomeriškai grynas 9-azabiciklo[3.3.1]nonano karkasas, nes prie 9-toje padėtyje esančios amino grupės galima prijungti įvairius funkcinius chromoforus. Pakaitai yra išsidėstę statmenai monomero ir nukreipti į išorę. Jie yra toliau nuo komplementarių vandeniliniais ryšiais sujungtų izocitozino fragmentų, tad jų dydis neturi įtakos ortogonaliai ciklinių tetramerų agregacijai, kurios metu nepoliniuose organiniuose tirpikliuose susidaro vamzdeliniai polimerai (20 pav.). Taipogi, įvestos didelės π-konjuguotas sistemos 9-toje pozicijoje turi teigiamą efektą polimero savitvarkai, nes struktūra yra papildomai stabilizuojama atsiradusios π-π sąveikos tarp plokščių aromatinių žiedų.
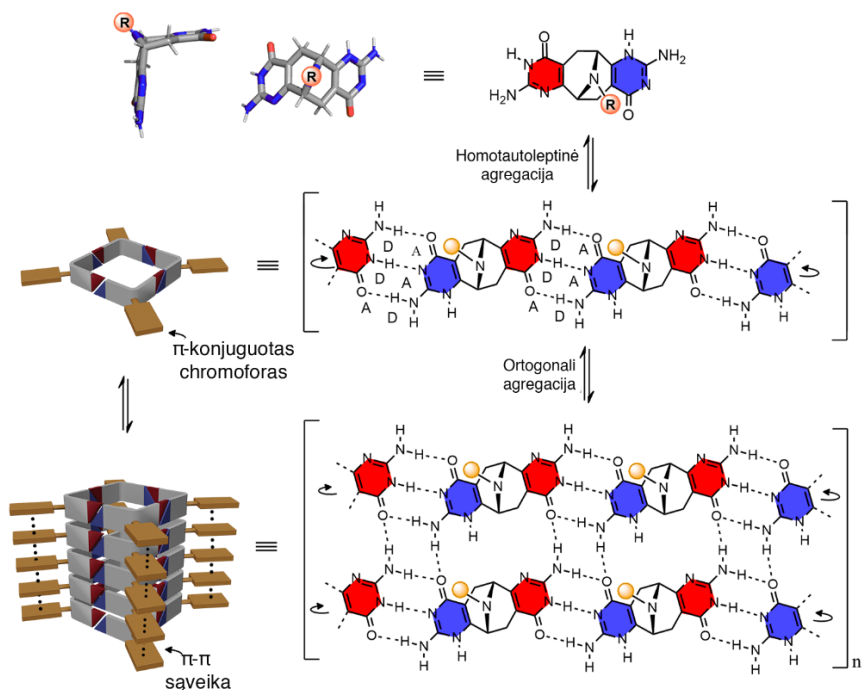
20 pav. 9-azabiciklo[3.3.1]nonano monomero agregacija į supramolekulinį tuščiavidurį vamzdelį.

Kooperatyvus efektas, tarp kryptingų stiprių vandenilinių ryšių ir van der Waals sąveikų, įgalina elektroniškai aktyvių supramolekulinių struktūrų kūrimą, kurios pasižymi aukštu savitvarkos laipsniu. π-konjuguotos sistemos yra plačiai naudojamos kaip aktyviosios medžiagos įvairiuose (opto)elektroniniuose įrenginiuose, pvz. lauko efekto tranzistoriuose (OFET), saulės elementuose, šviesos dioduose (OLED) ir fotovoltiniuose prietaisuose.[208]

Šiam tikslui buvo pasirinktas tetratiafulvalenas (TTF) dėl jo gerų skylių laidumo savybių. Pirmiausiai 1,3-ditiol-2-tiono fragmentas **128** buvo susintetintas geromis išeigomis atliekant anglies disulfido redukciją naudojant metalinį natrį su dimetilformamidu ir po to nukleofilinio pakeitimo reakciją su n-decilbromidu (21 pav.). Atliekant asimetrinio kopuliavimo reakciją tarp 1,3-ditiol-2-tiono **128** ir 1,3-ditiol-2-ono **134** buvo gautas TTF fragmentas 94 % išeiga. Toliau buvo atliktas monodekarboksilinimas veikiant junginį **135** LiBr. Gautas esteris **136** buvo suhidrolizuotas su LiOH vandeninėje terpėje ir galiausiai paverstas į tikslinį prekursorių acilchloridą **138** naudojant oksalilchloridą su piridinu tetrahidrofurane. TTF **138** buvo prijungtas prie azabiciklo ketoesterio **139** ir

galiausiai suformuotas komplementarus izocitozino fragmentas naudojant guanidino karbonatą. Nauji monomerai **140a** ir **140b** 9-azabiciklo[3.3.1]nonano pagrindu buvo susintetinti naudojant atitinkamai raceminį ir enantiomeriškai gryną ketoesterius **131a** ir **131b**.
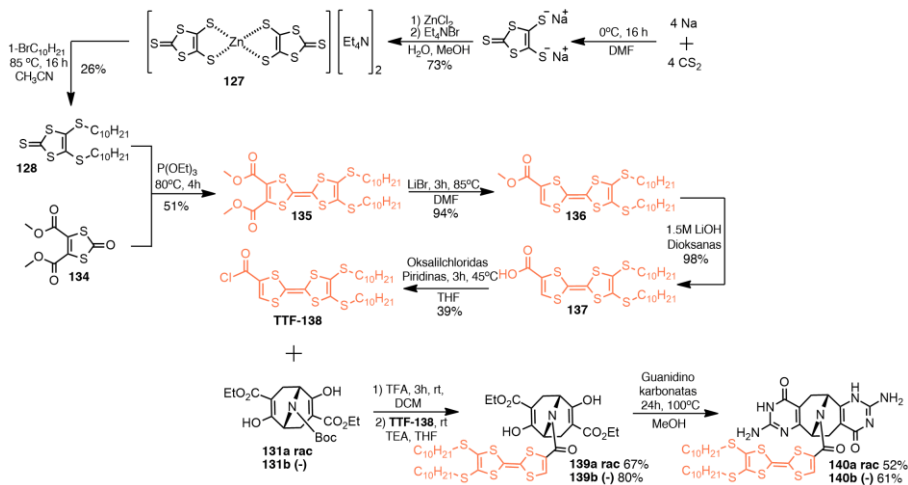

21 pav. Raceminio ir enantiomeriškai gryno monomerų **140a** ir **140b** sintezė.

Enantiomeriškai grynas monomeras **140b** tautoleptinės agregacijos metu susijungė į ciklinius tetramerus ir po to į supramolekulinius vamzdelius susidarant tarpmolekuliniams vandeniliniams ryšiams tarp gretimų tetramerų. Dėl stiprios agregacijos nepoliniuose tirpikliuose susidaro klampus gelis ir yra stebimas signalų išplatėjimas ^{1}H BMR spektruose (22 pav.). Poliniame DMSO tirpiklyje vandeniliniai ryšiai yra suardomi ir supramolekulinis agregatas disocijuoja į monomerą.
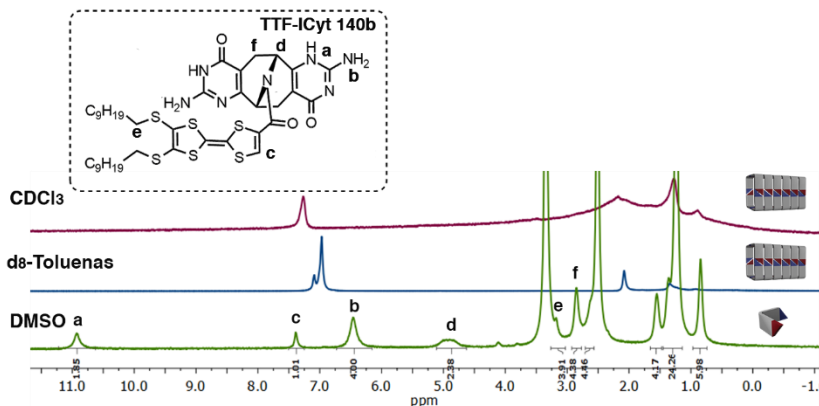
22 pav. Polimero (**140b4)n** ^{1}H BMR spektrai CDCl₃, d₈-toluene ir monomero **140b** ^{1}H BMR spektras DMSO.

Tetramero **140b₄** molekulinis modelis buvo optimizuotas pusiau empiriniu PM3 metodu naudojant Spartan'14 programą. Iš šių tetramerų sukonstruotas tuščiaviduris supramolekulinis vamzdelis (**140b₄)ₙ**, kuris optimizuotas molekulinės mechanikos jėgos lauko MMFF metodu. Elektrostatinis potencinio paviršiaus žemėlapis parodė, kad aukšto ir žemo elektronų tankio van der Waals paviršiai yra išsidėstę priešingose ciklinio tetramero pusėse (23a pav.). Toks priešingas elektronų tankio pasiskirstymas lemia dipolio momento atsiradimą išilgai vamzdelinės struktūros ir skatina ortogonalią agregaciją ta pačia kryptimi. Taipogi, iš molekulinio modelio matome, kad periferijoje išsidėstę plokšti TTF π-konjuguoti fragmentai yra beveik statmeni azabicklo[3.3.1]nonanui ir gali efektyviai susipakuoti išilgai sklidimo ašies (23b pav.).
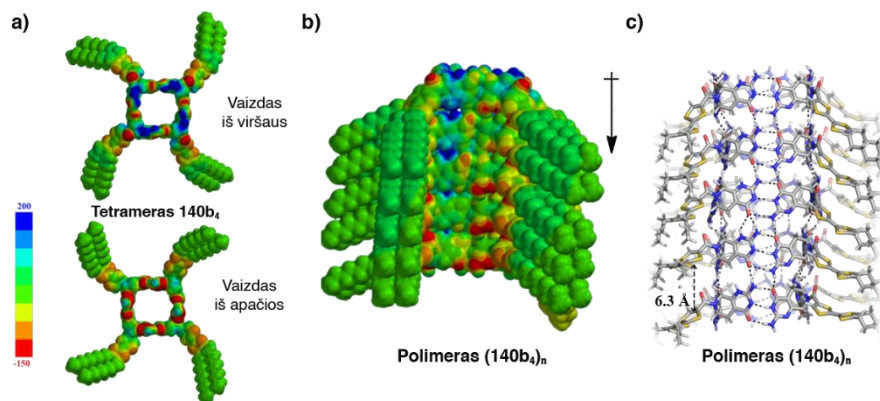

23 pav. a) Tetramero **140b₄** ir supramolekulinio vamzdelio (**140b₄)ₙ** elektrostatiniai potenciniai paviršiaus žemėlapiai; b) vamzdelinio polimero (**140b₄)ₙ** molekulinis modelis.

Svečio C_{60} įterpimo eksperimentai buvo atlikti kaitinant enantiomeriškai gryną monomerą **TTF-ICyt 140b** kartu su fulerenu 90 °C temperatūroje toluene (24a pav.). Sėkmingas polimerinio komplekso **C_{60}@(140b₄)ₙ** susidarymas buvo akivaizdus dėl spalvos pasikeitimo iš oranžinės į rudą, kuri būdinga C_{60} kompleksams (24b pav.). Gautas rudas tirpalas buvo paliktas atvėsti iki kambario temperatūros ir susidaręs gelis patvirtino, kad polimerinė struktūros topologija nebuvo pažeista. Absorbcijos spektre toluene užfiksuotas komplekso absorbcijos maksimumo 3 nm hipsochrominis poslinkis lyginant su laisvu fulerenu esančiu ties 336 nm (24c pav). TTF fragmento absorbcijos smailė liko nepakitusi, vadinasi jis nesąveikauja su svečio molekulėmis, kurios yra vamzdelio ertmėje.

Kontroliniai eksperimentai atlikti su raceminiu monomeru **TTF-ICyt 140a** parodė, kad vykstant heterochiralinei agregacijai tarp dviejų skirtingų enantiomerų ciklinės struktūros nesusidaro, tačiau gaunamos zigzaginės struktūros. Jos gali toliau asocijuotis į dvimates lakštines struktūras susidarant tarpmolekuliniams vandeniliniams ryšiams. Kadangi, susidariusios struktūros neturi ertmės į kurią galėtų įterpti svečio molekulę, fulereno kompleksavimo eksperimentai toluene buvo nesėkmingi.

Šiame skyriuje aprašytas vamzdelinis polimeras galėtų potencialiai būti puikus kandidatas kaip naujas supramolekulinis n,p-heterosandūros puslaidininkis, kur p ir n tipo kanalai yra pilnai atskirti. Vandeniliniai ryšiai kartu su π-π sąveikomis užtikrina tvarkingą chromoforų išsidėstymą. Išorėje esantys TTF fragmentai pasižymi geru skylių laidumu, o ertmėje esantis fulerenas puikiai tinka kaip elektronų pernešimo medžiaga, dėl savo elektronų akceptorinių savybių.
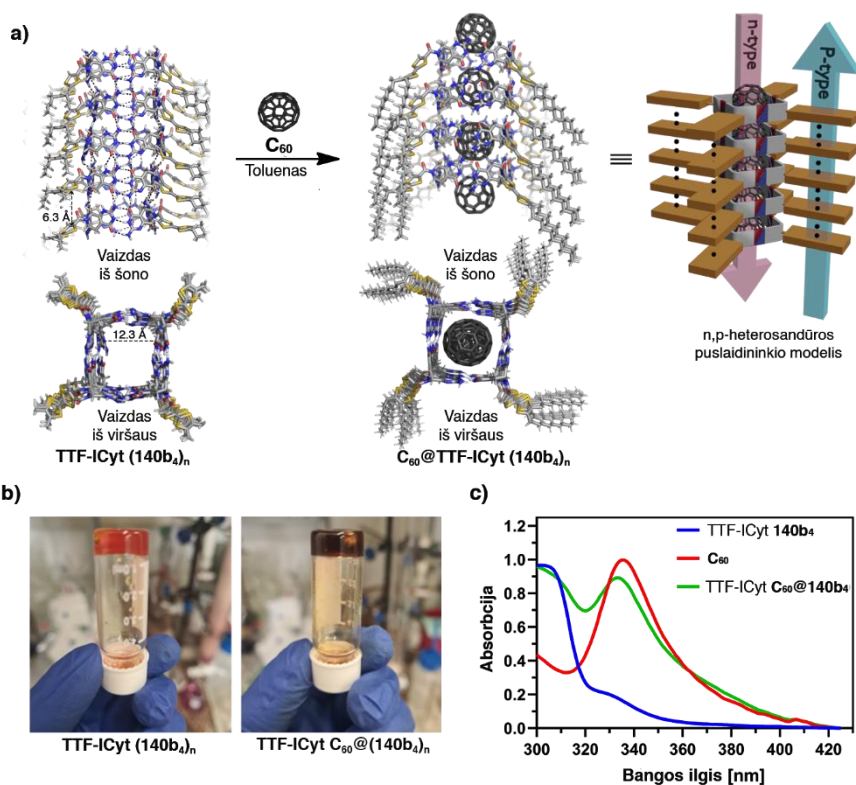

24 pav. a) Svečio C_{60} molekulių įterpimas į supramolekulinį vamzdelį toluene; b) susidarę polimero (**140b_4)_n** (kairėje) ir polimerinio komplekso C_{60}@(**140b_4)_n**

227

(dešinėje) geliai (c = 11 mM) toluene; c) absorbcijos spektrai polimero (**140b₄)ₙ**, laisvo fulereno ir komplekso **C₆₀@(140b₄)ₙ** toluene (c = 1 µM).
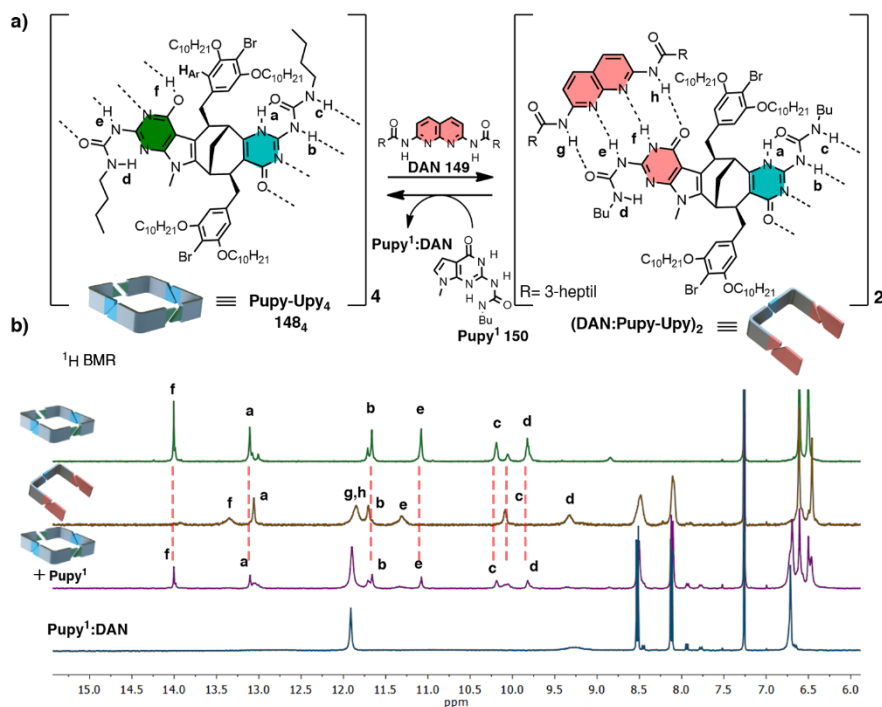
4. Dinaminės supramolekulinės žnyplės

Sekantis žingsnis norint sukurti funkcionalias supramolekulines struktūras yra gebėjimas kontroliuoti sistemos dinamiškumą ir grįžtamumą. Mūsų pasirinkta strategija rėmėsi galimybe valdyti pusiausvyrą tarp skirtingų tautomerinių formų veikiant sistemą išoriniu cheminiu ar šviesos stimulu. Šiam tikslui pasiekti buvo susintetintas C₁-simetrijos monomeras **Pupy-Upy 148**. Pupy fragmente ureidopirimidinonas yra sukondensuotas kartu su elektronų turtingu pirolo žiedu. Monomeras asocijuojasi į ciklinį tetramerą susidarant DDAA-AADD vandeniliniams ryšiams tarp Upy fragmentų keto formoje ir DADA-ADAD tarp Pupy fragmentų enolinėje formoje (25 pav.).
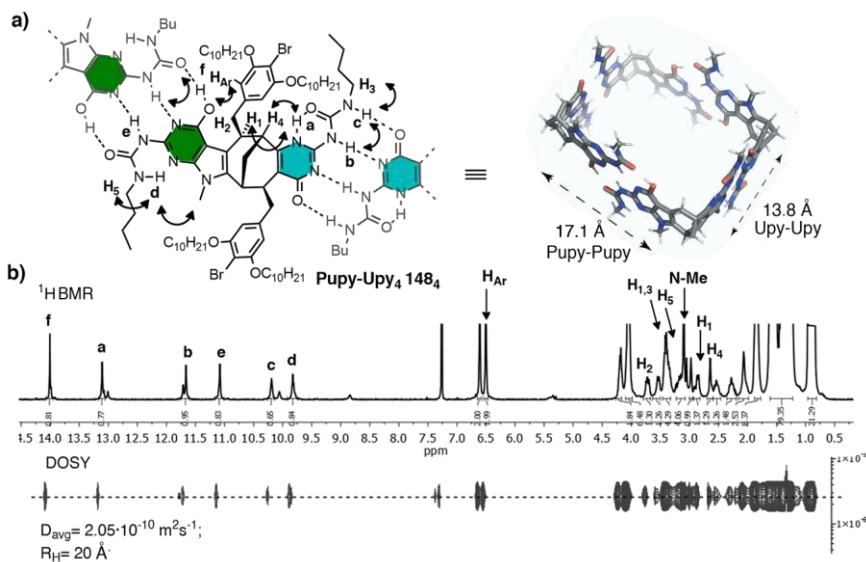
25 pav. a) Monomero **Pupy-Upy 148** asociacija į ciklinį tetramerą; b) tetramero **Pupy-Upy₄ 148₄** ¹H BMR spektras CDCl₃.

Tačiau jeigu sistemoje yra papildomas monomeras, sudarantis komplementarius DAAD tipo ryšius, tada Pupy fragmente dominuoja ADDA tipo keturgubi vandeniliniai ryšiai vietoje įprastų DDAA ar DADA. Taigi, naujai gautą tetramerą **Pupy-Upy₄** sumaišius su stechiometriniu kiekiu 2,7-diamino-1,8-naftiridino **149** (DAN), buvo selektyviai suardytas Pupy-Pupy homodimeras ir naujai susidarė DAAD-ADDA tipo Pupy-DAN heterodimeras. Įvedant konkuruojantį **DAN 149** motyvą, uždaro ciklinio

agregato topologija buvo transformuota į atviros formos dimerines žnyples (26 pav.). Sistemos polinkis sudaryti didžiausią galimų vandenilinių ryšių skaičių pastūmė dinaminę pusiausvyrą link supramolekulinių žnyplių susidarymo. [1]H BMR spektre CDCl$_3$ taip pat stebimas silpnesniuose laukuose naujai atsiradęs 8 NH rezonansų rinkinys. Remiantis stebimomis erdvinėmis sąveikomis COSY ir ROESY spektruose, šie signalai yra priskiriami vandeniliams, kurie dalyvauja susidarant dimerams Upy-Upy ir heterodimerams Pupy-DAN. ^{1}H-^{15}N HSQC spektras patvirtino, kad nebeliko enolinės tautomerinės formos, nes stebimos visos sąveikos tarp atitinkamų vandenilių ir azoto atomų. Hidrodinaminis spindulys R_H = 17,3 Å apskaičiuotas iš difuzijos koeficiento (2,38·10^{-10} m^{2}s^{-1}) parodė mažesnio agregato susidarymą lyginant su eksperimentiniu tetramero **Pupy-Upy$_4$** spinduliu (R_H = 20Å), kadangi ilgesnioji Pupy-Pupy tetramero kraštinė yra suardoma vykstant heterodimerizacijai su **DAN 149**.


26 pav. Grįžtamoji ciklinio tetramero agregacija į supramolekulines žnyples pridėjus konkuruojančio **DAN 149** motyvo CDCl$_3$.

Supramolekulinės žnyplės buvo suardytos pridėjus perteklių konkuruojančio junginio **Pupy^1 150** į **Pupy-Upy$_4$** ir **DAN 149** mišinį. Iš ^{1}H BMR spektro CDCl$_3$ matome, kad susidarė pirminis ciklinis tetrameras **Pupy-Upy$_4$** ir

heterodimeras **DAN-Pupy**[1]. DOSY spektre stebimos dviejų dydžių dalelės, kurių difuzijos koeficientai D = 1,90·10^{-10} m^2s^{-1} ir D = 3,63·10^{-10} m^2s^{-1} buvo priskirti atitinkamai tetramerui ir **DAN-Pupy**[1]. Pridėjus konkuruojantį fragmentą buvo indukuota monomerų saviatranka į homodimerus. Tai pademonstruoja galimybę grįžtamai valdyti supramolekulinio agregato topologiją tarp uždaros ir atviros formos.

Analogiškai, grįžtamai manipuliuoti supramolekulinio agregato asociaciją tarp ciklinio tetramero ir dimerinių žnyplių galima užmaskuojant vieną iš komplementarių vandenilinių ryšių motyvų (27 pav.). Šiam tikslui buvo pasirinktas redokso aktyvus junginys **red-DAN 151**. Kadangi naudojamas asimetrinis **red-DAN**, tai heteroasociacijos metu gaunamas žnyplių izomerinis mišinys ir ^{1}H BMR spektre C_6D_6 stebimas signalų išplatėjimas. Toliau, **red-DAN** yra paverčiamas į iminochinoną (**ox-DAN**) oksidacinėmis sąlygomis, naudojant Co(salen)$_2$ ir molekulinį deguonį. Tokiu būdu DAAD vandenilinių ryšių motyvas yra transformuojamas į nekomplementarų DAA motyvą, kuris negali asocijuotis su Pupy. Supramolekulinis agregatas yra atgal paverčiamas į ciklinį tetramerą.
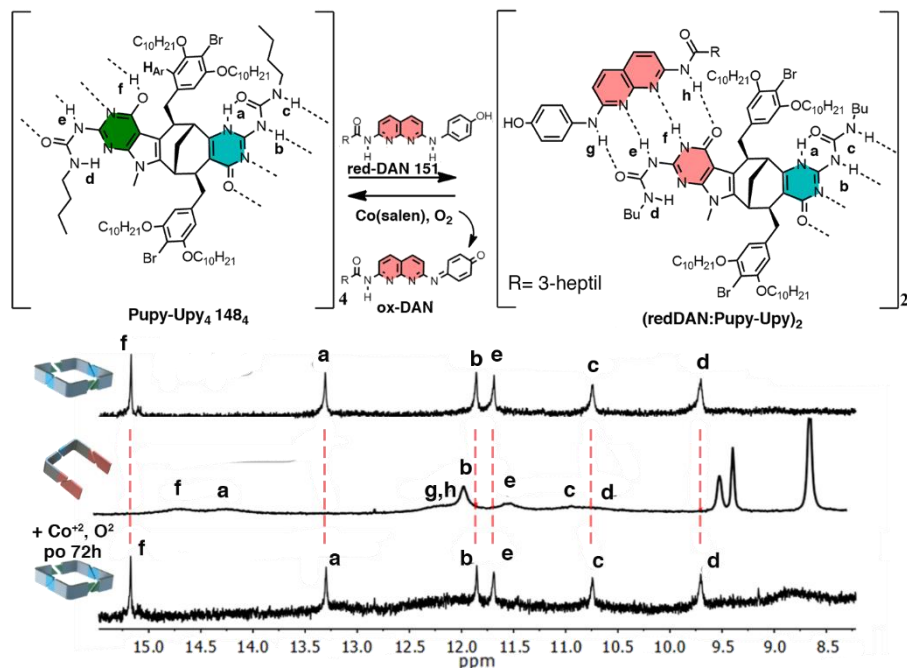
27 pav. Ciklinio tetramero **Pupy-Upy₄** grįžtama asociacija į dimerines žnyples pridėjus redokso aktyvaus junginio **red-DAN 151**.

Norint pilnai valdyti supramolekulinės struktūros topologiją ir grįžtamai suardyti vidinę ertmę, reikia užblokuoti Upy-Upy homodimero asociaciją. Tam buvo puikiai pritaikyta šviesa aktyvuojama cviterjoninė merocianino rūgštis, kuri mėlynos šviesos indukuotos nukleofilinės ciklizacijos metu išlaisvina protoną. Supramolekulinėse žnyplėse esantis Upy-Upy fragmentas yra suardomas selektyviai protonizuojant Upy motyvą. Iš DOSY eksperimento apskaičiuotas hidrodinaminis spindulys ($R_H = 11$ Å) patvirtina mažesnių dalelių buvimą, nes ši vertė yra daug mažesnė už ciklinio tetramero ar žnyplių spindulio vertę. Tamsoje supramolekulinė struktūra agreguojasi atgal į žnyples, nes gautas fotorūgšties ciklinis spiropiranas termiškai grįžta į merocianino cviterjoną atimdamas protoną iš protonizuoto Upy fragmento.
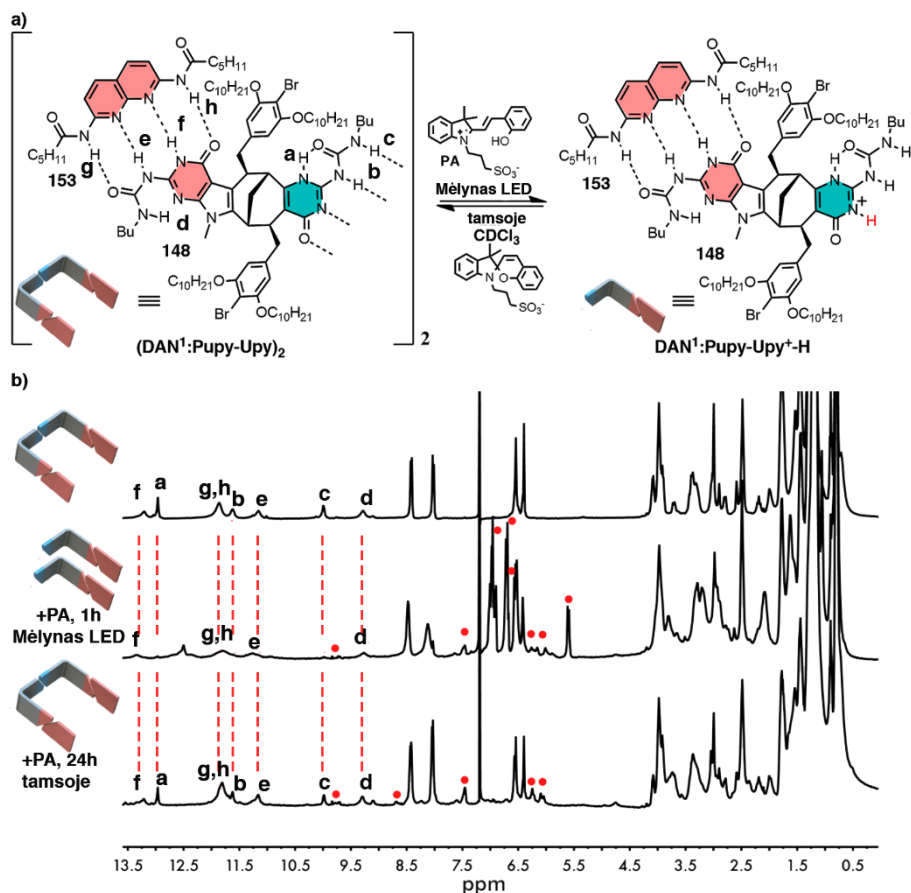
28 pav. Supramolekulinių žnyplių disociacija naudojant šviesa aktyvuojamą cviterjoninę merocianino rūgštį.

Apibendrinant, buvo sukurtos racionalios strategijos, kurios įgalina grįžtamą kontroliavimą tarp skirtingų supramolekulinių struktūrų topologijų naudojant cheminį ar šviesos stimulą. Toks grįžtamų pilnai nekovalentiniais ryšiais pagrįstų agregatų kūrimas atveria duris tolimesniam struktūrų pritaikymui medžiagų perneršimui ir selektyviam išlaisvinimui, taip pat kuriant įvairius cheminius receptorius ar kitas išmanias į dirgiklius reaguojančias medžiagas.

IŠVADOS

1. Šiame darbe buvo sukurti supramolekuliniai vamzdeliai ir diskretiškos kapsulės, turintys lankstų nukleofilinį jungtuką, kuris buvo prijungtas atliekant fotocheminę „click" reakciją. Taip pat pademonstruota, kad gautas nukleofilinis jungtukas įgalina supaprastintą įvairaus dydžio chromoforų įvedimą į sistemą, kurie neturi įtakos agregacijos laipsniui.

2. Buvo pademonstruota, kad gautos tuščiavidurės kapsulės gali į vidų įterpti svečio C_{60} molekulę nepoliniuose tirpikliuose – chloroforme, benzene ir poliniame – acetonitrile. Atrasta šeimininko-svečio komplekse unikali tamsoje vykstanti elektronų pernaša tarp artimai erdvėje išsidėsčiusių jungtukų turinčių sulfidines grupes ir svečio fulereno C_{60} molekulę.

3. Fulerenas ir jo pigi žaliava, fulereno suodžiai, buvo sėkmingai pritaikyti kaip heterogeniniai katalizatoriai chemoselektyvioje sulfidų fotooksidacijoje iki sulfoksidų puikiomis išeigomis. Šių katalizatorių universalumas buvo pademonstruotas juos pritaikant radikalinės ciklizacijos, aminų pavertimo į iminus ir boro rūgšties oksidacijos reakcijose. Sukonstruotas srautinis reaktorius leido reakcijas vykdyti gramų skalėje.

4. Buvo pademonstruotas dinaminės kapsulės, funkcionalizuotos tetrafenilporfirino fragmentais, gebėjimas pritaikyti lanksčią vidinę ertmę efektyviam svečio molekulės įterpimui. Svečio C_{60} kompleksavimo metu vyksta monomero tautomerizacija iš keto į enolinę formą. Konformacijos pokyčių metu papildomai atsiradusi π-CH sąveika kompensuoja energetinius nuostolius ir entropijos sumažėjimą, bei stabilizuoja naujai susidariusį kompleksą.

5. Sukonstruoti vamzdeliniai polimerai azabiciklo[3.3.1]nonano pagrindu, turintys π-konjuguotą tetratiafulveno chromoforą. Vandeniliniai ryšiai kartu su papildomomis π-π sąveikomis tarp plokščių konjuguotų pakaitų užtikrina aukštą savitvarkos laipsnį. Tokia savitvarkė sistema užtikrina n ir p tipo kanalų atskyrimą, kuris yra reikalingas skirtingų krūvių efektyviai pernašai kuriant ambipolinius organinius puslaidininkius.

6. Sukurta unikali strategija, kuri leidžia grįžtamai kontroliuoti agregato topologiją tarp ciklinio tetramero, dimerinių žnyplių ar pavienio monomero. Ši strategija paremta galimybe selektyviai valdyti vandenilinius ryšius sudarančių fragmentų Upy ir Pupy tautomerizacijos pusiausvyrą naudojant

konkuruojančio monomero komplementarų fragmentą, taip pat cheminį ar šviesos stimulą.

LIST OF PUBLICATIONS

Main publications:

- A. Jozeliūnaitė, D. Valčeckas, E. Orentas, Fullerene soot and a fullerene nanodispersion as recyclable heterogeneous off-the-shelf photocatalysts, *RSC Adv.,* **2021**, 11, 4104-4111. DOI: 10.1039/D0RA10147H;
- A. Jozeliūnaitė, T. Javorskis, V. Vaitkevičius, V. Klimavičius, E. Orentas, Fully Supramolecular Chiral Hydrogen-Bonded Molecular Tweezer, *J. Am. Chem. Soc*. **2022**, 144, 18, 8231 – 8241. DOI: 10.1021/jacs.2c01455.

Other publications not included in the thesis:

- E. Radiunas, S. Raišys, S. Juršėnas, A. Jozeliūnaitė, T. Javorskis, U. Šinkevičiūtė, E. Orentas, K. Kazlauskas. Understanding the limitations of NIR-to-visible photon upconversion in phthalocyanine-sensitized rubrene systems*, J. Mater. Chem. C*., **2020**, 8, 5525-5534. DOI: 10.1039/C9TC06031F;
- E. Radiunas, M. Dapkevičius, S. Raišys, S. Juršėnas, A. Jozeliūnaitė, T. Javorskis, U. Šinkevičiūtė, E. Orentas, K. Kazlauskas. Impact of t-butyl substitution in rubrene emitter for solid state NIR-to-visible photon upconversion, *Phys. Chem. Chem. Phys*., **2020**, 22, 7392-7403. DOI: 10.1039/D0CP00144A;
- C. Ye, W. Yuan, X. Wei, R. Liang, A. Jozeliūnaitė, J. de Mendoza, E. Orentas, Q. Shi. Metal coordination guided formation of discrete neutral three-component hydrogen-bonded architectures, *Org. Lett.* **2020**, 22, 23, 9215–9219. DOI: 10.1021/acs.orglett.0c03397
- E Radiunas, M. Dapkevičius, L. Naimovičius, P. Baronas, S. Raišys, S. Juršėnas, A. Jozeliūnaitė, T. Javorskis, U. Šinkevičiūtė, E. Orentas, K. Kazlauskas, NIR-to-vis photon upconversion in rubrenes with increasing structural complexity. *J. Mater. Chem. C*, **2021**, 9, 4359-4366. DOI: 10.1039/D1TC00296A;
- E. Radiunas, L. Naimovičius, S. Raišys, A. Jozeliūnaitė, E. Orentas, K. Kazlauskas, Efficient NIR-to-vis photon upconversion in binary rubrene films deposited by simplified thermal evaporation, *J. Mater. Chem. C*., **2022**, 10, 6314 – 6322. DOI: 10.1039/D1TC05332A

List of conferences:

- A. Jozeliūnaitė, A. Neniškis, D. Anderson, T. Javorskis, V. Vaitkevičius, E. Orentas. A General Approach Toward Hydrogen-bonded Supramolecular Nanotubes from Small Building Blocks, The 17th Symposium of the French – American Chemical Society, Orlean, 2018;
- A. Neniškis, A. Jozeliūnaitė, V. Vaitkevičius, E. Orentas. Supramolecular Large Cavity Nanotubes Based on Orthogonal Self-Assembly of Isocytosine, Balticum Organicum Syntheticum, Talinn, 2018;
- A.Jozeliūnaitė, D. Valčeckas, E. Orentas. Fullerene-C_{60}: From The Inoccent Guest Molecule to a Photocatalyst. Open Readings, Vilnius, 2020 – canceled due to COVID-19;
- A. Jozeliūnaitė, E. Orentas, An Efficient Heterogeneous Carbon-Based Photocatalyst For Selective Sulfide Oxidation To Sulfoxides. Open Readings, Vilnius, 2021;
- A. Jozeliūnaitė, E. Orentas, Enantiopure Hydrogen-Bonded Aggregates: From Discrete Tetramer to Tubular Polymer, Balticum Organicum Syntheticum, Vilnius, 2022.

Curriculum Vitae

Work experience:

2021.12.13 – Present

    Company: Thermo Fisher Scientific

    Position: R&D Scientist

Projects:

2021.04.01 – 2022.06.30

    Institution: Vilnius University

    Position: Chemist

    Project: "Addressing the lifetime issues of the latest generation OLEDs: analysis and possible solutions", Research Council of Lithuania, Grant S-MIP-21-12. Budget: 149 993 Eur.

2019.06.03 – 2022.06.30

    Institution: Center for Physical Sciences and Technology FTMC

    Position: Engineer

    Project: "Nanoscale probing and activation of surface-initiated polymerization", Research Council of Lithuania, Grant S-MIP-19-7. Budget: 149 996 Eur.

2018.01.01 – 2022.01.07

    Institution: Vilnius University

    Position: Project's junior research assistant

    Project: "Triplet state engineering in organic optoelectronics compounds", European Social Fund under Global Grand measure (09.3.3-LMT-K-712-01-0084). Budget: 594 350 Eur.

2018.01.02 – 2020.08.31

    Institution: Vilnius University

    Position: Laboratory assistant

    Project: "New entries into the chemistry of organic free-radicals (GoRadical)", Research Council of Lithuania, Grant S-MIP-17-46. Budget: 99 956 Eur.

Internships:

2021.09 – 2021.11

  University: University of Santiago de Compostela, Spain

  Description: During the internship I was working on the development of supramolecular frameworks used for nanoporous materials under supervision of Prof. Javier Montenegro.

2015.12 – 2016.08

  University: École polytechnique fédérale de Lausanne, Switzerland

  Description: Internship was carried out in the Laboratory of Macromolecular and Organic materials led by Prof. Holger Frauenrath at EPFL. Photochromic switching comprising various length of π-conjugated systems were developed under supervision of dr. Giuseppe Sforazzini.

2014.07 – 2014.08

  Company: BĮ "Nacionalinė visuomenės sveikatos priežiūros laboratorija"

  Description: During the internship assisted in quantitative anion analysis by liquid chromatography method.

2014.02.24– 2014.05.24

  University: Vilnius University

  Description: Scientific research project (SMT-14P-26/SMT14P-077) under supervision of Prof. Edvinas Orentas was performed during summer funded by the Research Council of Lithuania's project "Promotion of Students' Scientific Activities" (VP1-3.1-ŠMM-01-V-02-003).

2013.07– 2013.09

  University: Kaunas University of Technology

  Description: Scientific research project "Organic fluorescent dyes for light emiting diodes" (F5-90-860/SMP13-071) under supervision of dr. Ramūnas Lygaitis was performed during summer funded by the Research Council of Lithuania's project "Promotion of Students' Scientific Activities" (VP1-3.1-ŠMM-01-V-02-003).

Education:

2017.10 – 2022.09

University: Vilnius University

Field of Science: Chemistry

Degree: Doctorate

2015.09 – 2017.06

University: Vilnius University

Field of Science: Chemistry

Degree: Master's (Cum Laude)

2011.09 – 2015.06

University: Vilnius University

Field of Science: Chemistry

Degree: Bachelor's

Other:

- Promotional PhD scholarship from Research Council of Lithuania for actively conducting scientific research (2019 No. P-DAP-19-182);
- An award for the best oral presentation on Chemistry and Chemical Physics presented in the 62nd international conference for students of physics and natural sciences „Open Readings 2019", 2019, Vilnius, Lithuania;
- An ACS poster award in 17th Symposium of the French - American Chemical Society, Orlean, 2018.